2023

Influenza A virus inclusions are liquid condensates that can be pharmacologically hardened

Temitope Akhigbe Etibor

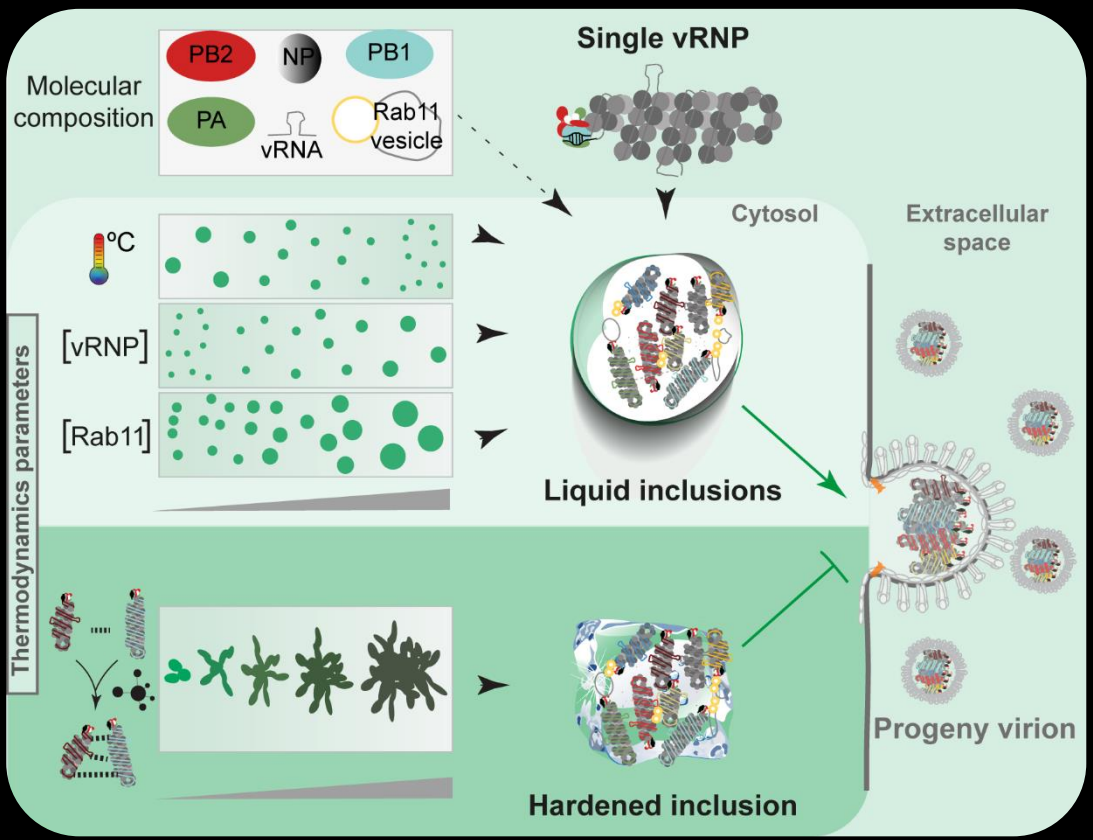

Dissertation presented to obtain the **Ph.D. degree in Integrative Biology and Biomedicine (IBB)**

Oeiras, March, 2023

INSTITUTO DE TECNOLOGIA QUÍMICA E BIOLÓGICA ANTÓNIO XAVIER | UNIVERSIDADE NOVA DE LISBOA

Influenza A virus Inclusions are Liquid Condensates that can be Pharmacologically Hardened

Temitope Akhigbe Etibor

Dissertation presented to obtain the Ph.D degree in Integrative Biology and Biomedicine

Instituto de Tecnologia Química e Biológica António Xavier | Universidade Nova de Lisboa

Research work coordinated by:

INSTITUTO GULBENKIAN DE CIÊNCIA

Oeiras, March, 2023

Declaration

I, Temitope Akhigbe Etibor hereby declare that this dissertation and the data herein contained, are the results of my own work conducted between August 2017 to November 2022 in the laboratory of Dr Maria João Amorim (PhD), at the Instituto Gulbenkian de Ciência (IGC), Oeiras, Portugal.

Financial support for this work was granted by a Doctoral Fellowship awarded to Temitope Akhigbe Etibor by Fundação para a Ciência e Tecnologia (FCT): PD/BD/128436/2017 and COVID/BD/151646/2021.

The Amorim Lab was awarded an ERC grant on LOFlu project (101001521) for which I was a beneficiary upon the expiration of my FCT fellowship.

I declare that all contributions have been acknowledged in the appropriate "Author contributions" or "Acknowledgments" sections.

Work developed during this period, resulted the in following publications:

Etibor T.A., Vale-Costa S., Sridharan S., Bras D., Becher I., Mello V.H., Ferreira F., Alenquer M., Savitski M.M., Amorim M.J. Rules for Hardening influenza A virus liquid condensates. bioRxiv (2022). doi.org/10.1101/2022.08.03.502602. (bioRxiv preprint, in revision).

Etibor T.A., Yamauchi Y., Amorim M.J. Liquid Biomolecular Condensates and Viral Lifecycles: Review and Perspectives. Viruses. (2021) 25;13(3):366. doi: 10.3390/v13030366. PMID: 33669141.

Alenquer M., Vale-Costa S., **Etibor T.A.**, Sousa A.L.., Ferreira F, Amorim M.J. Influenza A virus Ribonucleoproteins form liquid organelles at endoplasmic reticulum exit sites. Nature Communications 10, 1629 (2019). doi.org/10.1038/s41467-019-09549-4. PMID: 30967547.

Acknowledgements

"If I have seen further, it is by sitting on the shoulders of giants"

Sir Isaac Newton (1675).

My sojourn from scientific curiosity to discovery is by no means a solo endeavour. To attain balance in academia, the comingling of family and social support cannot be understated. For me, this feat was only achievable through the help of many giants who nurtured me.

First, I would like to thank my precious (in Gollum´s voice) supportive wife, Efemena Jennifer Etibor, whom there is not enough adulation to express her contribution to this success. With your endless love, sacrifice, and encouragement, I was able to sail through the difficult periods of my PhD. You and our children (Sofia Etibor and Manuel Etibor) were my inspiration and the source of love and laughter which kept me sane through this arduous period.

To my parents (Mr Babatunde Etibor and Mrs Ruth Etibor) and siblings (James, Blessing, Daniel, and Joshua Etibor), thank you for your enduring prayers, love and support that kept me grounded and focused on all times.

To my colleagues at the CBV whom I've had the honour of learning from as I venture into the world of science. Thank you for accompanying me through the peaks and troughs that came along. My special thanks to: Silvia Vale-Costa for the many chit-chats, jokes, discouraging me from smelling TEMED and helping with bureaucracies at the IRN, Marta Alenquer for keeping things serious and sane; on a less serious note, I hope you remember my prank about ruining your experiment (your countenance that day was a marvel), Filipa Sena, Victor Mello, Nuno Santos and João Diamantino, Monica Mendonça for always noting my eccentricities (such as making strange sounds of no origin other than me, infectious laughter etc). To Daniela Brás the fashionista who is always organized and meticulous, a trait I would like to phenocopy. Thank you for the special experiences you gave me and

many on your wedding day, I'm a tough lad but 'kind of' teared up that day, and for the first time in a long time, I felt nostalgic, to Camila, for always being piqued when I look or speak in your direction, the number one troublemaker who compelled me to wear a baby-face making eye glasses, and reminder of the surgical eating mechanism. To Chris, whom I have the honour of addressing as Krish, for your useful inventions (which I hope gets patency in the future), curiosity and important papers that you share, I see myself in you sometimes and thank you for your contribution to my work. To Mariette, a colleague who like me expresses the anti-coffee antibody. To Oleg, you are welcome to the CBV Lab, and I thank you for agreeing to review my dissertation. To Filipe, the Mcgyver and master regulator of the CBV lab, I sincerely appreciate your kindness, calm advice, and technical support throughout this period. It´s wonderful being your 'office mate'. When the market recovers from the current downturn, let´s get rich soon! Importantly, to every CBV member (old and new) with whom I have worked together, discussed in lab meetings and at launch, and unsuccessfully bugged me to no end on at least trying a bit of alcohol, coffee or both, I say a big thank you.

To my supervisor (the boss who is 'always' right) Maria João Amorim, I cannot express enough, my gratitude for your patience and perseverance especially in the early days of my PhD (which could have resulted in premature termination). You are one of a kind boss who cared about what I am going through in my personal life and mental space. In the future, I will take your advice and try to take as many breaks as possible. With your support and guidance, today, I can confidently say that I came, I saw, I conquered. Despite being naïve, you gave me the chance and confidence for independent thinking, critical reasoning, and scientific rigor. Many times, we brainstormed from what the best experiment or analysis could be to answer specific questions, giving me liberty to develop creative ideas and methods rooted in logical rationale. I truly enjoyed our scientific discourse, as it was a way for me to sharpen my mind when you come up with the why, how, which,

what questions. I was amazed by how well you took my idea of transitioning to the industry in the future and have been so supportive in getting this done. I could not have had a better supervisor.

I would like to thank the members of Mikhail Saviski's lab: Sindhuja Srinivasan and Isabelle Becher for their contribution to my work and many discussions via zoom. Without your collaboration, this work would not be so accomplished.

To my thesis committee members: Ivo Telley and Paula Duque, thank you for not recommending that I get kicked out of the PhD programme too early. The chances you have afforded me as well as your counsel and scientific input allowed me to think out of the box, thereby, aiding my work progress.

I would like to appreciate my IBB2017 colleagues (Catarina, Hugo, Tania, Margarida, Camilla, Marco, Andre and Andre, Sahar, Hermina and Bas) for the many social gatherings (launch, dinner, beer hour, etc), help with information and bureaucratic paper works. You were all there with me from the very beginning till the end. I couldn't have had better mates than you guys.

Importantly, my sincere appreciation goes to the IBB programme established by the IGC which incubated me into the scientific life and kept on providing support through the Élio Sucena, Alekos Athanasiadis (of blessed memory) and Jorge Caneiro, who were assisted by Ana Aranda Silva and Patricia Gomes. My sincere appreciation to Elio for your kind advice in the early and difficult days of my PhD, I am sure you are proud that it was not all in vain. To Jorge, who takes everyone's problems as his own, when I was almost evacuated from my home, you rendered assistance beyond imagination, and I cannot say thank you enough. My special thanks to Ana Aranda Silva and Patricia Gomes for being so instrumental to this success in all ways beyond mentioning. Many of your works were in the background, but today, their results are at the fore.

Also, I would like to say thank you to the Nigerian community (Abdulbasit, Ibukun, Bisola, Wilson and Tope) at the IGC for their support, care, and friendship beyond science.

To Ana Regalado, who made sure my life was always easy especially when it comes to paper works, registering kids at school, translation. You went out of your way to help me and my family, and we say a big thank you.

Finally, I acknowledge the advanced imaging, electron microscopy and quantitative biology units of the IGC for their support and assistance in this work (especially Gabriel Martins, Nuno Pimpão, Maria Hanulova, Jose Marques, Ana Laura Sousa, and Tiago Paixão).

If there was anything I have learnt enroute to achieving a PhD degree, it is that the PhD is a never-ending curiosity stream, we just must stop at some point and let others pick up thenceforth. In the name of eminent giants that treaded this path before me, I hereby drop my pipette, pen and lab coat with the hope of picking another in the future.

List of figures

List of tables

Table of contents

List of Abbreviations

Summary

Influenza A virus (IAV) is relevant to human and veterinary health as it causes seasonal epidemic and sporadic pandemics with excess mortality (Hampson and Mackenzie, 2006; Martin-Benito and Ortin, 2013; Vale-Costa et al., 2016a; Silvia Vale-Costa and Amorim, 2016). A way to reduce the risks of IAV disease is the yearly vaccination programmes, which has a reported 40-60% efficiency, pointing to the need for a more efficacious solution. This is only possible by gaining thorough understanding of IAV biology at the fundamental level, which could then inform the development of new antiviral therapeutics.

IAV is a negative sense, single stranded RNA virus with an eight-partite segmented genome in the form of viral ribonucleoproteins (vRNPs). Each vRNP consists of nucleoprotein (NP) encapsidated viral RNA (vRNA, which encodes specific viral proteins) with viral polymerase (consisting of PB2, PB1 and PA) at its base-paired 5'- and 3'-terminal ends. Viral genome assembly is yet a process that lacks molecular understanding and geographical characterization. It is known to be a selective process, whereby eight, and no more than eight, different vRNPs form a complex that is packaged into assembling virions at the plasma membrane. This thesis investigates where IAV genome assembly takes place and whether these compartments have specific properties that may be targeted. Upon infection, the vRNPs are released into the cytosol and imported into the nucleus for transcription and replication. However, as viral assembly takes place at the plasma membrane, the newly synthesized vRNPs are exported from the nucleus to the cytosol where they interact with Rab11 to form viral inclusions. Due to the increased colocalization of different vRNPs in the inclusions with time of infection, these sites were proposed as the hotspots of IAV genome assembly.

Having provided the state-of-the art in **Chapter 1**, we explored, in **Chapter 2,** the emergence of IAV inclusions and considered two hypotheses:

that intersegment vRNA-vRNA interactions gives rise to IAV inclusions, which would suggest that sub-bundles or bundles of vRNPs in the process of genome assembly, were contained in these sites or that such interactions are preceded by inclusion emergence, suggesting that IAV inclusions are sites specialised for genome assembly. Using a mini-replicon system that expresses only one or two species of vRNA(s) or IAV infection that produces all eight vRNAs, we showed that one vRNA type is sufficient to form inclusions, suggesting that IAV inclusion biogenesis precedes intersegment interactions. Correlative light and electron microscopy (CLEM) of these single vRNA type inclusions phenocopy infection induced inclusion; a non-membrane delimited cluster of vRNP-rich Rab11 vesicles, akin to biomolecular condensates that were postulated to originate by phase transition. In fact, these single vRNP type inclusions readily adapted to shock treatment and undergo fusion and fission dynamics. This indicates that IAV inclusions are liquid condensates.

One of the ways to alter the physiological function of biomolecular condensates is by changing their biophysical properties. This strategy could, for viruses, give rise to alternative antiviral therapies. In **Chapter 3**, we therefore asked whether it is possible to harden IAV inclusions and how. For this, we changed established parameters (such as temperature, molecular concentration, and type/strength of interactions) known to regulate the biophysical properties of biomolecular condensates as proxy of different biological processes regulating enthalpy, concentration or modulating the ligations between interacting components, such as post-translational modifications. For temperature, we used 4ºC, 37ºC and 42ºC; for concentration, we varied the concentration of characterised drivers of IAV inclusion' formation (vRNP and Rab11) and for number/strength of interactions, we used nucleozin (a well-known antiviral drug that oligomerizes either free NP or NP in vRNPs). Our data showed that inclusion hardening is best achieved by increasing the number/ strength of interactions over that

altering concentration and temperature. In fact, using different biophysical analysis such as coarsening assay, pulse-chase photobleaching, fluorescence loss after photoactivation and single particle tracking, we showed that in contrast to liquid IAV inclusions, hardened inclusions displayed rigidity, lacking dynamics and loss mobility.

Having understood that IAV leads to formation of insoluble condensates in the cell to organize viral reactions, in **Chapter 4**, we next aimed at understanding how IAV infection in general changed the landscape of soluble material in the cell. For this, we analysed the solubility proteome profile (SPP) during a time course of IAV infection to identify cellular and viral molecules that partition into condensates and to identify cryptic condensates induced by infection. Our analysis revealed changes in the abundance of 174 cellular proteins and 10 viral proteins and in the solubility of 413 proteins (within the 6,629 proteins detected occurring throughout infection). Phase transitions in the cell correlated with mitochondria, translation, cell-substrate junction proteins and established LLPS processes (stress granule formation, nucleoli function, splicing). Our assay showed that vRNP constituents (NP, PB1, PB2, and PA) become more insoluble with time, just as inclusions enlarge, in agreement with Chapter 2 in this thesis. To validate the screen, we repeated the SPP assay in infected Rab11a-DN cells that do not form inclusions and make vRNPs evenly distributed in the cytosol. Using this system, we found that vRNP components (NP, PB1, PB2 and PA) are soluble, indicating the need for a functional Rab11a to form inclusions, and validating their insoluble profile.

We, then used SPP to evaluate of the impact of nucleozin in the cellular solubility landscape and found that nucleozin did not lead to additional changes in solubility of cellular components, other than vRNPs. Crucially, this work opens new avenues to explore how alterations in cellular and viral material properties regulate cellular function and contribute to viral infection.

In **Chapter 5**, we discuss the findings and provide caveats and future perspectives of this study.

Título e resumo

O vírus influenza A (IAV) é relevante para a saúde humana e veterinária, pois causa epidemias sazonais e pandemias esporádicas com excesso de mortalidade (Hampson e Mackenzie, 2006; Martin-Benito e Ortin, 2013; Vale-Costa et al., 2016a; Silvia Vale -Costa e Amorim, 2016). Uma forma de reduzir os riscos da doença por IAV são os programas anuais de vacinação, que têm uma eficiência relatada de 40-60%, apontando para a necessidade de uma solução mais eficaz. Isso só é possível obtendo uma compreensão completa da biologia do IAV no nível fundamental, o que poderia informar o desenvolvimento de novas terapêuticas antivirais.

O IAV é um vírus de RNA de cadeia simples de sentido negativo com um genoma segmentado de oito partes na forma de ribonucleoproteínas virais (vRNPs). Cada vRNP consiste em RNA viral encapsidado por nucleoproteína (NP) (vRNA, que codifica proteínas virais específicas) com polimerase viral (consistindo em PB2, PB1 e PA) em suas extremidades 5' e 3' de pares de bases. A montagem do genoma viral ainda é um processo que carece de compreensão molecular e caracterização geográfica. É conhecido por ser um processo seletivo, pelo qual oito, e não mais que oito, diferentes vRNPs formam um complexo que é empacotado na montagem de vírions na membrana plasmática. Esta tese investiga onde ocorre a montagem do genoma do IAV e se esses compartimentos possuem propriedades específicas que podem ser alvo. Após a infecção, os vRNPs são liberados no citosol e importados para o núcleo para transcrição e replicação. No entanto, como a montagem viral ocorre na membrana plasmática, os vRNPs recém-sintetizados são exportados do núcleo para o citosol, onde interagem com Rab11 para formar inclusões virais. Devido ao aumento da colocalização de diferentes vRNPs nas inclusões com o tempo de infecção, esses locais foram propostos como os pontos críticos da montagem do genoma do IAV.

Tendo fornecido o estado da arte no Capítulo 1, exploramos, no Capítulo 2, o surgimento de inclusões de IAV e consideramos duas hipóteses: que as interações entre segmentos vRNA-vRNA dão origem a inclusões de IAV, o que sugeriria que sub-feixes ou feixes de vRNPs no processo de montagem do genoma, estavam contidos nesses sítios ou que tais interações são precedidas pela emergência de inclusão, sugerindo que as inclusões do IAV são sítios especializados para a montagem do genoma. Usando um sistema de mini-replicon que expressa apenas uma ou duas espécies de vRNA(s) ou infecção por IAV que produz todos os oito vRNAs, mostramos que um tipo de vRNA é suficiente para formar inclusões, sugerindo que a biogênese da inclusão de IAV precede as interações entre segmentos. Microscopia correlativa de luz e eletrônica (CLEM) dessas inclusões únicas do tipo vRNA; inclusão induzida por infecção por fenocópia; um aglomerado não delimitado por membrana de vesículas Rab11 ricas em vRNP, semelhante a condensados biomoleculares que foram postulados para se originarem por transição de fase. De fato, essas inclusões únicas do tipo vRNP se adaptam prontamente ao tratamento de choque e sofrem dinâmicas de fusão e fissão. Isso indica que as inclusões de IAV são condensados líquidos.

Uma das maneiras de alterar a função fisiológica dos condensados biomoleculares é alterando suas propriedades biofísicas. Essa estratégia poderia, para os vírus, dar origem a terapias antivirais alternativas. No Capítulo 3, portanto, perguntamos se é possível endurecer as inclusões de IAV e como. Para isso, alteramos parâmetros estabelecidos (como temperatura, concentração molecular e tipo/força de interações) conhecidos por regular as propriedades biofísicas de condensados biomoleculares como proxy de diferentes processos biológicos regulando entalpia, concentração ou modulando as ligações entre componentes interativos, como como modificações pós-traducionais. Para temperatura, usamos 4ºC, 37ºC e 42ºC; para concentração, variamos a concentração de drivers caracterizados de formação de inclusão de IAV (vRNP e Rab11) e para número/força de

interações, usamos nucleozina (uma conhecida droga antiviral que oligomeriza NP livre ou NP em vRNPs). Nossos dados mostraram que o endurecimento da inclusão é melhor alcançado aumentando o número/força das interações ao longo da alteração da concentração e temperatura. De fato, usando diferentes análises biofísicas, como ensaio de engrossamento, fotobranqueamento por pulso, perda de fluorescência após fotoativação e rastreamento de partícula única, mostramos que, em contraste com as inclusões líquidas de IAV, as inclusões endurecidas apresentavam rigidez, falta de dinâmica e perda de mobilidade.

Tendo entendido que o IAV leva à formação de condensados insolúveis na célula para organizar as reações virais, no Capítulo 4, procuramos entender como a infecção pelo IAV em geral mudou a paisagem do material solúvel na célula. Para isso, analisamos o perfil de proteoma de solubilidade (SPP) durante um período de infecção por IAV para identificar moléculas celulares e virais que se dividem em condensados e para identificar condensados crípticos induzidos pela infecção. Nossa análise revelou alterações na abundância de 174 proteínas celulares e 10 proteínas virais e na solubilidade de 413 proteínas (dentro das 6.629 proteínas detectadas ocorrendo durante a infecção). Transições de fase na célula correlacionadas com mitocôndrias, tradução, proteínas de junção célula-substrato e processos LLPS estabelecidos (formação de grânulos de estresse, função de nucléolo, splicing). Nosso ensaio mostrou que os constituintes do vRNP (NP, PB1, PB2 e PA) tornam-se mais insolúveis com o tempo, assim como as inclusões aumentam, de acordo com o Capítulo 2 desta tese. Para validar a triagem, repetimos o ensaio SPP em células Rab11a-DN infectadas que não formam inclusões e fazem vRNPs distribuídos uniformemente no citosol. Usando este sistema, descobrimos que os componentes vRNP (NP, PB1, PB2 e PA) são solúveis, indicando a necessidade de uma Rab11a funcional para formar inclusões e validando seu perfil insolúvel.

Nós, então, usamos o SPP para avaliar o impacto da nucleozina no cenário de solubilidade celular e descobrimos que a nucleozina não levou a alterações adicionais na solubilidade dos componentes celulares, além dos vRNPs. Crucialmente, este trabalho abre novos caminhos para explorar como as alterações nas propriedades do material celular e viral regulam a função celular e contribuem para a infecção viral. No Capítulo 5, discutimos os resultados e fornecemos ressalvas e perspectivas futuras deste estudo.

Chapter 1 - Introduction

1.1 Influenza A virus

1.1.1 Describing the Flu and its causative agent

Infectious agents pre-date humanity and have remained a major health, veterinary, social and economic concern despite the advancement in medicine and science (reviewed in (Pappas et al., 2008)). Like many other infection-related symptoms, early reports of flu-like symptoms date back to Hippocrates in ancient Greece around 5-4 B.C. (reviewed in (Pappas et al., 2008)). Despite ancient historians having attributed the disease outbreak to the influenza (reviewed in (Morens and Taubenberger, 2011)), the name originated from Italy in 1743 as 'influenza de cattaro' (epidemic of death) (Gosling, 2003). This became widespread at a period when flu outbreaks were thought to emanate from the 'influence' of astral alignment (reviewed in (Morens and Taubenberger, 2011)).

Two types of influenza viruses, influenza A (IAV) and B (IBV) virus, are the causal agents of the flu, a seasonal and highly contagious respiratory infection with variable disease severity ranging from mild illness to lethality (WHO, 2018). For the first time, in 1931, Shope isolated IAV from pigs (Shope, 1931), which was later identified as one of the aetiological agents of influenza in humans (Smith et al., 1933). Despite scientific advancement, IAV keeps perpetuating globally via aerosols, droplets and fomites (Asadi et al., 2020; Mubareka et al., 2009; Petrova and Russell, 2018; Smieszek et al., 2019), provoking yearly epidemics of about 3 to 5 million infections and 290,000 to 650,000 deaths (Iuliano et al., 2018; WHO, 2018).

Of note, IAV, but not IBV (Caini et al., 2019; CDC, 2021), also originates sporadic pandemics accompanied by devastating public health emergencies and socio-economic burdens of significant proportions relative to seasonal epidemics ((Iuliano et al., 2018) reviewed in (Krammer et al., 2018; Mettelman and Thomas, 2021; Morens and Taubenberger, 2011;

Neumann et al., 2009; Taubenberger and Kash, 2010; Taubenberger and Morens, 2006; WHO, 2018)). So far, the 1918 Spanish flu is historically the most fatal flu pandemic (reviewed in (Morens and Taubenberger, 2011; Saunders-Hastings and Krewski, 2016; Taubenberger and Morens, 2006)), as it infected up to 500 million people, resulting in about 20 to 50 million global deaths, while the recent 2009 swine flu pandemic caused a fatality of about 290,000 to 650,000 ((Iuliano et al., 2018) reviewed in (Hurt et al., 2012; WHO, 2018)).

Antivirals and vaccines are respectively critical for combating and preventing flu outbreaks, especially in susceptible groups such as the elderly and immunosuppressed. For flu epidemics, the use of antivirals is regulated as circulating strains may develop resistance against approved antivirals, making vaccination the most widespread and efficient weapon against flu (reviewed in (Hurt et al., 2012; Hussain et al., 2017)). IAV vaccines however, require frequent updates to respond to viral evolution, that are informed by tight epidemiological surveillance on circulating strains and on how vaccine administration protects viral infection (reviewed in (Krammer, 2019; Krammer et al., 2018; Mettelman and Thomas, 2021)). During IAV pandemics, novel strains emerge necessitating a rapid response. Here, vaccine development is further compounded by the necessity of its tailoring to the new circulating strain and their manufacture time, leaving antivirals as the first line of treatment and mitigation of symptoms.

These challenges therefore demand a better understanding of IAV infection biology as a means to explore alternative strategies for treatment and/or prevention.

1.1.2 Taxonomy

Influenza virus originates from the Orthomyxoviridae family (ICTV, 2017) and was recently classified into 7 genera (and 9 species) by the

International Committee on Taxonomy of Viruses (ICTV) (Adams et al., 2017; ICTV, 2017). This includes Alphainfluenzavirus (Influenza A virus, IAV), Betainfluenzavirus (Influenza B virus, IBV), Gammainfluenzavirus (Influenza C virus, .ICV), Deltainfluenzavirus (Influenza D virus, IDV), Isavirus (Salmon isavirus), Quaranjavirus (Johnston Atoll quaranjavirus, Quaranfil quaranjavirus) and Thogotovirus (Dhori thogotovirus and Thogoto thogotovirus) (Adams et al., 2017; ICTV, 2017).

The IAV has an extensive and diverse host range including reservoir animals (aquatic, migratory birds (Ren et al., 2016)) with spillover outbreaks and in some cases, establishment in animals such as pig, horses, seals, dogs, and cats (reviewed in (Joseph et al., 2017a; Kuiken et al., 2006; Webster et al., 1992; Wille and Holmes, 2020)). These spillover events require adaptation to a new host, which IAV can accommodate due to its inherent high rate of mutation and segmented genome that enables genomic mixing and fast adaptation to new environments ((Nobusawa and Sato, 2006) and reviewed in (Webster et al., 1992; Wille and Holmes, 2020; Yoon et al., 2014; Zambon, 1999)). However, IBV exclusively infects humans and seals, presenting a decreased mutation rate relative to IAV ((Nobusawa and Sato, 2006) and reviewed in (Hurt et al., 2012; Wille and Holmes, 2020; Yoon et al., 2014)). Co-circulating IAV and IBV cause seasonal epidemics (Iuliano et al., 2018) resulting in severe morbidity and mortality in humans, whereas pandemic events are associated only with IAV (reviewed in (Taubenberger and Morens, 2008)).

Humans are the primary hosts of ICV, displaying mild respiratory diseases (in contrast to IAV and IBV), which result in children hospitalization due to upper respiratory tract infections in < 6-year olds and lower respiratory tract infections in < 2-year olds ((Calvo et al., 2013; Fritsch et al., 2019; Kauppila et al., 2014; Matsuzaki et al., 2006; Shimizu et al., 2015) and reviewed in (Sederdahl and Williams, 2020). However, ICV has also been

detected in animals such as pig, dog, cow, with a rare swine-human transmission being reported ((Guo et al., 1983; Kimura et al., 1997; Manuguerra and Hannoun, 1992; Yamaoka et al., 1991; Zhang et al., 2018) and reviewed in (Sederdahl and Williams, 2020)).

Although, ICV was isolated more than 70 years ago (Taylor, 1949), IDV was only recently isolated and characterised in pig (Hause et al., 2013) and cattle (Collin et al., 2015). In the laboratory environment, IDV is capable of infecting guinea pigs (Sreenivasan et al., 2015) and ferrets, thus displaying broader tropism relative to ICV (Hause et al., 2013). For instance, serological test, PCR and sequencing analysis demonstrated that goats, buffalos, and humans can be positive for IDV (Zhai et al., 2017). IDV does not circulate in humans, and most human infections result from occupational exposure, especially in cattle exposed workers shown to express high of levels of neutralizing antibody ((White et al., 2016) and reviewed in (Asha and Kumar, 2019; Liu et al., 2020)). Phylogenetic analysis of IDV shows a 50% homology to ICV (Collin et al., 2015; Hause et al., 2013), with both genera being antigenically stable and not presenting high risk to humans (reviewed in (Su et al., 2017)).

Overall, IAV underlies most of the serious human influenza outbreaks. In fact, for the past 100 years, pandemic events including the 1918-1920 H1N1 Spanish flu, 1957-1958 H2N2 Asian flu, 1968-1970 H3N2 Hong Kong, 1977-1979 H1N1 Russian, and more recent 2009-2010 pH1N1/09 swine flu were caused by IAV infection with considerable mortality (reviewed in (Harrington et al., 2021; Saunders-Hastings and Krewski, 2016)). Since 2009, the pH1N1 displaced the previous H1N1 strain and is currently co-circulating with H3N2 in the global populace as one of the main aetiological factors of seasonal influenza outbreaks ((WHO, 2018) and reviewed in (Saunders-Hastings and Krewski, 2016)), jointly with IBV.

Essentially, the IAV is the only genus that poses a significant zoonotic threat to human health and therefore is the focus of this work.

1.1.3 Ecology

IAV spreads amongst many diverse species which is partly due to the migratory nature of its primary reservoirs, the aquatic wild birds ((Austin and Hinshaw, 1984; Hinshaw et al., 1980) reviewed in (Joseph et al., 2017a; Markwell and Shortridge, 1982; Webster et al., 1992)). Along the migratory flyways, viruses are shed via faeces in fresh water shared with other birds, which then acquire the new viral strain resulting in the diversified pool of viruses in birds ((Deibel et al., 1985; Hinshaw et al., 1980) reviewed in (Joseph et al., 2017a; Webster et al., 1992)).

IAVs are usually non-pathogenic in reservoir birds or at least clinically asymptomatic ((Markwell and Shortridge, 1982) reviewed in (Joseph et al., 2017a; Webster et al., 1992)). However, cross-species transmission of pathogenic strains take place either to poultry or humans directly or via intermediates such as pig (as reviewed in (Frymus et al., 2021; Parrish et al., 2015; Taubenberger and Kash, 2010; Webster et al., 1992; Wille and Holmes, 2020, 2020; Yoon et al., 2014)). Besides wild and domestic birds (Burnet and Bull, 1943; Deibel et al., 1985; Lebarbenchon et al., 2013; Wan et al., 2021), pigs (Shope, 1931) and humans (Kawaoka et al., 1989), IAV has been isolated from many other animals including bats (Kandeil et al., 2019; Tong et al., 2013, 2012), horses (Sovinova et al., 1958; Toh et al., 2019), dogs (Ou et al., 2022), felines (Hatta et al., 2018), and marine animals (Goldstein et al., 2013) (Figure 1.1).

IAV and IBV express two protruding surface glycoproteins, haemagglutinin (HA) (Wilson et al., 1981) and neuraminidase (NA) (Colman et al., 1983), contrasting with one haemagglutinin-esterase fusion (HEF) (Rosenthal et al., 1998) glycoprotein encompassing both HA and NA activities

on the surface of ICV and IDV (reviewed in (Liu et al., 2020)). ICV HEF is distinct to IDV HEF that expresses an open receptor-binding cavity able to accommodate diverse extended glycan moieties, thereby, underlying its broader tropism. Unlike most IAV serotypes that require HA binding to sialic acid receptor for cell entry (Weis et al., 1988), the bat IAV strains exceptionally utilise MHC class II HLA-DR receptor as they lack receptor binding pockets ((Giotis et al., 2019; Karakus et al., 2019; X. Sun et al., 2013) and reviewed in (Yang et al., 2021)).

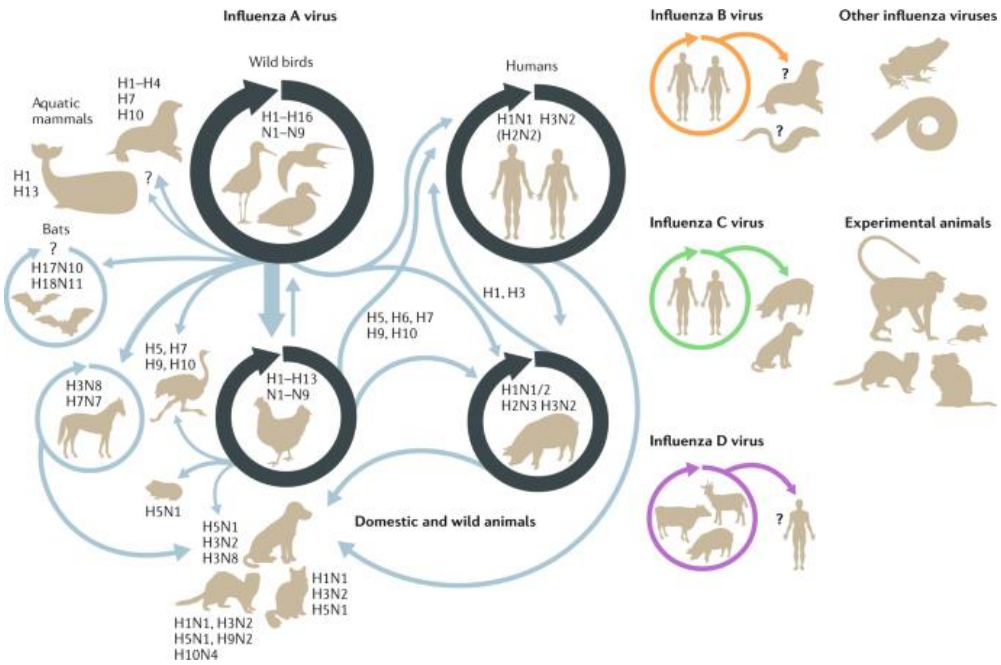

Figure 1.1- Diversity and ecology of influenza viruses.

Influenza A virus spreads amongst a plethora of hosts ranging from animals to humans. IAV has its natural ecology in wild birds or bats, however, spillovers result in its transmission to a diversity of species including humans. This image was published in (Long et al., 2019)).

Based on the antigenic properties of HA and NA that are expressed on the virion surface, avian influenza virus (AIV) is subtyped into sixteen HA

(H1 – 16) and nine NA (N1 – 9) (reviewed in (Wang et al., 2021)). Recently, two additional serotypes were isolated in bats- H17N10 and H18N11, but little is known regarding their ecological and epidemiological impacts ((Kandeil et al., 2019; Tong et al., 2013, 2012; Zhou et al., 2013) and reviewed in (Ciminski and Schwemmle, 2021)). Altogether, there are eighteen HA and eleven NA IAV serotypes.

Of all possible IAV subtypes, only two originating from birds or pandemic reassortants remain endemic in humans: 2009 H1N1, and 1968 H3N2 (reviewed in (Ito et al., 1998; Taubenberger and Kash, 2010; Wille and Holmes, 2020)). H1N1 and H3N2 are therefore included in the recommended trivalent or quadrivalent vaccines together with the conserved strain(s) of IBV (Yamagata and/ or Victoria) ((Caini et al., 2019; World Health Organization, 2022) reviewed in (Hutchinson and Yamauchi, 2018; Wille and Holmes, 2020)). The 2022 vaccines are therefore engineered against the following circulating strains; A/H1N1pdm09 and A/H3N2 as well as B/Victoria lineage (reviewed in (World Health Organization, 2022)).

Despite causing no disease in their natural reservoir ((Markwell and Shortridge, 1982) reviewed in (Joseph et al., 2017a; Webster et al., 1992)), in other birds, AIV infection may provoke disease and is divided into low pathogenicity avian influenza (LPAI) or high pathogenicity avian influenza (HPAI) (reviewed in (CDC, 2022)). Infection by LPAI presents mild or no symptom in birds, while HPAI caused by either H5N1, H5N6, H7N9 or H10N8 is highly contagious in birds and associated with high mortality ((Bi et al., 2019; CDC, 2022; Chang et al., 2020; Chen et al., 2006, 2015; WHO, 2018; Zhou et al., 2013) reviewed in (Bonilla-Aldana et al., 2020; Joseph et al., 2017b)). This difference in lethality is delineated by multifactorial traits such as virus genetics and host immune susceptibility and tropism (reviewed in (Schrauwen et al., 2014)).

The most well described factor of AIV lethality is based on viral HA protein. In LPAI, HA contain monobasic proteolytic sites (e.g. PQRET**R/**G) (Chen et al., 1998; Kawaoka and Webster, 1988) that are cleaved by proteases such as trypsin (Kawaoka and Webster, 1988; Klenk et al., 1975; Lazarowitz and Choppin, 1975), transmembrane protease serine (TMPRSS2 & 4 (Bertram et al., 2012; Böttcher et al., 2006; Chaipan et al., 2009)), human airway trypsin-like protease (HAT) (Böttcher et al., 2006) also called TMPRSS11D, blood clotting factor Xa (Gotoh et al., 1990), plasmin (Lazarowitz and Choppin, 1975), tryptase Clara (Kido et al., 1992), miniplasmin (Murakami et al., 2001), or tryptase TC30 (Sato et al., 2003). These proteases are only expressed in cells of the respiratory airway and gastrointestinal tract, thereby, limiting LPAI tropism. As a result, the disease outcome is mild and localised. On the other hand, HPAI HA are characterised by polybasic cleavage sites (e.g. PQRE**RRRKR**/G) (Stieneke-Gröber et al., 1992) proteolyzed by subtilisin-like endoproteases such as furin and proprotein convertases 5/6 (PC5/6) (Feldmann et al., 2000; Horimoto et al., 1994), which are ubiquitously expressed in all cells, thereby, causing systemic infection and death (90-100 % in chicken in about 48 hours) ((CDC, 2022) and reviewed in (Bertram et al., 2010; Böttcher-Friebertshäuser et al., 2013)).

These different viruses can spillover to humans and cause different types of diseases, with HPAI provoking more severe forms of the infection and systemic disease. Subtypes known to infect humans include H5N1, H5N6, H6N1, H7N2, H7N3, H7N7, H7N9, H9N2, H10N7 and H10N8 (reviewed in (Wang et al., 2021)). These infections are sporadic because of contact with infected animals or infected parts of animals. For zoonotic IAVs to cross the inter-species boundaries and establish in other species, including humans, specific adaptation processes must occur (reviewed in (Wang et al., 2021; Yoon et al., 2014)). For instance, IAVs replicate in the intestinal tract of aquatic birds with an average body temperature of 42ºC. Here, the viral

protein HA is known to preferentially recognise α-2,3-linked sialic acid receptors that have linear presentation with the PB2 viral protein containing glutamic acid at the position 627 ((Mehle and Doudna, 2008; Ng et al., 2012; Webster et al., 1978) and reviewed in (Jonges et al., 2014; Mänz et al., 2013; Wille and Holmes, 2020; Yoon et al., 2014). This is not the case in humans where endemic IAV have adapted to replicating in the upper respiratory tract at 35 - 37 °C, with HA preferring a 'bent' α-2,6-linked sialic acid receptors and a lysine occupying the 627 position of PB2 ((Mehle and Doudna, 2008; Ng et al., 2012; Webster et al., 1978) reviewed in (Mänz et al., 2013; Taubenberger and Kash, 2010; Wille and Holmes, 2020)).

1.1.4 IAV structure

The IAV is an enveloped, negative-sense, single stranded, segmented RNA (-ssRNA) virus. IAV viral particle (virion) is about 80 -120 nm in diameter, displaying pleiomorphic forms, with the smallest virions adopting elliptical shape and others adopting a bacilliform shape with more than 200nm bulbous head known as the Archetti body, while the filamentous virions can be up to 20 µm in length and 100nm in diameter (Figure 1.2) (Archetti, 1955; Calder et al., 2010; Dadonaite et al., 2016; Harris et al., 2006; Mosley and Wyckoff, 1946; Nakatsu et al., 2016; Noda, 2012; Seladi-Schulman et al., 2013; Sugita et al., 2011; Vijayakrishnan et al., 2013). Regardless of shape and size, IAVs are compositionally identical, as all are made of a viral envelope enclosing an octameric segmented genome. The viral envelope is composed of lipid membrane and proteins originating from the host cells they infected (Hutchinson et al., 2014; Shaw et al., 2008).

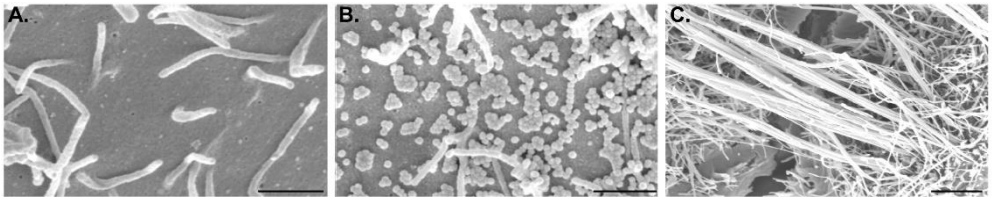

Figure 1.2- Structural pleiomorphism of IAV.

*IAV adopts different morphologies budding from apical surface of A549 lung epithelial cells that are **(A)** uninfected (as control); **(B)** infected with influenza A/Puerto Rico/8/34 (PR8), where virions bud as spheres; and **(C)** infected with a reassortant PR8 virus containing segment 7 from A/Udorn/301/72 that bud as filaments. Scale bar is 1μm. This image was published in (Amorim, 2019).*

Embedded in the outer surface of the viral envelope are 3 viral transmembrane proteins: trimeric HA, and tetrameric NA, with a homotetrameric proton-selective matrix protein 2 (M2) integrating through the membrane (**Figure 1.3**A) (Calder et al., 2010; Chlanda et al., 2015; Copeland et al., 1986; Gaymard et al., 2016; Harris et al., 2006; Wasilewski et al., 2012). HA is more abundant than NA in a ratio of 1:4 or 1:5 (also reported to be non-stoichiometric), which is more than M2 (Hutchinson et al., 2014). HA mediates entry of the encapsidated IAV genome by binding virions to host cells via sialylated receptors (Weis et al., 1988). NA cleaves highly enriched sialic acid decoys from airway secreted mucus to facilitate host cell attachment. NA also promotes progeny virion egress by cleaving sialic acids on the surface of infected cells and nascent virions (Cohen et al., 2013; Sakai et al., 2017).

Beneath the envelope is the viral capsid containing matrix protein 1 (M1) (Roberts et al., 1998) that encapsulates a central core of segmented genome (in a 1 + 7 configuration) (Nakatsu et al., 2016; Noda et al., 2018, 2006; Noda and Kawaoka, 2010) and its associated proteins including nuclear export protein (NEP; previously identified as non-structural protein 2,

NS2) (**Figure 1.3**A) (Hutchinson et al., 2014; Inglis et al., 1976; Richardson & Akkina,1991; Yasuda et al., 1993). Previously thought to be non-structural, a recent proteomic screen identified non-structural protein 1 (NS1) in purified IAV virions (Hutchinson et al., 2014). Although, its topological configuration in the virions is yet to be established, it was demonstrated that virion-associated NS1 does not form a complex with viral ribonucleoproteins (vRNPs) but is protected from proteases, suggesting that NS1 resides within the M1 capsid (Hutchinson et al., 2014).

The IAV genome is an eight-partite supramolecular complex of rod-shaped vRNPs (**Figure 1.3**A) (Pons et al., 1969), which range in diameter 10 – 15 nm and in length 30 – 120 nm (Compans et al., 1972; Noda et al., 2006). Each vRNP is made up of a unit of heterotrimetric RNA-dependent RNA polymerase complex (RdRp), multiple units of nucleoprotein, and a viral RNA (vRNA) copy that is distinct in nucleotide (nt) length (890 - 2341) (**Figure 1.3**A) and the viral protein(s) it encodes (**Figure 1.3**B, **Table 1.1**) ((Honda et al., 1990; Horisberger, 1980; Reich et al., 2014; Yuan et al., 2009) and reviewed in (Amorim, 2019)). Generally, the viral genome encodes 10 essential polypeptides. However, up to 22 proteins may be expressed in cells, depending on the viral strain and cell type (**Figure 1.3**B, **Table 1.1**) (reviewed in (Pinto et al., 2021)). Structurally, the vRNAs are similar, characterised by a large central negative-sense coding region flanked by shorter (19 - 58 nucleotides, nt) non-coding regions (NCRs, also known as untranslated region, UTR) at both 5’ and 3’ genomic ends (reviewed in (Ferhadian et al., 2018)).

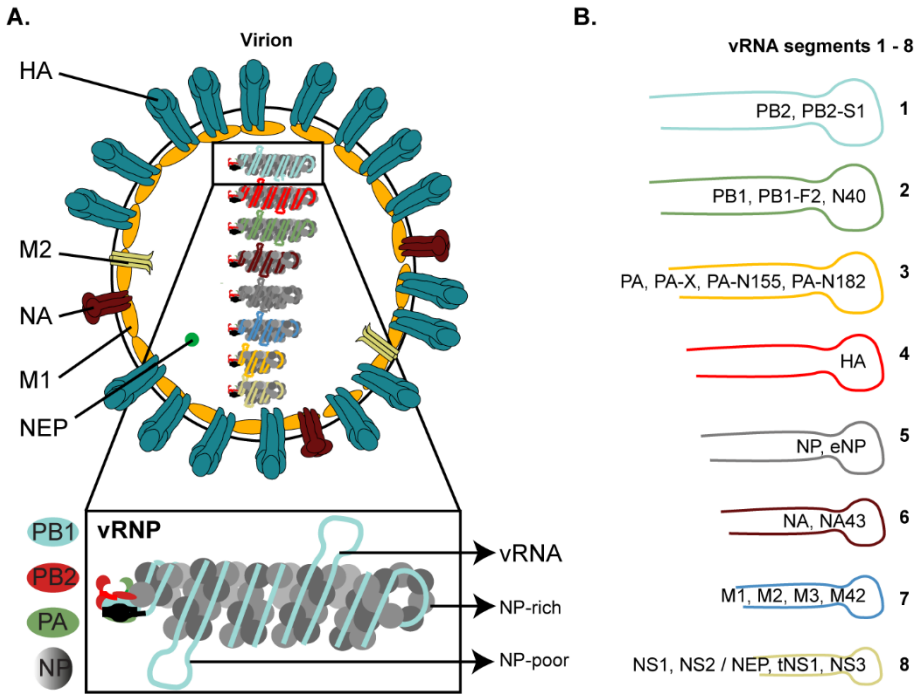

Figure 1.3- Graphical depiction of the IAV virion and genome structure.

(A) *Illustration of influenza A virion and vRNP structure (highlighted)* ***(B)*** *IAV genomic RNA segments showing the proteins they codify. The essential proteins are PB2 – Polymerase basic protein 2; PB1 – Polymerase basic protein 1; PA – Polymerase acidic protein; HA – Hemagglutinin; NP – Nucleoprotein; NA – Neuraminidase; M1/M2 – Matrix protein 1/ 2; NS1/2(NEP) – Non-structural protein 1/2(Nuclear export protein) ; vRNA – Viral RNA; vRNP – Viral ribonucleoprotein. Their functions are listed in* ***Table 1.1****.* ***Figure 1.3****A was a kind gift from Maria João Amorim and published in (Amorim, 2019).*

The NCRs consist of a highly conserved promoter (motif) sequence (12 and 13 nucleotides at the 3' and 5' termini respectively) among viral strains and the 8 segments themselves, and a non-conserved segment-specific regions of about 5-45 nucleotides (Fujii et al., 2003; Gog et al., 2007; Goto et al., 2013; Hutchinson et al., 2010, 2008; Liang et al., 2005, 2008;

Marsh et al., 2007; Muramoto et al., 2006; Tomescu et al., 2014; Watanabe et al., 2003) and reviewed in (Eisfeld et al., 2015; Ferhadian et al., 2018; Isel et al., 2016)). The conserved NCR of 5' and 3' termini alongside two adjacent nucleotides present partially complementary and base-pair to form an approximately 15-base pair-long panhandle (Detjen et al., 1987), where the RdRp assembles (Murti et al., 1988). The RdRp is composed of polymerase basic 1 (PB1), polymerase basic 2 (PB2) and polymerase acidic (PA) (Detjen et al., 1987; Murti et al., 1988; Tomescu et al., 2014). This results in a double-helical antiparallel vRNA hairpin that folds back on itself, opposite the base-pairing and RdRp-bound genomic ends (Hsu et al., 1987; Pons et al., 1969).

Table 1.1- IAV segments and respective encoded polypeptides.

Seg	Polypeptide	Function	Ref
1	PB2	Component of RNA transcriptase - 7m GpppNm recognition	(Biswas et al., 1998; Guilligay et al., 2008; Hagen et al., 1994; Reich et al., 2014)
	PB2-S1	Mitochondrial, inhibits RIG-I/MAVS	(Yamayoshi et al., 2015)
2	PB1	Component of RNA transcriptase - catalyzes nucleotide addition, inhibits innate immune response	(Biswas et al., 1998; Biswas and Nayak, 1994; Hagen et al., 1994; He et al., 2008; Reich et al., 2014; Zeng et al., 2021)
	PB1-F2	Mitochondrial, apoptosis induction, interferon response, and virulence factor	(Chen et al., 2001; McAuley et al., 2007; Mettier et al., 2021; Tauber et al., 2012; Wise et al., 2011; Zamarin et al., 2005)
	PB1-N40	Unclear - suggested role in replication and viral pathogenesis	(Tauber et al., 2012; Q. Wang et al.,

			2019; Wise et al., 2009, 2011)
3	PA	Component of RNA transcriptase - endonuclease, involved in cap snatching	(Dias et al., 2009; Hagen et al., 1994; Li et al., 1998; Plotch et al., 1981; Reich et al., 2014; Yuan et al., 2009)
	PA-X	Non-specific mRNA endonuclease, involved in host shut-off	(Bavagnoli et al., 2015; Firth et al., 2012; Jagger et al., 2012; Rigby et al., 2019)
	PA-N155	Unclear - suggested role in replication	(Muramoto et al., 2013; Q. Wang et al., 2018)
	PA-N182	Unclear - suggested role in replication	(Muramoto et al., 2013; Q. Wang et al., 2018)
4	HA	Sialic acid binding, fusion activity, and antigenic determinant	((Bullough et al., 1994; Chen et al., 1998; Kawaoka and Webster, 1988; Mehle and Doudna, 2008; Stieneke-Gröber et al., 1992; Webster et al., 1978; Wilson et al., 1981) reviewed in (Wiley and Skehel, 1987))
5	NP	vRNP formation, nuclear import and export and transcription, processivity factor of the polymerase, inhibit PKR activation, promotes viral RNA synthesis and viral replication	(Chutiwitoonchai and Aida, 2016; Digard et al., 1999; Elton et al., 2001, 1999; Gabriel et al., 2008; Hagen et al., 1994; Honda et al., 1988; Lin et al., 2017; Melen et al., 2003; Moisy et al.,

			2012; Momose et al., 2001; O'Neill et al., 1995; O'Neill and Palese, 1995; Pons et al., 1969, 1969; Ruigrok and Baudin, 1995; Sharma et al., 2011; Wang et al., 1997)
	eNP	Unclear - suggested role in gene expression	(Wanitchang et al., 2011)
6	NA	Sialidase activity, budding, cell exit and antigenic determinant	(Cohen et al., 2013; Colman et al., 1983; Sakai et al., 2017)
	NA43	Unclear	(Machkovech et al., 2019)
7	M1	Capsid uncoating, vRNP nuclear export, virus assembly and major virion protein, controls viral morphology	(Banerjee et al., 2014; Baudin et al., 2001; Calder et al., 2010; Elleman and Barclay, 2004; Li et al., 2014; K. Martin and Helenius, 1991; Ye et al., 1999; Zvonarjev and Ghendon, 1980)
	M2	Ion channel, HA maturation and virus uncoating and budding	(Chizhmakov et al., 2003, 1996; Czabotar et al., 2004; Hu et al., 2006; Leiding et al., 2010; Mould et al., 2000; Pinto et al., 1997; Stauffer et al., 2014; Tang et al., 2002; Wang et al., 1995)
	M3	Unclear - suggested to downregulate early segment 7 expression, essential to group A *Streptococcus* virulence in IAV superinfection	(Clohisey et al., 2020; Herrera et al., 2017)
	M42	Functionally replaces M2 upon its depletion	(Wise et al., 2012)

8	NS1	Inhibits host pre-mRNA processing, maturation and antiviral IFN responses, histone mimicry	(Gack et al., 2009; Gao et al., 2012; Marazzi et al., 2012; Min and Krug, 2006; Park et al., 2018; Pichlmair et al., 2006; Rajsbaum et al., 2012; Silverman and Weiss, 2014; Talon et al., 2000; Tsai et al., 2017)
	tNS1	Cytoplasmic, inhibits IRF3 and IFN-β	(Kuo et al., 2016)
	NS2/NEP	vRNP nuclear export	(Huang et al., 2013; Neumann et al., 2000; Yasuda et al., 1993)
	NS3	Unclear - suggested role in replication	(Selman et al., 2012)

Using photoactivatable ribonucleoside enhanced cross-linking and immunoprecipitation (PAR-CLIP) and high-throughput sequencing of RNA isolated by cross-linking immunoprecipitation (HITS-CLIP), NP was shown to bind to the vRNA non-uniformly and stoichiometrically (with a periodicity of approximately 12 nt, previously 24 nt per NP molecule (Labaronne et al., 2016; Lee et al., 2017; Ortega et al., 2000; Williams et al., 2018)) with high affinity along the internal region of vRNA polymer, allowing accessibility for base-pairing and replication priming (Arranz et al., 2012; Moeller et al., 2012; Yamanaka et al., 1990). Despite the earlier work reporting a lack of sequence specificity for NP, a recent study showed NP-vRNA binding sites are guanine (G)-rich and uridine (U)-poor. Of note, vRNA is partially sensitive to RNAse V1 digestion (Arranz et al., 2012; Moeller et al., 2012; Yamanaka et al., 1990), as higher order (secondary and tertiary) double stranded structures in its internal coding region emerge with low or no NP binding (Lee et al., 2017; Williams et al., 2018). Some of these higher order structures as well as sequences of the NCR and its adjacent coding regions were identified as

packaging signals able to establish intersegment vRNP-vRNP interactions for IAV genome packaging (Gog et al., 2007; Hutchinson et al., 2010, 2008).

1.1.5 IAV Life cycle

For a successful infection, influenza A virions must contain eight genomic segments and express all the essential structural proteins (Brooke et al., 2013; Nakatsu et al., 2016; Noda et al., 2018, 2006; Noda and Kawaoka, 2010). The multistep viral life cycle begins with virion attachment to target cells, followed by cell entry and nuclear delivery of the viral genome for replication (reviewed in (Amorim, 2019; Dou et al., 2018; Eisfeld et al., 2015; Etibor et al., 2021; Hutchinson and Yamauchi, 2018; Watanabe et al., 2010)). The cycle terminates with cellular egress of progeny virions that are propagated to vicinal cells or new host(s) via aerosols and/ or droplets. Every stage of the IAV life cycle is triggered by viral induced cellular cues which may involve enzymatic reactions, chemical- or receptor-mediated signals (reviewed in (Amorim, 2019; Dou et al., 2018; Eisfeld et al., 2015; Etibor et al., 2021; Hutchinson and Yamauchi, 2018; Watanabe et al., 2010)). Despite continued advances in understanding the key processes of IAV life cycle (reviewed in (Amorim, 2019; Dou et al., 2018; Eisfeld et al., 2015; Etibor et al., 2021; Hutchinson and Yamauchi, 2018; Watanabe et al., 2010)), many unknowns are yet to be clarified, justifying the need for further investigation.

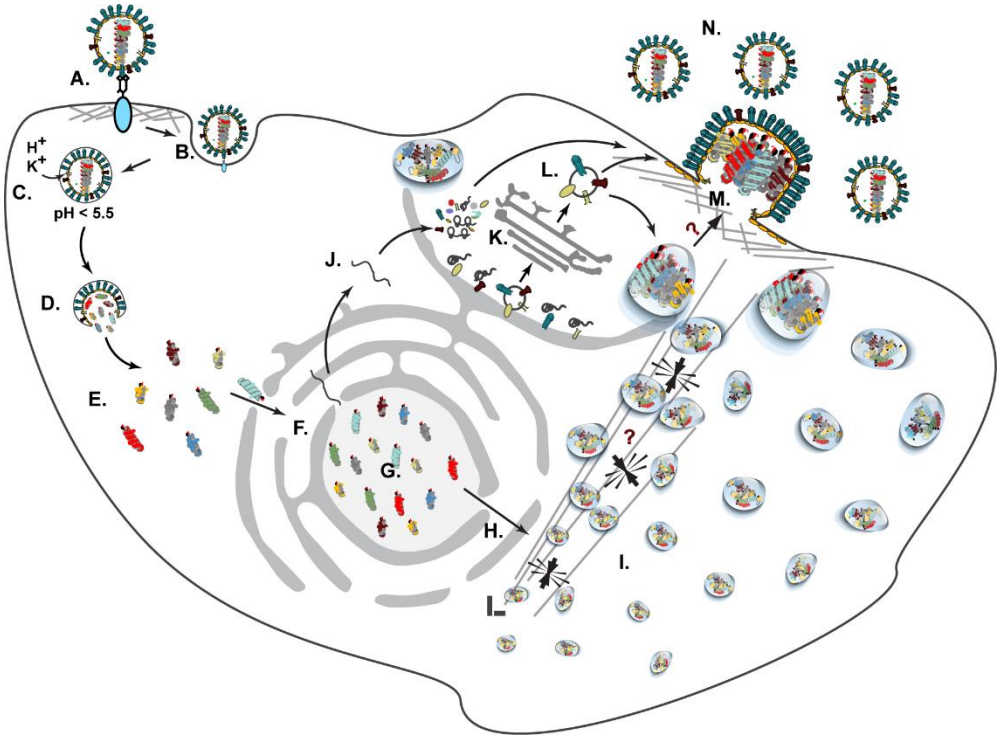

Figure 1.4- Graphical summary of the IAV life cycle.

(A) *attachment,* ***(B)*** *internalization,* ***(C)*** *acidification,* ***(D)*** *capsid uncoating,* ***(E)*** *genome debundling,* ***(F)*** *nuclear import,* ***(G)*** *genome transcription and replication,* ***(H)*** *nucleocytoplasmic shunt of vRNPs into inclusion,* ***(I)*** *genome assembly,* ***(J)*** *nuclear export of mRNAs,* ***(K)*** *viral translation and protein synthesis,* ***(K - L)*** *viral protein translocation,* ***(M)*** *virion assembly and budding at the plasma membrane, and* ***(N)*** *progeny virion release.*

1.1.5.1 Attachment, internalization and uncoating

IAV infection is initiated by the binding of HA to sialic acid receptor on the host cell surface (**Figure 1.4**A) (Ito et al., 2000; Suzuki et al., 2000; Weis et al., 1988) and reviewed in (Kuchipudi et al., 2021)), followed by virus internalization (**Figure 1.4**B). Virus internalization involves dynamin and Epsin-1 in clathrin-mediated endocytosis (Chen and Zhuang, 2008; Roy et al., 2000). Alternatively, a non-clathrin caveolin-independent endocytosis

(Rust et al., 2004; Sieczkarski and Whittaker, 2002) or an unconventional entry route such as macropinocytosis (de Vries et al., 2011) and sialic-acid independent endocytosis may be used (Kajiwara et al., 2020). Upon internalization, the low endosomal pH (< 5.5, **Figure 1.4**C) (reviewed in (Huotari and Helenius, 2011)) activates M2 ion channel (Chizhmakov et al., 2003, 1996; Czabotar et al., 2004; Holsinger and Alams, 1991; Hu et al., 2006; Leiding et al., 2010; Mould et al., 2000; Pinto et al., 1997, 1992; Tang et al., 2002; Wang et al., 1995), allowing the influx of H^+ and K+ (Stauffer et al., 2014). This weakens the capsid M1-M1 oligomeric interactions (Stauffer et al., 2014), while acidifying the virion core (Holsinger and Alams, 1991; Pinto et al., 1992; Stauffer et al., 2014) to prime HA for conformational change (**Figure 1.5**A-E) (Benhaim et al., 2020; Bullough et al., 1994).

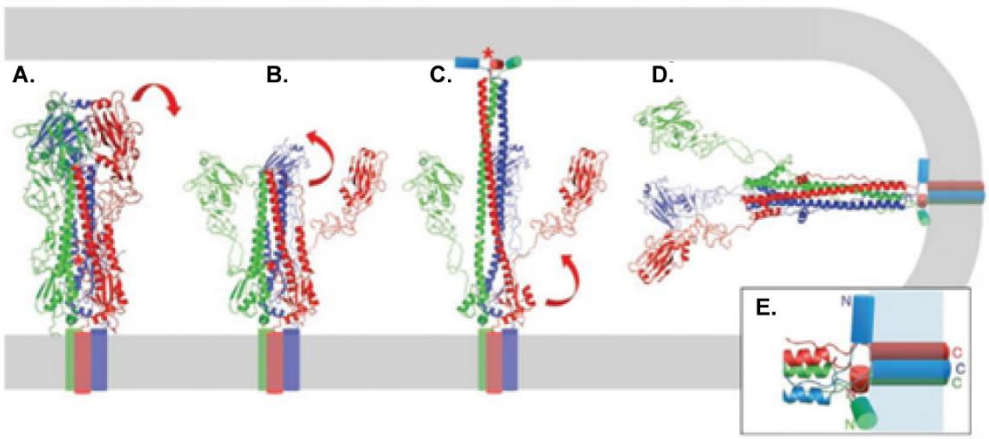

Figure 1.5- Proposed mechanism of fusogenic conformational changes in IAV haemagglutinin.

(A) *The pre-fusion conformation,* ***(B)*** *HA1 dissociation from its tightly docked position in response to proton (H^+) binding,* ***(C)*** *the extended intermediate, which collapses via a helix-loop-helix transition,* ***(D, E)*** *Collapse of the extended intermediate by zipping up the trimers to generate the post-fusion conformation that causes hemifusion and pore formation. This image was published in* (Harrison, 2008).

Since HA is synthesised as a 75kDa precursor protein (HA0) that is modified (by N-glycosylation, palmitoylation) and translocated along the secretory pathway to the PM, it must first be cleaved by trypsin-like or furin-based endo-proteases (**Figure 1.6**) (as detailed above in the "Ecology" section) at specific arginine residue (R) into two subunits: HA1 (55 kDa) and HA2 (25 kDa) (**Figure 1.6**) (reviewed in (Böttcher-Friebertshäuser et al., 2013)). Cleavage is a key prerequisite for HA conformational changes at low pH in the endosome, as it triggers membrane fusion and is essential for the infectivity and spread of influenza viruses ((**Figure 1.6E,F**) reviewed in (Böttcher-Friebertshäuser et al., 2013)). The proteolyzed HA0 exposes the embedded fusion peptide on the N-terminus of HA2 for insertion into the endosomal membrane, with the C-terminal transmembrane domain anchoring HA2 in the viral membrane (**Figure 1.5**) (Benhaim et al., 2020; Bullough et al., 1994). This creates a hairpin structure as the HA2 homotrimer folds back on itself (**Figure 1.5**) (Das et al., 2018), to position the endosomal and viral membranes in proximity until fusion is completed (Maeda et al., 1981; Maeda and Ohnishi, 1980; White et al., 1982; Yoshimura and Ohnishi, 1984). These events result in the IAV genome release from the weakened capsid into the cytosol.

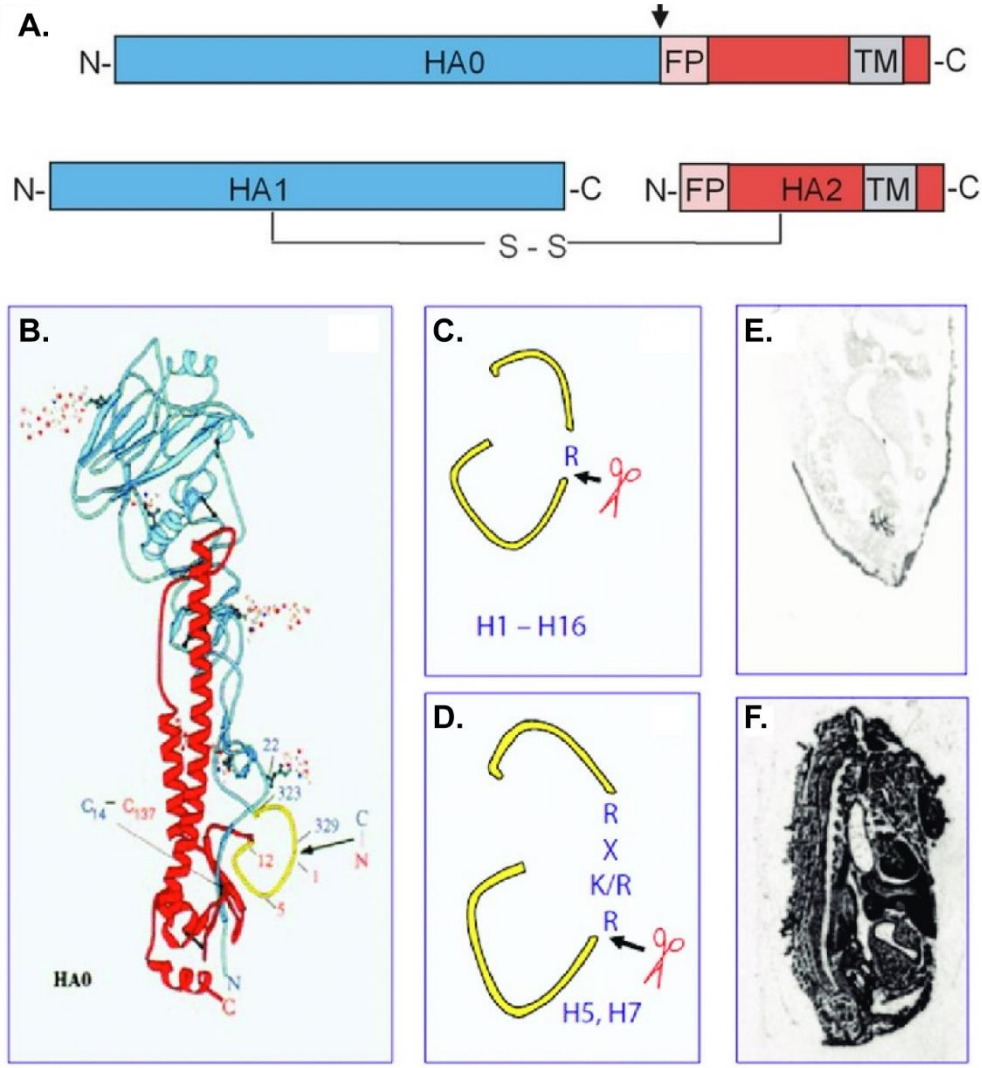

Figure 1.6- Cleavage of HA0 into HA1 and HA2 at a specific cleavage site determines pathogenicity.

(A) Scheme illustrating the HA0 precursor and its cleaved HA1 (blue) and HA2 (red) subunits. (B) Structure of the monomeric HA0 precursor of IAV (A/HongKong/68 strain) with a cleavage resistant mutation, R329Q. The cleavage site is in the prominent yellow loop (arrow). (C). LPAI virus' monobasic cleavage site (R) that is cleaved by tissue-specific trypsin-like endoproteases (D). HPAI viruses (e.g. serotypes H5 and H7) contain a

multibasic site- RX(K/R)RX, cleavable by the ubiquitously expressed furin and furin-like endoproteases (E) Spread of the LPAI virus, and of (F) HPAI virus. This image was published in (Böttcher-Friebertshäuser et al., 2013).

Next, viral capsids are disassembled (**Figure 1.4**D) for the release of IAV genome into the cytosol (**Figure 1.4**E). This is mediated by E3 ubiquitin ligase; Itch (Su et al., 2013), Speckle-type POZ protein-like/ Cullin-3 (CUL3-SPOPL) E3 ubiquitin ligase complex (Gschweitl et al., 2016; Huotari et al., 2012) and reviewed in (Huotari and Helenius, 2011)) and the aggresome processing machinery (Banerjee et al., 2014). The aggressome protein, histone deacetylase 6 (HDAC6) targets M1-associated unanchored ubiquitin for IAV capsid uncoating, with microtubule motors (dynein and dynactin) and actin motors (myosin II) generating the physical forces necessary for uncoating (Banerjee et al., 2014). Finally, Karyopherin beta (importin-β) family member transportin-1 (TNPO-1) facilitates vRNP debundling and nuclear import (**Figure 1.4**F) (Miyake et al., 2019).

1.1.5.2 Nuclear Import

Debundled cytosolic vRNPs that were released from dissociated viral capsids are transported into the nucleus for subsequent transcription and genome replication (Amorim and Digard, 2006; Herz et al., 1981; Jackson et al., 1982; López-Turiso et al., 1990; Shapiro et al., 1987). Since each vRNP is exceedingly more than 40 kDa, its transport is not physically possible by passive diffusion but largely depends on an active energy-dependent process that is mediated by the classical nuclear import pathway (Kemler et al., 1994). Nuclear translocation of vRNPs is directed by the nuclear localization signals (NLS) of NP and PB2 (Jones et al., 1986; Lin and Lai, 1983; K Martin and Helenius, 1991; Ozawa et al., 2007) that recruit the adapter protein importin-α (IMPα), which is recognised by importin-β (IMPβ) receptor for vRNP translocation through the nuclear pore complex (NPC) (K Martin and Helenius, 1991; O'Neill et al., 1995).

Alternative pathways reported include, the J domain of DnaJ Heat Shock Protein Family (Hsp40) member B1 (Hsp40/ DnaJB1) that promotes vRNPs nuclear entry via its interaction with the N-terminal domain of NP as well as IMP-α (Batra et al., 2016). Furthermore, nucleoporin 85 interacts with PB1 via Ran-binding protein 5 (RanBP5) and PB2 through importin-α 1&7 (IMP-α1 and IMP-α7) to promote vRNPs nuclear import and replication (Ling et al., 2022). Following nuclear translocation and release of vRNPs, IMPα and IMPβ are individually recycled back to the cytosol. In the nucleus, the error prone (low fidelity) viral RdRp directs transcription and replication of the viral genome (**Figure 1.4**G) (reviewed in (Fodor, 2013; Fodor and Velthuis, 2020; Wandzik et al., 2021)).

1.1.5.3 Viral transcription and replication

The IAV genome consists of negative sense vRNAs that are unable to directly translate into viral proteins. Therefore, incoming vRNPs need to be transcribed into mRNAs, and replicated into progeny vRNA and form vRNPs. Viral mRNAs are initially transcribed directly from incoming vRNPs (Etkind and Krug, 1975) in the nucleus as well as from newly synthesised vRNAs later in infection (**Figure 1.7**) (Muramoto et al., 2006; Shapiro et al., 1987). On the other hand, Replication is not a direct process but rather requires an intermediate complementary RNA (cRNA) synthesis step (**Figure 1.7**) (Etkind and Krug, 1975; Vreede and Brownlee, 2007; York et al., 2013). To make viral cRNAs and progeny vRNAs, *de novo* synthesis and nuclear import of viral proteins (NP, PB1, PB2 and PA) are required, as they form the ribonucleoprotein (cRNP and vRNP) complex with each transcript (Pflug et al., 2017; Shapiro et al., 1987). Through their NLS, NP (Cros et al., 2005; Neumann et al., 1997) and PB2 (Pumroy et al., 2015; Tarendeau et al., 2007) viral proteins are imported individually into the nucleus, while PB1 and PA are imported as heterodimers (Swale et al., 2016).

The processes that originate viral mRNA and cRNA are different, resulting in a capped and polyadenylated mRNA that lacks 15-16 nt from the 5´-teminus of the template vRNA, or a full complementary version of the vRNA encapsidated into cRNPs (**Figure 1.7**). Importantly, both viral transcription and replication processes are catalysed by the RdRp complex (**Figure 1.8**), consisting of the polymerase core (formed by PB1, C-terminal and N-terminal regions of PA and PB2 respectively), and flexible peripheral appendices (made of the endonuclease domain of PA and key PB2 domains- including the cap-binding, mid-link, 627, and NLS domains) (reviewed in (Eisfeld et al., 2015; Fodor, 2013; te Velthuis and Fodor, 2016)).

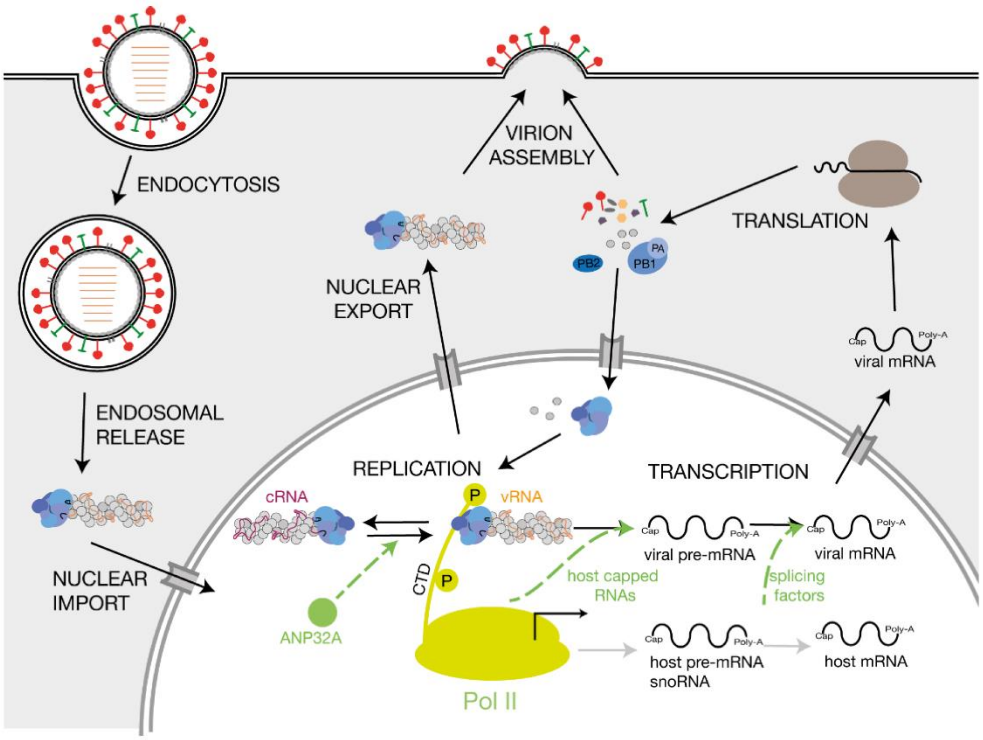

Figure 1.7- Schematics of IAV genome transcription and replication.

Key host factors that play a role in viral RNA synthesis are indicated in green. PB1 (blue), PB2 (dark blue) and PA (grey) host factors (green). This image was published in (Weis and Te Velthuis, 2021).

1.1.5.3.1 Viral transcription

Aided by the association with cellular RNA polymerase II (Pol II) C-terminal domain (Engelhardt et al., 2005; Lukarska et al., 2017; Martínez-Alonso et al., 2016), the IAV mRNA transcription is primed by a cap snatching process (**Figure 1.8**A) (Cianci et al., 1995; Fechter et al., 2003; Hagen et al., 1994; Li et al., 2001, 1998; Plotch et al., 1981; Rao et al., 2003; Reich et al., 2014; Yuan et al., 2009). Here, PB2 binds to the 5´ 7-methylguanosine (5´ 7mG) cap of selected host transcripts (Beaton and Krug, 1981; Cianci et al., 1995; Fechter et al., 2003; Rao et al., 2003; Reich et al., 2014), preferably, small nuclear RNAs (snRNAs), small nucleolar RNAs (snoRNAs) and promoter-associated capped small RNAs (generated from paused Pol II during transcription initiation) rather than (pre)-mRNA (Beaton and Krug, 1981; Gu et al., 2015; Koppstein et al., 2015; Shaw and Lamb, 1984; Sikora et al., 2014). The PB2-snatched transcripts are then cleaved 10-13 nucleotides downstream of the 5´-7mG-cap (at CA-cleavage site on the 3´-terminus (Beaton and Krug, 1981; Rao et al., 2003; Shaw and Lamb, 1984)) by PA endonuclease domain (Hagen et al., 1994; Li et al., 2001, 1998; Plotch et al., 1981; Yuan et al., 2009).

Passing through the product exit channel of the polymerase complex, the snatched capped primer is then positioned into the PB1 catalytic active centre by PB2 cap-binding domain for primer extension using the vRNA as template (**Figure 1.8**A) (Reich et al., 2014; Sugiyama et al., 2009). After transcription initiation, PB2-cap binding domain dissociates from the 5´-m7G capped primer to allow the elongation process (Reich et al., 2014). Transcription elongation, whose processivity is facilitated by NP (Honda et al., 1988), continues as the vRNA template is pulled along the catalytically active site of RdRp until a 5-7 nt poly-U sequence that is about 16 nt from the 5´-teminus of the template vRNA is encountered. In this U-stretch, polymerase stuttering occurs, resulting in the recursive incorporation of adenosine monophosphate (AMP) to produce polyadenylated (polyA) tail on

the nascent viral mRNA (Poon et al., 2000, 1999; Robertson et al., 1981). The nascent viral mRNA exits the catalytically active site of the polymerase (same as the route taken by the 5´7mG-capped primer) via the exit channel of the complex (**Figure 1.8**A). Thereafter, the 5´m7G-cap of the nascent mRNA may then bind to the host cap-binding complex for the assembly of a messenger ribonucleoprotein (mRNP) ((Bier et al., 2011) and reviewed in (te Velthuis and Fodor, 2016; York and Fodor, 2013)). Due to the limitation imposed by the size (~13.5 kb) of its genome, the IAV employs host factors to maximize its coding capacity through splicing or ribosomal frameshift, which result in the translation of its multifunctional proteins (**Table 1.1**).

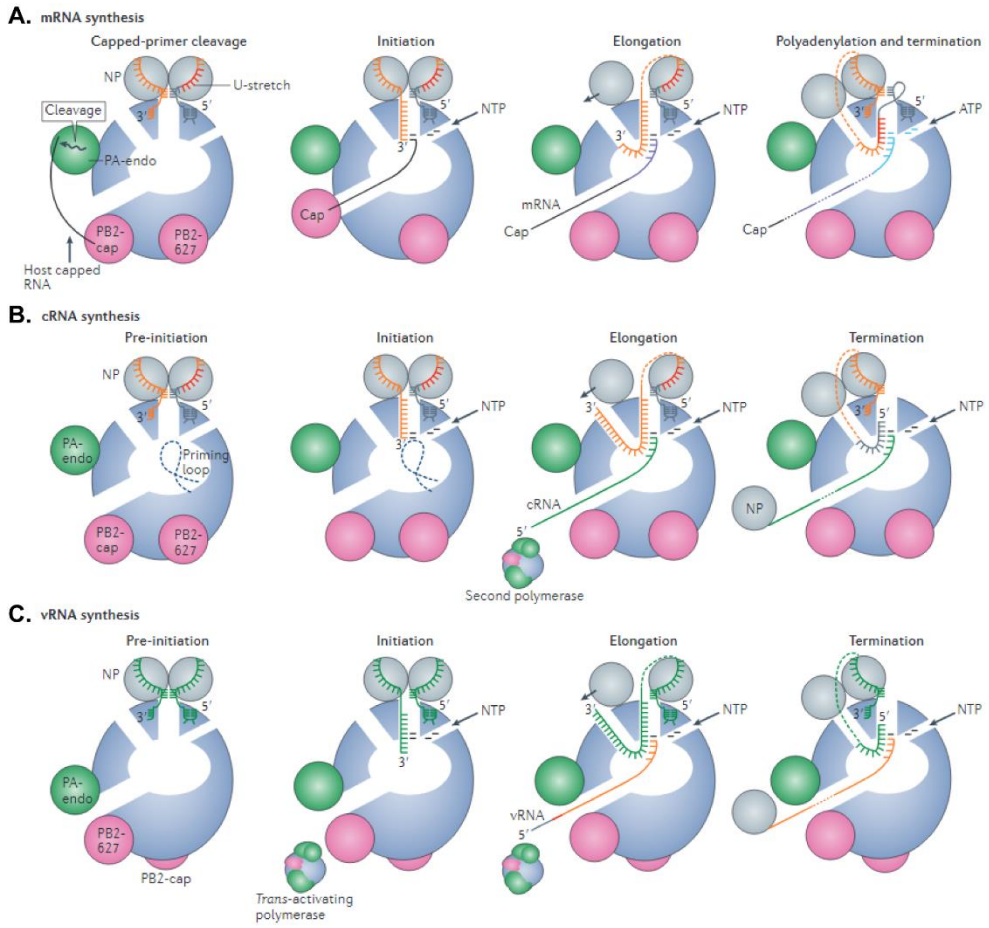

Figure 1.8- Models of IAV genome transcription and replication.

(A) Viral mRNA transcription. (B) Intermediate synthesis of complementary RNA (cRNA; green), (C) vRNA synthesis, as the second step in replication of the viral genome. This image was published in (te Velthuis and Fodor, 2016).

1.1.5.3.2 Viral replication

Unlike viral transcription, vRNA replication is a two-step process (**Figure 1.8**). In the first step, a replicative positive sense antigenome intermediate known as cRNA is formed in a primer independent manner (Etkind and Krug, 1975; Vreede and Brownlee, 2007; York et al., 2013). Next, the 3´-teminus of the template vRNA enters the catalytically active site of the polymerase for terminal initiation by pppApG dinucleotides (Beaton and Krug, 1986; Deng et al., 2006), which is supported by the priming loop (a β-hairpin structure) that must be displaced upon elongation (**Figure 1.8**B) (Reich et al., 2014; Te Velthuis et al., 2016). Although the elongation process is like that of viral mRNA, to achieve cRNA chain termination, the 5´-terminus of the vRNA must be released from the polymerase binding pocket for it to be copied. This termination process is distinct from mRNA chain termination in a yet unclear process. As the cRNA exits the product exit channel of the RdRp, a second polymerase recruits NP to form a helical cRNP complex, with the NP along the RNA and RdRp on the 5´- and 3´- termini (**Figure 1.8**B) (Chan et al., 2010; Ng et al., 2008; Turrell et al., 2013; Ye et al., 2006; York et al., 2013).

In a second step, the synthesized cRNA serves as template for vRNA synthesis via internal initiation directed by pppApG dinucleotide (Te Velthuis et al., 2016), which enables vRNA elongation along the template Crna (**Figure 1.8**C). Although, this process is independent of a full-length priming loop, different models suggest that it requires a trans-activating or trans-acting helper polymerase (Jorba et al., 2009; Tshierry et al., 2016; York et al., 2013) with catalytically inactive and active properties respectively. It is possible that the trans-activating polymerase could bind nascent vRNA exiting the catalytically active polymerase during elongation and termination

steps (**Figure 1.8**C) (reviewed in (te Velthuis and Fodor, 2016)). Together with the helper polymerase, NP will encapsidate the emerging vRNA to form vRNP (Jorba et al., 2009; Moeller et al., 2012).

1.1.5.3.3 Regulation of transcription and replication

As the IAV genome translocate into the nuclear matrix, they associate with chromatin components for transcription and replication (Chase et al., 2011; Jackson et al., 1982; López-Turiso et al., 1990; Robb et al., 2011; Takizawa et al., 2006). For instance, IAV RdRp interact with nuclear matrix proteins 2 (NXP2, also called MORC3), remodellers of chromatin (chromodomain helicase DNA binding protein1 and 2, CHD1 and CHD2), and host RNA polymerase II (Pol II) and viral RdRp modulator, chromosome 14 open reading frame 166 (C14orf166, also called CLE) (Alfonso et al., 2011; Marcos-Villar et al., 2016; Rodriguez et al., 2011; Ver et al., 2015). Also, the minichromosomal maintenance (MCM) complex interacts with the PA subunit of the RdRp to support transition from *de novo* initiation to elongation on the vRNA template (Kawaguchi and Nagata, 2007). Acidic leucine-rich nuclear phosphoprotein 32 family member A and B (ANP32A and ANP32B (also known as APRIL, PAL31, PHAP1b)) were reported as host specificity factors that interact with actively replicating viral RdRp to facilitate mammalian-adapted avian cRNA and vRNA replication (Bradel-Tretheway et al., 2011; Long et al., 2016; Nilsson-Payant, 2022; Peacock et al., 2020a, 2020b; Staller et al., 2019; Sugiyama et al., 2015; Swann et al., 2022; York et al., 2014). Other cellular factors such as DDX39B (also known as BAT1 or UAP56), TAT-SF1 (also known as HTATSF1) FMR1 reinforce NP interaction with the viral RdRp to enhance vRNA replication, while also supporting NP recruitment to nascent vRNA and cRNA for vRNP and cRNP assembly, respectively (Kawaguchi et al., 2011; Naito et al., 2007; Zhou et al., 2014).

For mRNA synthesis, the viral RdRp directly recruits the serine-5-phosphorylated form of Pol II large subunit carboxy-terminal domain (CTD)

(Engelhardt et al., 2005; Martínez-Alonso et al., 2016), providing access to nascent host capped RNAs and a high concentration of splicing factors (Vreede and Brownlee, 2007) such as RED (also known as RER or IK), SMU1, SF2 (also known as ASF1 or SRSF1), SFPQ (also known as PSF), heterogeneous nuclear RNP-K (hnRNP-K) and NS1-binding protein (NS1-BP) (Fournier et al., 2014; Landeras-Bueno et al., 2011; Shih and Krug, 1996; Tsai et al., 2013). In fact, SFPQ is a splicing factor that enhances the efficiency of viral mRNA polyadenylation (Landeras-Bueno et al., 2011).

The switch from viral transcription to replication is a regulated process shown to involve the viral proteins NEP and NP (Mänz et al., 2012; Robb et al., 2009; Shapiro and Krug, 1988; Skorko et al., 1991). In fact, high level of NEP expression was shown to inhibit viral genome transcription and replication (Bullido et al., 2001; Mänz et al., 2012), while low expression levels stimulate cRNA and vRNA accumulation (Mänz et al., 2012; Robb et al., 2009), leading to the proposal that NEP is essential for determining viral mRNA:cRNA ratio. Due to the ability of NEP to directly bind PB1 and PB2 via its C-terminal α-helices, it was speculated as a polymerase co-factor that stimulates viral replication, by controlling polymerase switch from transcription to replication ((Fodor et al., 1993; S González and Ortín, 1999; Susana González and Ortín, 1999; Jung and Brownlee, 2006; Li et al., 1998; Mänz et al., 2012; Perales et al., 1996) and reviewed in (Paterson and Fodor, 2012)). Additionally, a small viral RNA (svRNA, 22-27 nt long), which depends on RdRp, NP and NEP for formation, was required for viral transcription-replication switch (Perez et al., 2010; Umbach et al., 2010). Importantly, NEP was reported to be essential for the genome replicative competence of avian flu (H5N1) during mammalian adaptation (Mänz et al., 2012). Furthermore, I32T mutant of NEP results in the suppression of cRNA synthesis, thereby, forming defective interfering (DI) particles that lack intact PA gene segment (Odagiri et al., 1994; Odagiri and Tobita, 1990).

1.1.5.4 Nuclear export

After viral genome transcription and replication in the host nucleus, the mRNPs and vRNPs are released into the cytosol for protein synthesis and genome assembly, respectively. Similar to the active principle of importin-based vRNP nuclear translocation, nucleocytoplasmic shuttling of newly synthesized vRNPs is facilitated by chromosomal region maintenance 1 (CRM1, also known as exportin 1, XPO-1) pathway. Importantly, viral factors such as M1 ((Bui et al., 2000; K. Martin and Helenius, 1991) reviewed in (Whittaker et al., 1996)) and NEP (NS2) (O'Neill et al., 1998) are crucial mediators of vRNP nuclear export. The C-terminus of M1 binds to the vRNP through direct interaction with NP ((Baudin et al., 2001; Noton et al., 2007) and reviewed in (Paterson and Fodor, 2012; Portela and Digard, 2002)). On the other hand, NEP establishes an intermediate connection that bridges the M1-vRNP complex (Akarsu et al., 2003; Baudin et al., 2001; Noton et al., 2007; Shimizu et al., 2011; Ward et al., 1995; Yasuda et al., 1993) and a complex of CRM1 and its co-factor GTP-binding nuclear protein Ran (Ras-related nuclear protein) (Ran-GTP) i.e. CRM1-Ran-GTP (Dong et al., 2009; Elton et al., 2001; Güttler et al., 2010; Huang et al., 2013; Ma et al., 2001; Neumann et al., 2000), forming a daisy chain (reviewed in (Paterson and Fodor, 2012)) that facilitates nuclear vRNP export.

The NEP binds to M1 (via its nuclear localization signal, NLS on its N-terminus (Akarsu et al., 2003; Baudin et al., 2001; Noton et al., 2007; Shimizu et al., 2011; Ward et al., 1995; Yasuda et al., 1993)) and CRM1 (also known as exportin, XPO1) via its prominent hydrophobic tryptophan residue (W78) on the C-terminal domain (Akarsu et al., 2003; Shimizu et al., 2011) and nuclear export signal (NES) at the N-terminus (Dong et al., 2009; Elton et al., 2001; Güttler et al., 2010; Huang et al., 2013; Ma et al., 2001; Neumann et al., 2000) respectively. In fact, inhibition of the CRM1 pathway using pharmacological blocker of nuclear export viz. leptomycin B (LMB) (Watanabe et al., 2001), anti-NEP antibody treatment (O'Neill et al., 1998), or

infection with nonviable recombinant viruses that are unable to encode NEP protein (Neumann et al., 2000), result in the retention of vRNPs in the nucleus. Upon nuclear egress of vRNPs, it was suggested that M1 blocks the NLS of NP to prevent potential reimportation into the nucleus (Akarsu et al., 2003; Shimizu et al., 2011).

Asides the CRM1 pathway, some host factors were proposed to contribute to the nucleocytoplasmic shunt of vRNPs. An example is nucleolin, which directly interacts with NP to promote vRNP nuclear exit (Terrier et al., 2016). Interestingly, plasma membrane (PM) accumulation of HA was reported to activate the RAF/ MEK/ ERK (MAPK) anti-apoptotic signalling pathway via protein kinase C α (PKCα) for timely regulation of vRNP export (Marjuki et al., 2007, 2006). Of note, inhibition of MAPK pathway impairs the nuclear egress of vRNPs (Pleschka et al., 2001). At the same time, activation of pro-apoptotic regulator Caspase 3 (Casp 3) also promotes nucleocytoplasmic shunt of vRNPs, possibly by increasing nuclear membrane porosity (Wurzer et al., 2003).

1.1.5.5 Genome assembly

Late in the viral life cycle, nucleocytoplasmic shunt of vRNPs terminates at the plasma membrane (PM) (Momose et al., 2011) where progeny virions are assembled, bud and are released from the cell. Upon nuclear exit (**Figure 1.4**H), vRNPs accumulate around the microtubule organizing centre (MTOC) for Y-box binding 1 (YB-1)- and HIV Rev-binding (HRB) proteins-dependent porting to Ras related in brain protein 11 (Rab11, especially Rab11a) GTPase recycling endosomes (Amorim et al., 2011; Bruce et al., 2010; Eisfeld et al., 2011b; Kawaguchi et al., 2012; Momose et al., 2007; Nturibi et al., 2017). Rab11 loads vRNPs via PB2 (with the RdRp portion facing the endosome) (Veler et al., 2022) and was suggested as a quality control mechanism to ensure that progeny virions incorporate a polymerase-containing vRNP.

In infected cells, Rab11 displays a very different distribution to that occurring in infected cells (Amorim et al., 2011; Bhagwat et al., 2018; Bruce et al., 2010; Momose et al., 2011; Nturibi et al., 2017; Vale-Costa et al., 2016b). In fact, Rab11-bound vRNPs have been shown to concentrate in larger cytosolic puncta. In these puncta all the 8 different vRNPs can be detected (Haralampiev et al., 2020). Two pathways have been proposed for originating these Rab11 positive puncta. In one model, these puncta concentrate in the cytoplasm at endoplasmic reticulum (ER) exit sites (ERES) ((Alenquer et al., 2019; Amorim et al., 2011; Vale-Costa et al., 2016b) and reviewed in (Amorim, 2019)). Alternatively, progeny vRNPs reaching the cytosol initially bind to the ER to originate Rab-11 irregularly coated vesicles that are delivered to the PM, possibly via ER tubulations (de Castro Martin et al., 2017). Despite the role of microtubules (Amorim et al., 2011; Momose et al., 2007) and ER (de Castro Martin et al., 2017) in vRNP trafficking, the process of transferring completely or semi assembled viral genome to sites of virion assembly at the PM is unknown but proposed to involve Rab11 (reviewed in (Amorim, 2019)).

The presence of vRNP-enriched cytoplasmic punctae is concomitant with altered distribution (Amorim et al., 2011; Bruce et al., 2010; Eisfeld et al., 2011a; Lakdawala et al., 2014; Momose et al., 2011, 2007; Nturibi et al., 2017), and functional impairment of Rab11 endocytic recycling (Vale-Costa et al., 2016b). Particularly, correlative light and electron microscopy (CLEM) and immunogold labelling of these structures displayed hotspots of electron dense elements (vRNPs) and Rab11 vesicular clusters, which lack membrane delimitation akin to classical biomolecular condensates (Sousa et al., 2017; Sílvia Vale-Costa and Amorim, 2016a). Biomolecular condensates are abundant in the viral world and are known as viroplasms, viral factories, aggresomes, or virosomes, to indicate sites of viral replication (reviewed in (Netherton et al., 2007; Wileman, 2007)). Viruses can also form viral inclusions, which are sites of accumulation of viral proteins, nucleic acids and

selected host proteins and can include (or not) viral factories (reviewed in (Netherton et al., 2007)). Given this definition, IAV vRNP hotspots were re-classified as viral inclusions (Alenquer et al., 2019) (**Figure 1.4**I).

Being enriched hotspots of IAV genomic segments (Alenquer et al., 2019; Amorim et al., 2011; Chou et al., 2013; Dou et al., 2017; Lakdawala et al., 2014) that display liquid properties (such as fusion and fission, dynamic exchange of materials, spherical shape and no membrane delimitation) (Alenquer et al., 2019), increasing in size to accommodating more vRNPs as infection progresses (Etibor et al., 2022; Vale-Costa et al., 2016b), viral inclusions were postulated as sites containing partially formed or completely formed IAV genomes (Chou et al., 2013; Haralampiev et al., 2020; Lakdawala et al., 2014), or be sites of IAV genome assembly (Alenquer et al., 2019; Amorim et al., 2011). In support of both hypothesis, as vRNPs travel through the cytosol to the PM, studies have shown increased co-localization of different vRNPs in viral inclusions (Amorim et al., 2013; Lakdawala et al., 2014), suggesting that these structures could be hotspots of IAV genomes. However, the mechanism by which the segmented IAV genome assembles or package into a 1+7 vRNP configuration is yet to be elucidated.

There have been two proposed models of the IAV genome assembly; random and selective packaging. The random model assumes an unregulated assembly process that is dictated by chance, whereas the selective model uses a controlled mechanism that ascertain the packaging of a genome consisting of eight distinct vRNPs into nascent virions (Compans et al., 1972; Fujii et al., 2003; Gog et al., 2007; Hatada et al., 1989; Hutchinson et al., 2010; Kingsbury, 1970; Lee et al., 2017; Williams et al., 2018). Accumulating evidence, especially the finding that most virions contain exactly 8 different vRNPs, give a strong support to the selective model of genome assembly which is currently the most accepted model (as reviewed in (Amorim, 2019)). Thus far, sequence specific vRNA-vRNA interactions and packaging signals support the selective model of genome assembly and no

proteins have been reported to be critical for vRNP-vRNP interactions (Compans et al., 1972; Fujii et al., 2003; Gog et al., 2007; Hatada et al., 1989; Hutchinson et al., 2010; Kingsbury, 1970; Lee et al., 2017; Williams et al., 2018).

1.1.5.6 Virion assembly and egress

Prior to PM translocation, major viral structural proteins HA, NA and M2 are translated in ER-associated ribosomes (**Figure 1.4**J) (Bos et al., 1984; Daniels et al., 2003; Dou et al., 2014; Hull et al., 1988). HA and NA proteins are then sialylated in the ER for subsequent transport through the classical secretory pathway (**Figure 1.4**L) to cholesterol- and sphingolipids enriched regions on the PM (**Figure 1.4**M) ((Barman et al., 2004; Chen et al., 2007; Ohkura et al., 2014; Sato et al., 2019; Wang et al., 2008; Yondola et al., 2011) reviewed in (Nayak et al., 2009)). These sites are called lipid rafts (Takeda et al., 2003) and serve as viral budding sites (known as budozones), where nascent virions assemble and bud from prior to release (**Figure 1.4**N).

Transfection system singly expressing either HA, NA, or M1 demonstrated their capability to independently induce budding of virus-like particles (VLPs) (Chen et al., 2007; Gómez-Puertas et al., 2000; Lai et al., 2010; Wang et al., 2010). However, in infectious state, only HA and NA proteins can initiate viral budding (Gómez-Puertas et al., 2000; Hughey et al., 1992; Valcárcel et al., 1991; Wang et al., 2010) reviewed in (Rossman and Lamb, 2011)). Here, M1 requires membrane targeting mediated by either M2 or the cytoplasmic tails of HA and NA (Ali et al., 2000; Barman et al., 2004; Jin et al., 1997; Zhang et al., 2000). Unlike HA and NA, M2 expression is delayed (Zebedee et al., 1985), making it unable to initiate budding and allowing HA and NA to serve as the primary early drivers of viral budding (reviewed in (Rossman and Lamb, 2011)).

M1 may polymerise to facilitate filamentous virion formation, typical of clinical isolates ((Calder et al., 2010) and reviewed in (Dadonaite et al.,

2016)). Upon binding to a lipid membrane, M1 oligomerizes into a helical matrix, a trait which contributes to the morphology of nascent virions (Calder et al., 2010; Hilsch et al., 2014). In filamentous virions, M1 can oligomerise to form a rigid cylindrical helix, while spherical virions form a less ordered spherical spiral just similar to the topology of M1 at the poles of filamentous virions (Calder et al., 2010). Sometimes, the filamentous poles can form enlarged bulbous structure known as Archetti body, which retains a contiguous matrix layer, sometimes containing non-membrane associated M1-like material (Archetti, 1955; Vijayakrishnan et al., 2013).

Of note, M1 may confer curvature to viral membranes or block the curvature-enabling properties either through its interaction with HA or NA (Ali et al., 2000; Barman et al., 2004; Jin et al., 1997; Zhang et al., 2000) or with NP (Bui et al., 1996; Noton et al., 2007; Zhang and Lamb, 1996) when recruiting vRNPs to the budozone. This way, M1-mediated inhibition of membrane curvature may be an intrinsic viral mechanism to ensure complete genome assembly prior to the delayed M2 recruitment to the neck of budding virions (reviewed in (Rossman and Lamb, 2011)). At the neck, M2 may insert its amphipathic helix into the membrane, exerting a positive membrane curvature, which may produce the final force required for membrane scission (reviewed in (Rossman and Lamb, 2011)).

Asides the aforementioned viral proteins, NEP (possibly through its interaction with M1) (Akarsu et al., 2003) and host proteins (with some host factors being viral strain specific) are also incorporated into the newly egressed virus (Hutchinson et al., 2014). In fact, NEP-associated ATPase-F_1F_0 was shown to localise at the budozone underneath budding virions to facilitate cellular egress of progeny virions (Gorai et al., 2012). Since the egressed virions are tethered via HA to the cell surface, NA enzymatically cleaves the cellular sialic acid moiety to release nascent virions (Calder et al., 2010; Cohen et al., 2013; Sakai et al., 2017). Currently used antivirals block NA activity and viral egress (WHO, 2018). Finally, the released virions are

propagated to other cells or individuals, thereby, terminating the viral life cycle (**Figure 1.4**N).

1.1.6 Viral evolution

IAV is at a constant evolutionary arms race with its host (reviewed in (Hutchinson and Yamauchi, 2018; Joseph et al., 2017a; Krammer et al., 2018; Wille and Holmes, 2020; Yoon et al., 2014)) due to the selective pressure mounted by the host immune system in response to infection. Additionally, aberrant viral products such as chimeric viral-host hybrid proteins (Ho et al., 2020) defective interfering particles, and defective ribosomal products (DRiPs) (Yewdell et al., 1996) can generate host cellular responses, thereby, contributing to the host-viral fitness. A genetic mutation can result in the aberrant virion production. However, mutations may lead to an antigenic drift (**Figure 1.9**A), producing viruses that are fit to replicate and are highly adapted to a range of hosts (reviewed in (Hutchinson and Yamauchi, 2018; Jones et al., 2021; Krammer et al., 2018; Wille and Holmes, 2020)).

The IAV evolves rapidly due to its in-built low-fidelity RdRp with an error-prone replicative capacity (Lin et al., 2019). This is responsible for the emergence of heterogeneous quasispecies with novel antigenicity (Pauly et al., 2017), which is most evident in circulating seasonal IAV strains. The erroneous nature of the RdRp is exemplified in A/Puerto Rico/8/1934 (PR8, H1N1) with an estimated mutation rate of 0.92 to 1.8 x 10^{-4} substitutions per nucleotide per strand copied, meaning 1.2 to 2.4 mutations per replicated genome (Lin et al., 2019; Naito et al., 2019; Pauly et al., 2017).

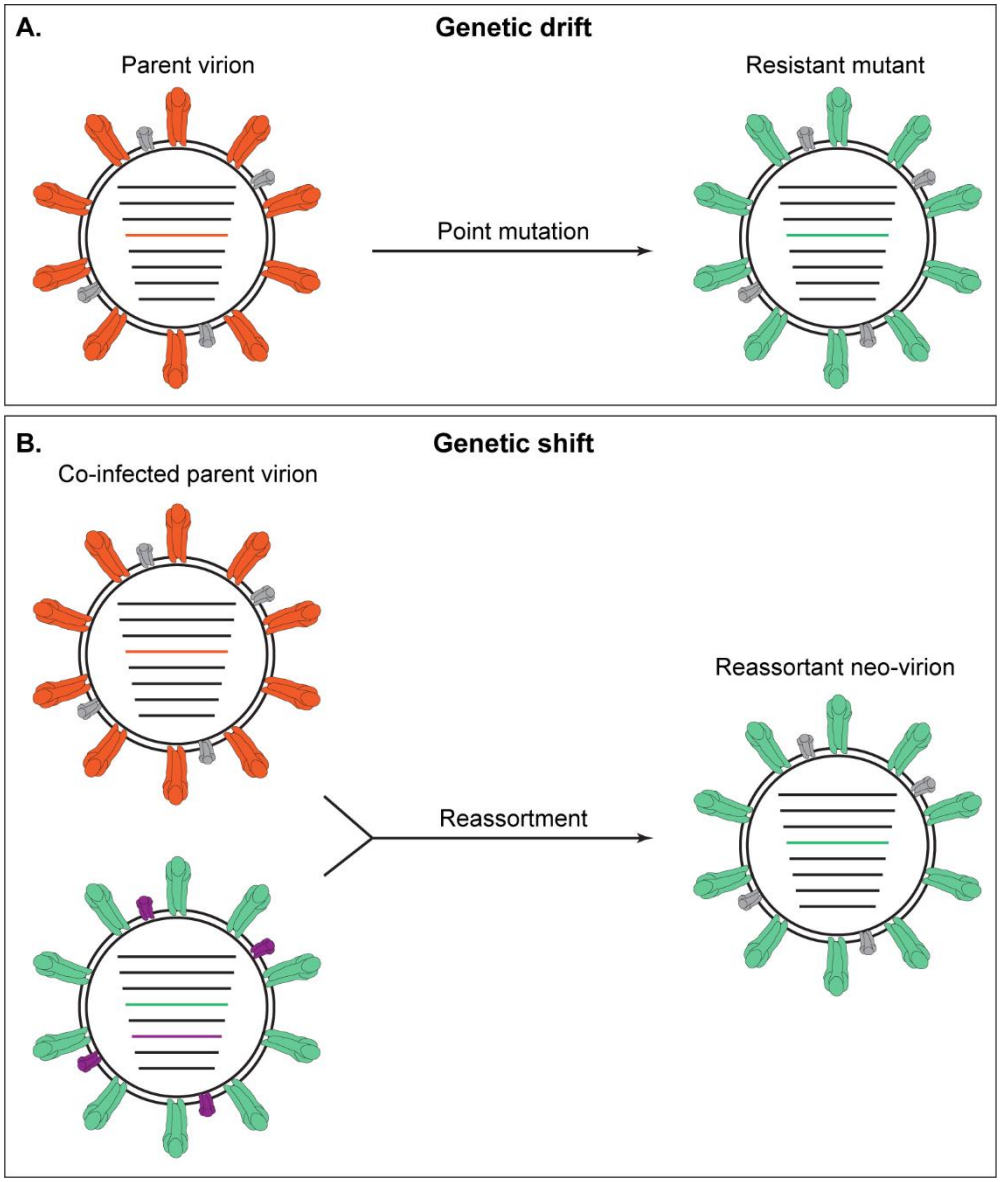

Figure 1.9- IAV evolutionary mechanisms.

(A) *Mutational error during IAV genome replication results in the emergence of resistant viral strains in a process known as antigenic/ genetic drift; an underlying factor of annual epidemics* ***(B)*** *Co-infection of the same cell with different IAV strains allows genetic reassortment, which produces neo-variant of pandemic potential in a process called antigenic/ genetic shift.*

The segmentation of the IAV genome being a mechanism driving faster evolution, albeit less frequent than genetic drift, imposes challenges in the assembly of each virion (**Figure 1.9**B). This is because infectious virions must incorporate only one copy of each vRNP, while containing all eight vRNPs. Therefore, simultaneous co-infection of antigenically dissimilar viruses in the same host cell allows genetic reassortment among distinct parental strains (**Figure 1.9**B) (reviewed in (Krammer et al., 2018; Taubenberger and Kash, 2010; Wille and Holmes, 2020)). This results in the emergence of neo-variants in a process called antigenic shift that in combination with environmental factors have been associated with pandemic events (reviewed in (Krammer et al., 2018; Taubenberger and Kash, 2010; Wille and Holmes, 2020)).

1.2 Phase transition

Having proposed that IAV inclusions are biomolecular condensates with liquid properties that may facilitate genome assembly, it is pertinent to understand the state-of-the-art in the field of phase transitions and its essentiality to cellular virology.

1.2.1 Phase transition of biomolecular condensates

The cell is a chaotic crowd of biomolecules including proteins, nucleic acids, carbohydrates, and lipids, which are maintained by active processes and organized in membrane-bound organelles such as mitochondria, ER, endosomes, lysosome, peroxisome and nucleus (reviewed in (Banani et al., 2017; Etibor et al., 2021; Falahati and Haji-Akbari, 2019)). But, phase transition is another recently described process; a thermodynamically driven mechanism for assembling biomolecules within viscoelastic membraneless organelles (MLOs) known as biomolecular condensates (reviewed in (Alberti and Hyman, 2021; Banani et al., 2017; Shin and Brangwynne, 2017)). Of note, phase transition extends beyond intracellular organelles, but has also been proposed as an organizing principle at the molecular and organismal levels as exemplified in tardigrade (Tanaka et al., 2022), *Caenorhabditis elegans* (Brangwynne et al., 2009) and yeast (Franzmann et al., 2018; Fuller et al., 2020).

Biomolecular condensates were described in the early 1900s by many, including Edmund B. Wilson who viewed the cytoplasm as a mixture of liquids in a form of emulsion (Wilson, 1899). Over decades, phase transitions were evoked several times to describe “lipid rafts” (Simons and Ikonen, 1997) as well as intracellular micro-compartmentalization (Runnström, 1963). Recently, Brangwynne *et al.* proposed that RNA and protein-rich P granules are asymmetrically distributed to the posterior end of the one-cell embryo by a phase transition process resembling the condensation and dissolution of liquids (Brangwynne et al., 2009), and this

mechanism is essential to establish the first germ cell of *Caenorhabditis elegans*. The initial observation of liquid behaviour (Brangwynne et al., 2009), set in motion a series of seminal studies to explain the driving forces of biomolecular condensate formation (reviewed in (Banani et al., 2017)).

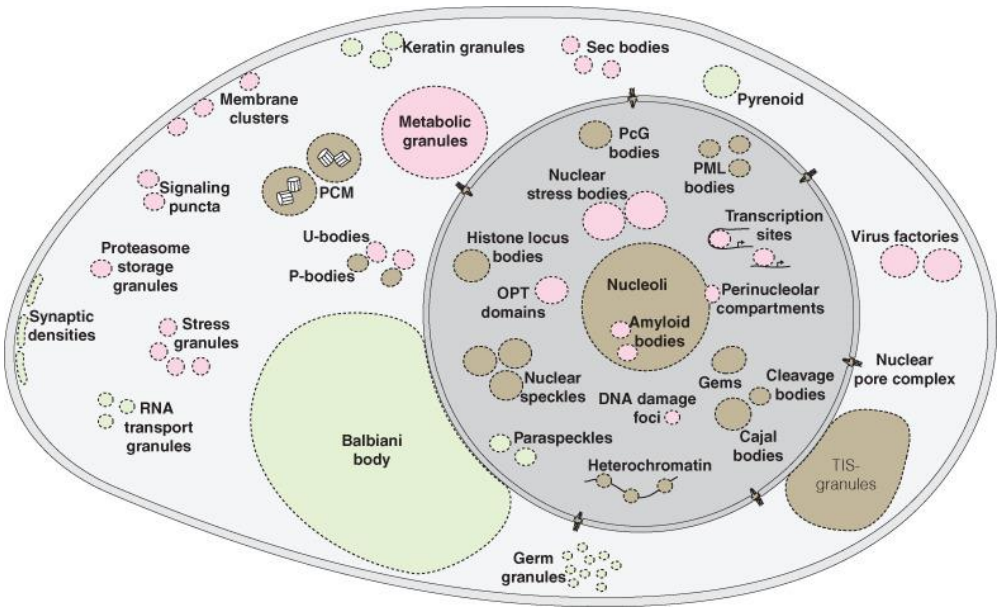

Figure 1.10- Representation of biomolecular condensates of the cell.

Depiction of biomolecular condensates formed within living cells either constitutively or induced by specific environmental or molecular stimuli.. Abbreviations: PCM- pericentriolar matrix, OPT domain- oct-1, PTF and transcription domain. This image was published in (Spannl et al., 2019).

Ever since, biomolecular condensates such as nucleolus, Balbiani body, stress granules, processing bodies (P granules), Cajal bodies, purinosomes, synaptic vesicles, nuclear speckle, nuclear paraspeckle, etc (**Figure 1.10**, reviewed in (Spannl et al., 2019)) were reported to be dissimilar from classical membrane-bound organelles due to their permeability, ability to spontaneously form or dissipate, yet still able to functionally compartmentalize cellular reactions (reviewed in (Alberti and Hyman, 2021; Banani et al., 2017; Spannl et al., 2019)). Hence, the presence of a phase

boundary allows biomolecular condensates to behave as functional compartments (reviewed in (Banani et al., 2017; Spannl et al., 2019)) that select components and buffer molecular noise (reviewed in (Riback and Brangwynne, 2020)).

The cellular functions of these biomolecular condensates have been described in a growing number of papers. For example, phase separation has been shown to promote the efficient spatiotemporal organization of cellular biochemistry (Freeman Rosenzweig et al., 2017; Oltrogge et al., 2020; Wan et al., 2018; H. Wang et al., 2019; Wunder et al., 2018), tune and accelerate / repress biochemical reactions (Hondele et al., 2019; Kim et al., 2019; Klosin et al., 2020; Li et al., 2012; Patel et al., 2017; Peeples and Rosen, 2021; Saini and Mukherjee, 2022), modulate signal transduction (Case et al., 2019b; Huang et al., 2016; W. Y. C. Huang et al., 2019; Su et al., 2016), maintain proteostasis (Danieli and Martens, 2018; Dao et al., 2018; Frottin et al., 2019) and nuclear structure (Cuylen et al., 2016; Feric et al., 2016; Frottin et al., 2019; Weber and Brangwynne, 2015; Yao et al., 2019; Zhu et al., 2019), regulate nucleic acid functions (Du and Chen, 2018; Nott et al., 2016; Sheu-Gruttadauria and MacRae, 2018; Van Treeck et al., 2018), sequester molecules for storage (Parchure et al., 2022), and respond to cellular stress (Fuller et al., 2020; Guillén-Boixet et al., 2020; Patel et al., 2015; Tanaka et al., 2022; Van Treeck et al., 2018; Yang et al., 2020), thereby facilitating cellular fitness ((Franzmann et al., 2018) (**Figure 1.11**)).

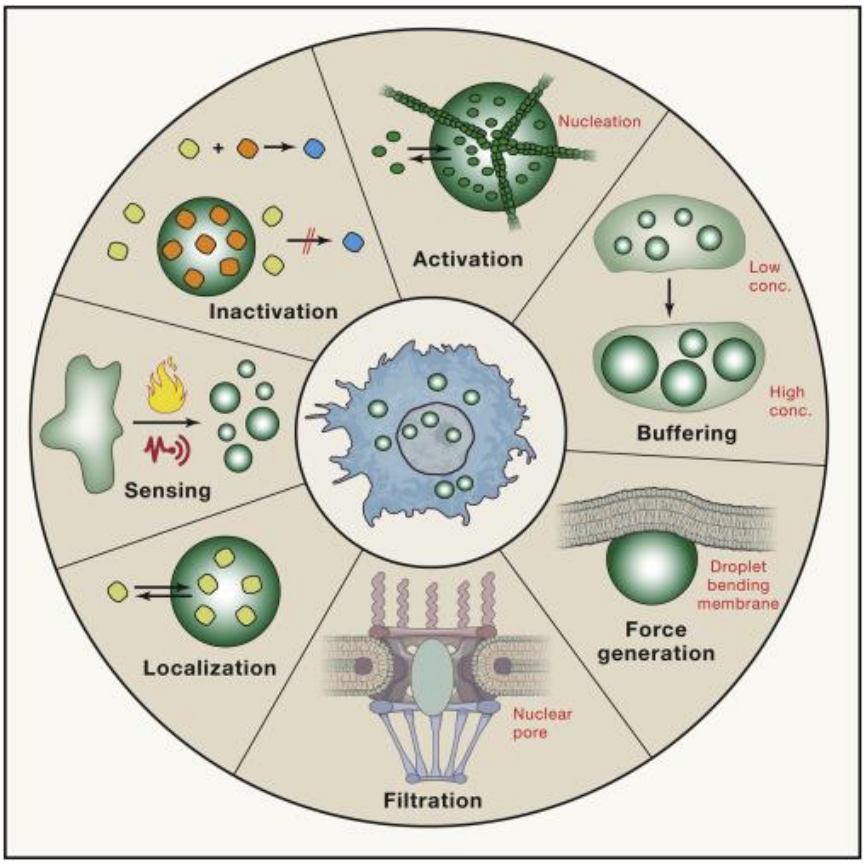

Figure 1.11- A repertoire of key functions of biomolecular condensates in the cell.

This image was published in (Alberti et al., 2019).

Phase transition is exemplified in biology using a well-mixed suspension colloid (emulsion) of oil and vinegar (reviewed in (Hyman and Simons, 2012)). In this colloid, the system seems to be in one phase if well mixed; however, when left unperturbed, the oil and vinegar begin to separate/ demix into two phases containing oil in one phase and water in another (**Figure 1.12**) (reviewed in (Hyman and Simons, 2012)). Due to affinity differences of oil and vinegar, phase separation thermodynamically favours the co-assembly of oil molecules in one phase and the demixing of vinegar molecules in another phase, resulting in a 2-phase system (reviewed in (Hyman and Simons, 2012)).

Figure 1.12- Vinaigrette.

A demixed phase of vinegar (black droplets) and oil (yellow phase). This image was published in (Wikipedia, 2022).

Accumulating evidence suggests that the self-assembly of condensates generates compartments permeable to selected components that quickly exchange material with its surroundings (Brangwynne et al., 2009; Weber and Brangwynne, 2015) (reviewed in (Brangwynne et al., 2015; Hyman et al., 2014; Hyman and Simons, 2012; Mittag and Parker, 2018; Perry, 2019; Weber and Brangwynne, 2012)). These biomolecular condensates have properties akin to liquid droplets i.e., they divide and fuse, rearrange quickly internally, are highly dynamic and respond to stress and stimuli (reviewed in (Banani et al., 2017; Brangwynne, 2011; Hyman et al., 2014; Hyman and Simons, 2012)). Importantly, the application of this concept to biology has several implications to our understanding of cellular processes and disease pathologies.

Given that viral infections exploit cellular structure and organization, to co-opt or subvert important metabolic pathways, antiviral responses, as well as biochemical resources that are essential for successful viral replication, it is expected that viruses would also take advantage of

biomolecular condensates. Therefore, it is imperative to shed light on virus-induced condensate biophysics and their functions.

1.2.2 Thermodynamic attributes of phase transitions

In classical physics, phase transition is a transient process whereby a ***homogeneous solution*** whose molecules are at equilibrium and have achieved the maximum ***entropy*** (ΔS_{max})-driven dissolution limit, transforms into an equilibrated ***demixed*** assembly (

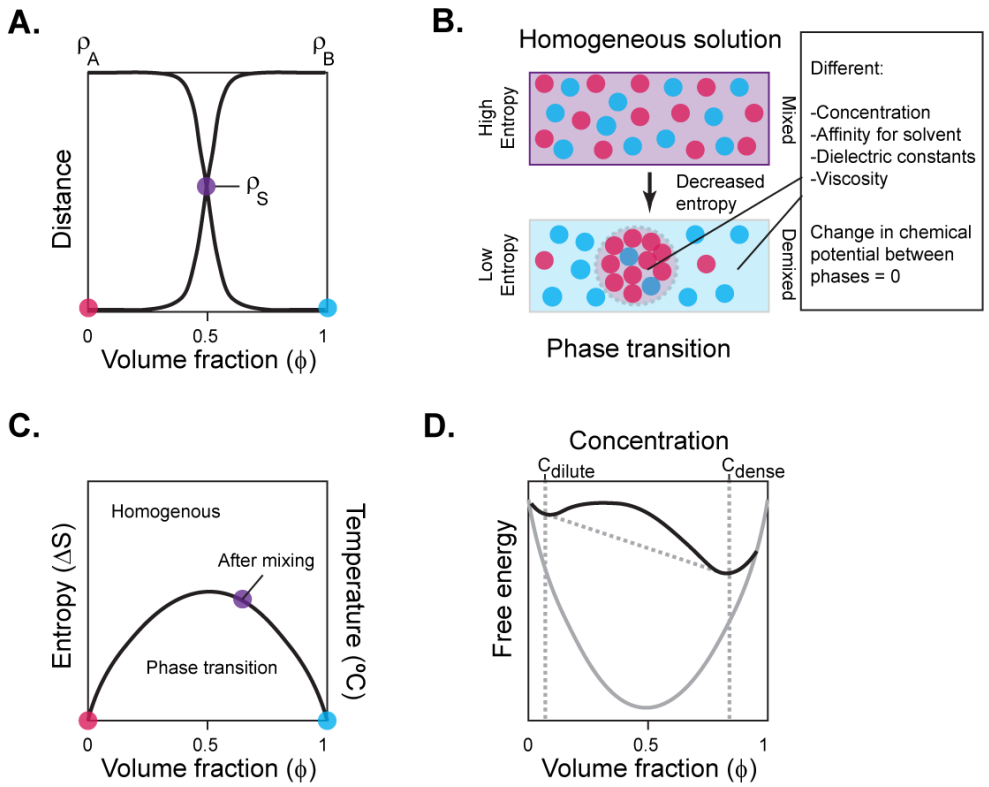

Figure 1.13A-C) (reviewed in (Banani et al., 2017; Berry et al., 2018; Boeynaems et al., 2018; Dignon et al., 2020; Hyman et al., 2014; J. Li et al., 2022; Ong and Torres, 2020)). In an ideal homogeneous mixture with negligible interaction energies, ***enthalpy*** (ΔH) is zero, and the ***free energy*** (ΔG) is an inverse function of the system´s entropy (ΔS) (reviewed in (Falahati and Haji-Akbari, 2019; Hyman et al., 2014)). Hence, at maximum entropy

(ΔS_{max}), free energy (ΔG) of the homogeneous mix is minimal (decreased), resulting in a system of thermodynamic equilibrium that favours mixing (reviewed in (Falahati and Haji-Akbari, 2019; Hyman et al., 2014; Riback et al., 2020)). In this mixed state, the ΔS is positive when the **volume fraction** (Φ) of the component molecules is $0 < \Phi < 1$ (**Figure 1.13**C). However, when $\Delta S \leq 0$, the system is more energetically favourable by demixing into assemblies with distinct **concentration** and Φ that can vary between 0 and 1, (**Figure 1.13**C). In this case, a ***phase boundary*** (**Figure 1.13**B) with selective permeability is formed at the interface of the assemblies and its surrounding solution (**Figure 1.13**B) (reviewed in (Hyman et al., 2014)). Selective permeability may be regulated by charge of condensate components as well as size, shape and surface properties (e.g., viscosity and surface tension) of the condensate. Any difference in the molecular *concentration* across the phase boundary is counterbalanced by diffusive fluxes driven by an equal ***chemical potential*** (μ) across the gradient (**Figure 1.13**D) (reviewed in (Banani et al., 2017; Hyman et al., 2014)).

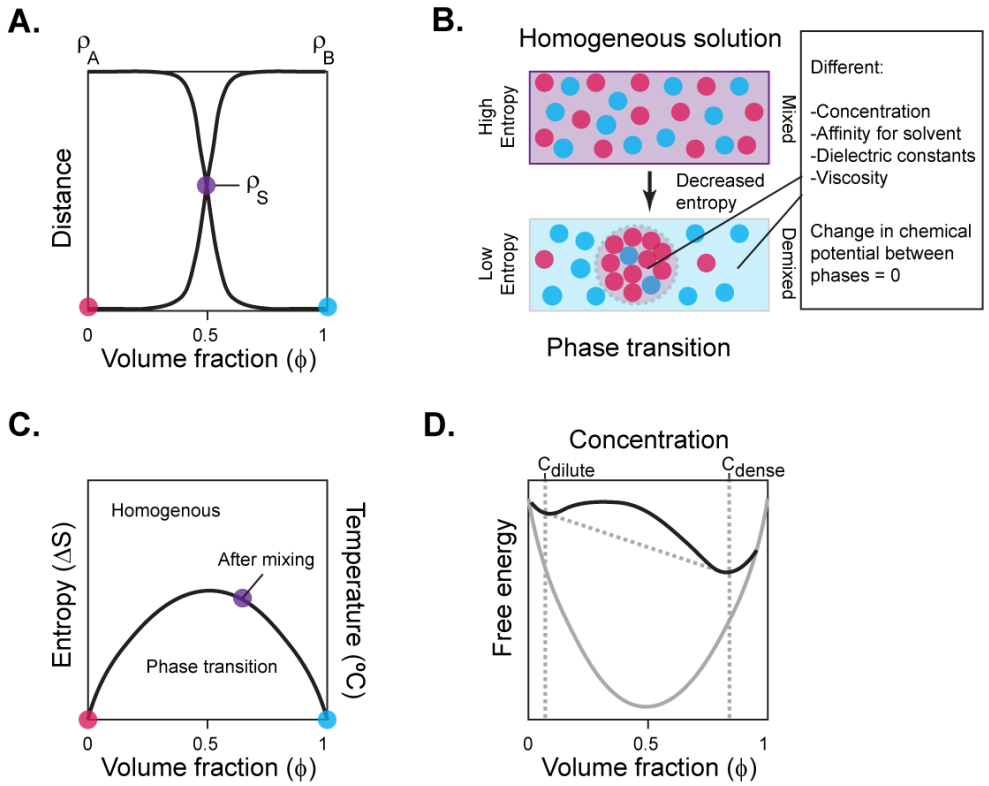

Figure 1.13- Schematic of the thermodynamics principles of phase transitions.

(A) *In an aqueous mixture of molecules A (magenta) and B (blue) that independently make favorable interaction with the solvent S (purple), but incompatible interactions with one another results in the demixing of A and B into two coexisting phases, rich in one component over the other with distinct volume fractions and densities. In this case, the density of A (ρ_A) in the B-rich phase is low, and the density of B (ρ_B) in the A-rich phase is low. However, the solvent density (ρ_S) is the same across the two phases, hence the differential densities of A and B is governed by their molecular concentration, interaction strength and volume fractions.* ***(B)*** *A mixed state of A and B (magenta and blue respectively) of high entropy demixes into two non-interacting phases of low entropy, separated by partition boundary (grey dotted circle)* ***(C)*** *Entropic contribution as a function of volume fraction. In a*

homogenously mixed state of A and B (purple dot), entropy (ΔS) is highest, demixing in one of two volume fractions (0, magenta or 1, blue), when ΔS ≤ 0. ***(D)*** *Free energy (ΔG) is a function of volume fraction and concentration of molecules.* C_{dense} *and* C_{dilute} *are the concentrations of a specific molecule within and outside the condensates respectively. Homogeneously mixed system is in the region between the dotted diagonal line and the lower grey convex curve, while partitioned (demixed) phases exist above the dotted diagonal line into the black upper curve.* This image was adapted from *(Hyman et al., 2014; Mittag and Pappu, 2022)) publications.*

The threshold concentration above which condensates begin to emerge from a metastable, homogeneous solution is known as ***saturation concentration*** (C_{sat}) (**Figure 1.14**) and the initiation of such emergence is called ***nucleation*** ((Martin et al., 2021; Sarkies and Frankel, 1971; Vekilov, 2010) and reviewed in (Berry et al., 2018; Hyman et al., 2014; Nakashima et al., 2019)). Homogeneous nucleation is a rare process that occurs spontaneously and rapidly, leading to the simultaneous emergence of numerous tiny droplets of identical sizes (Binder and Stauffer, 1976; Huang et al., 1974; Sarkies and Frankel, 1971; Vekilov, 2010). Heterogeneous nucleation is a slow process occurring in a few selected pre-existing sites that results in fewer nucleation events with droplets of varying sizes, such as ribosomal RNA, centriole and chromatin in case of nucleolus, centrosome and spindle respectively ((Vekilov, 2010) and reviewed in (Hyman et al., 2014; Malinovska et al., 2013). Therefore, nucleation is critical for size control, localization, and distribution of condensates (Hyman et al., 2014; Shimobayashi et al., 2021; Vekilov, 2010).

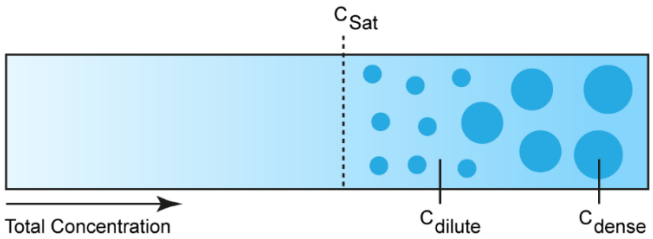

Figure 1.14- Schematic depiction of saturation concentration.

A system would remain in a homogenously mixed state until reaching a threshold concentration known as C_{sat} (dashed line), after which phase transition of condensates emerges. Here, molecules partition into condensates of dense concentration (C_{dense}) from a dilute external milieu (C_{dilute}).

In a post-nucleation supersaturated system, there is a flux of molecules between condensates exhibiting distinct Laplace pressures (i.e. differential pressure between the inside and outside of a curved surface forming an interfacial boundary between two fluid regions; as for example, two spherical bodies (Butt et al., 2006)) that generates a gradient of chemical potential (**Figure 1.15**), ((Butt et al., 2006) and reviewed in (Hyman et al., 2014)). This gradient results in a size control mechanism known as ***Ostwald ripening*** (**Figure 1.15**); a process whereby matured droplets are formed via absorption of smaller droplets into bigger ones leading to droplet growth, aging and hardening of condensates by coarsening (fusion between two droplets) ((Exner and Lukas, 1971; Lifshitz and Slyozov, 1961; Nakach et al., 2016) and reviewed in (Berry et al., 2018; Hyman et al., 2014; Voorhees, 1992)). Condensate growth is driven by the reduction of interfacial energies (surface tension) between fusing droplets (Feric et al., 2016). This hydrodynamics mechanism of condensate maturation (growth) may be coupled with Brownian motion, sedimentation, or surface attachment, enabling molecular flux into large condensates. Such directional flux would therefore increase the component concentration and transition densities of

these structures, which may result in hardening (Alberti and Hyman, 2021; Berry et al., 2018; Hyman et al., 2014; Mittag and Pappu, 2022)).

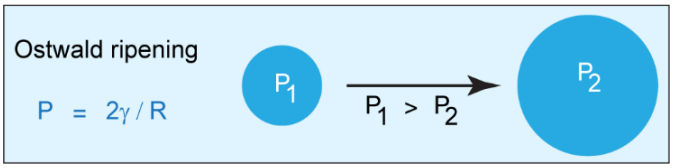

Figure 1.15- Schematic representation of Ostwald ripening.
Chemical potential differences in differently sized condensates results from differing Laplace pressures. The Laplace pressure ($P = 2\gamma/R$, where γ = droplet surface tension and R = droplet radius) is greater in small condensate relative to big condensates. This interfacial energy differences results in the ripening where the small condensate shrinks, feeding the growth of the bigger condensate (black arrow), which eventually coarsen. This image was adapted from (Butt et al., 2003; Hyman et al., 2014; Rosowski et al., 2020)) publication.

The propensity to undergo phase transition can be mapped in a phase diagram, defined by changes in a set of parameters (like temperature, concentration, pH and valency) that may result in a homogeneous mixture or promote phase transition (**Figure 1.16**A-C) (reviewed in (Alberti et al., 2019; Mitrea et al., 2022)). Generally, phase diagrams are depicted for a simple binary system, consisting of 2 regimes of molecules (**Figure 1.16**A) ((Klosin et al., 2020; Riback et al., 2020) reviewed in (Alberti et al., 2019; Berry et al., 2018; Riback and Brangwynne, 2020)). At ***sub-saturation concentration***, molecules mix homogeneously outside the binodal curve until saturation concentration (C_{sat}) is reached, after which the binodal is crossed and molecules demix to nucleate condensates (**Figure 1.16**A) (reviewed in (Alberti et al., 2019; Berry et al., 2018; Mittag and Pappu, 2022)).

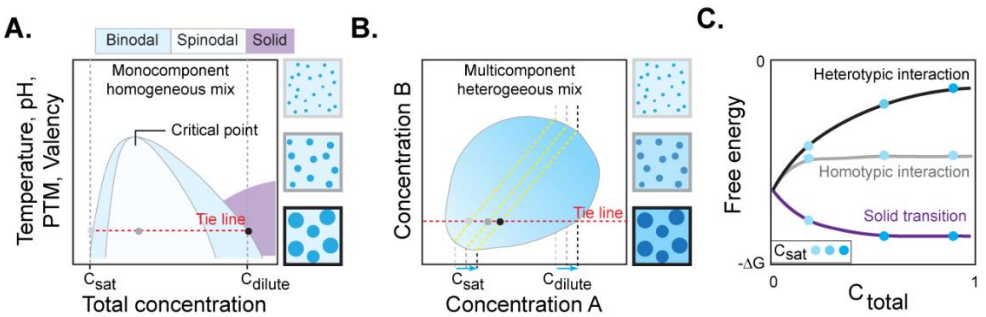

Figure 1.16 – Schematics of Phase diagrams.

The phase diagram is a function of the thermodynamic parameters that regulate phase behaviour such as temperature, pH, valency, and post-translational modifications (PTMs) ***(A)*** *A simple binary phase diagram showing the partition of a homogeneously mixed system after C_{sat} is crossed. The binodal regime (light blue region) is reached via nucleation after which spinodal decomposition (white region) takes place. As depicted by the tie line, the C_{sat} is always the same regardless of the total concentration of the system.* ***(B)*** *Multicomponent phase diagram of a ternary system displaying an unstable C_{sat}.* ***(C)*** *Free energy in binary (grey line) and multicomponent ternary (black line) systems are fixed or destabilizing respectively. Liquid-to-solid phase transitions result in a stabilizing free energy (purple line).These images were adapted from (Alberti et al., 2019; Riback et al., 2020; Riback and Brangwynne, 2020) publications.*

As concentration reaches the critical point and the spinodal line is crossed, highly dynamic phase separated domains with a minimized or negligible nucleation barrier and ability to coarsen, spontaneously emerge in a process known as ***spinodal decomposition*** (**Figure 1.16**A) (reviewed in (Alberti et al., 2019; Berry et al., 2018)). This ***homotypic*** binary system with a fixed C_{sat} (**Figure 1.16**A) is easily recapitulated in an *in vitro* system that mimics physiological state but lacks cellular noise from other biomolecules ((Klosin et al., 2020; Riback et al., 2020) reviewed in (Riback and Brangwynne, 2020). However, the rules of thermodynamics do not linearly

translate into living systems that actively consume energy, and important examples are starting to emerge on how phase transitions are regulated in living cells (Bracha et al., 2018). Of note, *in vivo* biological systems exhibit condensates formed by hundreds of distinct proteins and RNA components (Banerjee et al., 2017) and reviewed in (Hondele et al., 2020)). This ***heterotypic*** multicomponent trait results in a complex phase diagram with unfixed C_{sat} (**Figure 1.16**B) ((Riback et al., 2020) and reviewed in (Mittag and Pappu, 2022)).

Biological systems are very far from being in ***thermodynamic equilibria***, and this lack of equilibria is an absolute requirement for life (reviewed in (Berry et al., 2018; Mitrea et al., 2022; Mittag and Pappu, 2022)). Not only is the composition of the cell and liquid compartments complex, it is also extremely variable, oscillating and adapting in response to several stimuli (like the nutritional state, several types of stress including microbes, extracellular signalling) ((Patel et al., 2017; Wippich et al., 2013) and reviewed in (Drino and Schaefer, 2018; Rabouille and Alberti, 2017)). Phase transitions in biology are ***non-equilibrium thermodynamics*** processes (**Figure 1.16**B,C) (reviewed in (Alberti and Hyman, 2021; Berry et al., 2018)), nevertheless, some general principles are being understood regarding the intrinsic properties of the components able to self-assemble into biomolecular condensates.

The formation of these condensates is regulated in ways that are still being understood, but their deregulation can result in pathological conditions. Importantly, the type of interactions they establish and how biomolecular condensates may be kept away from equilibria or mature with time are being elucidated, as these have important consequences for cellular structure and organization. This has elegantly been shown for proteins associated with neurodegenerative disorders by revealing mutations that cause liquid-to-solid transitions and the formation of aggregates or crystals (**Figure 1.16**A) ((Patel et al., 2017, 2015; Vekilov, 2010) and reviewed in (Alberti, 2017)).

1.2.3 Properties of biomolecular condensates

The critical concept of biomolecular condensates arising by LLPS constituting a new framework in biology, is that the concentration of a molecule in two phases can be orders of magnitude apart without the assistance of a physical barrier. Importantly, reaching this difference in concentration does not require energy, as compartmentalization through LLPS is a spontaneous process, and so is its maintenance or transport across the boundaries (reviewed in (Perry, 2019)). In such a two-phase system, diffusion does not have to occur from higher to lower concentration, because the difference in the chemical potential at the interface is zero (reviewed in (Hyman et al., 2014)).

The two phases might have different material properties including distinct dielectric constants and affinities for the solute molecules. As a result, the interior of a condensate can be constituted by a solvent closer to an organic solvent rather than displaying aqueous properties and partition certain components while excluding others (Nott et al., 2016). The consequences of this differential behaviour are that these compartments can achieve an exquisite level of selection for partitioning molecules inside. For example, in vitro assembled DEAD box helicase 4 (Ddx4) compartments absorb single or hairpin-containing RNAs but exclude double-stranded RNA (Nott et al., 2016), which means that a fine-tuning in selection for inclusion in LLPS compartments is achieved.

Furthermore, the formation of biomolecular condensates is reversible, and liquid condensates can assemble and dissolve in response to very small changes in conditions, including ***concentration*** and ***valency*** of components, ***ions***, ***PTMs***, and nucleic acids that result from environmental conditions or integrated cell signalling (An et al., 2008; Banani et al., 2016; Banerjee et al., 2017; Berry et al., 2018, 2015; Du and Chen, 2018). This leaves the cell with the potential to form functional biomolecular condensates under certain

conditions and dissolve them when they change, responding quickly to metabolic alterations or to stress. Examples include how related enzymes can cluster to form the purinosome (An et al., 2008; Zhao et al., 2013) and how their enzymatic products dissolve these structures or how stress granules form/disassemble into liquid organelles in response to signalling (Marrone et al., 2018; Molliex et al., 2015; Van Treeck et al., 2018; Wippich et al., 2013). This provides an efficient means for regulating reactions in response to variations in conditions or for rearranging structures using a minimal investment of energy or allocated resources.

There are many other molecular modulators that can alter the phase threshold of molecules in *in vitro* reductionist models. These include chaperones, ***ATP*** (energy) (Patel et al., 2017), ***pH*** (Koga et al., 2011), ***ionic strength*** (*salt concentration*) (Nakashima et al., 2018), ***temperature*** (Nott et al., 2015), and ***PTMs*** (phosphorylation, ubiquitination, SUMOylation, methylation, acetylation, etc.) ((Case et al., 2019b; Nott et al., 2015; Patel et al., 2017; Rai et al., 2018; Reineke et al., 2017; Saito et al., 2019) and reviewed in (Hofweber and Dormann, 2019, p. 109; Snead and Gladfelter, 2019)). Particularly, PTMs may either decrease or increase the C_{sat}. Examples are: the phosphorylation of nephrin decreasing the condensation/partitioning of N-WASP and non-catalytic region of tyrosine kinase (NCK) (Li et al., 2012); and arginine methylation of Ddx4 increasing the saturation concentration (C_{sat}) of Ddx4 (Nott et al., 2015).

Interestingly, ***membranes and endomembrane surfaces*** can lower the phase concentration threshold ((Banjade and Rosen, 2014; Case et al., 2019b; W. Y. C. Huang et al., 2019; Li et al., 2012; Ma and Mayr, 2018; Snead et al., 2022; Su et al., 2016) and reviewed in (Case et al., 2019a)). These may either restrict movement (from 3D to 2D) or increase the valency of components in order to generate LLPS nucleation sites, including actin assembly at membrane surfaces ((Case et al., 2019b) and reviewed in (Snead and Gladfelter, 2019)), synaptic vesicles in synapsin clusters

(Milovanovic et al., 2018), membrane contact sites (Lee et al., 2020; Ma and Mayr, 2018; Snead et al., 2022), and a linker for activation of T cells (LAT)-based network of Ras signalling (W. Y. C. Huang et al., 2019). Importantly, there is a need to better understand membrane-condensates interaction and their regulatory mechanisms (reviewed in (Zhao and Zhang, 2020)).

Typically, cells are maintained within a tight temperature range and display adaptive responses to thermal fluctuations. Depending on the molecular composition, thermoregulation is especially key for the emergence and maintenance of condensates (Quiroz and Chilkoti, 2015). It was shown that biomolecular condensates can exhibit either upper critical solution temperature (UCST), lower critical solution temperature (LCST) or re-entrant phase transition (**Figure 1.17**A) ((Falahati and Haji-Akbari, 2019) and reviewed in (Quiroz and Chilkoti, 2015)). UCST is the most common and its phase diagram is the most described in biology to date. In ***LCST transition***, the system remains as a homogoneous mix until the temperature increases beyond the critical point (Figure 1.17A) ((Falahati and Haji-Akbari, 2019) and reviewed in (Quiroz and Chilkoti, 2015)). In contrast, ***UCST transition*** only emanate as demixed phase from the mix if the temperature lies below the critical temperature (**Figure 1.17**A) ((Falahati and Haji-Akbari, 2019) and reviewed in (Quiroz and Chilkoti, 2015)).

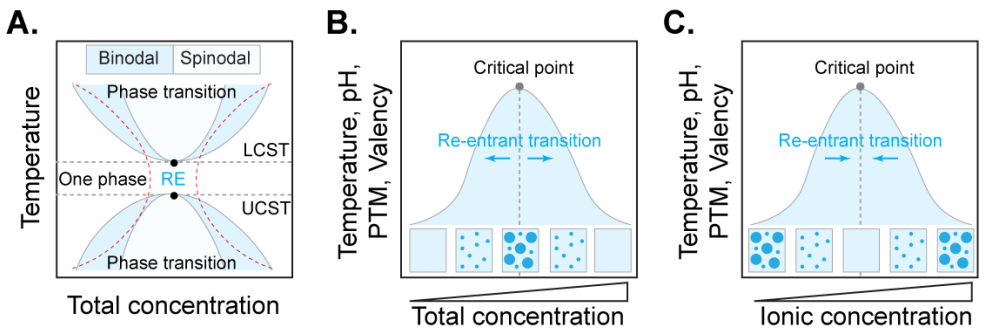

Figure 1.17- Schematic phase diagram of re-entrant phase transitions.

Phase diagrams of different systems are distinct and dependent on the modulators of phase transitions such as temperature, ionic concentration etc ***(A)*** *Phase transition may occur if the lower critical solution temperature (LCST) or upper critical solution temperature (UCST) is reached. A re-entrant phase regime (RE) exists between the LCST and UCST, resulting in an hourglass shaped diagram (red dashed concave lines) exists during re-entrant* ***(B – C)*** *Re-entrant phase transitions. These images were adapted from (Falahati and Haji-Akbari, 2019; Quiroz and Chilkoti, 2015)) publications.*

Interestingly, there are conditions known as ***re-entrant phase transition*** where molecular demixing occurs at both low and high temperatures, concentration, or ionic strength (**Figure 1.17**B,C) ((Alshareedah et al., 2019; Banerjee et al., 2017; Krainer et al., 2021; Portz and Shorter, 2021; Quiroz and Chilkoti, 2015; Su et al., 2022) and reviewed in (Falahati and Haji-Akbari, 2019; Tom and Deniz, 2021)). Between these high and low temperatures or ionic concentrations, a miscibility zone exists, which results in a hour-glass phase diagram (**Figure 1.17**B,C) ((Krainer et al., 2021) reviewed in (Falahati and Haji-Akbari, 2019; Milin and Deniz, 2018)). Re-entrant phase transitions are also concentration dependent (**Figure 1.17**A-C) (Krainer et al., 2021). Several manuscripts describe the role of RNA in promoting phase separation at a certain concentration, but when the critical concentration is crossed, a resultant re-entrant phase transitions ensues (**Figure 1.17**A) ((Alshareedah et al., 2019; Banerjee et al., 2017; Krainer et al., 2021; Quiroz and Chilkoti, 2015; Su et al., 2022) and reviewed in (Portz and Shorter, 2021; Tom and Deniz, 2021)). This means that after a concentration threshold RNA promotes the dissolution of biomolecular condensates. This offers an opportunity for a feedback loop in which the reaction products, in this case RNA, controls the formation or disassembly of biomolecular condensates, as observed in ribosomes or spliceosomes (Alshareedah et al., 2019; Banerjee et al., 2017; Kaur et al., 2019; Mitrea et al., 2018).

1.2.4 Molecular grammar of phase transitions

It became established that the formation of biomolecular condensates depends on the properties of their constituents that are normally proteins and nucleic acids, mostly RNA, in still poorly defined compositions, that interact weakly and transiently with each other whilst avoiding interacting with the milieu (reviewed in (Banani et al., 2017; Hondele et al., 2020; Hyman et al., 2014; Milin and Deniz, 2018; Shin and Brangwynne, 2017)). The molecules that reside in biomolecular condensates are of two types: molecules that drive their formation (drivers or scaffolds) and molecules that through interaction with the drivers /scaffolds are dragged to the condensates (clients or residents) ((Banani et al., 2016) reviewed in (Banani et al., 2017)).

In a series of seminal reports, the rules governing the driving forces and properties of condensate formation are beginning to be understood using LLPS models adapted from the field of ***associative polymers*** and hence considering macromolecules as polymeric chains. Examples include FUS, TATA-binding protein-associated factor 15 (TAF15), Ewing sarcoma breakpoint region 1 (ESWR1), and heterogeneous nuclear ribonucleoprotein A1 (hnRNPA1) analysed in light of the stickers-and-spacers framework ((Brangwynne et al., 2015; J. Wang et al., 2018) reviewed in (Choi et al., 2020; Harmon et al., 2017; Holehouse and Pappu, 2018; Perry, 2019; Posey et al., 2018).

Drivers of LLPS compartments comprise ***multivalent proteins***. Many systems have been reported in which drivers of biomolecular condensates also contained ***intrinsically disordered proteins/regions/domains*** (IDPs/IDRs/IDDs) that have low complexity and can also be called low-complexity domains (LCD) or prion-like domains (PrLD) (Alberti and Carra, 2018; Banani et al., 2016; Bergeron-Sandoval et al., 2016; Riback et al., 2020; Strom and Brangwynne, 2019; Taylor et al., 2016; Vantomme and Meijer, 2019; J. Wang et al., 2018; Wheeler and Hyman, 2018; Yoshizawa et al.,

2020). However, it is now clear that existence of IDRs is not the only essential driver for the formation of biomolecular condensates. Multivalency is a key feature to promote condensation. Multivalent proteins are composed of N repeats of sticky domains/motifs that provide N-specific interactions ((Alshareedah et al., 2021) and reviewed in (Mittag and Pappu, 2022)). Sticky interacting domains or ***stickers*** also called ***scaffolds*** (reviewed in (Choi et al., 2020; Choi and Pappu, 2020), that correlate with valency (number of ligations established), can be short linear motifs such as those found in IDP or folded domains such as for example RNA recognition motifs, SRC Homology 3 (SH3), PDZ (an initialism combining the first letters of the first three proteins discovered to share the domain- post synaptic density protein (PSD95), Drosophila disc large homolog 1 tumor suppressor (Dlg1)), zonula occludens-1 protein (zo-1) or small ubiquitin-like modifier (SUMO) ((Ranganathan and Shakhnovich, 2020; Yang et al., 2019) and reviewed in (Van Roey et al., 2014)).

Stickers control the ability to form biomolecular condensates. They are composed of charged and aromatic amino acids, especially arginine and tyrosine. Stickers preferentially interact with other stickers in homotypic and heterotypic interactions (reviewed in (Berry et al., 2018; Choi et al., 2020; Choi and Pappu, 2020; Perry, 2019)), rather than interacting with the solvent, and thus establish high-order networks that are key in driving condensation (Bergeron-Sandoval et al., 2016; Berry et al., 2018; Perry, 2019). Stickers determine the C_{sat} of a phase diagram in an inverse proportional manner, i.e., more stickers results in lower C_{sat} (reviewed in(Choi and Pappu, 2020)).

Other important contributors of phase separation are regions in between the sticky domains or ***spacers***. These regions provide flexibility and structure to the network and can be structural domains or IDRs of low complexity. Space residues comprise glycine, serine, and glutamine ((J. Wang et al., 2018) and reviewed in (Holehouse and Pappu, 2018)). Spacers are responsible for the material properties of the biomolecular condensates, as

changing these residues leads to changes in diffusion and across phase boundaries of condensates ((J. Wang et al., 2018) and reviewed in (Holehouse and Pappu, 2018)). Changes in glycine or serine to alanine result in the hardening of condensates and the change in glutamine to glycine results in increased fluidity (J. Wang et al., 2018). Spacers control the rate at which cross-links are established and broken, which is a function of the number of possible ligations on space residues ((Brangwynne et al., 2015) and reviewed in (Choi et al., 2020)).

The types of interactions shown so far to permit phase separation include ***electrostatic***, ***dipole–dipole***, ***cation–π***, ***and π–π*** interactions (reviewed in (Mitrea et al., 2022)). Having cationic and aromatic stickers allows attracting molecules at a long range but also establishing specific cohesive interactions at a short range. As such, stickers can be said to encode the interaction range and strength in biomolecular condensates (Choi and Pappu, 2020). These interactions are possible on specific types of amino acids and nucleic acids prevalent on the types of proteins mentioned above ((Mittag and Parker, 2018; Qamar et al., 2018; Sanders et al., 2020) and reviewed in (Weber and Brangwynne, 2012)).

Due to their length, flexibility, and multivalency, RNAs have been demonstrated to be a critical ***scaffold*** of proteins bearing RNA recognition motifs (RRM) for **client** binding and to control phase separation (Maharana et al., 2018). However, their behaviour is different depending on the identity of the biomolecular condensates (in some cases helping the formation, by enabling nucleation or establishing networks and in other cases permitting dissolution by electrostatic charge inversion, for example) ((Berry et al., 2015; Garcia-Jove Navarro et al., 2019; Maharana et al., 2018; Shevtsov and Dundr, 2011; J. Wang et al., 2018; Wilson, 1899; Zhang et al., 2015) and reviewed in ((Brangwynne and Johnson, 2013; Langdon and Gladfelter, 2018; Weber and Brangwynne, 2012)). Phase transition also depends on the

properties of the solvent in the intracellular milieu, which needs to disfavour solute–solvent interactions to drive spontaneous condensation.

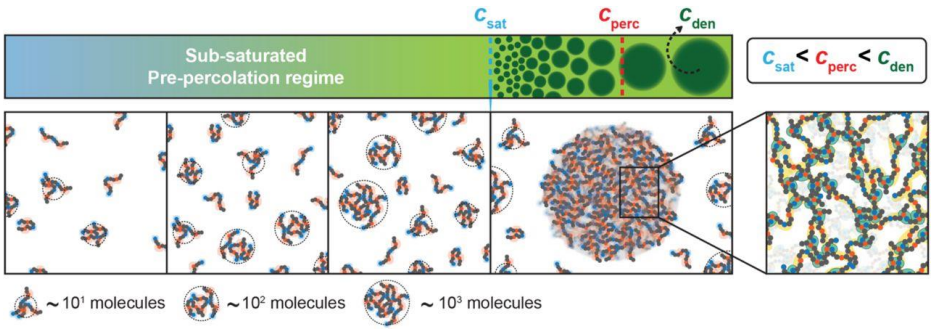

Figure 1.18 - Schematic of percolation coupled to phase transition.

Reversible physical crosslinks amongst sticker networks forms finite-sized clusters with increasing size and density even at sub-C_{sat}. Beyond C_{sat}, the clusters form mesoscale assemblies via phase transition. Such condensate spanning network is achieved by the addition of monomers and coalescence due to $C_{sat} < C_{perc} < C_{dense}$. This images was published in *(Kar et al., 2022).*

1.2.5 Types and tunability of phase transitions

The liquid property refers to an amorphous state, which lacks both long range translational order and ability to withstand shear deformation, resulting in a rapid adaptive relaxation (reviewed in (Falahati and Haji-Akbari, 2019)). Liquids display viscosity when an external force is exerted while solids can resist shape deformation due to shear elasticity (reviewed in (Hyman et al., 2014)). However, complex fluids such as gels are viscoelastic; sharing spectral properties of liquids and solids (reviewed in (Hyman et al., 2014)). Biomolecular condensates formed by LLPS can mature or transition into a slowly relaxing viscous ***gel*** or may aggregate/ precipitate into ***solid*** fibres or crystals (**Figure 1.16**A) (reviewed in (Alberti et al., 2019; Brangwynne et al., 2015; Falahati and Haji-Akbari, 2019; Hyman et al., 2014)).

The function of biomolecular condensates has been postulated to be intimately associated with the material properties and their mobility: a condensate needs to have highly dynamic components for operating as signalling hubs or reactions centres, whilst elasticity and a degree of rigidity is important when condensates function as scaffolds (reviewed in (Falahati and Haji-Akbari, 2019; Hyman et al., 2014; Mitrea et al., 2022)). Howeverchanges in the material properties of condensates may occur and result from changes in concentration, conformation, amino acids availability for engaging in interactions, or strength/type of interactions or from changes in surface tension and viscosity. Applied to biological systems, changes in liquid condensates may occur via mutations, PTMs, availability of ions, metabolites, or occurrence of energetic reactions (reviewed in (Alberti and Hyman, 2021; Falahati and Haji-Akbari, 2019; Hyman et al., 2014)). This is exemplified by the solid fibrous polymerization of actin filaments from a liquid Nephrin-Nck-N-WASP condensate (Case et al., 2019b) and aberrant neuropathological aggregates of fused in sarcoma (FUS) in diseases like amyotrophic lateral sclerosis (ALS) and frontotemporal dementia (FTD) (Patel et al., 2015). In the context of viral infection, measles virus (MeV) inclusion bodies have been shown to mature from liquid to a gel-like structure as infection progresses (Zhou et al., 2019), but the impact of this change on its function is unknown.

1.2.6 Phase transitions in viral infections

Recently, many viruses were shown to assemble biomolecular condensates with the properties of liquids (Alenquer et al., 2019; Davis et al., 2019; Heinrich et al., 2018; Hidalgo and Gonzalez, 2019; Nikolic et al., 2017, 2016; Tarakhovsky and Prinjha, 2018; Zhou et al., 2019) (**Figure 1.19**), but our knowledge of liquid biomolecular condensates and especially of phase separation in viral infections is still in its infancy.

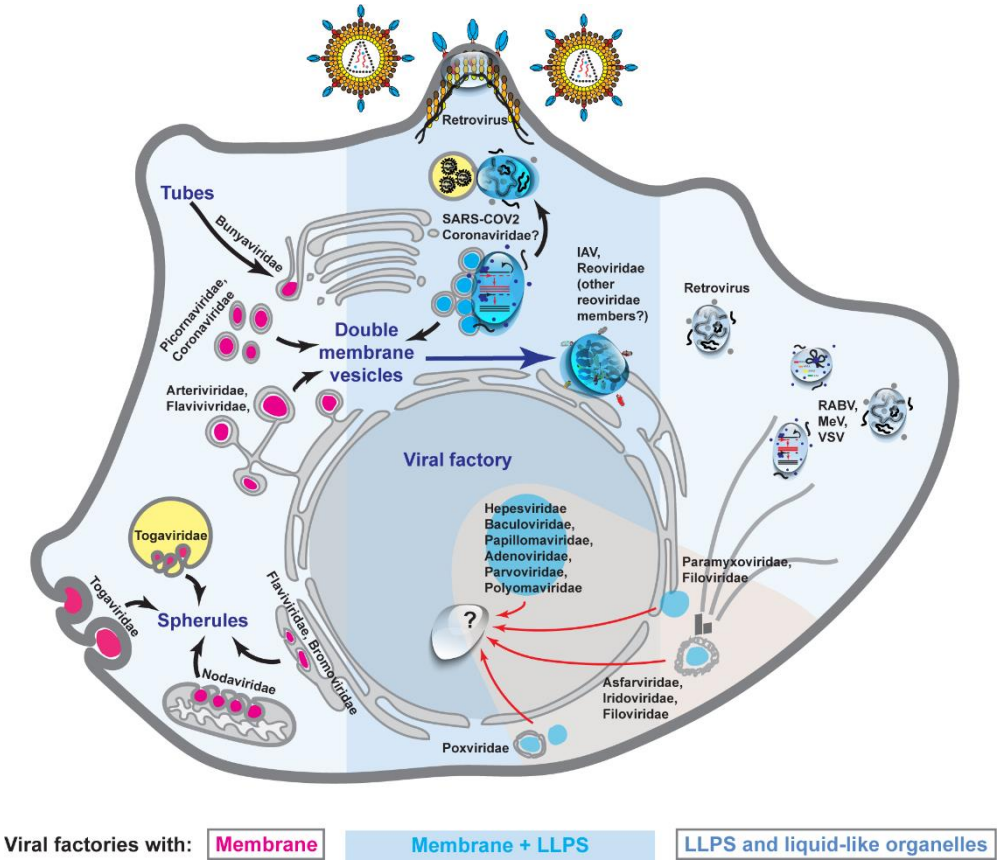

Figure 1.19- Viral infection alters cellular structure and organization.

Seminal studies have shown several examples of viruses that re-shape membrane-bound organelles to facilitate their replication, which are depicted in the left side of the figure. Recent reports suggest that viruses may also induce the de novo formation of other types of cellular compartments, which lack delimiting membranes and display the properties of liquids. Interestingly, several viruses such as reovirus, influenza A virus (IAV), human immunodeficiency virus-1 (HIV), and severe acute respiratory syndrome coronavirus-2 (SARS-CoV-2) show an intimate association between the two types of cellular organelles, and the membrane interface has been shown to actively modulate protein LLPS in several ways. It has been shown to lower C_{sat} for protein LLPS by restricting the movement of drivers and clients and

even by operating as platforms for multivalent interactions. Additionally, it can build special environments to enable function; it can amplify signal transduction and even facilitate the fusion and fission of condensates, increasing their dynamics and avoiding that they reach equilibrium. This image was published in (Etibor et al., 2021).

Considering recent findings, such discovery suggests a change in paradigm on how viruses organize biochemical reactions. Despite being early days, compartments with liquid properties have been suggested to play roles in every step of viral lifecycles: viral entry, genome replication, assembly, and genome packaging (**Figure 1.20**) (reviewed in (Dolnik et al., 2021; Etibor et al., 2021; Wei et al., 2022; Wu et al., 2022)).

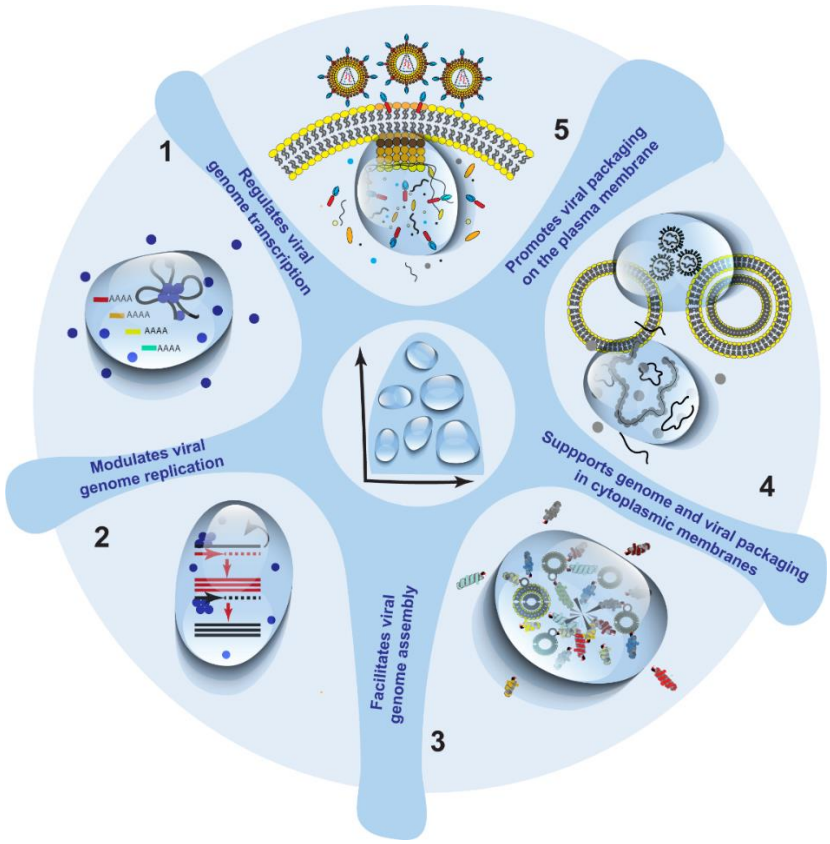

Figure 1.20- Liquid organelles can play different roles in viral infections.

Despite being early days, liquid organelles have already been hypothesized to play many different functions in viral infections such as genome transcription, replication, assembly, and virion packaging. This image was published in (Etibor et al., 2021).

Studies have shown that Mononegavirales (such as rabies virus; RABV, measles virus; MeV, respiratory syncytial virus; RSV, vesicular stomatitis virus; VSV, ebola virus, human- metapneumovirus; hMPV) (reviewed in (Etibor et al., 2021)), SARS-CoV-2 (Carlson et al., 2020; Cascarina and Ross, 2020; Chen et al., 2020; Iserman et al., 2020b; Savastano et al., 2020; Tai et al., 2021), HIV (Krasnopolsky et al., 2019; Krishnamoorthy et al., 2003; Lyonnais et al., 2021), rotavirus (Dhillon and Rao, 2018; Geiger et al., 2021) and IAV (Alenquer et al., 2019) have broadly evolved mechanisms to assemble proteins and/ or nucleic acids into liquid micro-condensates (**Table 1.2**). Although, each virus has a minimal molecular requirement necessary to induce condensates with specialized functions, studies showed that nucleoprotein is central to most viral condensates (**Table 1.2**).

Table 1.2- Viral condensates and function

Virus	Liquid Compartment	Minimal Components	System	Validation	Ref
RABV	Negri body	N, P	Transfection	Infected cells	(Nikolic et al., 2017)
VSV	Viral Inclusion	P, (N, L)	Transfection	-	(Heinrich et al., 2018)
MeV	Viral factory	N, P	Transfection; In vitro reductionist assay	-	(Guseva et al., 2020; Zhou et al., 2019)]
		N	Transfection;	-	

SARS-CoV-2	Replication transcription complex (RTC)		In vitro reductionist assay		(Carlson et al., 2020; Cascarina and Ross, 2020; Chen et al., 2020; Iserman et al., 2020b; Savastano et al., 2020; Tai et al., 2021)
IAV	Viral Inclusion	NP, vRNA, Rab11	Transfection	Infected cells	(Alenquer et al., 2019)
HIV	Budding site	Gag/NC	Transfection In vitro reductionist assay	Infected cells	(Monette et al., 2020; Sengupta et al., 2019)

The Negri bodies formed during RABV infection were the first described liquid viral condensates to support genome transcription and replication (Lahaye et al., 2009; Nikolic et al., 2017, 2016). Ever since, other viruses were shown to organise functional condensates. For example, rotavirus assemble viral replication factories (Geiger et al., 2021), VSV, MeV and SARS-CoV-2 form compartments for genome transcription, replication, SARS-CoV-2 and IAV form condensates for genome assembly (in the case of SARS-CoV-2 and IAV) (Alenquer et al., 2019; Cascarina and Ross, 2022, 2020; Heinrich et al., 2018; Zhou et al., 2019), while HIV compartments are involved in genome and virion assembly (Krasnopolsky et al., 2019; Krishnamoorthy et al., 2003; Xue et al., 2012).

1.2.7 Phase transitions in IAV infection

The IAV entry factors HDAC6 and importin (TNPO-1) are known to respectively promote stress granule maturation (Saito et al., 2019) and disassembly of FUS condensates (Guo et al., 2018; Yoshizawa et al., 2020), serving as precedence for potential IAV-induced condensate

(patho)physiology. Importantly, during the later stage of IAV infection, nucleocytoplasmic shunt of vRNPs and its interaction with Rab11a results in the appearance of cytoplasmic punctae known as viral inclusions (Alenquer et al., 2019) that contain concentrate Rab11a and constitute hotspots, which concentrate different vRNPs. These inclusions were hypothesised to be involved in IAV genome assembly since different vRNPs increasingly colocalise with these condensates as they enlarge while being transported to the PM (Amorim, 2019; Chou et al., 2013; Haralampiev et al., 2020; Lakdawala et al., 2014; Ramos-Nascimento et al., 2017; Sousa et al., 2017; Vale-Costa et al., 2016b).

Our group showed that IAV inclusions lack delimiting membranes despite being enriched in a clusters of Rab11a vesicles and vRNPs akin to liquid condensates containing clusters of synaptic vesicles at synaptic junctions (Alenquer et al., 2019; Milovanovic et al., 2018). Interestingly, we also demonstrated that IAV inclusions share the liquid properties that are typical of biomolecular condensates (Alenquer et al., 2019). These includes the ability to fuse and divide, to rapidly exchange materials, to coalesce into sphere-like structures, and to react fast to several stimuli such as hypotonic shock (Hyp), 1,6-hexanediol (Hex) and Brefeldin A (Alenquer et al., 2019).

Up to this moment, we lack an in vitro reconstitution system and have been unable to designate the mechanism governing the formation of IAV liquid inclusions. However, we speculate that during IAV infection, vRNPs engage in multiple and distinct intersegment interactions bridging cognate vRNP-Rab11 units on flexible membranes leading to demixed viral inclusions (Chou et al., 2013; Gavazzi et al., 2013b; Haralampiev et al., 2020; Le Sage et al., 2020; Shafiuddin and Boon, 2019; Sugita et al., 2013). How demixing could promote formation of complete genomes and how these would be excluded from viral inclusions to reach the plasma membrane remains unknown.

Given that the material properties in IAV inclusions may be essential for genome assembly, which is a key step for the assembly and release of infectious progeny virions, we hereby propose that perturbing the material properties of IAV inclusions could provide an avenue for abrogating viral infection, thereby, serving as a novel antiviral strategy.

1.3 Final remarks

The maintenance of host-virus interaction is key for viral survival and evolution. Due to the limited number of proteins synthesized by viruses, they essentially depend on host cellular machinery to complete their life cycles (reviewed in (Amorim, 2019; Etibor et al., 2021)). While some cellular processes are co-opted (like receptor cues), others are suppressed or circumvented (such as innate immune responses) (reviewed in (Amorim, 2019; García-Sastre, 2017)). Many cellular processes occur in membrane bound organelles as well as membraneless biomolecular condensates (reviewed in (Alberti, 2017; Alberti et al., 2019; Banani et al., 2017; Hyman et al., 2014; Mittag and Pappu, 2022)). Similarly to classical organelles, viruses have been recently shown to also utilise or make *de novo* biomolecular condensates for functional compartmentalization of reactions as seen in **Figure 1.20** ((Alenquer et al., 2019; Cascarina and Ross, 2020; Heinrich et al., 2018; Zhou et al., 2019) reviewed in (Cascarina and Ross, 2022)).

Like many viruses, IAV utilizes the host cell machinery for replication. However, the presence of a segmented genome complicates its assembly process. Eight unique vRNPs must be packaged into the progeny virion for it to be infectious, making the assembly process complex and challenging ((Noda et al., 2018, 2006; Sugita et al., 2013) and reviewed (Noda and Kawaoka, 2010)). Since each genomic vRNA segment contains sites that facilitate cognate vRNA-vRNA interactions, the vRNPs were proposed to assemble by a selective instead of a random process ((Gog et al., 2007; Goto et al., 2013; Hutchinson et al., 2010; Lee et al., 2017; Williams et al., 2018) and reviewed in (Amorim, 2019)). Also, cytoplasmic vRNPs were shown to localize to liquid-like Rab11a-positive viral inclusions proposed to deliver assembled or assembling vRNPs to the PM (Amorim et al., 2011; Bhagwat et al., 2018; Chou et al., 2013; Lakdawala et al., 2014). A pertinent question that arises is therefore, whether biogenesis of viral inclusions and their material properties facilitate IAV genome assembly.

To resolve the cellular location where viral genome assembly takes place, two hypotheses emerged: ***dispersal*** and ***compartmentalization*** models (**Figure 1.21**) (Amorim, 2019). The dispersal model is based on reports showing that inclusions transiently collide with one another and become bigger while simultaneously allowing stochastic mixing of vRNPs enroute the PM (Chou et al., 2013; Dou et al., 2018; Eisfeld et al., 2011a; Gerber et al., 2014; Hutchinson and Fodor, 2013; Lakdawala et al., 2014; Pohl et al., 2016). However, an alternate mechanism may be justified due to the reduced recycling competence of Rab11a during infection (Amorim et al., 2011) and reports linking the ER to vRNP transport (Alenquer et al., 2019; de Castro Martin et al., 2017; Vale-Costa et al., 2016a). The compartmentalization model stems from the impairment of Rab11a recycling function due to either out-competition of its normal interactome (family interacting proteins (FIPs) (Vale-Costa et al., 2016b)) by viral protein (e.g. PB2) (Veler et al., 2022) or by activating unknown cellular pathways that re-route of Rab11a vesicles to inclusions (Alenquer et al., 2019; Sousa et al., 2017; Sílvia Vale-Costa and Amorim, 2016a).

Crucially, the later model is further supported by the characteristic liquid properties of IAV inclusions (Alenquer et al., 2019). Here, materials such as Rab11a aggregate and concentrate vRNPs to enhance vRNA-vRNA intersegment interactions in a small surface area per volume ratio, where assembly can progressively take place away from spurious non-viral RNA-RNA interaction in the large cytosolic volume. In either model, IAV inclusions are critical for viral genome assembly. To better understand the genome assembly process, it is therefore pertinent to unravel the cellular mechanisms driving IAV inclusion biogenesis. Importantly, abrogating these material properties of IAV inclusions may block viral replication and be pursued as a novel antiviral approach.

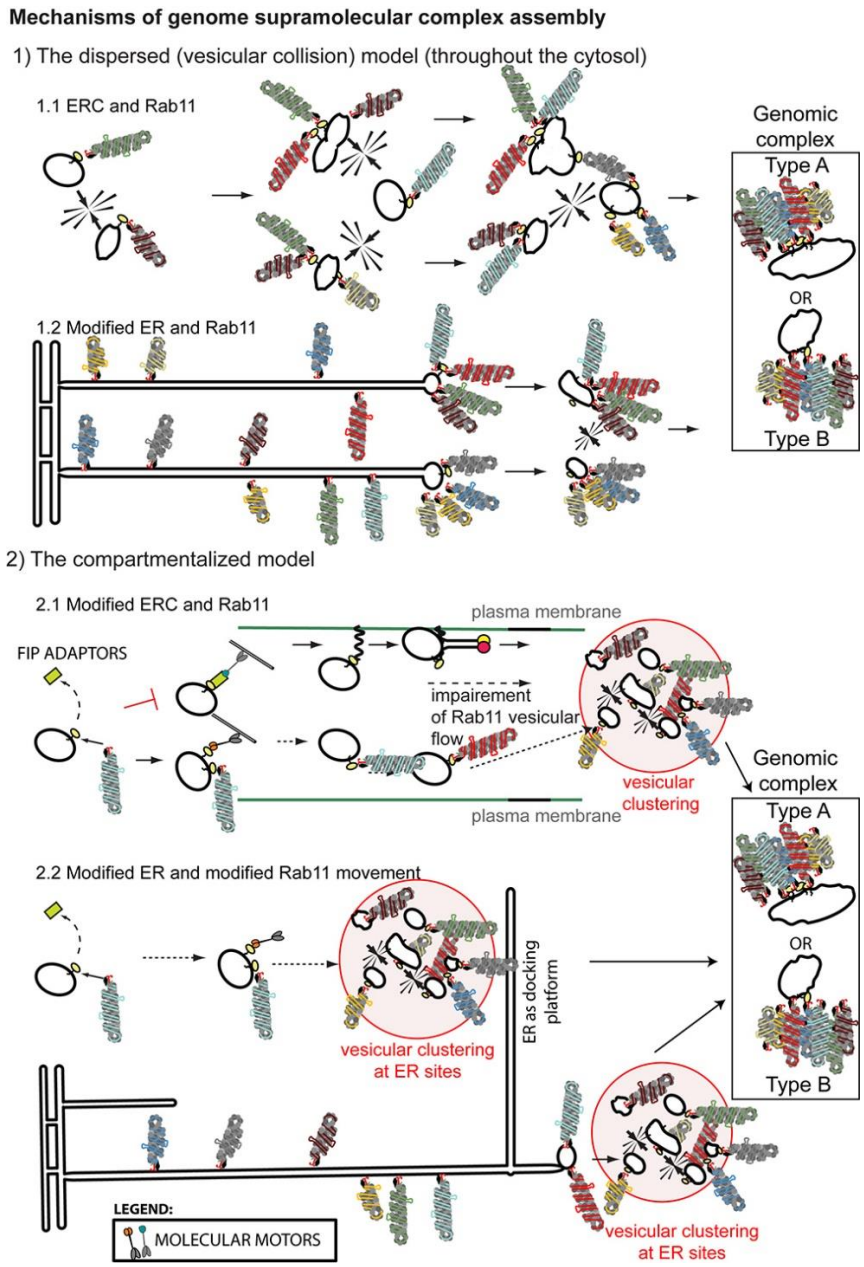

Figure 1.21- Schematics illustrating the mechanism of IAV genome supramolecular complex assembly

*In **model (1)**, the dispersed (vesicular collision) model proposes a genomic complex formation coupled to vRNP transport on Rab11-containing-vesicles. Here, inter-segment interactions would occur in a sequence-based manner*

as vesicles transition to the PM and collide to form of sub-bundles until a complete genomic complex is assembled (with eight different segments). In this model, vesicles may fuse (leading the genomic complex type A) or vRNPs could be transferred from one vesicle to the next by vesicular "kissing" events (genomic complex type B). The model assumes that type A and B differs in the number of molecules of Rab11 (with type A having at least 8 segments) and the size of the vesicles (with type A having enlarged structures). Several mechanisms are proposed based on the literature: ***(1.1)*** *Collision of endocytic recycling compartment (ERC) vesicles containing Rab11 and vRNPs could take place in the entire cytosol.* ***(1.2)*** *Collision of irregularly coated vesicles (containing vRNPs and Rab11) from IAV modified ER would take place close to the plasma membrane.* ***Model (2)*** *is a compartmentalized model, which predicts that IAV infection would induce the re-routing and/ or impairment of Rab11 pathway, leading to compartmentalization of different vRNP segments inside viral inclusions to facilitate viral genome assembly* ***(2.1)*** *in multiple docking platforms or* ***(2.2)*** *at precise cellular hotspots defined by the ER. Viral inclusions could be formed if vRNPs are transported: (A) on ERC vesicles to the ER or (B) attached to the ER and subsequently released onto Rab11 vesicles that are routed to the plasma membrane.* These images were published in *(Amorim, 2019)).*

1.4 Aims and general objectives

The overarching goal of this PhD project is to understand whether IAV viral inclusions are functional, for example to support genome assembly in a compartment, and whether the liquid properties are important for function. For simplicity, this PhD project is divided into three result chapters:

1.4.1 Chapter 2- The minimal molecular requirement for IAV inclusion biogenesis

Numerous studies have shown that IAV inclusions are enriched with host Rab11a and viral ribonucleoproteins (vRNPs). Using single molecule fluorescence *in situ* hybridization (smFISH), inclusions were shown to colocalize different vRNP types and proposed as sites facilitating intersegment vRNA-vRNA interactions. However, the contribution of individual IAV genomic segments in the biogenesis of inclusions has not been elucidated. Additionally, when Rab11a knock out (Rab11 KO) or Rab11a dominant negative (DN) cell lines are infected with IAV, inclusions are not formed and viral titre drops by at least 1 log, indicating that Rab11a as an essential host factor for inclusion biogenesis. We therefore probed the minimal viral genomic RNAs necessary to form inclusions in the presence of Rab11a. Since all vRNAs are known to colocalise in IAV inclusions, we would assess the relationship between intersegment interactions and inclusion emergence by determining the number of vRNA types that is required to form viral inclusions.

1.4.2 Chapter 3- Thermodynamics rules for hardening IAV inclusions

In the previous chapter, we identified the minimal vRNA requirements to form inclusions and established that inclusions formed by single or multiple vRNP types have liquid properties. In this thesis, we hypothesise that the liquid character is essential for function, ask the question whether it is possible to alter their material properties and aim at determining by which means. As

liquid condensates are known to be driven by key thermodynamics parameters (such as temperature, concentration, and number/strength of interaction), in this chapter, we will explore the thermodynamics rules that facilitates liquid inclusion biogenesis and their maturation. Importantly, this data will be used to determine the key thermodynamics drivers of inclusion hardening, which may serve as a potential novel antiviral approach.

1.4.3 Chapter 4- Solubility proteome profiling of liquid and hardened IAV inclusions

Next, we will assess the proteome-wide profile for proteins that change solubility upon infection, therefore assessing if there is a new layer in viral-host interactions that govern cellular function and that should be explored in the future. Due to density transition exhibited by biomolecular condensates, we expect molecules that are evenly distributed in the cytoplasm to show high solubility relative to the insolubility of molecules that partition into viral-induced cytoplasmic condensates such as IAV inclusions. Importantly, this screen would serve two purposes; to yield unknown proteins that may partition into inclusions and identify novel condensates and their molecular factors. We would validate this screen using cells (Rab11a-DN) able to release vRNPs into the cytosol but unable to form inclusions. Given that the multivalency-inducing antiviral (nucleozin) changes the biophysical properties of IAV inclusions by hardening, we will further assess the solubility profile of Rab11a-DN inclusions rescued by nucleozin.

Chapter 2 - The minimal molecular requirement for IAV inclusion biogenesis

2.1 Author contributions

The experiments presented in this chapter were designed and planned by Temitope Akhigbe Etibor and Maria João Amorim. All experiments and data generated were performed by Temitope Akhigbe Etibor. Temitope Akhigbe Etibor wrote the chapter with Maria João Amorim supervision. Some sections of this chapter are part of a published manuscript which can be assessed from:

Alenquer M, Vale-Costa S, **Etibor TA**, Ferreira F, Sousa AL, Amorim MJ. Influenza A virus ribonucleoproteins form liquid organelles at endoplasmic reticulum exit sites. Nature Communications. (2019) 9;10(1):1629. doi: 10.1038/s41467-019-09549-4. PMID: 30967547; PMCID: PMC6456594. The rest of the data will be published soon.

2.2 Summary

Influenza A virus has an eight-partite RNA genome that during viral assembly forms a complex containing one copy of each RNA in the form of viral ribonucleoproteins (vRNPs). This is an essential process as infectious particles must contain eight RNPs and one of each kind. IAV genome assembly is a selective process driven by vRNA-vRNA interactions and is hypothesized to lead to discrete punctate structures (known as viral inclusions) scattered through the cytosol. Here, we show that contrary to the accepted view, formation of IAV inclusions precedes genomic vRNA-vRNA interactions among distinct vRNPs, as they assemble in cells expressing only one vRNP type.

Importantly, we demonstrated that inclusions formed by one vRNP type phenocopies the behaviour of infection-derived inclusions. These inclusions display characteristics of liquid organelles, segregating from the cytosol without a delimitating membrane, dynamically exchanging material and adapting fast to environmental changes. We hereby propose that viral inclusions segregate vRNPs from the cytosol to facilitate selected vRNA-vRNA interactions in a liquid environment.

2.3 Introduction

Influenza A infection is a serious threat to human health, causing annual epidemics, and occasional pandemics (reviewed in (Kumar et al., 2018)). The virus contains an eight-partite RNA genome, with each segment encapsidated as an individual viral ribonucleoprotein (vRNP) complex. vRNPs are composed of single-stranded negative-sense RNA, with base paired terminal sequences originating a double-stranded RNA portion to which binds the RdRp. The remaining sequence attaches several copies of unevenly bound nucleoprotein (NP) (Lee et al., 2017). The advantages of having a segmented genome are evident for viral evolution (reviewed in (Lowen, 2017)) and for better gene expression control (reviewed in (Belshaw et al., 2008)), but increase the complexity of the assembly of fully infectious virions ((Noda et al., 2018) and reviewed in (Ferhadian et al., 2018)).

Viral assembly occurs at the plasma membrane (**Figure 2.1**). For an influenza particle to be fully infectious, the eight vRNPs must be packaged in a virion ((Nakatsu et al., 2016; Noda et al., 2018, 2006) and reviewed in (Noda, 2012; Noda and Kawaoka, 2010)). Virions do not usually package more than eight segments (**Figure 2.1**) (Nakatsu et al., 2016) and each segment generally occurs once per virion. In agreement, full-length segments compete with corresponding segments that have internal deletions, known as defective interference particles (Davis et al., 1980; Duhaut and Dimmock, 1998; Duhaut and Mccauley, 1996). Together, the data indicate that vRNP segments of the same type do not interact. At the budding sites, complexes of eight interlinked vRNPs have been imaged (**Figure 2.1**), meaning that, at some point during infection, a selective process allows the eight segments to self-assemble via intersegment vRNA-vRNA interactions ((Hutchinson et al., 2010; Lee et al., 2017; Noda et al., 2018; Williams et al., 2018) and reviewed in (Ferhadian et al., 2018)). However, it is under debate whether vRNPs reach the plasma membrane already as complete genome bundles.

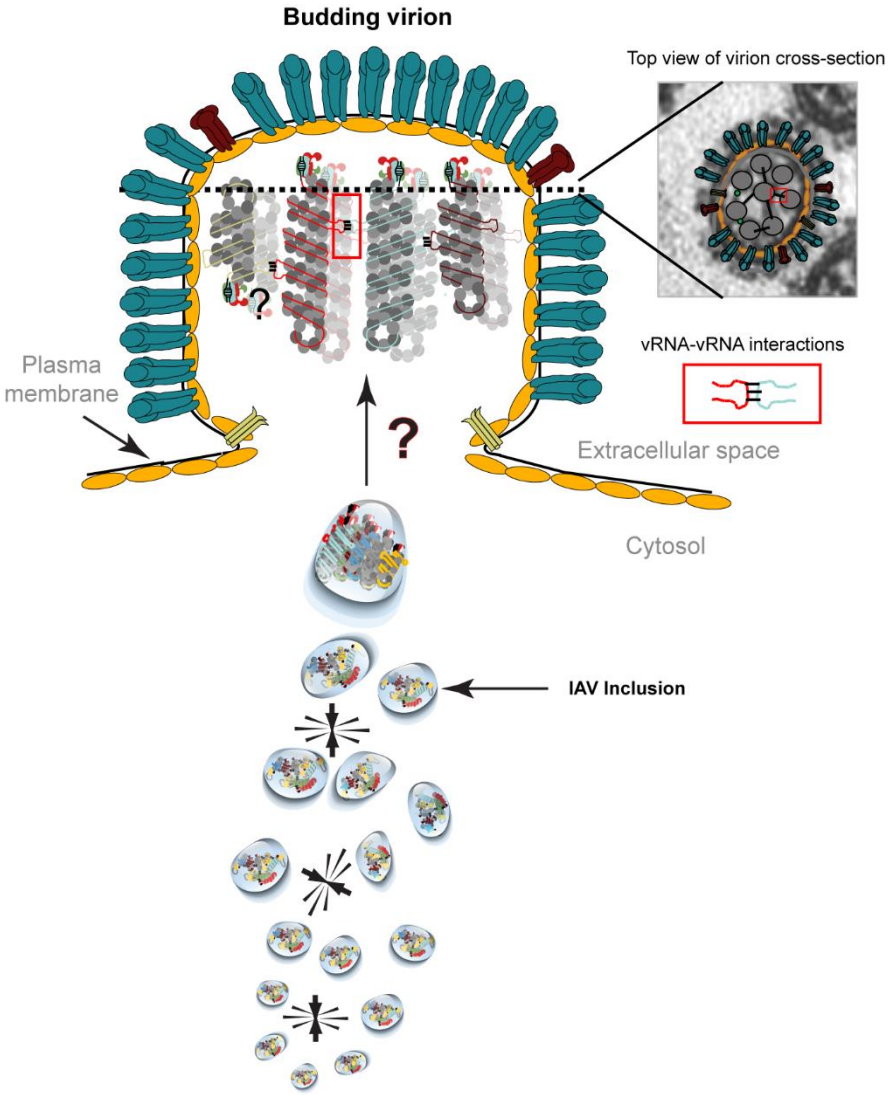

Figure 2.1- Schematics of a proposed model of IAV genome and virion assembly.

vRNP-rich IAV inclusions exchange materials enroute the budozone where they are packaged into virions as an interacting supramolecular complex (red rectangles). This image was adapted from *(Amorim, 2019) publication.*

After viral replication, vRNPs are exported from the nucleus, reach the cytosol and concentrate with Rab11a to form viral inclusions that distributes

throughout the cytoplasm and increase in area as infection progresses (Amorim et al., 2011; Bruce et al., 2010; Chou et al., 2013; Eisfeld et al., 2011a; Lakdawala et al., 2014; Momose et al., 2011, 2007; Nturibi et al., 2017; Vale-Costa et al., 2016b). Each inclusion accommodates different vRNP segments, with higher co-localisation amongst different vRNPs as inclusions get closer to the plasma membrane (Lakdawala et al., 2014). These observations (Chou et al., 2013; Lakdawala et al., 2014; Nturibi et al., 2017; Vale-Costa et al., 2016b; Sílvia Vale-Costa and Amorim, 2016a) led to the proposal that genome assembly precedes vRNP packaging into budding virions by a process linked with the formation of the viral inclusions.

Studies on the biogenesis of IAV inclusions showed that their formation required the cellular GTPase Rab11a (Amorim et al., 2011; Bruce et al., 2010; de Castro Martin et al., 2017; Eisfeld et al., 2011a; Lakdawala et al., 2014; Lopez et al., 2021; Momose et al., 2011; Nturibi et al., 2017). In uninfected cells, Rab11 is the master regulator of the endocytic recycling compartment (ERC), a system used for delivering endocytosed material and specific cargo from the trans-Golgi network (TGN) to the cell surface. Rab11a-GTP regulates ERC transport by recruiting molecular motors, tethers, and SNAREs to, respectively, drive, dock, and fuse vesicles to the PM (reviewed in (Sílvia Vale-Costa and Amorim, 2016b)).

Despite initial reports showing that the role of Rab11a was to deliver vRNPs to the cell surface (Amorim et al., 2011; Avilov et al., 2012a; Bruce et al., 2010; Chou et al., 2013; Eisfeld et al., 2011a; Lakdawala et al., 2014; Momose et al., 2011; Nturibi et al., 2017), accumulating evidence strongly indicates that Rab11 trafficking is impaired during IAV infection (de Castro Martin et al., 2017; Kawaguchi et al., 2015; Vale-Costa et al., 2016b). In agreement, competition assays in cells or by *in vitro* binding assays demonstrated that vRNPs can outcompete Rab11a effectors for Rab11a binding, rendering the recycling process sub-optimal (Kawaguchi et al., 2015;

Vale-Costa et al., 2016b; Veler et al., 2022). Further corroborating the scenario that Rab11 pathway is impaired by infection, recent publications suggested that Rab11 was re-routed to the ER during IAV infection (de Castro Martin et al., 2017). The redistribution of Rab11a during infection, changing from discrete to enlarged puncta can be observed by correlative light and electron microscopy (CLEM). Here, sites that are not delimited by membranes, but consisting of clustered vesicles observed by electron microscopy matched well with Rab11 and vRNPs staining observed by fluorescence microscopy. Altogether, the data indicates that viral inclusions constitute hotspots of vRNPs (Vale-Costa et al., 2016b).

The formation of viral inclusions was postulated in a dispersal model to be dependent on the establishment of sequential vRNA-vRNA interactions occurring as Rab11a vesicles transporting vRNPs collided (Chou et al., 2013; Lakdawala et al., 2014; Nturibi et al., 2017). However, impairment of endocytic recycling and the ability to use the ER, ERES and the ER-Golgi cycling for inclusions formation argues against this hypothesis but supports the compartmentalization model of IAV genome assembly. Nevertheless, the existence of vRNP-Rab11a inclusions indicates segregation from the cytosol akin to liquid-like condensates, in the sense that they are not delimited by membranes, are dynamic, able to fuse and divide, and dissolve upon shock ((Brangwynne et al., 2009) and reviewed in (Hyman et al., 2014)).

Importantly, IAV inclusions were previously shown to colocalise with different vRNP species (Amorim et al., 2011; Chou et al., 2013; Lakdawala et al., 2014; Nturibi et al., 2017). We therefore asked if these inclusions are precursors or consequences of intersegment vRNP-vRNP interactions. Since, this hypothesis results from an infection system which contains all 8 vRNP segments, it is pertinent to determine whether intersegment interactions drive formation of viral inclusions or otherwise. We therefore explored the minimal vRNP requirements necessary to form IAV inclusions. For this, we used a mini-replicon system to express one or two vRNPs and

test if viral inclusions are formed. Our expectation was that if viral inclusion formation required inter-segment interactions, then expressing one single vRNP would result in failure to form viral inclusions. Conversely, should one vRNP type be sufficient to form inclusions, we hypothesised that intersegment interactions are not necessary for inclusion formation (**Figure 2.2**).

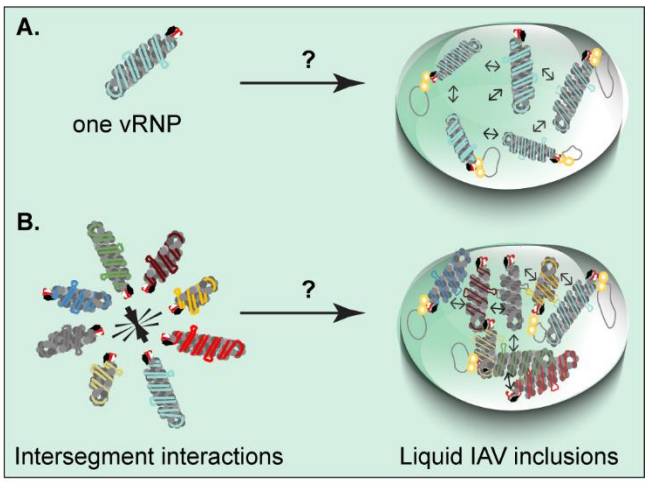

Figure 2.2- Schematics for testing the hypothesis that IAV inclusions originate due to intersegment interactions.

*Proposed model that **(A)** one vRNP type is sufficient to form viral inclusions, or **(B)** intersegment interactions precede IAV inclusion formation.*

In this work, we demonstrated that viral inclusions are formed when a single vRNP type is expressed in a cell. Furthermore, single vRNP inclusions display liquid properties akin to infected cells that express all 8 vRNP segments. Therefore, we postulate that viral inclusions are not formed by intersegments interactions established *a priori*, but their biogenesis precedes and facilitates stochastic vRNP–vRNP interactions in a liquid environment of crowded vRNPs.

2.4 Results

2.4.1 IAV inclusions form when a single vRNP type is expressed.

To address the question of whether viral inclusion formation requires inter-segment interactions, we assessed the formation of vRNP hotspots and the subcellular distribution of Rab11a in a mini-replicon system expressing a single segment type (i.e. segment 7 or 8) of influenza A/Puerto Rico/34/8 virus (PR8) (**Figure 2.3**). It is well established that vRNPs from the same type compete for packaging into virions, and, therefore, do not interact (Duhaut and Mccauley, 1996; Inagaki et al., 2012; Venev and Zeldovich, 2013). As positive control, we used cells expressing two types of PR8 vRNPs, segments 7 and 8, previously shown to form viral inclusions (Amorim et al., 2011).

Cells were transfected with plasmids expressing the RdRp (3P: PB1, PB2, PA) and a 4:1 mixture of NP:GFP-NP to make 3P-NP that supports vRNA replication. To make vRNA, pPolI plasmids of segment 7 or 8 (that expresses NS1 and NS2) were added and co-transfected with NS2 and M1 protein encoding plasmids respectively, which permits nucleocytoplamic egress of newly synthesized vRNPs. Positive controls were transfected with both pPolI plasmids for segments 7 and 8 and 3P-NP plasmids. This mini-replicon has been validated before, by showing that vRNPs incorporated GFP-NP, and that complete vRNPs were exported from the nucleus, colocalizing with vRNA from all segments (Amorim et al., 2011).

The way that the system works in brief is as follows: segment transcription originates a complete negative-sense vRNA to which NP and the RdRp bind, amplifying the system and mimicking viral transcription and replication. For negative control, we established the same system, but deficient in vRNA replication due to polymerase PB2 deficit (2P-NP). Alternative negative controls include segment 7 or 8 vRNA (with 3P-NP) replication competent system that lacks the corresponding NS2 or M1 proteins respectively, which result in nuclear accumulation of vRNPs (that are

unable to exit the nucleus). In another negative control, all helper plasmids that support replication and nucleocytoplasmic egress of vRNPs were expressed but the system lacks pPolI plasmids for both segment 7 and 8 vRNAs.

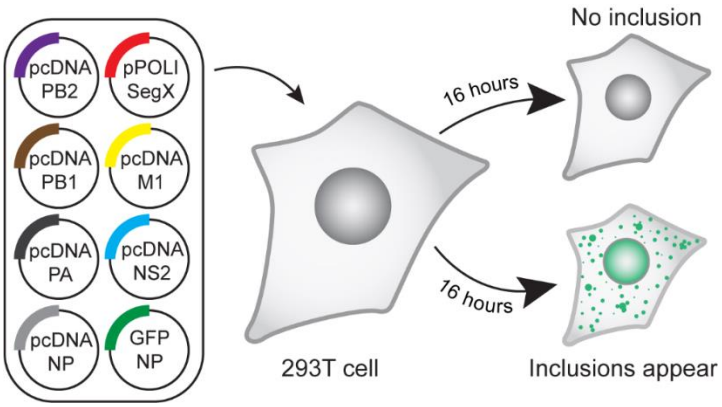

Figure 2.3- Experimental scheme of plasmid-based minireplicon assay.

To recapitulate infection-like inclusions in a system expressing only one genomic vRNA type, we transfected cells with plasmid (pPolI-SegX) encoding one vRNA type (vRNA-X). For nuclear transcription and replication of the vRNA (vRNA-X), cells were co-transfected with plasmids (pcDNA-PB1, pcDNA-PB2 and pcDNA-PA) encoding the three polymerase proteins which are the minimal protein components of an influenza vRNP. Additionally, plasmids encoding IAV proteins (pcDNA-NS2 and pcDNA-M1) which facilitate vRNA nuclear export were co-transfected with GFP-NP expressing plasmids that served as a proxy for inclusion localization.

In the present study, we confirmed that the system was fully functional by western blotting, immunofluorescence imaging and fluorescence *in situ* hybridization (FISH) (**Figure 2.4 - Figure 2.7**). The expression of all components of the mini-replicon, in each condition, was evaluated by Western blotting, except that of NS2, for which no good commercial antibody

is available (**Figure 2.4**). As expected, the expression of the proteins of a specific segment was detected only in 3P-NP samples (**Figure 2.4**).

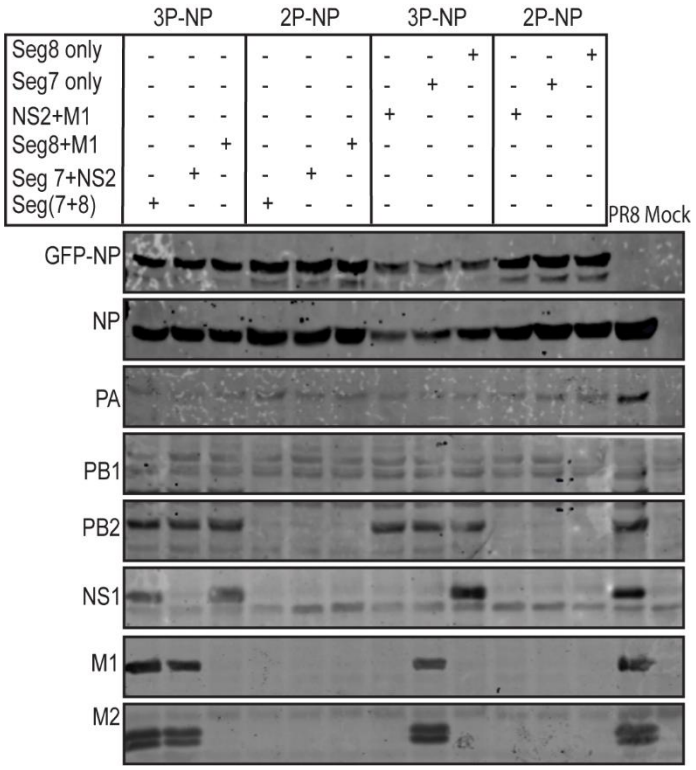

Figure 2.4- Western blot of minireplicon assay.

In a plasmid-based minireplicon assay, 293T cells were transfected for 16 hrs with plasmid(s) encoding one and/ or two IAV genomic vRNA type (Seg 7 and/ or Seg8), replication and transcription proteins such as the RdRp (PB1, PB2, PA), NP (and GFP-NP) and nuclear export proteins (M1 and NS2). Negative controls lacked at least one polymerase protein (PB2) or nuclear export protein (M1 or NS2). 16 hours post-transfection, cells were lysed, and the indicated proteins were detected for western blotting, with PR8- and mock-infected cells serving as positive and negative reference controls.

We then investigated Rab11 subcellular distribution by immunofluorescence and observed that it did not change in any of the 2P-NP conditions as well as in other negative control systems, consistently with

previous reports (**Figure 2.5**B-D) (Amorim et al., 2011). However, in the 3P-NP condition, Rab11 redistributed, forming the characteristic enlarged puncta regardless of expressing one or two vRNPs, indicating that one vRNP type is sufficient to form viral inclusions (**Figure 2.5**A).

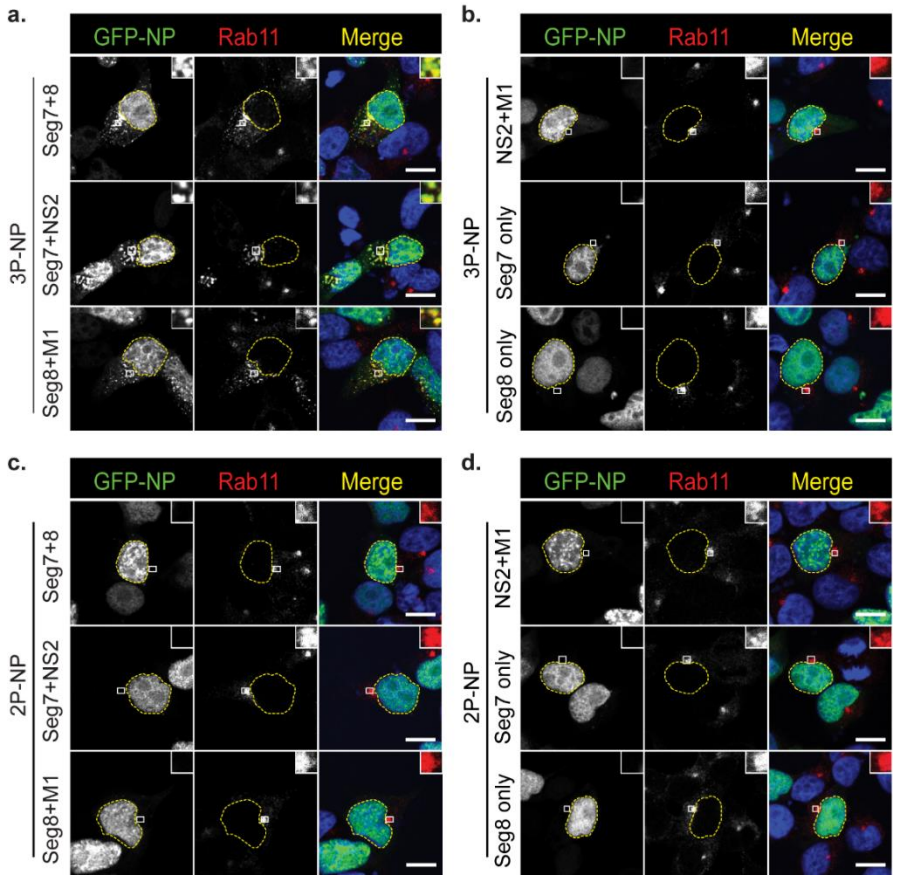

Figure 2.5 - Immunofluorescence images showing that viral inclusions form in the absence of intersegment vRNA interactions.

293T cells were transfected for 16 hrs with the minimal protein components of an influenza vRNP; the three polymerase proteins (3P), ***(A)****, (or, as a non-functional control expressing either two polymerase proteins lacking PB2 - 2P,* ***(C, D)****, or 3P, and 2P, lacking a vRNP nuclear export protein- M1 or NS2*

***(B, D)**) and NP, as well as with plasmids expressing GFP-NP. Cells were fixed and stained for Rab11 (red). Furthermore, cells were transfected with plasmids expressing vRNA from segments 7 and 8, or segment 7 or 8 alone with- a plasmid encoding NS2 or M1 respectively or expressing no segment together with plasmid encoding NS2 and M1 proteins. White boxes show areas of co-localization between NP and Rab11. Nuclei are delineated by yellow dashed lines. Bar = 10 µm.*

The areas of Rab11 puncta, when one or two vRNPs were expressed, were significantly different between the 3P-NP and 2P-NP conditions, when quantified, and ranked based on their size: small inclusions up to 0.15 µm^2, intermediate inclusions between 0.15 and 0.30 µm^2, and large inclusions over 0.30 µm^2 (**Figure 2.6**A,B), as before (Vale-Costa et al., 2016b). Consistent with our work, in the absence of NS2 or M1 in segment 7 and segment 8 conditions respectively expressing 3P-NP, vRNPs were retained in the nucleus and Rab11 distribution was similar to that of 2P-NP condition (**Figure 2.6**A,B).

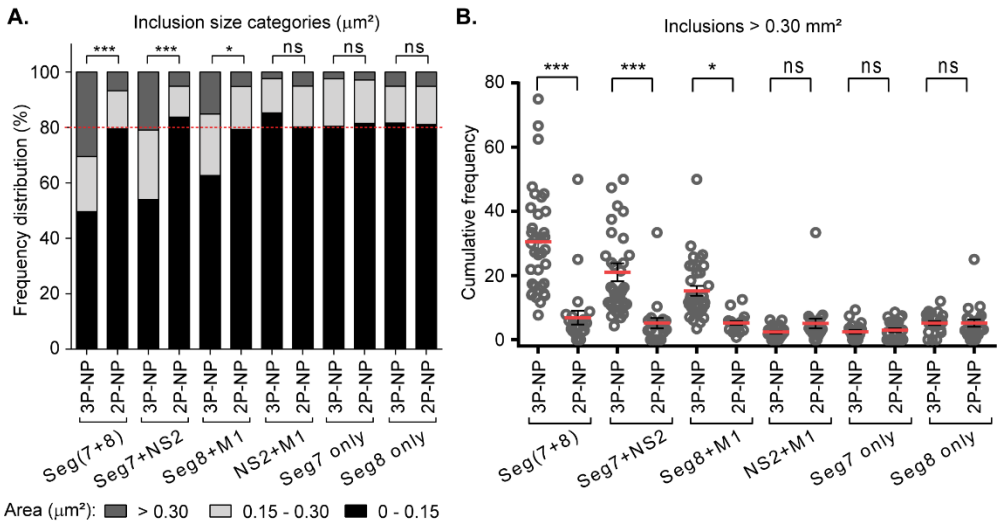

Figure 2.6- Size categories and quantification of minireplicon inclusions in a minireplicon setup.

*Rab11 Inclusions from **Figure 2.5** were segmented and quantitatively analysed. Statistical analysis of data was performed using a non-parametric Kruskal–Wallis test, followed by Dunn's multiple comparisons test (***p < 0.001). Between 30 and 70 cells were analysed per condition and 3 independent experiments were performed. **(A)** The frequency distribution of Rab11 inclusions within the three area categories (in μm^2) was plotted for each condition. **(B)** Cumulative frequency of Rab11 inclusions with area greater than 0.30 μm^2 was plotted for each condition. The red line is the median cumulative frequency.*

Finally, we assessed the distribution of segment 7 and 8 RNA by fluorescent *in situ* hybridization (FISH). In the case of 2P-NP conditions, probes against the vRNA of segments 7 or 8 detected discrete dots in the nucleus (**Figure 2.7**B), consistent with DNA polymerase I transcription but absence of amplification, as described before (Amorim et al., 2011). In the case of 3P-NP, and independently of the number of segments expressed, vRNAs of each type were detected in enlarged puncta, and co-localized between them (when expressed together) and with NP, showing that vRNP hotspots are formed without requiring RNA interactions among distinct segments (**Figure 2.7** A). However, 3P-NP conditions expressing segment 7 vRNA (without NS2), 8 vRNA (without M1), or a combination of NS2 and M1 proteins only, phenocopies the 2P-NP conditions, which failed to produce viral inclusions (**Figure 2.7**C).

Collectively, the results obtained demonstrate that viral inclusions assemble in the presence of a single vRNP type. The data also indicate that formation of Rab11 enlarged puncta is dependent on vRNPs reaching the cytosol but precedes and does not require vRNA-vRNA intersegment interactions.

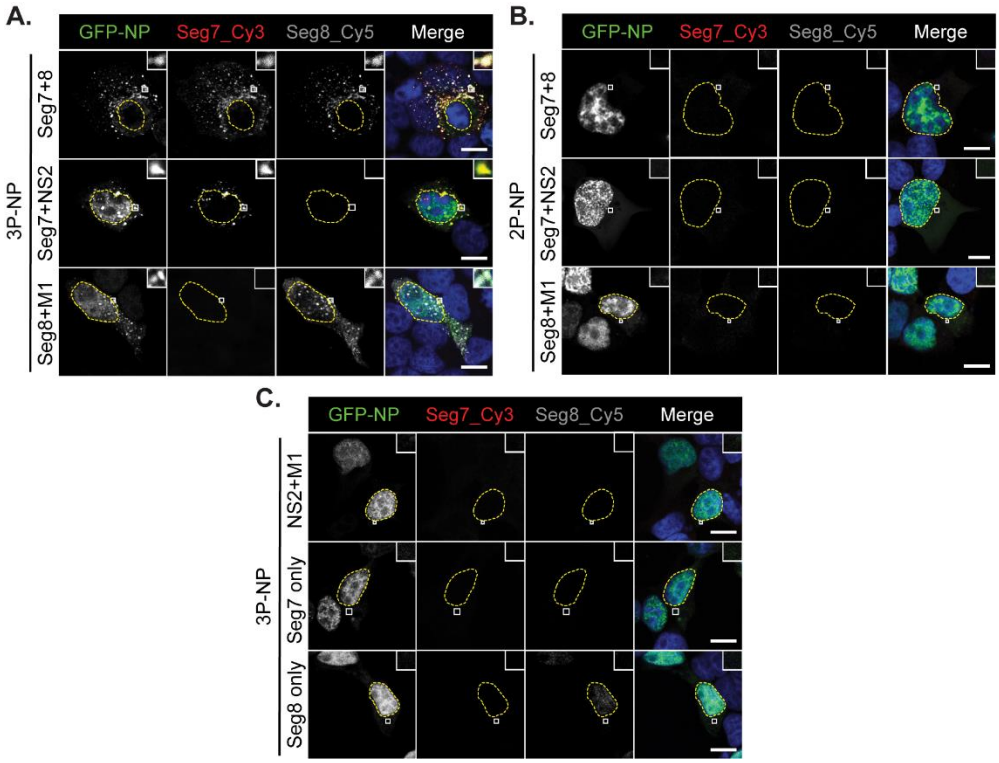

Figure 2.7- Fluorescence in situ hybridization (FISH) images of minireplicon system.

Minireplicon assay was done as described in ***Figure 2.5****, and duplicate samples were processed to detect segment 7 (Cy3, red) and segment 8 (Cy5, gray) vRNA by fluorescence in situ hybridization (FISH). Insets (White boxes) show areas of co-localization between NP (GFP-NP as proxy) and viral segments. Nuclei are delineated by yellow dashed lines. Bar = 10 µm.* ***(A)*** *Cells expressing segment 7 and /or 8 vRNA(s) with all RdRp (PB1, PB2, PA) forming viral inclusions* ***(B)*** *Cells expressing segment 7 and /or 8 vRNA(s) in the absence of one RdRp (PB2) do not form viral inclusions.* ***(C)*** *Cells*

expressing segment 7 or 8 vRNA only, or viral export protein (NS2 and M1) only, with all RdRp subunits (PB1, PB2, PA) do not form inclusions.

2.4.2 Single vRNP inclusions are non-membrane delimited condensates.

Numerous studies have demonstrated phase transition as a biophysical mechanism for the emergence of cellular and virus-induced biomolecular condensates, which are enriched in nucleic acids and proteins (reviewed in (Etibor et al., 2021; Hyman et al., 2014)). These condensates were shown to lack a delimiting membrane (Alenquer et al., 2019; Caragliano et al., 2022a; Cascarina and Ross, 2020, 2022; Geiger et al., 2021; Heinrich et al., 2018; Iserman et al., 2020a; Nikolic et al., 2017; Zhou et al., 2019). In fact, our lab revealed that IAV infection induced vRNP-enriched vesicular clusters of heterogeneous sizes (Vale-Costa et al., 2016b), which were recently renamed as irregularly coated vesicles (de Castro Martin et al., 2017). Of note, these inclusions were not membrane delimited (Alenquer et al., 2019).

In the present study, we showed that inclusion biogenesis precedes and does not require intersegment interactions. We assessed if the inclusions formed by single vRNP share similar ultrastructural traits to inclusion formed during IAV infection. Using correlative light and electron microscopy (CLEM) we examined the inclusions formed with our established minireplicon system (**Figure 2.8**) consisting of segment 7 vRNA, NS2 and 3P-NP proteins and compared it to the positive control (GFP-NP transfected and PR8 infected cell (**Figure 2.9**).

As previously reported in PR8 infected and GFP-NP transfected cells, we were able to recapitulate vRNP enriched clusters of Rab11 vesicles, which concentrate in non-membrane delimited inclusions (**Figure 2.9**). Similarly to infected cells expressing all eight vRNAs, we observed that the minireplicon system expressing only segment 7 vRNA display areas of clustered vesicles,

which were not delimited by a membrane(**Figure 2.8**). This suggests that single vRNP inclusions are formed independently of the vRNA-vRNA interactions, representing the ultrastructure of infection-derived inclusions, which lack membrane delimitation.

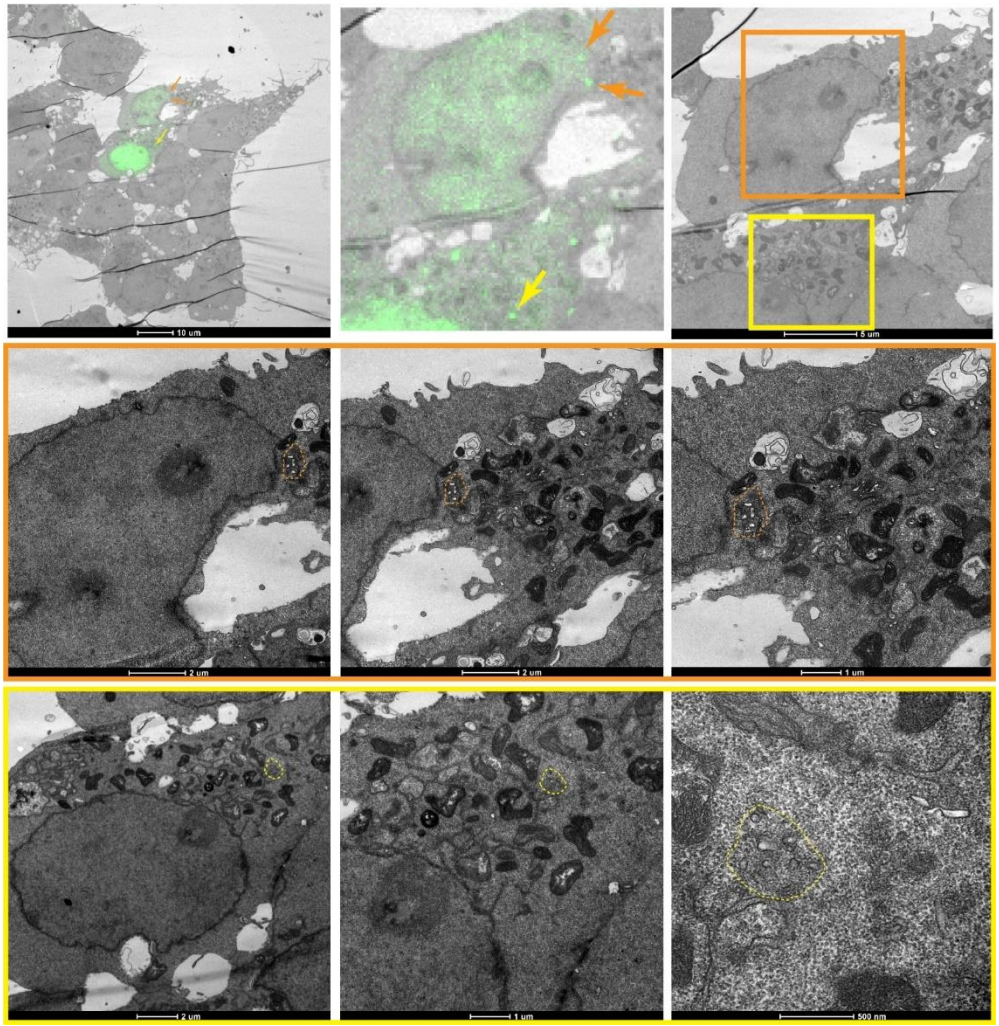

Figure 2.8- Correlative light and electron microscopy (CLEM) of inclusions originating from single vRNP type.

293T cells were transfected with minireplicon plasmids that would only express segment 7 vRNP together with GFP-NP (for CLEM) for 16 hours. Insets (orange and yellow) are the cells where inclusions were imaged, and

dotted ellipses (orange and yellow) show viral inclusions origination from segment 7 vRNP only. The inclusions consist of non-membrane delimited clustered Rab11 vesicles and electron dense vRNPs.

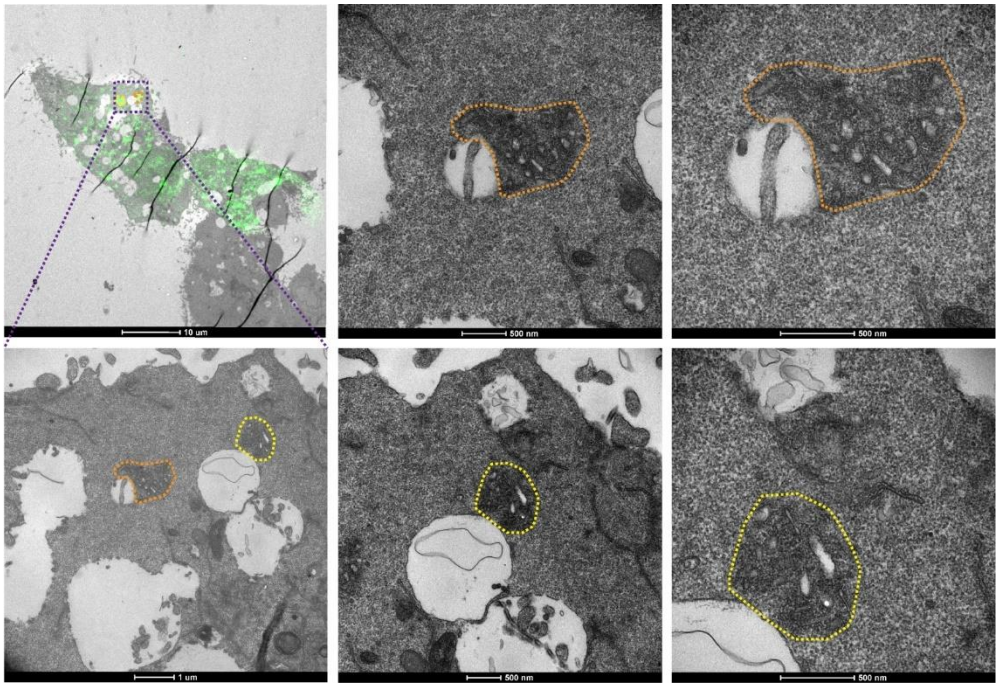

Figure 2.9- Correlative light and electron microscopy (CLEM) of PR8 infected inclusions.

293T cells were PR8-infected and transfected with GFP-.NP (for CLEM) for 16 hours. The dotted ellipses (orange and yellow) show the non-membrane bound viral inclusions originating from infection. IAV inclusions are enriched with Rab11 vesicles clusters and electron dense vRNPs.

2.4.3 Single vRNP inclusions display properties of liquid organelles.

Amongst other types of phase transitions, a number of membraneless biomolecular condensates were shown to emerge by liquid–liquid phase separation and have liquid-like properties (reviewed in (Hyman et al., 2014)). These liquid-like properties include deformability promoted by fusion and

fission events, quick response to stimuli, dynamic exchange of material, ability to internally reorganize and rounded shape (reviewed in (Alberti and Hyman, 2021; Banani et al., 2017; Hyman et al., 2014; Shin and Brangwynne, 2017)). Similar properties were shown for SARS-CoV-2 condensates, Negri bodies and viroplasms formed during rabies and vesicular stomatitis viral (VSV) infections and measles, replication factories of rotavirus and human cytomegalovirus (hCMV), etc. (Caragliano et al., 2022a; Carlson et al., 2020; Cascarina and Ross, 2022; Chen et al., 2020; Geiger et al., 2021; Heinrich et al., 2018; Iserman et al., 2020a; Nikolic et al., 2017; Savastano et al., 2020), and it was postulated that other viral factories or viral inclusions may assemble by liquid–liquid phase separation.

Interestingly, our laboratory showed that the IAV inclusions express similar phenotype (Alenquer et al., 2019) leading us to probe when this behaviour was initiated. Having demonstrated that cytoplasmic intersegment vRNP interactions is contingent on the formation of non-membrane delimited inclusions, we hypothesise that single vRNP inclusions (enriched with an association of multiple identical vRNP type) have inherent liquid properties to support subsequent vRNP-vRNP interactions. To formally validate this notion, we used two strategies for monitoring their dynamic nature and properties in live cells. First, we captured the movement and fusion-fission dynamics of single type vRNP inclusions. Second, we enquired their adaptability to shock treatments.

To analyse the dynamics of single vRNPs, we used the segment 7 minireplicon system. 293T cells were transfected with plasmids expressing segment7 vRNA and 3P-NP and NS2 proteins and compared it to positive controls expressing two vRNA types (segments 7 and 8). Careful analyses revealed many fusion and fission events amongst individual inclusions at varying distances (**Figure 2.10**), which indicates constant exchange of material and deformability. After fusion or fission events, viral inclusions reacquired a rounded shape (**Figure 2.10**), indicating occurrence of internal rearrangements. Furthermore, these inclusions appear to be constantly

exchanging material amongst them (**Figure 2.10**), postulated to be an essential trait to promote viral genome assembly.

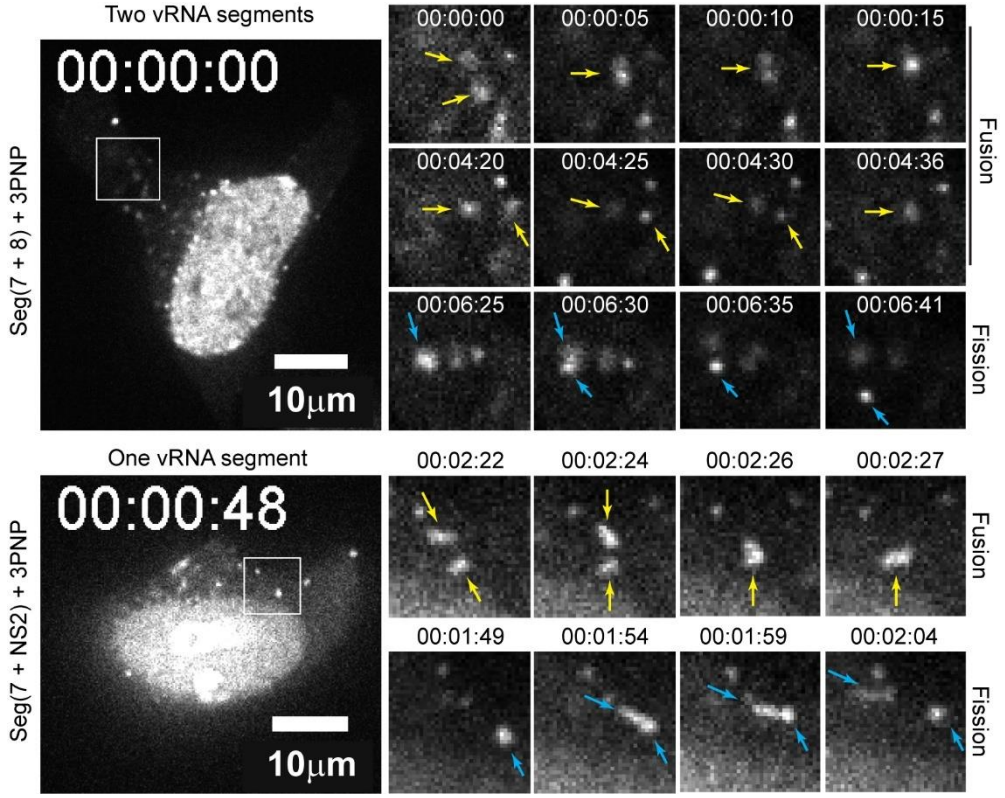

Figure 2.10- Inclusions composed of one or two vRNP type can fuse and divide.

293T cells were transfected with plasmid(s) encoding one (segment 7, with nuclear export protein NS2) or two (segments 7 and 8) IAV genomic vRNA type(s) together with plasmids encoding RdRp (PB1, PB2, and PA), NP and GFP-NP. 16 hours post-transfection, fission (yellow arrow) and fusion (blue arrow) dynamics of the inclusions (GFP-NP, as proxy) were tracked by live imaging. Scale Bar = 50 µm.

To investigate how single vRNP inclusions react to physiological changes, we subjected them to the well-established hypotonic and

hexanediol shock treatments and assessed their adaptation to shock according to **Figure 2.11.**

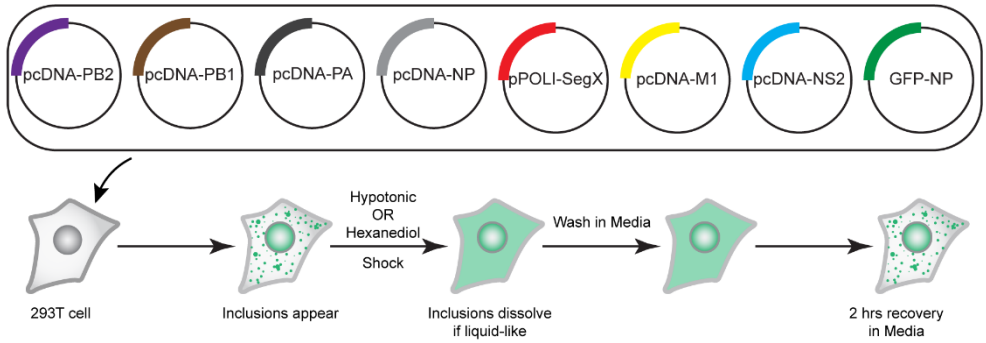

Figure 2.11- Experimental scheme of minireplicon-derived inclusion adaptation to shock treatments.

Model of inclusions formed via plasmid-based minireplicon assay respond after hypotonic or 1,6-hexanediol shock treatments. Liquid inclusions are expected to dissolve and reappear in the presence and absence of shock treatments respectively.

293T cells expressing minireplicon plasmids able to synthesize at least one vRNP (Segment 7 and NS2 protein, or segment 8 and M1 protein, or both segments 7 and 8; with all expressing 3P-NP) to form inclusions were exposed to a 10 mins hypotonic shock (ionic strength changing from 150 to 30 mM by diluting media with water), fixed, and imaged by confocal microscopy. As observed in infection-derived inclusions (Alenquer et al., 2019), single vRNP inclusions dissolve and were no longer visible after hypotonic shock (**Figure 2.12**). This effect was reversible as upon substitution of hypotonic solution by normal media for 2 h, inclusions were reformed (**Figure 2.12)**.

In the same minireplicon system, upon 5% 1,6-hexanediol treatment, we observed some cell blebbing, which was absent with hypotonic shock.

However, this has been described as a normal consequence of this treatment, and noted that it does not cause cell death, as cells recover upon washing out hexanediol (Kroschwald et al., 2017). Prolonged incubations with hexanediol are, nevertheless, toxic to the cells and lead to aberrant appearance of stress structures promoted by cell shrinkage (Kroschwald et al., 2017). Therefore, we treated cells only for 30 min with 5% hexanediol before fixing them for quantifications, or before allowing cells to recover by washing out hexanediol and replacing with media (**Figure 2.12**A,B). Like hypotonic shock, hexanediol treatment resulted in dissolution of inclusions which reappeared after 2h recovery in normal media (**Figure 2.12**A,B).

The ability of IAV inclusions to react to hypotonic dilution and to hexanediol treatment suggests they are liquid condensates (Kroschwald et al., 2017; Nott et al., 2015). Together, these data reveal that single vRNP inclusions, containing both Rab11 and vRNPs, can respond to changes in the cellular environment and their constituents can self-organize into fluxional structures in live cells. In sum, the data indicate that single type vRNP form inclusions that are dynamic and react quickly to stress.

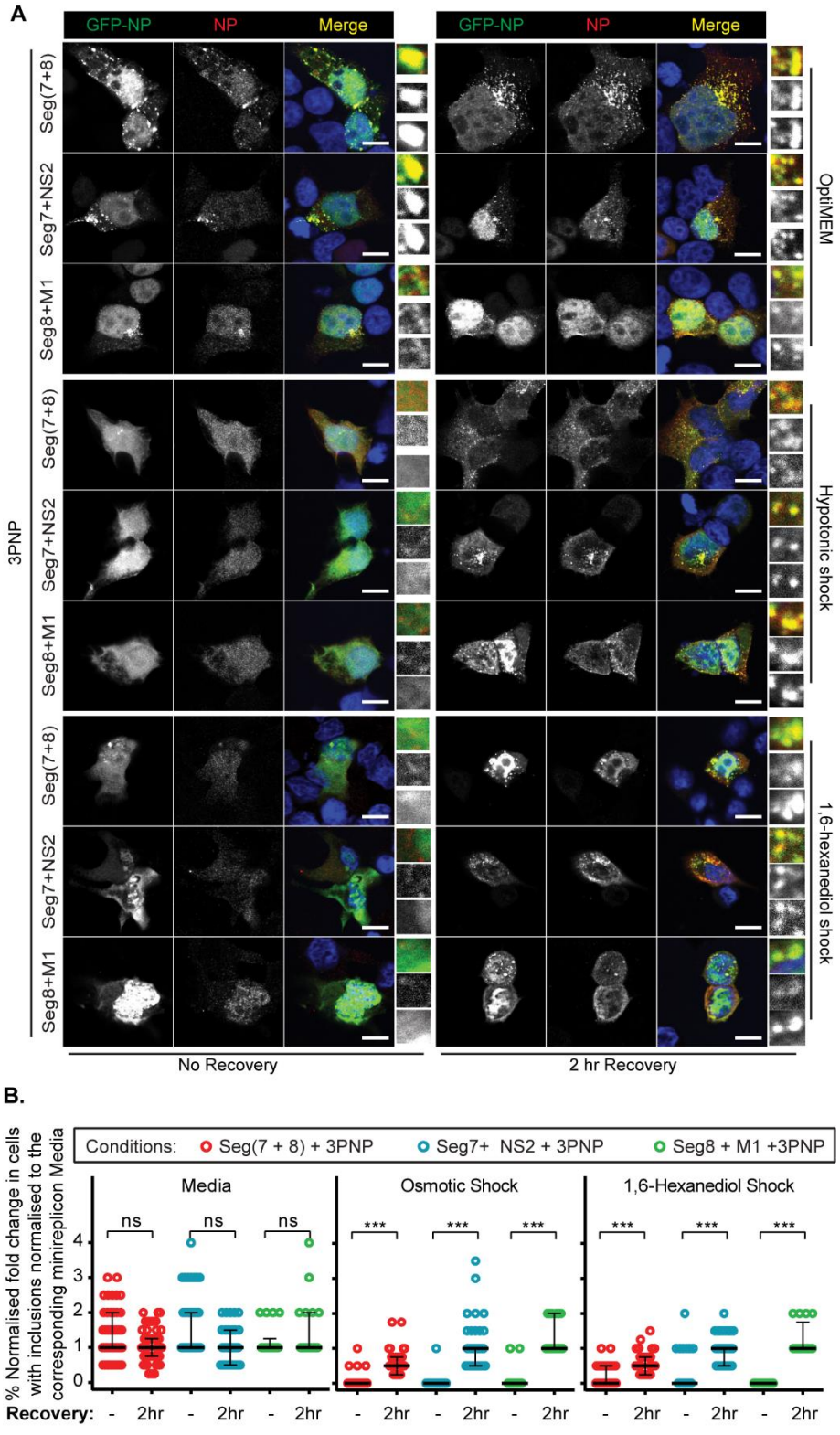
A
GFP-NP
NP
Merge
GFP-NP
NP
Merge
3PNP
Seg(7+8)
Seg7+NS2
Seg8+M1
Seg(7+8)
Seg7+NS2
Seg8+M1
Seg(7+8)
Seg7+NS2
Seg8+M1
OptiMEM
Hypotonic shock
1,6-hexanediol shock
No Recovery
2 hr Recovery
B.
% Normalised fold change in cells with inclusions normalised to the corresponding minireplicon Media
Conditions:
Seg(7 + 8) + 3PNP
Seg7+ NS2 + 3PNP
Seg8 + M1 +3PNP
Media
Osmotic Shock
1,6-Hexanediol Shock
ns
***
0
1
2
3
4
Recovery:
-
2hr

Figure 2.12- Single vRNP inclusions respond to shock treatments.

293T cells were transfected with plasmid(s) encoding one (segment 7, with nuclear export protein NS2, or segment 8, with nuclear export protein M1) or two (segments 7 and 8) IAV genomic vRNA type(s) together with plasmids encoding RdRp (PB1, PB2, and PA), NP and GFP-NP. 16 hours post-transfection, cells were exposed to either hypotonic shock, 5% 1,6-hexanediol or control vehicle (optiMEM) followed by a 2hr recovery in optiMEM before fixing and immunofluorescence staining of NP. ***(A)*** *immunofluorescence images showing inclusion (GFP-NP and NP as proxy of inclusions) response to shock treatments.* ***(B)*** *Quantification of cells expressing inclusions. The number of cells per view area that display inclusions were manually counted and normalised to those formed when treated with their corresponding media (optiMEM). Statistical analysis of data was performed using a non-parametric Kruskal–Wallis test, followed by Dunn's multiple comparisons test (***p < 0.001).*

2.5 Discussion

Viral inclusions that emerge during IAV infection have been linked to genome assembly. In this work, we provide evidence that viral inclusions are formed when cells express a single vRNP type (**Figure 2.13**). Given that vRNPs of the same type compete for incorporation in virions (Davis et al., 1980; Duhaut and Dimmock, 1998; Duhaut and Mccauley, 1996; Fujii et al., 2003), our findings indicate that formation of these structures precedes vRNP–vRNP interactions (**Figure 2.13**). This leads to a paradigmatic change in the model of IAV genome assembly. We propose that viral inclusions are microcompartments that spatiotemporally facilitate the genome assembly process (**Figure 2.13**). Such mechanism would require concentrating vRNPs from the cytosol into inclusions.

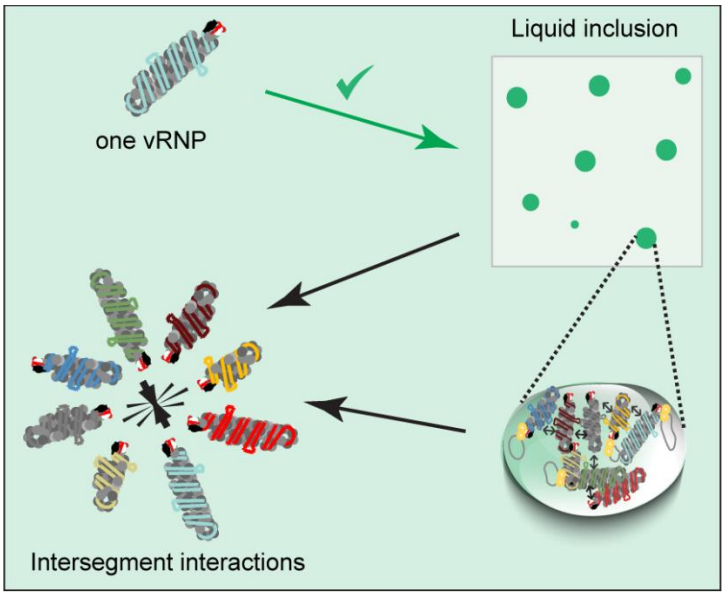

Figure 2.13- Single vRNP specie forms liquid-like IAV inclusions that promote genome assembly via vRNA-vRNA interactions.

Supporting this premise are the numerous studies describing phase transition mechanisms for segregating selected molecules from the cytosol to microcompartments that lack membrane delimitation (reviewed in (Alberti and

Hyman, 2021; Banani et al., 2017)). Such compartmentalization, driven by liquid demixing, originates functional phase-separated organelles of components and reactions. Several membraneless organelles in the cell (e.g. nucleolus, centrosomes, stress granules, DNA repair foci, or G bodies) respond and adapt quickly to stimuli (reviewed in (Alberti and Hyman, 2021; Banani et al., 2017)). Like steady-state physiological condition, , these traits have also been observed in stressed conditions including viral infections. Interestingly, viral-induced membraneless microcompartments have been known for decades and functionally associated with host immune escape, viral replication, and assembly ((Caragliano et al., 2022a; Cascarina and Ross, 2020; Geiger et al., 2021; Guseva et al., 2020; Lahaye et al., 2009; Morgan et al., 1954; Nikolic et al., 2017; Wu et al., 2014; Zhou et al., 2019) and reviewed in (Caragliano et al., 2022a, 2022b; Etibor et al., 2021; Lopez et al., 2021; Netherton et al., 2007)). Despite the similarities, the two biological assemblages have been treated as unrelated phenomena and the link between them only recently started to emerge.

Herein, we report that IAV inclusions originating from a single type vRNP species display liquid-like properties akin to the inclusions that contain all eight vRNP types during viral infection. Like classical biomolecular condensates, single vRNP inclusions display the physical characteristics of liquid condensates. This behaviour is shared with infection-derived vRNPs as well as Negri bodies found in rabies virus-infected cells, or SARS-CoV-2 condensates, vesicular stomatitis viral (VSV) and measles viroplasms, rotavirus replication factory and hCMV replication compartment (Caragliano et al., 2022a; Carlson et al., 2020; Cascarina and Ross, 2022; Chen et al., 2020; Geiger et al., 2021; Heinrich et al., 2018; Iserman et al., 2020a; Nikolic et al., 2017; Savastano et al., 2020) in terms of shape, dynamism, and ability to deform and react quickly to physiological changes (reviewed in (Boke and Mitchison, 2017; Hyman et al., 2014; Woodruff et al., 2018)). Importantly, single vRNP inclusions are not involved in the viral genome replication (which

takes place in the host cell nucleus) but originate as dynamic liquid cytoplasmic hub that may facilitate intersegment vRNA-vRNA interactions (**Figure 2.13**).

However, our work lacks an *in vitro* reconstitution system able to formally demonstrate the underlying molecular process governing formation of inclusions that arise from single or multiple vRNP types. The ability of single vRNP inclusions to deform by fusion and fission, form non-membrane delimitated clustering of vRNP-rich Rab11 vesicles, shock adaptation, and spherical shape allow us to speculate that they may form by phase transition. In fact, such phase transition may involve vRNP binding to membranes such as Rab11 vesicles (since inclusions do not form in their absence) or the association of Rab11-positive inclusions with ER and ERES.

Our results permit us to speculate that IAV induced inclusions may serve as site for genome assembly. IAV genome assembly was proposed to occur via either dispersed model (where vRNPs assemble via vesicular collision enroute the budozone) or compartmentalized model (where Rab11 are impaired/ rerouted to concentrate vRNPs in viral inclusions) as reviewed in (Amorim, 2019). The dynamic liquid characteristics of single vRNP inclusions is in line with the dispersed model. However, in agreement with the clustering model, CLEM of single vRNP displayed inclusions enriched with vesiculated structures (Rab11) that are in close proximity to the ER, which may then deliver them to the PM. It is also possible that clusters of vRNP-coated Rab11 vesicles inside IAV inclusions collide with one another to establish cognate intersegment interactions which may then release the fully assembled genome via the ER or other unidentified processes. Whether Rab11 is involved in material exchange among inclusions remains to be evaluated.

Interestingly, cross-talks between membrane-bound and membraneless organelles (e.g. ER) are starting to emerge (Lee et al., 2020;

Ma and Mayr, 2018). Importantly, our lab previously demonstrated that inclusions are spatially regulated, developing close to, and synchronously moving with the ER at the ERES, which promotes the fusion and fission dynamics of IAV inclusions. This raises the possibility that viral inclusions move using the ER. This hypothesis, together with the finding that vRNPs attach the ER (Alenquer et al., 2019; de Castro Martin et al., 2017) to form irregularly coated vesicles viz. viral inclusions, might help answering the unresolved question of vRNP transport to the plasma membrane. Compelling evidence to validate a model in which upon nuclear export, vRNPs move using the ER and concentrate near the ERES to assemble viral genomes for posterior delivery to the plasma membrane by Rab11 vesicles is still needed.

2.6 Materials and methods

2.6.1 Cell culture

Human embryonic kidney 293 cells expressing a mutant version of the SV40 large T 158 antigen (HEK293T aka 293T; a kind gift of Prof Paul Digard, Roslin Institute, UK.) were cultured in complete media constituting Reduced Serum Medium Glutamax™ (OptiMEM™; Gibco™, ThermoFisher, 51985026) supplemented 200 mM L-glutamine (Life Technologies, 25030-024). Every 3-4 days, confluent 293T cells were sub-cultured in T75 flasks using trypsin-EDTA (Biowest, X0930-100).and incubated at 37ºC, 5% CO_2. Cells used were within a maximum passage of 20.

2.6.2 Transfection

To reconstitute GFP-tagged vRNPs, 293T cells grown to 70% confluency in 24-well poly-D-lysine coated plates were transfected with plasmids pcDNA PB1, PB2, PA (150 ng each), NP (150 ng), GFP-NP (50 ng), pPol-I segments 7 and/ or 8 (150 ng each), and/ or pcDNA-NS2 (150ng each) or pcDNA-M1 (150ng each), using Lipofectamine 2000 (ThermoFisher, 11668027) or jetPRIME (Polyplus, 101000015) in Opti-MEM (ThermoFisher, 51985026) according to the manufacturer's instructions, and incubated for 16 hours at 37º C in an incubator with 5% CO2.

2.6.3 Influenza A virus strains

Reverse-genetics (RG) derived A/Puerto Rico/8/34 (PR8, H1N1) (kindly provided by Prof. Ron Fouchier) was used as model virus. Viruses were grown in eggs as following: embryonated chicken eggs were incubated at 37ºC for 10 days. After that, the eggshell was lightly sanded with a rotary tool and a hole was pierced with a sterile 27G needle on top of the egg and on the opposite side of the embryo. Through that hole, 100 PFU of virus diluted in 200µl PBS were injected into the allantoic fluid of the egg. Infected

eggs were incubated at 37ºC for 2-3 days, and then at -20ºC for 2h. Viruses were collected by opening the eggs and carefully retrieving the allantoic fluid. After centrifugation at 3500g, 5min, 4ºC to remove debris, the virus solution titrated by plaque assay and aliquoted and kept at -80ºC.

2.6.4 Infection

Cells were seeded in culture plates at appropriate density and incubated overnight. Virus inoculum was added in serum-free DMEM at the MOI of 10 and incubated for 45min. Afterwards, cells were overlaid with complete media and incubated at 37ºC, 5% CO2 for 15.4 h.

2.6.5 Western blotting

Samples were collected in Laemmli's sample buffer (20% (v/v) glycerol (Sigma-Aldrich, 1.04093) / 2% (v/v) SDS (NZYtech, MB01501) / 100µM DTT (NZYtech, MB03101) / 24µM Tris-HCl (VWR, 28.811.295) pH 6.8 / 0.04% (w/v) Xylene Cyanol FF (Sigma-Aldrich, X4126) / 0.04% (w/v) Bromophenol Blue (Sigma-Aldrich, B0126)) and denatured by heating at 95°C for 10min. Protein samples were loaded into a resolving gel containing 8 or 12.5% (v/v) acrylamide (GRiSP, GB16.3037) with a 4.3% (v/v) acrylamide stacking gel and ran in PAGE buffer (0.25M Tris / 0.192M Glycine (PanReac AppliChem, A1067) / 1% (v/v) SDS) at 150V in a Mini-PROTEAN Tetra Vertical Electrophoresis Cell (BioRad).

Proteins were transferred to a 0.45 µm nitrocellulose blotting membrane (GE Healthcare, 10600003) using a Trans-Blot SD Semi-Dry Electrophoretic Transfer Cell (Bio-Rad, 1703940). Membranes were blocked overnight at 4ºC or 1hr at 37ºC in 5% (w/v) dried non-fat milk (Nestlé, Molico) in PBS-T (0.1% (v/v) Tween-20 (SigmaAldrich, P1379) in PBS), followed by washing with PBS-T. Membranes were subsequently stained with primary antibodies for 1h at room temperature or overnight at 4ºC, while rocking. After

incubation, membranes were washed with PBS-T, then incubated with secondary antibodies for 45 min at room temperature, while rocking.

Membranes were then washed again with PBS-T and PBS and visualized on a LI-COR Biosciences Odyssey near-infrared platform (LI-COR, 9120). Red (700nm) and green (800nm) channels were split and converted to gray scale using ImageJ (NIH, version 1.51h). Except when quantifying band intensities, corrections were made to improve visualization by adjusting brightness and contrast of the entire image. All antibodies were diluted in PBS-T and are indicated in **:**

https://doi.org/10.5281/zenodo.7473398.

Table S2.1

Antibodies used included: virus NP (1:1000), PB1, PB2, PA, and NS1 (all at 1:500), kindly provided by Prof. Paul Digard, Roslin Institute, UK; goat polyclonal against green fluorescent protein (GFP) (1:2000; Sicgen, AB0020), and virus M1 (1:500; Abcam, 20910); mouse polyclonal against virus M2 (1:500; Abcam, 5416) (see **Table S2.1**). Unfortunately, there is no working antibody for NS2. The secondary antibodies used were from IRDye range (1:10000; LICOR Biosciences).

2.6.6 Fluorescence *in situ* hybridization (FISH)

Cells were fixed for 10 min using 4% (v/v) formaldehyde in PBS, washed three times in PBS and permeabilized using 0.2% (v/v) Triton-X-100 in PBS for 7 min followed by 3 washes in PBS. Thereafter, cells were postfixed using a 1%(v/v) formaldehyde solution in PBS for 10 min and washed again with PBS. Next, a prehybridization mix (60% formamide, 0.3 M sodium chloride, 30 mM sodium citrate pH 7.0, 10 mM EDTA pH 8, 35 mM dextran sulphate (w/v), 250 ng mL^{-1} tRNA) was added to the cells and incubated for 1 h at 37 °C. During this period, Cy3-, or Cy5-labelled ribonucleotide probes were boiled for 5 min and placed on ice for further 5 min prior to dilution to a final concentration of 0.5% (v/v) in 0.3 mL of

prehybridization solution containing 1 µL Ribolock RNAse inhibitor (ThermoFisher).

Cells were then incubated with the probe mix for at least 16 h at 37°C, then washed three times for 15 min at room temperature with a mix consisting of 60% formamide, 0.3 M sodium chloride, 30 mM sodium citrate pH 7.0. Next, the cells were washed two times with PBS for 5 min, while the third wash was done in 0.10 (v/v) Hoechst in PBS for 5mins. Finally, the cells mounted on a slide with Dako Faramount Aqueous Mounting Medium and single optical sections were imaged with a Leica SP5 live confocal microscope.

To generate FISH probes, pcDNA3 plasmids containing viral segments were linearized with XbaI and transcribed with T7 RNA polymerase (Life Technologies) to produce a positive-sense probe to detect vRNA. Probes were directly labelled using cy3 or cy5-UTP (Perkin Elmer)11. Plasmids used to synthesize FISH probes to detect vRNA from PR8 segments 7 and 8 were constructed by PCR-amplifying NS and M sequences, and cloning them into pCDNA3, using XbaI restriction sites respectively

2.6.7 Immunofluorescence.

Cells were fixed for 10 min with 4% (v/v) formaldehyde and permeabilized for 7 min with 0.2% (v/v) Triton-X-100 in PBS. Thereafter, they were incubated with the indicated primary antibodies for 1 h at RT, washed thrice with 1% (v/v) NCS or FBS in PBS and incubated for 45 min with Alexa fluor conjugated secondary antibodies and Hoechst. Antibodies used were rabbit polyclonal against Rab11a (1:100; Life Technologies, 715300), and mouse monoclonal against NP (1:1000; Abcam, 20343 (see **Table S2.1**)). Secondary antibodies were all from the Alexa Fluor range (1:1000; Life Technologies) (see **Table S2.1**). Following washing, cells were mounted with Dako Faramount Aqueous Mounting Medium and single optical sections were imaged with a Leica SP5 live confocal microscope. The frequency

distributions of the inclusion areas were calculated and categorised as small (0–0.15 μm^2), intermediate (0.15–0.30 μm^2) and big (0.30 μm^2) using GraphPad Prism.

2.6.8 Image segmentation and analysis.

Immunofluorescence images were converted to 8-bit or used as 16 - bit colour, background was removed, and the threshold was adjusted. Thereafter, we used a custom FIJI (Fiji Is Just) ImageJ 2.1.0/1.53p) script to quantify and categorise the area of segmented inclusions in the selected cell. Images were postprocessed using FIJI and Adobe Illustrator.

2.6.9 Live cell Imaging

PR8 infected or minireplicon expressing cells were grown in chambered 8-well glass-bottomed dish (Ibidi) containing OptiMEM medium (Gibco) and incubated for 14 h at 37 ºC and 5% CO_2. Media was substituted for Leibovitz L-15 media to buffer CO_2 and data acquisition started on a Roper TIRF Spinning Disk (Yokogawa CSU-X1) with a cage incubator to control temperature at 37 °C. After excitation with a 491 nm laser (Cobolt 491, 100 mW), fluorescence from GFP was detected with a ×100 oil immersion objective (Plan Apo 1.49), a bandpass filter (525/45 Chroma), and a photometrics 512 EMCCD camera. Images were post-processed with ImageJ (NIH) and Adobe Illustrator.

2.6.10 Particle (inclusion) tracking

FIJI (Fiji Is Just) ImageJ 2.1.0/1.53p) Trackmate plugin was used to track inclusions at a timescale of 1 s/frame in live imaging samples and their XY trajectories and fusion-fission dynamics were subsequently mapped.

2.6.11 Condensate shock assay

Cells grown in OptiMEM media were replaced with either 80%(v/v) of H_2O or 5%(w/v) 1,6-Hexanediol in OptiMEM for 10 min or 30 min respectively. Thereafter, cells were either directly fixed or allowed to recover in OptiMEM for 2 hrs before fixing and processing for immunofluorescence. The number of cells expressing inclusions were quantified manually and normalised to the corresponding normal media for each minireplicon state using R.

2.6.12 Correlative light and electron microscopy (CLEM)

Cells, seeded onto gridded dishes (MatTek Corporation, P35G-2-14-C-GRID), were transfected with either the segment 7 minireplicon system or GFP-NP that was simultaneously infected with PR8 at an MOI of 10. After 16 h, cells were fixed, imaged using the Airyscan microscope, and finally processed for electron microscopy imaging, as described previously (Sílvia Vale-Costa and Amorim, 2016a). Sections of 70 nm thickness were cut using a Leica EMFC7 Ultramicrotome. The regions of interest were acquired with a Hitachi H7650 operating at 100 keV equipped with a XR41M mid mount AMT digital camera. Images were post-processed using FIJI, Icy (licence GPLv3) and Adobe Illustrator.

2.6.13 Quantification and statistical analysis

Data were analysed using Microsoft Excel and GraphPad Prism 9.4.1 (681). To quantify the sizes of inclusions, we extracted data from fixed images using an Image J custom plugin. We compared multiple groups that either express or do not express viral inclusions. Since the data is not homogenously distributed and multiple groups were involved, we performed statistical analysis of the data using a non-parametric Kruskal-Wallis test, followed by Dunn's multiple comparisons test (***$p < 0.001$).

2.7 Acknowledgement

We thank members of the CBV lab for helpful discussion and general input in this project, as well as Prof. Ron Fouchier (Erasmus University, Rotterdam) who provided reverse genetics virus, and Prof. Paul Digard (Roslin Institute, UK) for providing cells and antibodies. We gratefully acknowledge the advanced imaging and electron microscopy units of the Instituto Gulbenkian de Ciência (IGC) for their support & assistance in this work (especially Gabriel Martins (PhD), Nuno Pimpão (M.Sc.), Ana Loura Sousa (M.Sc.)).

Financial support for this work was provided by Fundaçao para a Ciencia e a Technologia (**FCT**) (PD/BD/128436/2017 and COVID/BD/151646/2021).

2.8 Supplementary Information

For **Figure 2.10**, the timelapse images of fusion and fission events of segment 7 inclusions and infection-derived inclusions were extracted from videos that can be assessed from:

https://doi.org/10.5281/zenodo.7473398.

Table S2.1- Antibodies used in western blot.

Western blot	Target	Brand	Catalog	Clone	Host	Diluted 1:
Primary antibodies						
NP	IAV	Homemade	NA	Poly	Rb	1000
PB1	IAV	Homemade	v1916	Poly	Rb	500
PB2	IAV	Homemade	N580 Final Bleed	Poly	Rb	500
PA	IAV	Homemade	v35 Bleed7	Poly	Rb	500
NS1	IAV	Homemade	v29	Poly	Rb	500
M1	IAV	Abcam	Ab20910	Poly	Gt	500
M2	IAV	Abcam	Ab5416	Poly	Rb	500
GAPDH	Human	Sicgen	Ab0049	Poly	Gt	2000
Beta-actin	Human	Sigma-Aldrich	A5441	AC-15	Ms	2000
GFP	NA	Sicgen	Ab0020	Poly	Gt	2000
Secondary antibodies						
Goat IRDye 680RD	Gt	LICOR Biosciences	926-68074	NA	Dk	10000
Goat IRDye 800CW	Gt	LICOR Biosciences	926-32214	NA	Dk	10000
Mouse IRDye 680RD	Ms	LICOR Biosciences	926-68072	NA	Dk	10000
Mouse IRDye 800CW	Ms	LICOR Biosciences	926-32212	NA	Dk	10000
Rabbit IRDye 800CW	Rb	LICOR Biosciences	926-32213	NA	Dk	10000
Rabbit IRDye 680RD	Rb	LICOR Biosciences	926-68073	NA	Dk	10000

Chapter 3 - Thermodynamics rules for hardening IAV inclusions

3.1 Author contributions

The experiments presented in this chapter were designed and planned by Temitope Akhigbe Etibor and Maria João Amorim. All experiments and data generated were performed by Temitope Akhigbe Etibor except the live imaging of infected cells expressing endogenous and high levels of Rab11, which was done by Silvia Vale-Costa and FRAP acquisition and analysis of inclusions in PR8 infected cells that was carried out by Maria João Amorim. Temitope Akhigbe Etibor wrote the chapter with Maria João Amorim supervision. This chapter is part of a manuscript currently undergoing peer-review in an open-source journal which can be assessed from bioRxiv:

Temitope Akhigbe Etibor, Sílvia Vale-Costa, Sindhuja Sridharan, Daniela Brás, Isabelle Becher, Victor Hugo Mello, Filipe Ferreira, Marta Alenquer, Mikhail M Savitski and Maria João Amorim. Rules for hardening influenza A virus liquid condensates (2022) bioRxiv 2022.08.03.502602; doi: https://doi.org/10.1101/2022.08.03.502602

3.2 Summary

Multiple viruses including IAV form biomolecular condensates in the host cell to facilitate viral replication. Accumulating evidence indicates that these viral condensates may be hardened, a strategy with potential for exploitation as novel antiviral therapy since viral reactions rely on specific material properties for function. However, there is no molecular understanding on how to efficiently modify the material properties of viral condensates, a pre-requisite for overcoming off-target effects by rational drug design. The material properties of biological condensates are modified by different thermodynamic parameters, including free energy, concentration, and type/strength of interactions.

Here, we used influenza A virus liquid cytosolic condensates, viz. viral inclusions, to provide a proof of concept that modulating the type/strength of transient interactions among the interactome in IAV inclusions is more efficient at hardening these structures than varying the temperature or concentration. Importantly, we showed that inclusions are heterotypic and provide a proof of concept that stabilizing vRNP interactions by a known pharmacological sticker called nucleozin (Ncz) more efficiently hardens these structures than varying temperature or concentration *in situ*. Our work supports the development of antivirals targeting the material properties of biomolecular condensates in viral infections. It also provides a framework for the selection of compounds with this activity for general application and thus provides an advance in disease therapy.

3.3 Introduction

Viruses are obligatory intracellular parasites that are highly dependent on the machinery of the hosts they infect. Inside cells, the adaptive plasticity of viruses to their cellular milieu is notable (reviewed in (Kaján et al., 2020; Netherton and Wileman, 2011; Wolff et al., 2020)). Seminal studies showed that viral adjustments to the cellular environment comprise sophisticated strategies for co-opting, readapting, and antagonizing different cellular pathways to facilitate viral replication, escape immune-related surveillance, and perpetuate viral transmission (reviewed in (García-Sastre, 2017; Tarakhovsky and Prinjha, 2018; Sílvia Vale-Costa and Amorim, 2016b)).

Recently, another layer of complexity— the physical properties of molecules in the cell emerged as a key determinant in cellular organization (reviewed in (Alberti, 2017; Alberti et al., 2019; Banani et al., 2017; Hyman et al., 2014; Mittag and Pappu, 2022)). It was demonstrated that cells can achieve active and functional compartmentalization via phase transition without recurring to membrane-bound organelles to form biomolecular condensates ((Brangwynne et al., 2009) reviewed in (Alberti, 2017; Alberti et al., 2019; Banani et al., 2017; Hyman et al., 2014; Mittag and Pappu, 2022)). This shift in paradigm adds layers of complexity to the healthy and infected cellular structures, and it offers new possibilities to the understanding of how organisms work, control reactions, and adapt to stimuli. As contemporary biology refocused to understand the biophysical properties and principles for organizing biomolecular condensates, it became apparent to explore virus-induced condensates and how we can manipulate them to block infection.

Evidence shows that viruses co-opt biomolecular condensates to facilitate viral replication and genome assembly, using similar strategies to other cellular condensates systems (reviewed in (Brocca et al., 2020; Cascarina and Ross, 2022; Dolnik et al., 2021; Etibor et al., 2021; Lopez et al., 2021; Wu et al., 2022; York, 2021)). Importantly, our Laboratory showed

for the first time that IAV inclusions are biomolecular condensates that display liquid-like properties (Alenquer et al., 2019). As the list of viruses utilizing liquid biomolecular condensates is rapidly growing, including reoviruses, hCMV, HIV, rabies, measles, SARS-CoV-2 (reviewed in (Brocca et al., 2020; Cascarina and Ross, 2022; Dolnik et al., 2021; Etibor et al., 2021; Lopez et al., 2021; Wu et al., 2022; York, 2021)), it becomes pertinent to ask whether targeting the material properties could constitute a novel antiviral approach.

Many studies have reported unique ways to modify biomolecular condensates by molecules classified known as c-mods, in the sense that they are able to either induce, dissolve, localize, or harden (morph) the condensates (reviewed in (Mitrea et al., 2022; Patel et al., 2022)). To name a few, examples include dissolvers (GSK626616, RK33, ION363 and tamoxifen targeting Dyrk3, DDX3, FUS, MED1 proteins respectively), inducers (Nusinersen ASO, PCG, Olaparib targeting SMA, Brd4, PAP proteins respectively), and localizers (Selinexor (KPT-330), Avrainvillamide, UNC6934 targeting CRM1/XPO1, NPM1, NSD2) (reviewed in (Mitrea et al., 2022; Patel et al., 2022)). Unfortunately, very little is known regarding hardening c-mods (known as morphers).

Recently, the Sonic hedgehog (Shh) pathway antagonist cyclopamine and its analogue A3E were demonstrated to inhibit human respiratory syncytial virus (hRSV) replication by altering the material properties of viral condensates (Risso-Ballester et al., 2021) and therefore classified as morphers. However, compounds targeting hRSV-related (Risso-Ballester et al., 2021) and cancer-associated (Klein et al., 2020) condensates exhibited off-target effects. Therefore, a critical advance in condensate disease therapy, including in viral infections, requires the defining of the yet unknown rules for efficiently and specifically targeting only selected biomolecular condensates. Such knowledge would create a path towards rational design

of molecules targeting biomolecular condensates and hence reduce off target effects.

In several studies it was demonstrated that the properties of biological condensates respond to many factors in a system-dependent manner (reviewed in (Alberti et al., 2019; Boeynaems et al., 2018; Falahati and Haji-Akbari, 2019; Hyman et al., 2014; Milovanovic and De Camilli, 2017; Mittag and Parker, 2018; Riback and Brangwynne, 2020; Snead and Gladfelter, 2019)). Entropic free energy (Quiroz and Chilkoti, 2015), concentration (Banani et al., 2016; Maharana et al., 2018; Riback et al., 2020), type and strength of interactions (Banjade and Rosen, 2014; Li et al., 2012; Oltrogge et al., 2020; Riback et al., 2020; Sanders et al., 2020) were demonstrated as having profound effects on the formation and material properties of biomolecular condensate. This suggests that cellular strategies able to modify these parameters could offer solutions for drug development. For example, pathways affecting local energy production, consumption or metabolism could alter the free energy landscape of biomolecular condensates (Munder et al., 2016; Patel et al., 2017; Riback et al., 2020). Similarly, pathways that regulate the local density of condensate drivers could affect concentration (Banani et al., 2016; Riback et al., 2020). Finally, pathways involved in post-translational modifications (Rai et al., 2018), pH (Kroschwald et al., 2018; Munder et al., 2016) or ionic strength (Yang et al., 2020) of condensate microenvironment as well as cell permeable compounds promoting aggregation or dissolution of condensate interactomes could affect the type and strength of interactions (Bracha et al., 2018; Seim et al., 2022; Snead et al., 2022; Zhu et al., 2019).

Having established that inclusions of single vRNP origins display liquid properties, corroborating our earlier report (Alenquer et al., 2019) that inclusions are inherently liquid biomolecular condensates, the next logical course was to use c-mod (morphers) to modify their material properties using for better understanding of their function. In this work, we meet the critical need to identify efficient strategies to harden IAV liquid inclusions. For this,

we compared the impact of well-characterized thermodynamic variables in the material properties of biological condensates by altering temperature (as a measure of the entropic contribution of free energy), concentration of drivers (by overexpression strategies) and number/strength of ligations within the condensate interactome (by using previously characterized stickers of vRNPs find the correct paper KAO (Amorim et al., 2013). We found that pharmacological stabilization of intersegment interactions is possible and is the most efficient strategy for hardening IAV inclusions. Furthermore, we showed that unlike liquid inclusions, pharmacologically hardened inclusions are rigid, immobile and lacking dynamism since they lack fusibility, flux of component molecules and internal rearrangement. Overall, our study supports the development of a new class of antiviral drugs (known as morphers) targeting the material properties of viral induced biomolecular condensates.

3.4 Results

3.4.1 Framework to identify perturbations that harden IAV liquid inclusions

As reported in (Alenquer et al., 2019), we demonstrated that viral inclusions formed by IAV infection display a liquid profile in the sense that they drip, acquire a spherical shape upon fusion and dissolve in response to hypotonic shock or brefeldin A treatment. Here, we identify the best strategies to harden viral inclusions to investigate if altering their material properties may be a novel antiviral therapy. For this, we systematically probed and compared the impact of temperature, concentration, and number/strength of interactions on the material properties of liquid viral inclusions, as a proxy of entropic, molecular and valency contributions, respectively.

We selected these parameters as they are well understood to regulate the interactions amongst components and the material properties of condensates (Quiroz and Chilkoti, 2015; Riback et al., 2020; Sanders et al., 2020; Shimobayashi et al., 2021) (**Figure 3.1**A). Methodologically, we employed established protocols for the thermodynamic perturbations to directly compare the effect of several parameters in one study. We quantified the impact of these perturbations on the number, nucleation density ($\rho = \frac{number\ of\ inclusion}{Cytoplasm\ Area}$, μm^{-2}), size, shape, dynamics, supersaturation ($S = ln\ \frac{Cdilute}{Csat}$, in which C_{sat} is the concentration above which molecules demix from an homogenous system), and the Gibbs free energy of partitioning (henceforth called free energy, $\Delta G = -RT ln K$, in which $K = \frac{Cdense}{Cdilute}$ is the partition coefficient) (**Figure 3.1** and **Figure 3.20 S1**).

Material concentrations inside (C_{dense}) and outside (C_{dilute}) viral inclusions were measured using the analytical strategies described in (Riback et al., 2020; Shimobayashi et al., 2021) and shown in (**Figure 3.1**B and validated in ***Figure 3.21* S2**). For this, we used the mean fluorescence intensity (MFI) of

NP as proxy of vRNP concentration (Amorim et al., 2011; Vale-Costa et al., 2016b), as it is well established that most cytosolic NP is in the form of vRNPs (Amorim et al., 2011; Avilov et al., 2012a; Bruce et al., 2010; Eisfeld et al., 2011a; Momose et al., 2011; Nturibi et al., 2017). With these values, it is possible to assess the change in free energy between conditions (ΔG = -RT*ln*K), given that the partition coefficient K (K= $\frac{Cdense}{Cdilute}$), which is the ratio between the concentrations of vRNPs in C_{dense} and C_{dilute} (**Figure 3.1**B).

Our goal was to identify which perturbations translated into significant shifts in ΔG to further explore whether these resulted in dramatic alterations in the material properties of viral inclusions, by assessing their kinetics and dynamics (**Figure 3.1**C) and determine how they impact viral replication.

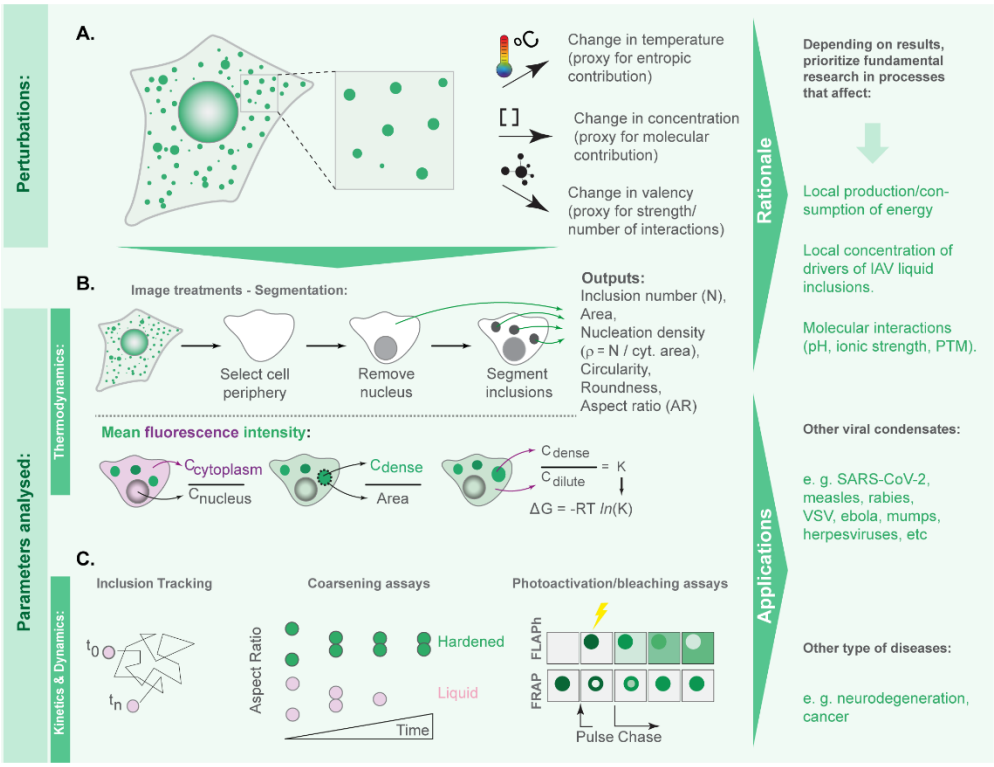

Figure 3.1- Framework applied to define the rules for hardening IAV liquid inclusions or other condensates.

(A) *To compare the contributions of entropy, concentration, and valency/strength/type of interactions, we subjected infected cells to the different perturbations; temperature, concentration of viral inclusion drivers (vRNPs and of Ras-related in brain 11a (Rab11a)) and number or strength of interactions between different vRNPs using the well-studied vRNP pharmacological sticker, nucleozin.* ***(B)*** *Our aim is to determine which amongst these perturbations impact more dramatically viral inclusions number, shape, size or Gibbs free energy of partitioning (free energy, ΔG). For this, we segmented circa 20 cells under the different conditions to measure the number of inclusions, area, aspect ratio, nucleation density and the amount of material inside (C_{dense}) and outside (C_{dilute}) viral condensates. With this, we calculated the partition coefficient K and extrapolated the ΔG.* ***(C)*** *When ΔG dramatically changed, we assessed how perturbations altered the material properties of IAV inclusions by determining how fast and how much they moved (using coarsening assays, particle tracking, fluorescence recovery after photobleaching (FRAP) and fluorescence loss after photoactivation (FLAPh)). The overall goal of this framework is to determine, for IAV, if and how liquid inclusions may be efficiently hardened. Additionally, the framework may be applied to other systems, including other viruses, for informed decisions on how to harden condensates.*

3.4.2 Changes in temperature mildly perturb IAV inclusions.

Cellular homeostasis state is maintained at a narrow permissive physiological range, including temperature. However, biomolecular condensates respond to fluctuations in temperature, and we took advantage of this to assess the entropic contribution of free energy and evaluate whether regulating host cell metabolism could offer future solutions to harden IAV liquid inclusions (**Figure 3.2**A). We quantitatively analysed the viral inclusions formed in cells incubated at 4 ºC, 37 ºC and 42 ºC for 30 minutes at 8 hours post-infection (hpi) (representative images in **Figure 3.2**B).

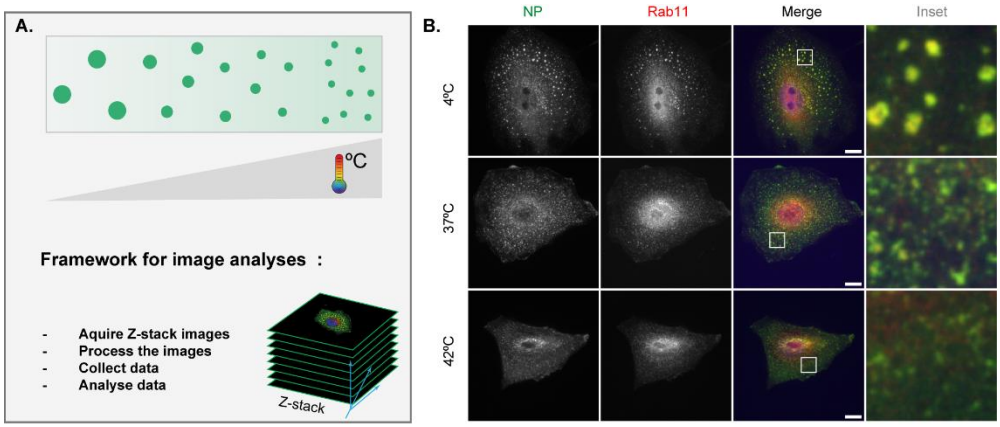

Figure 3.2- Immunofluorescence images demonstrating changes in inclusions at different temperatures.

*A549 were infected at a multiplicity of infection (MOI) of 3 with PR8 virus for 8 hrs (being the period of the lowest free energy), incubated at different temperatures (4ºC, 37ºC, 42ºC), fixed, and analysed by immunofluorescence using antibody staining against Rab11 and NP. (**A**) Schematic depiction of the experimental analysis workflow and (**B**) Representative images of fixed cells showing alterations in inclusions at different temperatures. Scale Bar = 10 µm.*

This short duration in temperature shift did not alter the levels of cytosolic vRNPs, as expected (**Figure 3.3**A). Increasing the temperature from 37º to 42ºC did not significantly change the size (**Figure 3.3**B), aspect ratio or number of viral inclusions (**Figure 3.3**B-E),but decreased the concentration of vRNPs in condensates (C_{dense}), and increased the nucleation density despite not altering the concentration of vRNPs in the milieu (C_{dilute}) (**Figure 3.3**F-K). This means that increasing the temperature up to 42 ºC still maintains the system in a two-phase regime, but affects the nucleation capacity, increasing the number of inclusions. Of note, vRNPs become homogenously distributed in the cytosol at 43.5 ºC (data not shown). Importantly, this increase in temperature modestly destabilized the structure,

as observed by an increase in Gibbs free energy (-2167.3 ± 2361 J.mol^{-1}@ 37 ºC to -1477.9 ± 228 J.mol^{-1}@ 42 ºC, mean ± SD, **Figure 3.3**L,M). Conversely, decreasing the temperature until 4ºC leads to an increase in the size of inclusions that is statistically significant from 42 ºC to 4ºC only (shift in area from 0.2896 ± 0.02 μm^2 at 42 ºC to 0.3474 ± 0.05 at 4ºC), rounds up liquid inclusions, and decreases their nucleation capacity and abundance (the latter significant only considering 42 ºC and 4ºC, **Figure 3.3**B-F). A drop in temperature increases the concentration of vRNPs in inclusions (C_{dense} at 37ºC of 3116.0 ± 0.05 AU, mean ± sd, and at 4ºC of 2144.5 ± 0.04 AU), and does not significantly change the stability of IAV inclusions as determined by Gibbs free energy (-2415.6±273 J.mol^{-1}@ 4 ºC, **Figure 3.3**L,M). Overall, the data indicate that the temperature increasing from 4ºC to 42ºC shifts our system to smaller inclusions that have less vRNPs. However, C_{dilute} did not change but there is an increase in nucleation density which indicates that heat disruption of weak molecular interactions leads to alterations in nucleation, fusion, and fission, as reported previously (Iserman et al., 2020). However, we did not observe significant alterations in the stabilization of our system, supporting that alterations in the conditions tested for temperature do not affect the material properties of viral inclusions.

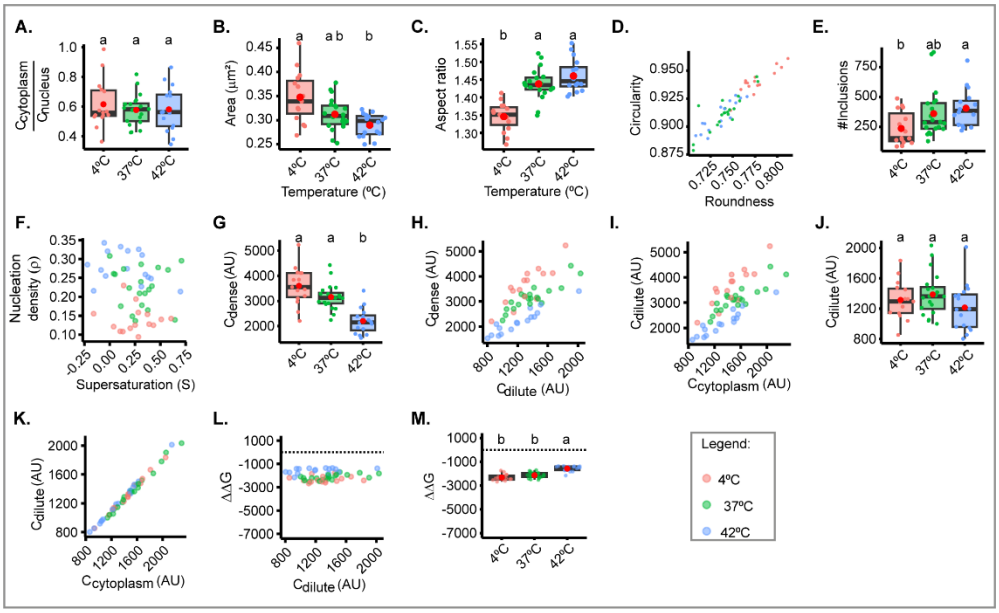

Figure 3.3- Temperature changes confer a modest alteration to inclusions properties.

Biophysical parameters were extracted from images described in ***Figure 3.2****, measuring NP intensity as a proxy for vRNPs (n = 15 - 20) by adapting the method published by (Riback et al., 2020; Shimobayashi et al., 2021) to determine concentration* C_{dense} *as the mean fluorescence intensity of vRNPs in the segmented IAV inclusions, while concentration* C_{dilute} *was extrapolated from the cytoplasmic vRNP intensity outside the inclusions. Each dot is the average value of a measured parameter within or outside IAV inclusions per cell, while the continuous black lines are non-linear fitted models for all data. Also, size and shape of inclusion was extracted from inclusions after image segmentation. Parameters that were normalized to an infection without IAV inclusions (3hpi) are indicated by a dashed horizontal line. Above each boxplot, same letters indicate no significant difference between them, while different letters indicate a statistical significance at* $\alpha = 0.05$*. Abbreviations: AU, arbitrary unit. (**A**). Boxplot depicting the fold change in cytoplasmic to nuclear vRNP concentration; P = 0.684 by one-way ANOVA followed by*

*Tukey multiple comparisons of means. (**B**) Boxplot of viral inclusion area (μm^2) per cell; P = 0.00234 by Kruskal Wallis Bonferroni treatment. (**C**) Boxplot of aspect ratio of inclusions; P < 0.001 by one-way ANOVA followed by Tukey multiple comparisons of means. (**D**) Scatter plot of inclusions circularity versus roundness. (**E**) Boxplot showing number of viral inclusions per cell; P < 0.001 by one-way ANOVA, followed by Tukey multiple comparisons of means. (**F**) Scatter plot of nucleation density (ρ = $\frac{number\ of\ inclusion}{Cytoplasm\ Area}$, μm^{-2}) versus degree of supersaturation (S = In $\frac{Cdilute}{Csat}$), as a measure of propensity to remain dispersed in the cytoplasm. (**G**) Boxplot of vRNP concentration within inclusions (C_{dense} (AU) P < 0.001 by one-way ANOVA, followed by Tukey multiple comparisons of means. (**H**) Scatter plot of C_{dense} (AU) versus surrounding cytoplasm (C_{dilute}, AU). (**I**) Scatter plot C_{dense} (AU) versus its total cytoplasmic vRNP concentration ($C_{cytoplasm}$, AU). (**J**) Boxplot showing C_{dilute} (AU); P = 0.203 by one-way ANOVA followed by Tukey multiple comparisons of means. (**K**) Scatter plot of C_{dilute} (AU) versus $C_{cytoplasm}$ (AU). (**L**) Scatter plot of fold change in free energy of partition (ΔΔG, J.mol^{-1}) where ΔG = -RTInK, and K = ($\frac{Cdense}{Cdilute}$), and ΔΔG = ΔG – $ΔG_{3\ hpi}$, versus C_{dilute} (AU). (**M**) Boxplot of ΔΔG (J.mol^{-1}); P < 0.001 by one-way ANOVA followed by Tukey multiple comparisons of means.*

3.4.3 Changes in concentration of viral inclusions' drivers do not impact their liquid profile.

Two factors were shown to drive the formation of IAV inclusions - vRNPs and Ras-related in brain 11a (Rab11a) (Amorim et al., 2011; Bruce et al., 2010; Eisfeld et al., 2011a; Lakdawala et al., 2014; Nturibi et al., 2017; Vale-Costa et al., 2016b; Veler et al., 2022). In fact, vRNP accumulation in liquid viral inclusions requires its association with Rab11a directly via the viral polymerase PB2 (Amorim et al., 2011; Veler et al., 2022), and the liquid character is maintained by an incompletely understood network of intersegment interactions bridging several cognate vRNP-Rab11 units on

flexible membranes. As the concentration of material is a key determinant for the physical properties of condensates (Hernández-Vega et al., 2017; Maharana et al., 2018; Riback et al., 2020; Weber and Brangwynne, 2015), we evaluated how concentration of these two drivers impacts the behaviour of IAV inclusions.

For this, we took advantage of the fact that vRNP levels increase during infection (Kawakami et al., 2011), and we analysed viral inclusions over a time course, in two conditions: with endogenous levels of Rab11a (using cells expressing GFP, as in (Alenquer et al., 2019), **Figure 3.4**A) and overexpressing Rab11a (in the form of GFP-Rab11a, as in (Alenquer et al., 2019), **Figure 3.4**B). With this approach, we aimed at analysing whether the material properties of viral inclusions changed over time and whether increasing the levels of Rab11 would alter these properties. This strategy would reveal if regulating Rab11a activity could harden IAV liquid inclusions.

In GFP expressing cells, as the progeny vRNP pool reaches the cytosol (**Figure 3.5**A), viral inclusions augment in size (from 0.172 ± 0.04 to 0.289 ± 0.06 μm^2, mean ± SD, **Figure 3.5**B), with similar aspect ratio (**Figure 3.5**C,D). There is a mild reduction in the number of inclusions from 8hpi onwards, as measured by the nucleation density (ρ) (**Figure 3.5**E-G). As infection progresses, the concentration of vRNPs inside condensates increases until 8 hpi (**Figure 3.5**H-J), accompanied by an increase in the diluted cytosolic phase (**Figure 3.5**I,K,L), and both parameters stabilise thereafter, indicating that the critical concentration occurs around 8 hpi.

Importantly, Gibbs free energy (normalised to 3 hpi) is lowest at 6 hpi (-1799.0 ± 623 $J.mol^{-1}$) and destabilises mildly onwards (-1139.8 ± 382, -1131.2 ± 444 and -833.8 ± 342 $J.mol^{-1}$ @ 8, 12 and 16 hpi, respectively) (**Figure 3.5**M-O). These results are consistent with the increase in cytosolic vRNP leading to bigger sized inclusions (**Figure 3.5**B) that overall maintain

the same concentration although becoming modestly destabilised, suggesting that the material properties are also modestly affected.

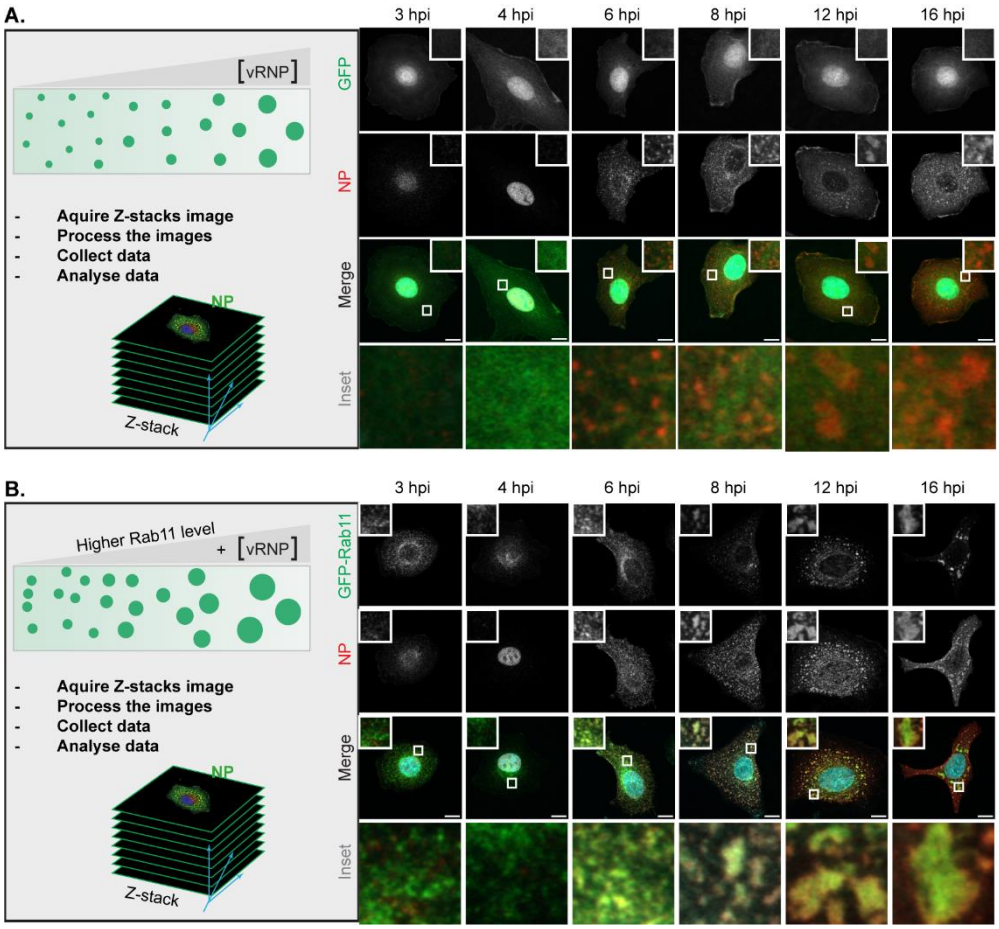

Figure 3.4- Immunofluorescence images demonstrating a concentration-dependent change in inclusions properties.

*A549 cells stably expressing **(A)** GFP, or **(B)** Rab11a-WT were infected at a MOI of 3 with PR8 virus and, at the indicated time points, were fixed, and analysed by immunofluorescence (IF) using antibody against NP (as a proxy for vRNPs).*

Schematic depiction of the experimental analysis workflow and representative immunofluorescence images of infected and fixed cells at different hpi (a

proxy for changing cytoplasmic vRNP concentration); NP (green), Rab11 (red), and nucleus (blue). Scale bar = 10 µm.

When overexpressing Rab11a, cytosolic vRNPs also accumulated in viral inclusions that increased with infection (**Figure 3.5**A,B, from 0.243 ± 0.03 to 0.385 ± 0.04 μm^2), but were significantly bigger than viral inclusions in GFP expressing cells, revealing a higher nucleation density (**Figure 3.5**E-G) and similar aspect ratio (**Figure 3.5**C,D), C_{dense} (**Figure 3.5**H-J) and C_{dilute} (**Figure 3.5**I,K,L). The lowest value of Gibbs free energy occurs at 8 hpi (-1337.7 ± 331 $J.mol^{-1}$) and destabilises from then onwards (-1145.3 ± 443 and -895.3 ± 394 $J.mol^{-1}$ @ 12 and 16 hpi, respectively, **Figure 3.5**M-O). This is consistent with Rab11a overexpression giving rise to bigger viral inclusions that overall contained the same vRNP concentration and destabilise slightly later.

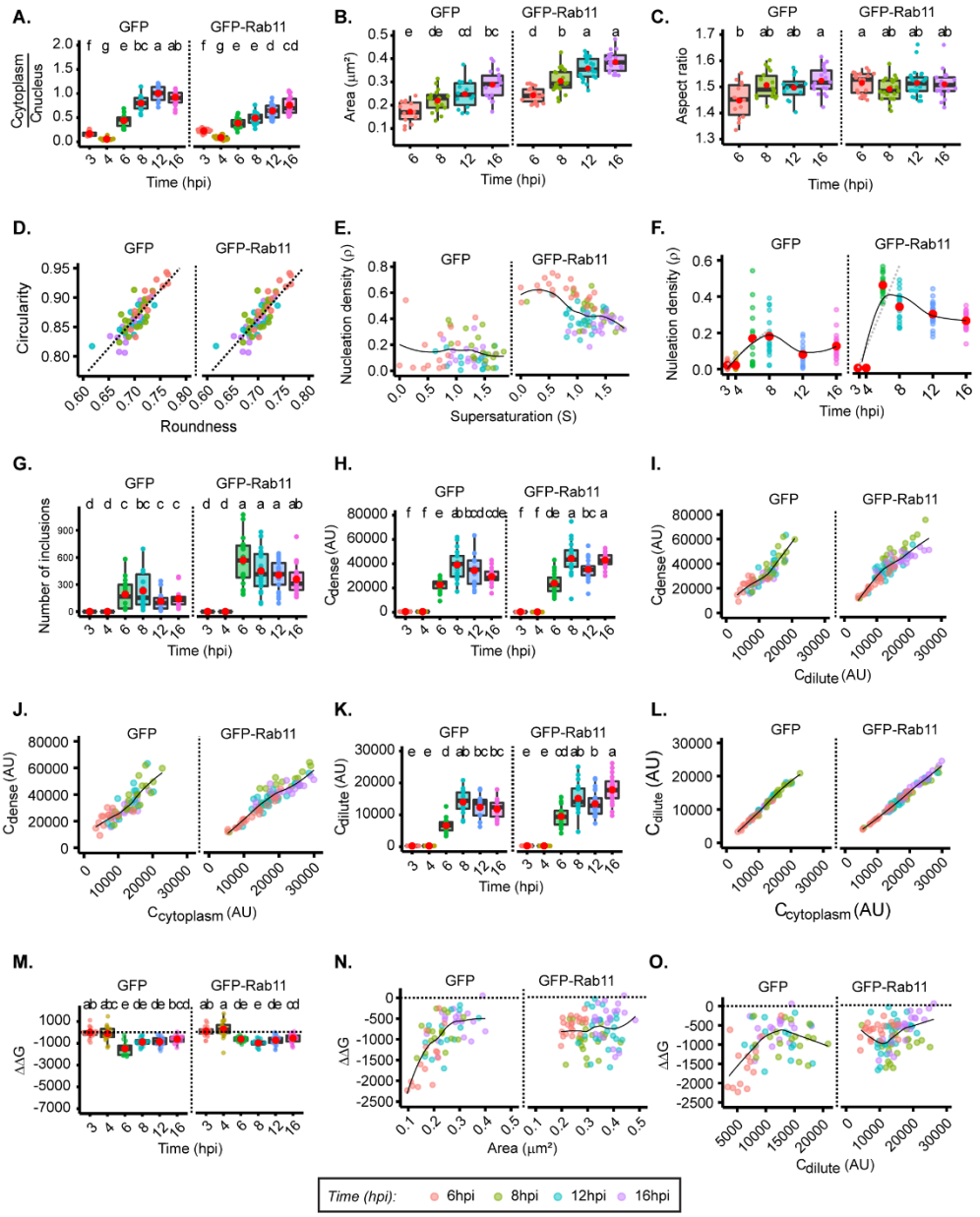

Figure 3.5- Concentration changes modestly alter inclusions properties.

Each dot is the average value of measured parameter per cell, and the continuous black lines are non-linear fitted models for all data. Above each boxplot, same letters indicate no significant difference between them, while different letters indicate a statistical significance at α = 0.05 using one-way

ANOVA, followed by Tukey multiple comparisons of means for parametric analysis, or Kruskal-Wallis Bonferroni treatment for non-parametric analysis. Abbreviations: AU, arbitrary unit. ***(A)*** *Boxplot depicting the fold change in the ratio of cytoplasmic to nuclear vRNPs concentration at different times of infection, with endogenous and overexpressed Rab11a at 8hpi. P < 0.001; Kruskal Wallis Bonferroni treatment.* ***(B)*** *Boxplot of inclusion area per cell; P < 0.000216; one-way ANOVA, followed by Tukey multiple comparisons of means.* ***(C)*** *Boxplot of inclusion aspect ratio; P = 0.033422; Kruskal Wallis Bonferroni treatment.* ***(D)*** *Scatter plot of inclusion circularity versus roundness.* ***(E)*** *Scatter plot showing nucleation density (ρ, μm^{-2}) versus degree of supersaturation (S).* ***(F)*** *Dot plot and model depicting nucleation density (ρ, μm^{-2}).* ***(G)*** *Boxplot of inclusion number per cell at different hpi. P = 0.001; Kruskal Wallis Bonferroni treatment.* ***(H)*** *Boxplot of C_{dense} (AU); P < 0.001; Kruskal Wallis Bonferroni treatment.* ***(I)*** *Scatter plot of C_{dense} (AU) versus C_{dilute} (AU).* ***(J)*** *Scatter plot of C_{dense} (AU) and $C_{cytoplasm}$ (AU).* ***(K)*** *Boxplot of C_{dilute} (AU); P < 0.001; Kruskal Wallis Bonferroni treatment.* ***(L)*** *Scatter plot of C_{dilute} (AU) versus $C_{cytoplasm}$ (AU) with time of infection.* ***(M)*** *Boxplot of ΔΔG ($J.mol^{-1}$); P < 0.001; Kruskal Wallis Bonferroni treatment.* ***(N)*** *Scatter plot of ΔΔG ($J.mol^{-1}$) relative to 3 hpi versus area of inclusion.* ***(O)*** *Scatter plot of ΔΔG versus C_{dilute} (AU).*

Importantly, in the two conditions and over the course of infection, viral inclusions maintained a liquid character with fusion and fission events taking place (**Figure 3.6**). Therefore, these data indicate that altering the concentration of vRNPs and/or Rab11a affects the size but modestly impact IAV inclusions' material properties.

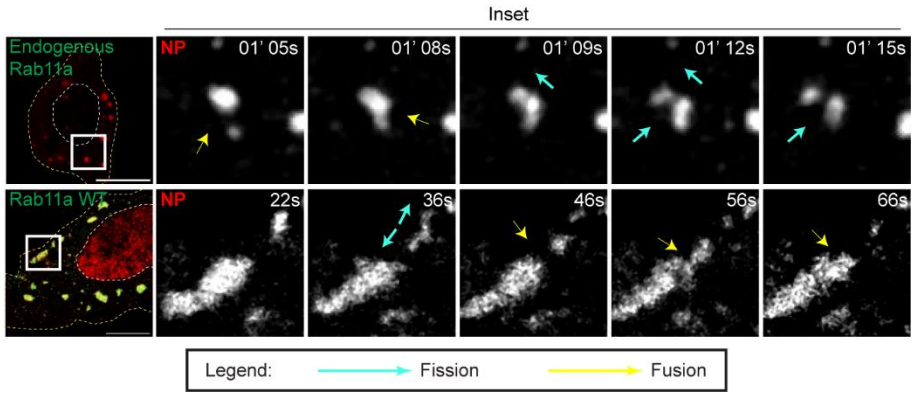

Figure 3.6- IAV inclusions containing endogenous Rab11a undergo fusion and fission.

A549 cells stably expressing GFP (top panel, extracted from live cell imaging videos), or Rab11a-WT (bottom panel, extracted from live cell imaging videos) were transfected with a plasmid encoding mCherry-NP and simultaneously co-infected with PR8 virus at an MOI of 10 and were live imaged at 12 – 16 hpi. Representative time lapse image of fission (blue arrow) and fusion (yellow arrow) dynamics of viral inclusions.

3.4.4 The increase in type/ strength of interactions dramatically stabilizes IAV inclusions.

Another critical regulator of condensate properties is how its components interact (reviewed in (Alberti and Hyman, 2021)). Therefore, we predict that oligomerizing vRNPs to each other or to Rab11a will change the viscoelasticity of condensates similar to chemically cross-linked iPOLYMER for intracellular hydrogels (Nakamura et al., 2018). For IAV, it was shown by many independent groups that the drug nucleozin operates as a pharmacological sticker that oligomerizes all forms of NP (Amorim et al., 2013; Kao et al., 2010; Nakano et al., 2021). In fact, it was demonstrated that the drug nucleozin has affinity for 3 different sites of NP (Kao et al., 2010) chemically polymerizing NP either free or vRNPs in a reversible manner (Amorim et al., 2013).

Interestingly, nucleozin was described as a novel class of influenza antivirals targeting the viral protein NP, potently inhibiting IAV replication in *ex-vivo* and in mouse model of influenza infection (reviewed in (Cianci et al., 2013)). However, it readily caused escape mutant viruses carrying a single substitution Y289H in NP (Kao et al., 2010). Despite the capacity to promote resistance, our strategy is to use nucleozin as a well-known tool to probe the effects of increasing the number and type of intra and inter-vRNP interactions in the material properties of IAV inclusions (***Figure 3.7***).

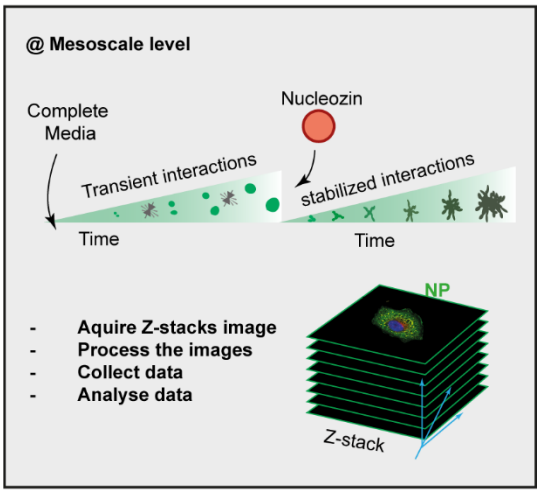

Figure 3.7- Schematics demonstrating nucleozin as a tool to harden IAV.

IAV inclusions in PR8 infected cells growing in complete media displayed liquid-like properties. Upon exposure to nucleozin, inclusions form a hardened meshwork.

With this reasoning, we evaluated the thermal stability of inclusions in the presence or absence of nucleozin in order to confirm its pharmacological sticker activity (Sridharan et al., 2019). It is well established that increasing temperature shifts a thermodynamics system to a homogeneous mix. In agreement, when we exposed IAV infected cells to a range of temperatures (4ºC, 37ºC and 42ºC), we found that higher temperatures yield smaller inclusions tending towards its homogenous distribution in the cytoplasm (***Figure 3.8***). Interestingly, when infected cells were exposed to the same

thermal conditions after nucleozin treatment, inclusions were irresponsive to thermal fluctuation, maintaining their stability (***Figure 3.8***).

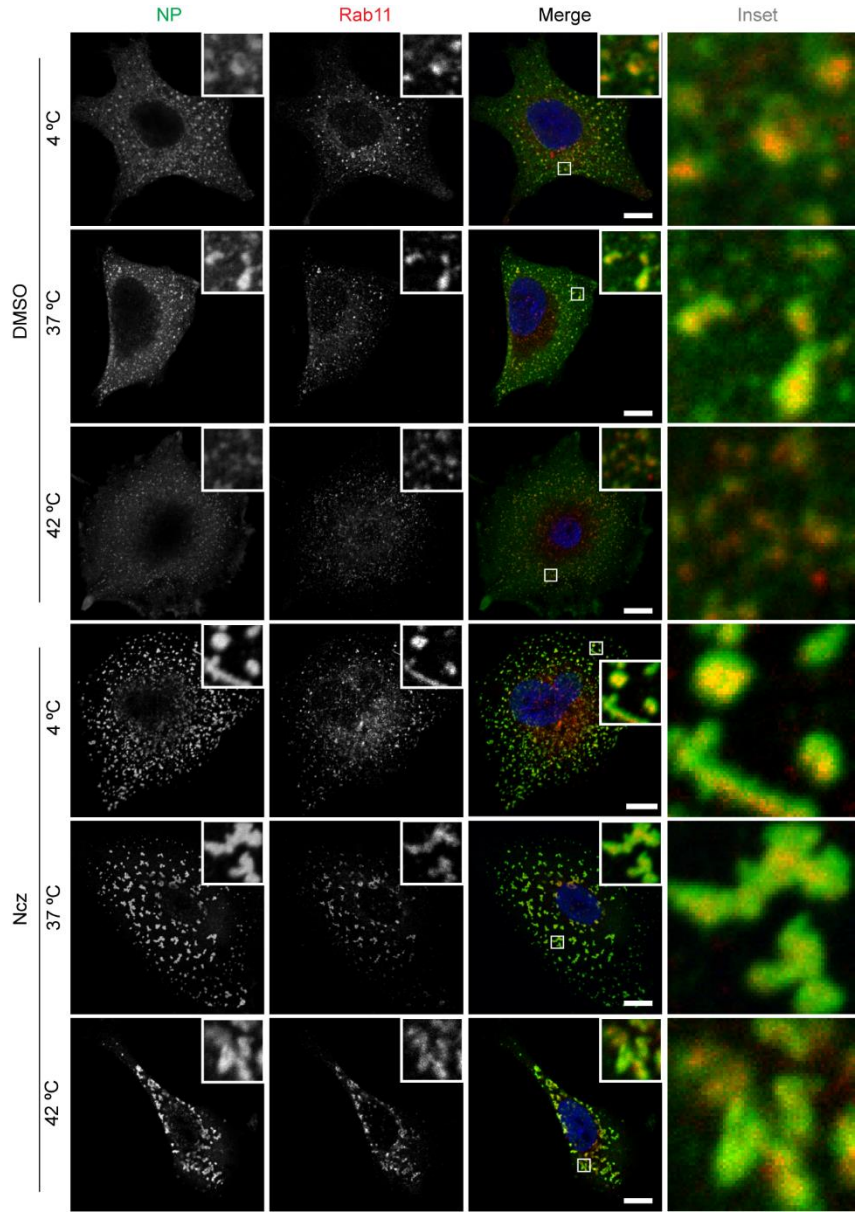

Figure 3.8- Hardened inclusions are thermally stable.

A459 cells were infected with PR8 at a MOI of 3. At 7.5 hpi the infected cells were treated with 5 μM Ncz or DMSO for 30 mins at 37ºC before being

subjected to thermal stress at 4ºC, 37ºC and 42ºC for 20mins and fixed for immunofluorescence analysis by staining with antibody against NP (green), Rab11 (red) and nucleus (blue). Representative image with Scale Bar = 10 µm.

Next, we tracked how nucleozin affected IAV liquid inclusions, by exposing the infected cells to this drug for different periods ranging from 5 min to 2h. We observed that nucleozin-treated inclusions form a multi-shaped meshwork unlike the rounded liquid droplets formed without nucleozin from 20 min post addition (***Figure 3.9***).

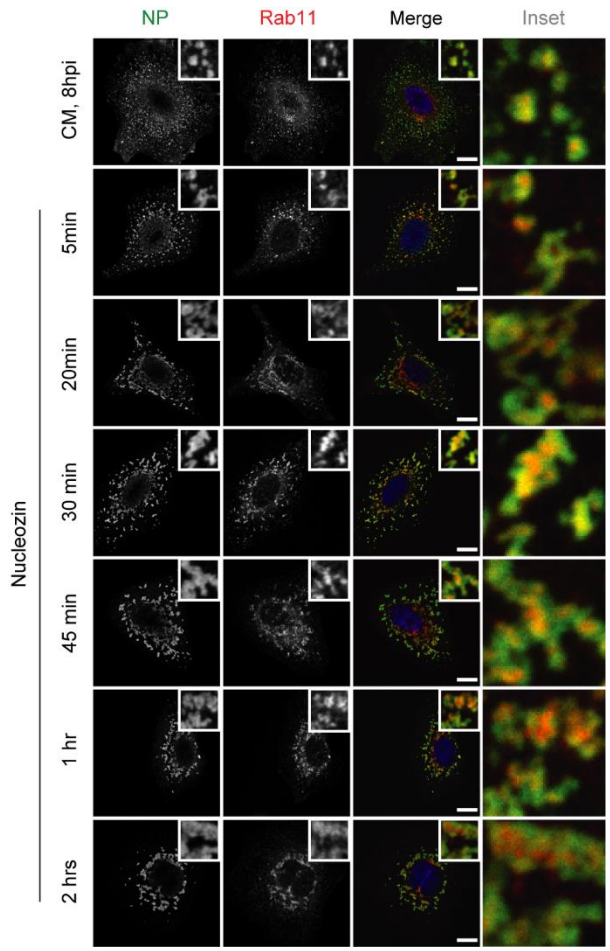

Figure 3.9- Nucleozin induces a mesoscale meshwork of IAV inclusions.

A549 cell were infected at a MOI of 3 with PR8 virus for 8 hrs, then incubated with a vRNP pharmacological sticker, nucleozin (Ncz) for different time periods from 5mins to 2hrs before fixing and analysis by immunofluorescence using antibody staining against NP (green) and Rab11 (red). Schematic depiction of the experimental analysis workflow and representative image of infected cells, fixed before and after Ncz treatment. Scale bar = 10µm.

Nucleozin affected the concentration of vRNPs in the cytosol that decreased with the time of treatment (**Figure 3.10**A), presumably by blocking vRNP nuclear export and/ or changes accessibility of antibodies to oligomerized NP. Conversely, nucleozin-treatment increased the size of viral inclusions (from 0.284 ± 0.04 without nucleozin to 1.02 ± 0.18 μm^2 with 2 h treatment, **Figure 3.10**B), which lost circularity (0.893 ± 0.02 without nucleozin to 0.761 ± 0.02 2h treatment, **Figure 3.10**C,D) and roundness (0.734 ± 0.01 without nucleozin to 0.672±0.02 with 2h treatment, **Figure 3.10**C,D) and decreased in number (from 366.2 ± 133,6 to 48.1 ± 34.0 after 2h treatment **Figure 3.10**E,F), suggesting that they were stiffer.

Interestingly, C_{dense} increased dramatically (from 2125.8 ± 0.09 without nucleozin to 3650.0 ± 0.03 with 2h nucleozin), **Figure 3.10**G-I) and C_{dilute} decreased and became stable after 20 min treatment (from 766.2 ± 213.0 without nucleozin to 330.2 ± 94.0 after 2h treatment, **Figure 3.10**H,J,K). Importantly, these structures were energetically more stable, with lower free energy (from -1711.1 ± 397 $J.mol^{-1}$ without nucleozin to -5388.4 ± 808 $J.mol^{-1}$ 2 h post nucleozin addition (**Figure 3.10**L,M).

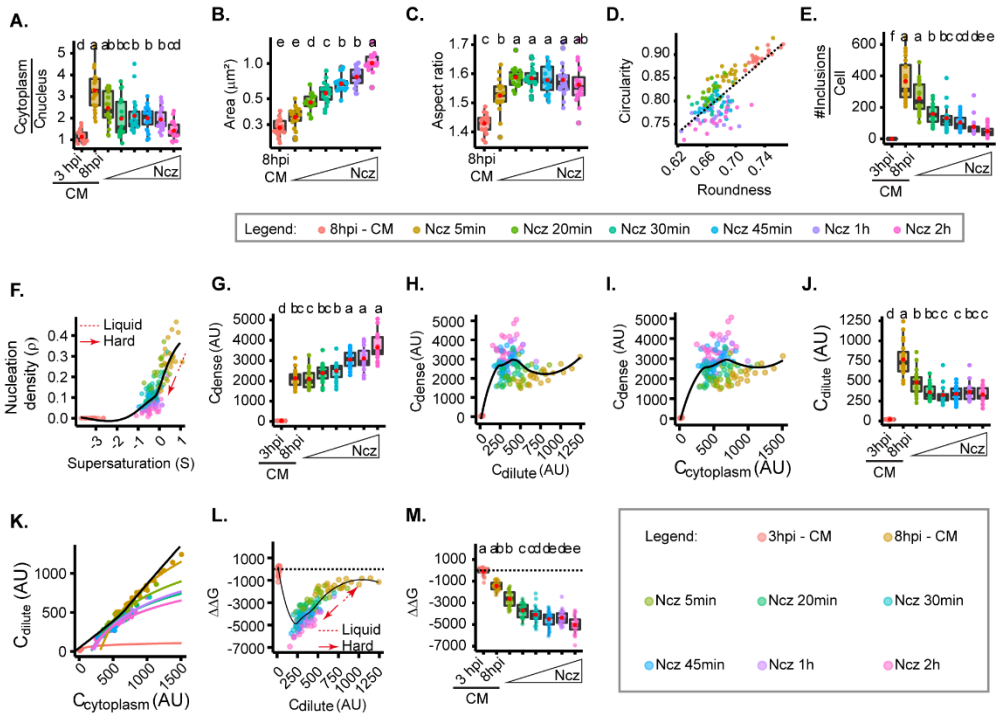

Figure 3.10- Increased interaction number and strength IAV inclusions.

Using images in ***Figure 3.9****, biophysical parameters were extracted and analysed as shown in* **Figure 3.4***. Each dot is the average value of measured parameter per cell, while the continuous black lines are non-linear fitted models for all data. Conditions normalized to an infection state without IAV inclusions (3 hpi) are indicated by a dashed black horizontal line. Above each boxplot, same letters indicate no significant difference between them, while different letters indicate a statistical significance at α = 0.05 using one-way ANOVA, followed by Tukey multiple comparisons of means for parametric analysis, or Kruskal-Wallis Bonferroni treatment for non-parametric analysis. Abbreviations: AU, arbitrary unit, CM, complete media and Ncz, nucleozin.* ***(A)*** *Boxplot depicting the fold change in the ratio of cytoplasmic to nuclear vRNPs concentration before and after Ncz (5 mM) treatment at 8hpi; P = 6.16e-14; Kruskal Wallis Bonferroni treatment.* ***(B)*** *Boxplot of inclusion area per cell; P < 0.001; Kruskal Wallis Bonferroni treatment.* ***(C)*** *Boxplot of inclusion aspect ratio; P < 2e-16; Kruskal Wallis Bonferroni treatment.* ***(D)***

Scatter plot of inclusion circularity versus roundness. ***(E)*** *Boxplot showing the number of inclusions per cell; P < 0.001; Kruskal Wallis Bonferroni treatment.* ***(F)*** *Scatter plot of nucleation density (ρ, μm^{-2}) versus degree of supersaturation (S).* ***(G)*** *Boxplot showing increasing inclusion C_{dense} (AU) with increasing Ncz incubation period. P < 0.001; Kruskal Wallis Bonferroni treatment.* ***(H)*** *Scatter plot of C_{dense} (AU) versus C_{dilute} (AU).* ***(I)*** *Scatter plot of C_{dense} (AU) and $C_{cytoplasm}$ (AU).* ***(J)*** *Boxplot showing C_{dilute} (AU; P < 0.001; Kruskal Wallis Bonferroni treatment.* ***(K)*** *Scatter plot of C_{dilute} (AU) versus $C_{cytoplasm}$ (AU). Coloured lines are non-linear fitted models of grouped data points in the graph.* ***(L)*** *Scatter plot of ΔΔG, J.mol^{-1} versus C_{dilute}, (AU).* ***(M)*** *Boxplot of fold change in free energy of partition (ΔΔG, cal.mol^{-1}); P < 0.001; Kruskal Wallis Bonferroni treatment.*

Together, the data suggest that stabilizing vRNP interactions changes inclusions more efficiently than the other strategies tested above (**Figure 3.11**).

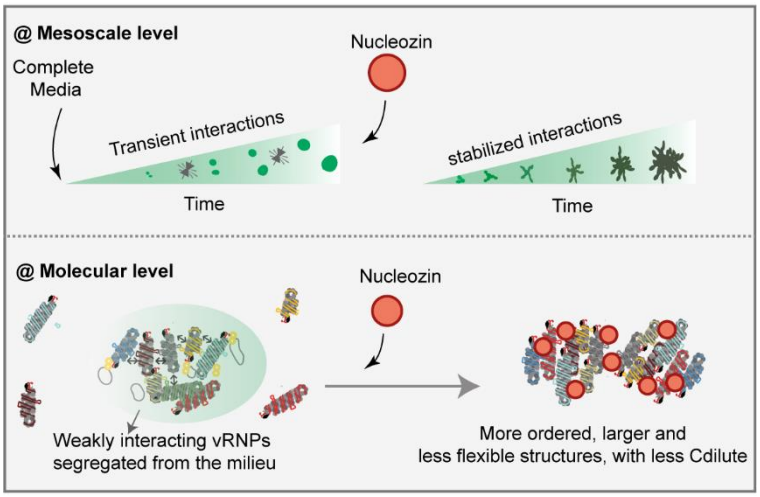

Figure 3.11-Model depicting a nucleozin-dependent interaction strength of IAV inclusions.

The mesoscale inclusion hardening, size augmentation and shape alterations are the consequences of nucleozin-induced vRNP stabilization at the molecular level.

3.4.5 Modifiers of strength/type of interaction between vRNPs harden liquid IAV inclusions.

Changing the strength of interactions amongst vRNPs impacted viral inclusions' thermodynamics the most. Therefore, we next sought to characterize if nucleozin altered their material properties. To achieve this, we first established the ability of IAV inclusions to respond to shock treatments by exposing them to hypotonic and 1,6-hexanediol shock treatments at different concentrations and time (**Figure 3.12**A-C). Our data showed that native inclusions are maintained in complete media (**Figure 3.12**A,C) but begin to dissolve in a manner that is proportional to the concentration and exposure time of 1,6-hexanediol (**Figure 3.12**B,C) and hypotonic shocks (**Figure 3.12**B,C). A 5 min or 30min shock in 80% H_2O or 1,6-hexanediol respectively (**Figure 3.12**B,C) is sufficient to dissolve viral inclusions and will therefore be used onwards.

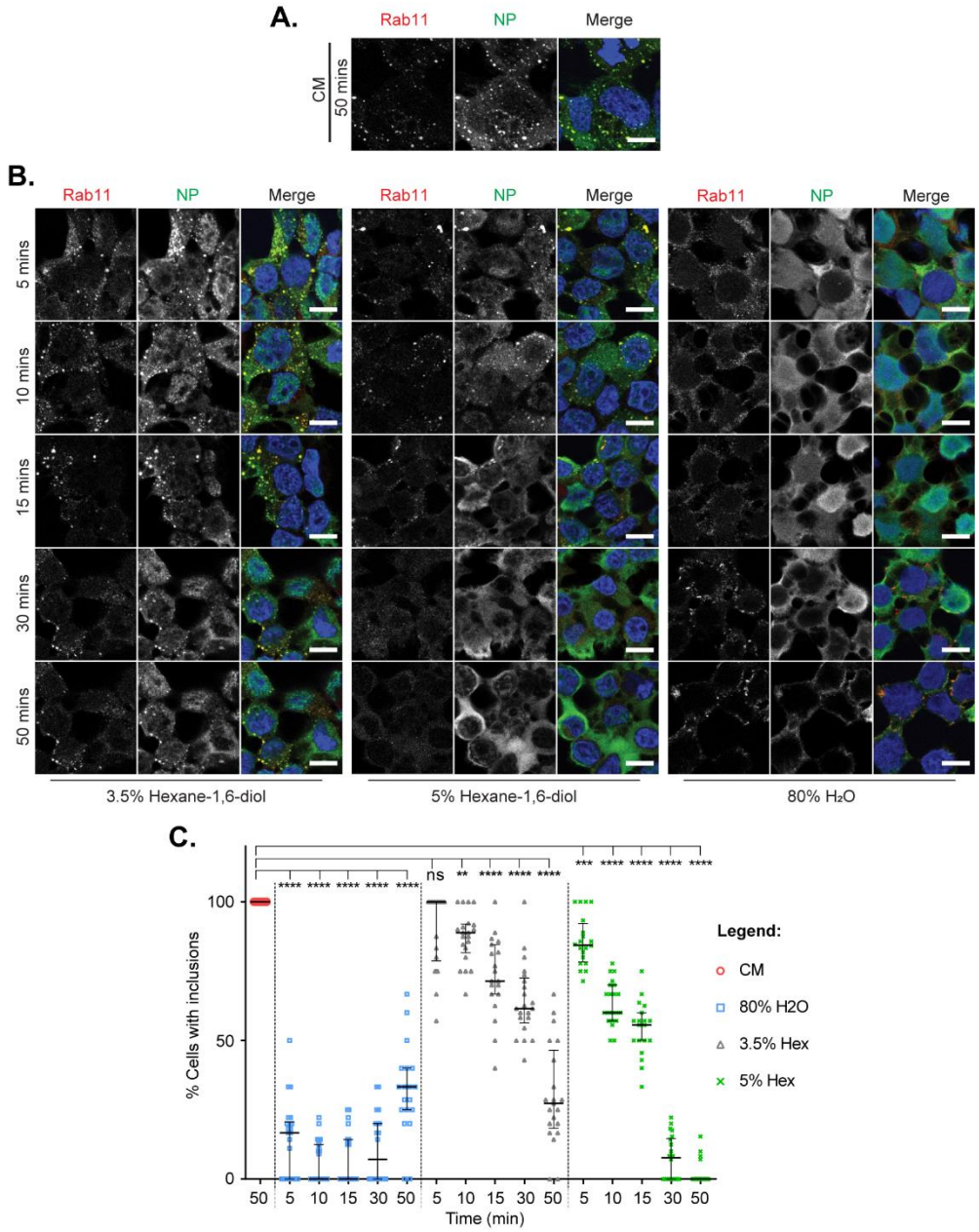

Figure 3.12- Inclusions respond to shock treatments in a time-dependent manner.

293T cells were infected with PR8 for 7 hrs at a multiplicity of infection (MOI) of 3, grown in ***(A)*** *complete media for 50mins as control or* ***(B)*** *incubated for*

5-50 mins with 3.5% 1,6-Hexanediol, 5% 1,6-hexanediol or 80% water (hypotonic shock). Representative immunofluorescence images show IAV inclusions (NP, green, Rab11, red). Scale bar = 5 µm. ***(C)*** *quantification of cells expressing inclusions before and after exposure to shock treatments, *** P < 0.0001; one-way ANOVA.*

We then examined if nucleozin-treated viral inclusions maintained the ability to dissolve upon shock treatments. We observed that native inclusions responded to shock treatment as expected, however, nucleozin strongly held inclusions together that did not dissolve when exposed to either hypotonic or 1,6-hexanediol shock treatments (**Figure 3.13**A-C). This lack of response to shocks suggests that IAV inclusions undergo hardening when vRNP interactions are stronger.

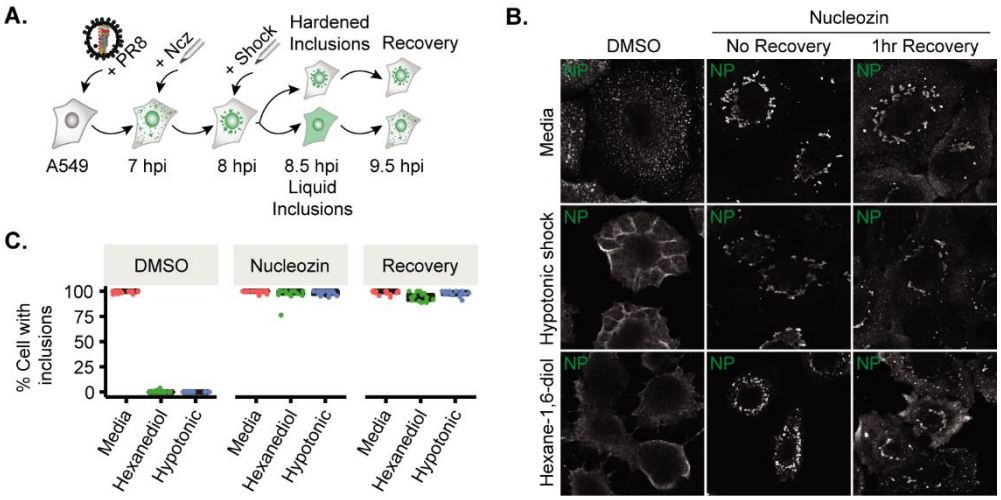

Figure 3.13- IAV inclusion response to hypotonic and 1,6-hexanediol shocks is lost when pre-treated with nucleozin.

A549 cells were infected with PR8 for 7 hrs at a multiplicity of infection (MOI) of 3, treated with 5 µM nucleozin (Ncz) or vehicle (DMSO) for 1hr and shocked with 80% water (hypotonic shock, Hyp, 5% 1,6-hexanediol (Hex) or complete media (CM) as control. ***(A)*** *Schematics of inclusion shock adaptation after*

Ncz or DMSO treatments. ***(B)*** *Representative immunofluorescence image showing IAV inclusions (NP, as proxy) response to shock treatments.* ***(C)*** *Boxplot showing percentage cells with inclusions after manual scoring. P < 0.001; Kruskal Wallis Bonferroni treatment.*

To formally establish that IAV liquid inclusions can be hardened, we compared the dynamics of viral inclusions in the presence or absence of nucleozin using four different approaches. First, we assessed their movement and measured speed and displacement from their point of origin (**Figure 3.14**A). Native liquid inclusions (treated with sham vehicle - DMSO) display a highly stochastic movement and long displacement, whilst nucleozin-hardened inclusions were less mobile with smaller displacement, as observed by analysing loss of movement in individual tracks (**Figure 3.14**B). There is an overall reduction in mean square displacement (MSD) with nucleozin (**Figure 3.14**C,D) that results in a lower MSD at 100 sec (MSD_{100sec} = 0.838 ± 1.17 μm^2 without nucleozin, shifting to 0.057 ± 0.22 μm^2 with treatment, median ± SD, **Figure 3.14**C,D).

In a second approach, we measured the time that two droplets take to relax to a sphere upon fusion by coarsening assays (shifting the aspect ratio from 2 to 1, **Figure 3.15**A). DMSO-treated inclusions relax fast to a single sphere upon fusion (5.8 ± 1.94 s; mean fusion time ± SEM, **Figure 3.15**B), shifting the aspect ratio from 2 to 1 (**Figure 3.15**C,D). Nucleozin-treated inclusions retain a stable aspect ratio over time (**Figure 3.15**D), as they are unable to fuse (**Figure 3.15**C,D). The results demonstrate that nucleozin stiffens IAV inclusions.

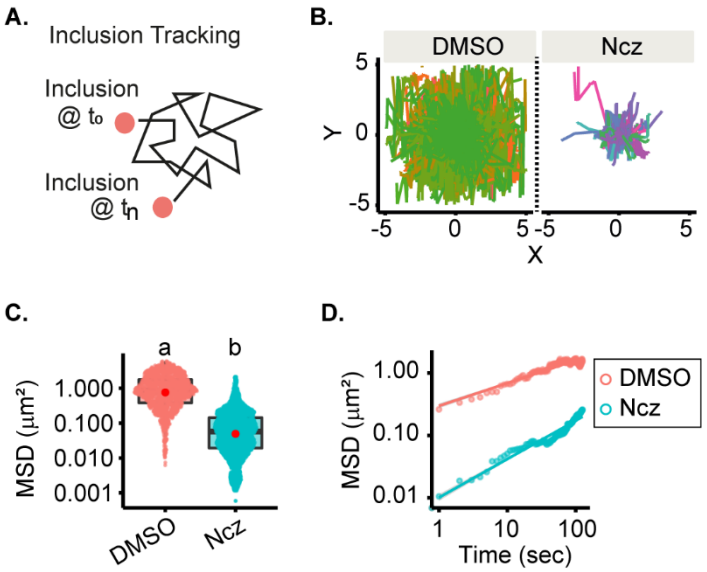

Figure 3.14- Nucleozin treated inclusions lose mobility.

A549 cells were transfected with plasmids encoding either GFP-NP and co-infected with PR8 virus at a multiplicity of infection (MOI) of 10. After 12 h, the cells were incubated in 5 µM Ncz or DMSO for 1 h and live imaged for tracking inclusion movements. ***(A)*** *Scheme showing how IAV inclusions were tracked over time from the point of origin at time zero (t_0)* ***(B)*** *Line graph the trajectories of IAV inclusions (GFP-NP, as proxy) after DMSO or nucleozin (Ncz) treatments* ***(C)*** *Boxplot of the mean square displacement (μm^2) of IAV inclusions.* ***(D)*** *Graph showing the mean square displacement (μm^2) versus time (sec) of IAV inclusions (NP, as proxy).*

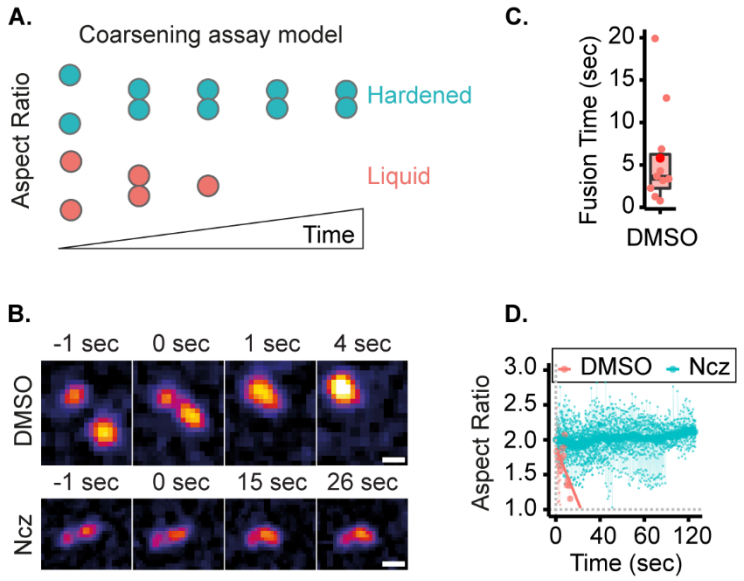

Figure 3.15- Inclusion liquid-like coalescence is lost upon nucleozin treatment.

A549 cells were transfected with plasmids encoding either GFP-NP and co-infected with PR8 virus at a multiplicity of infection (MOI) of 10 for 12 hrs, before a 1 hr treatment with 5 µM Ncz or DMSO and live imaging of inclusions fusion dynamics. ***(A)*** *Schematics of the coarsening assay model, in which liquid and hardened IAV inclusions are represented by orange and blue dots, respectively. Unlike hardened inclusions, native liquid inclusions are expected to fuse into a spherical droplet upon touching.* ***(B)*** *Pseudo-coloured time-lapse images of coalescing viral inclusions (GFP-NP used as proxy; extracted from live cell videos). Scale bar = 2 µm.* ***(C)*** *Aspect ratio was used as a measure of IAV inclusion coalescence into a sphere. Mean aspect ratio per time was fitted to a linear model (bold coloured lines). Horizontal grey dash lines depict a perfect sphere (aspect ratio = 1).* ***(D)*** *Boxplot of the fusion time (sec) of IAV liquid inclusions treated with DMSO. Dots represent fusion time of individual fusion event.*

In a third approach, the molecular dynamics of IAV inclusions was assessed by Fluorescence Loss After Photoactivation (FLAPh). In a live imaging experiment, a region of interest (ROI) was photoactivated and its decay profile monitored for 120 seconds (**Figure 3.16**).

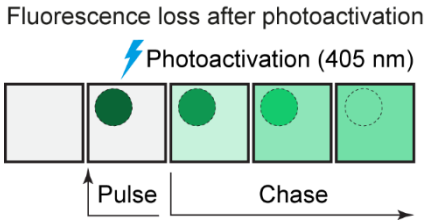

Figure 3.16- Schematic representation of a pulse-chase fluorescence loss after photoactivation (FLAPh).

At steady state there is no fluorescence, but when pulsed by light (405 nm) at a region of interest (ROI), the fluorophores in the ROI are activated emitting at 455nm (green fluorescence). In the ensuing chase period, the green, fluorescent particles can be tracked over time as materials are exchanged with particles in the inactivated regions. Therefore, fluorescence in the activated ROI is diluted while the fluorescence is gained at the inactivated region. This exchange is proposed to happen only in fluid materials but not in rigid materials.

After fitting data with a single exponential model, the plot showed that DMSO- and nucleozin-treated inclusions exhibited distinct decay profiles, rate constant and mobile fractions, with half-life of 14.41 ± 0.9 s (mean ± SEM) and 85.02 ± 19.8 s, respectively (**Figure 3.17**A-F). This indicates that nucleozin treated inclusions become more static (less mobile).

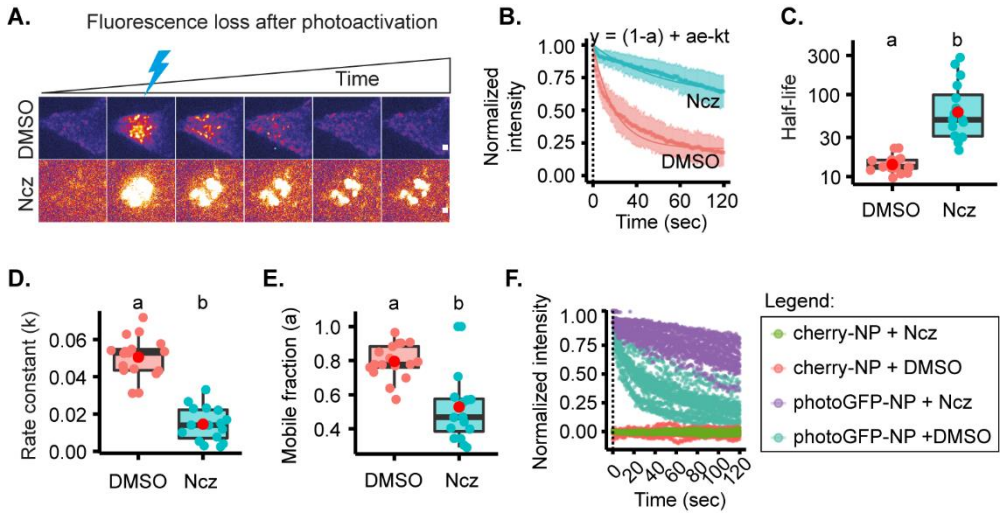

Figure 3.17- The native IAV Inclusion dynamicity is lost when treated with nucleozin.

A549 cells were co-transfected with plasmids encoding photoactivatable GFP-NP (paGFP-NP) and mcherry-NP (internal control) and simultaneously infected with PR8 virus at an MOI of 10. At12hpi, cells were treated for 1hr with 5 µM Ncz or DMSO, after which inclusions (paGFP-NP and cherry-NP as proxy) at specific region of interest (ROI) were photoactivated with 405 nm light and tracked by live-imaging for 120 sec. Above each boxplot, same letters indicate no significant difference between them, while different letters indicate a statistical significance at α = 0.05. ***(A)*** *Time lapse pseudo-colour images showing the fluorescence loss in photoactivated IAV inclusions (photoactivatable GFP-NP used as proxy) upon treatment with Ncz or DMSO)* ***(B)*** *Normalized fluorescence intensity decay of photoactivated IAV inclusions. Coloured lines are single exponential model fitting ($y_0 = (1\text{-}a) + ae^{-kt}$) of the data point, dots are the mean of the data per second, and vertical lines denote the standard deviation (SD) per time (sec).* ***(C)*** *Half-life ($t_{1/2} = \frac{In(2)}{k}$, $k = rate\ constant$) of IAV inclusions decay post-activation (sec). P = 1.386e-6; Kruskal Wallis Bonferroni treatment. (**D**) Decay constant (sec^{-1}) of inclusions. P = 1.386e-6; Kruskal Wallis Bonferroni treatment.* ***(E)*** *Mobile fraction of*

inclusions. P = 0.000475; Kruskal Wallis Bonferroni treatment. ***(F)*** *Dot plot showing every data point of normalized fluorescence decay of photoactivated IAV inclusions. Coloured lines are single exponential model fitting ($y_0 = (1-a) + ae^{-kt}$) of the data point, dots are the mean of the data per second, and vertical lines denote the standard deviation (SD) per time (sec).*

Lastly, we measured the internal rearrangement in viral inclusions. Because of the small size and highly dynamic nature of IAV inclusions, previous attempts to perform Fluorescence Recovery After Photobleaching (FRAP) experiments resulted in highly variable recovery rates. Therefore, we were unable to accurately determine if internal rearrangements were taking place viral inclusions (**Figure 3.18**A-D) (Alenquer et al., 2019; Amorim et al., 2011).

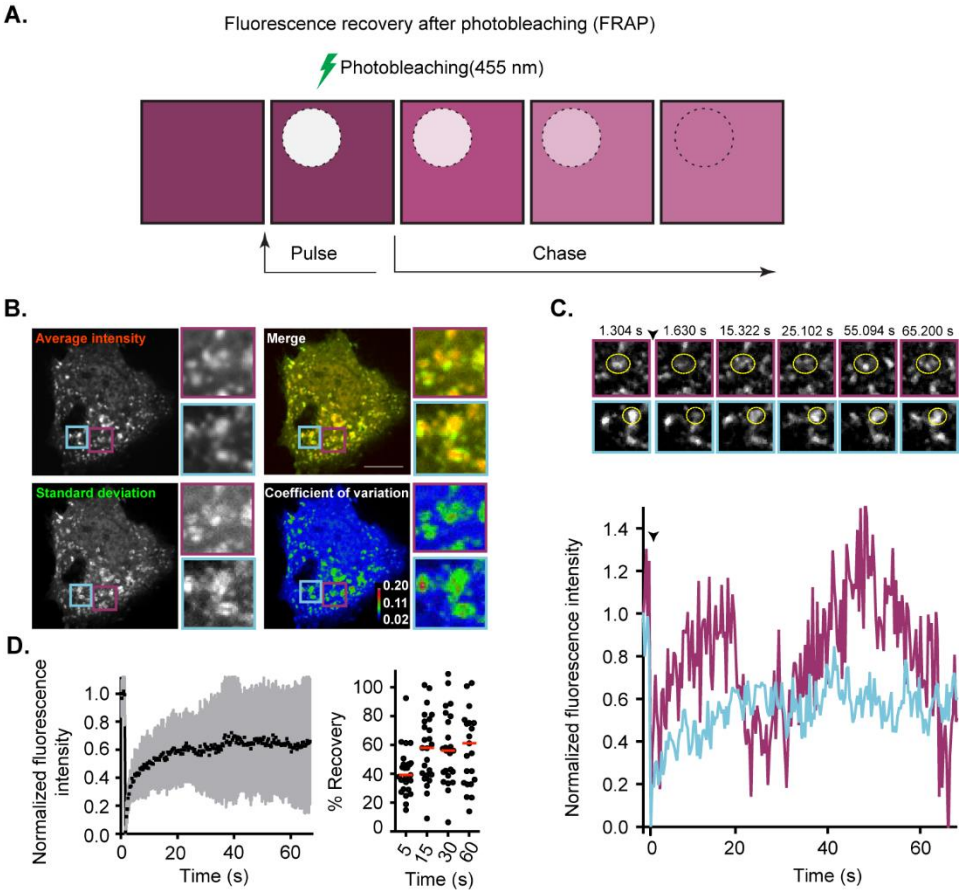

Figure 3.18- Fluorescence recovery after photobleaching (FRAP) demonstrating dynamic material exchange and rearrangement between inclusions

(Adapted from Alenquer et al 2019).

***(A)** Schematic representation of the FRAP experiment. Upon photobleaching of fluorescent particles in a region of interest (ROI), material exchange with inactivated particles outside the ROI results in fluorescence recovery in the ROI. **(B - D)** A549 cells were transfected with a plasmid encoding GFP-NP and infected with PR8 virus, at an MOI of 5. From 10-16hpi, individual inclusions were photobleached to fluorescence recovery of IAV inclusions (GFP-NP as proxy) **(B)** A representative cell is shown. The fluorescence*

signal of viral inclusions in this cell is depicted as: average intensity (in red), standard deviation (in green), the merge of both, and coefficient of variation. Two areas of viral NP inclusions, highlighted in purple and cyan boxes, were selected for fluorescence recovery after photobleaching (FRAP). Bar = 10 µm. ***(C)*** *R.F.I. was plotted as a function of time for the means of 25 FRAP events (left graph). The means are shown (black) with error bars representing the standard deviation (gray). The percentage of recovery of each photobleached region is shown for specific times (right graph), with medians represented as red bars. A single experiment representative of two independent experiments is shown.* ***(D)*** *The photobleached regions are marked by a yellow circle. The black arrowhead indicates the time of photobleaching. Relative Fluorescence Intensity (R.F.I.) was plotted as a function of time for each particle.*

As the microtubule depolymerising drug nocodazole largely blocks the movement of IAV inclusions, rendering them larger and more spherical (Amorim et al., 2011; Avilov et al., 2012a; Nturibi et al., 2017), we opted for bleaching IAV inclusions upon treating them with nocodazole (**Figure 3.19**A,B). In native conditions, the photobleached region quickly disappeared, consistent with internal rearrangement of vRNPs inside IAV inclusions, whilst in nucleozin-treated inclusions, the photobleached area remained unaltered, revealing stiffness (several examples in **Figure 3.19**B).

Taken together, DMSO- and nucleozin-treated IAV inclusions exhibit distinct responses to shocks, dynamics, internal rearrangement and coalescing properties, supporting that nucleozin hardens IAV liquid inclusions.

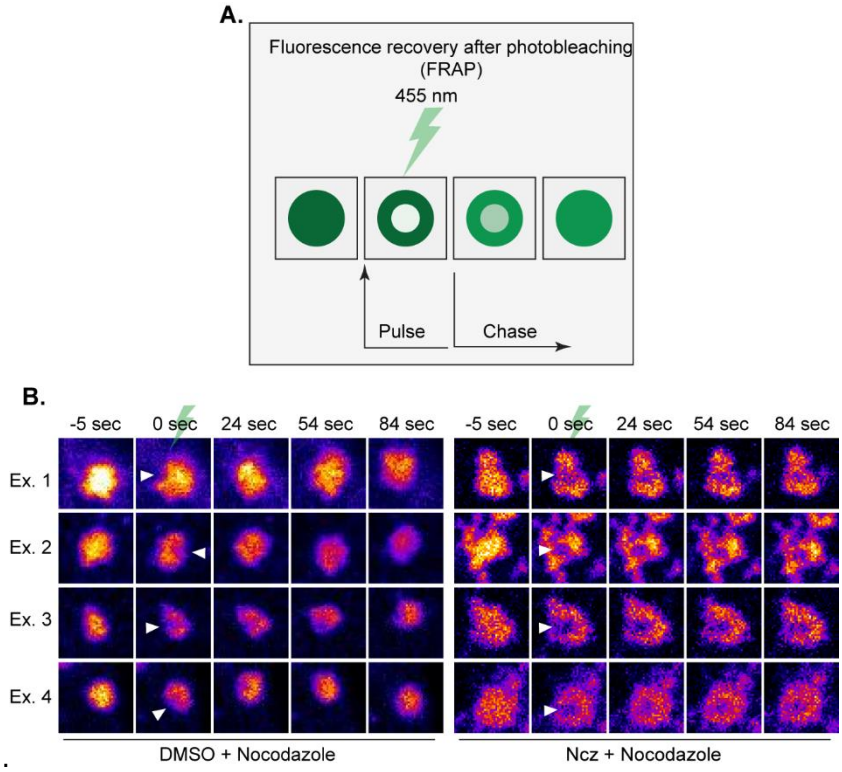

Figure 3.19- Fluorescence loss after photobleaching (FRAP) demonstrating the lack of dynamic material exchange and rearrangement in inclusions treated with nucleozin.

A549 cells were transfected with plasmids encoding mcherry-NP and co-infected with PR8 virus at an MOI of 10. At 12hpi, cells were treated with nocodazole (10 µg/mL) for 2h to reduce the highly stochastic motion of liquid IAV inclusions and subsequently treated with DMSO or nucleozin (Ncz, 5µM). Small regions inside IAV inclusions were photobleached to assess internal rearrangement of vRNPs (mCherry-NP as proxy). ***(A)*** *Schematics of experimental workflow.* ***(B)*** *Time lapse pseudocolor images shows the fluorescence recovery after photobleaching (FRAP).*

3.5 Discussion

Phase transitions are important for the regulation of key cellular programmes including transcriptional control (Hnisz et al., 2017), signal transduction (Case et al., 2019a), molecular biochemistry (Banani et al., 2017; Wheeler and Hyman, 2018), cellular noise (Riback and Brangwynne, 2020), granulostasis (Alberti et al., 2017; J. Wang et al., 2018), amongst others. However, aberrant phase transitions that originate from changes in material properties such as liquid to solid phase transition (reviewed in (Alberti and Dormann, 2019)) have been implicated in stress adaptation (reviewed in (Franzmann and Alberti, 2019; Rabouille and Alberti, 2017)), neurodegenerative diseases (reviewed in (Elbaum-Garfinkle and Brangwynne, 2015; Nedelsky and Taylor, 2019)) and cancer (reviewed in (Spannl et al., 2019)).

Condensates formed during viral infections namely IAV, SARS-CoV-2, measles, Rabies virus, VSV etc, are known to display a liquid profile that may support critical function (such as viral genome transcription, replication and assembly) during their life cycles (reviewed in (Etibor et al., 2021; H. Li et al., 2022; Lopez et al., 2021; Luzak, 2022; Wei et al., 2022; Wu et al., 2022)). Therefore, we and others hypothesised that changing the material properties of liquid viral condensates results in the alteration of their function and may abrogate viral replication. This is important as liquid viral condensate hardening was recently reported to abrogate hRSV replication (Risso-Ballester et al., 2021).

In our work, we provided a framework for assessing the impact of the well-known and modifiable biophysical parameters of intracellular phase transitions namely temperature, concentration, and type/ strength of interactions. Assessment of these parameters demonstrated that modulation of the type/ strength of molecular interactions within IAV inclusions generated

the most profound effect on the condensates and is therefore the best strategy to harden IAV inclusions for hampered function.

In the presence of thermal fluctuations, IAV Inclusions appear bigger at a low temperature (4ºC) and begin to dissolve into smaller but numerous microstructures at a high temperature (42ºC). This behaviour is most common for *in vitro* biomolecular condensates exhibiting a UCST phase diagram ((Quiroz and Chilkoti, 2015) and reviewed in (Falahati and Haji-Akbari, 2019)). Here, phase transition occurs only below the critical temperature. Beyond this upper critical temperature, a regime of homogeneous mixture that starts to emerge like IAV inclusions at 42ºC and beyond. This homogeneous behaviour may be due to destabilization of interactions within the components of viral inclusions. Importantly, IAV inclusions do not display a hardened profile irrespective of the thermal state.

Furthermore, changes in the concentration of molecules that are known to partition into IAV inclusions (viz. vRNPs and Rab11a) only increased the sizes and saturation concentration as infection progresses with time. However, the inclusion densities at high vRNP and Rab11a concentrations were not sufficient to yield hardened inclusions. In fact, these inclusions readily exhibited a fluid fusion and fission dynamics regardless of size and concentration, as is expected of a liquid viral condensate. Moreover, IAV inclusions displayed a non-fixed C_{sat} that is typically exhibited by *in vivo* condensate systems governed by multicomponent thermodynamics (Riback and Brangwynne, 2020). Due to the heterogeneity of its component molecules, the behaviour of IAV inclusions does not fit with biomolecular condensates originating from a binary system where C_{sat} is fixed (reviewed in (Riback and Brangwynne, 2020)). Despite changes in the concentration of its molecular constituents, IAV inclusions retain their innate liquid behaviour including the ability to fuse and divide, adapt readily to shock, and display rapid dynamics.

Interestingly, upon exposure to pharmacological sticker, nucleozin, the thermodynamics landscape of IAV inclusions was drastically changed. This resulted in the free energy stabilization of a rather destabilizing liquid IAV inclusion as would be expected for c-mods. Stabilization of the free energy landscape was previously reported for high valency interactions (Riback et al., 2020), which in the case of IAV led to the hardening of liquid inclusions. This hardening phenotype is characteristic of aberrant biomolecular condensates exemplified by neurodegenerative diseases and cataract (reviewed in (Elbaum-Garfinkle and Brangwynne, 2015; Nedelsky and Taylor, 2019; Vekilov, 2010)). However, pharmacological hardening during IAV infection creates a unique opportunity that favours normal cellular physiology over viral replication by forming aberrant viral inclusions with significantly reduced dynamics, mobility, and fusibility.

In sum, increasing interaction type/ strength is the key to hardening IAV inclusions; a process that is not dependent on thermal or concentration changes. This are unexpected results that, in practical terms, suggest that regulating endothermic reactions close to viral inclusions or the concentration of components within viral inclusions is unlikely to yield an efficient strategy to harden these structures in a way that could be used to block IAV infection. Conversely, investing in strategies able to increase the strength of interactions between inclusions, or reducing the flexibility of vRNPs may provide innovative solutions to block viral infections. Here we did not test what are the parameters that could result in abrogation of the formation or dissolution of viral inclusions. These strategies are known to reduce viral titres (Alenquer et al., 2019; Amorim et al., 2013; Bruce et al., 2010; Eisfeld et al., 2011a; Ganti et al., 2021; Han et al., 2021; Kao et al., 2010).

Our framework for assessing the material properties may be applied to other cellular and viral condensates to determine the best therapeutic strategies. Since we were able to target liquid inclusions for pharmacological

hardening, drug selectivity of c-mods would be a vital to the advancement of condensate therapeutics.

As a result of the off target effects observed in hRSV condensate inhibitors cyclopamine and A3E (Risso-Ballester et al., 2021), in the next chapter, we will address the condensate drug selectivity challenge.

3.6 Materials and methods

3.6.1 Cell lines

GFP-Rab11a-WT and GFP-Rab11a-DN cell lines were produced in-house and characterised in (Alenquer et al., 2019), while human basal alveolar epithelial cell (A549) and human embryonic kidney 293 cells expressing a mutant version of the SV40 large T 158 antigen (HEK293T aka 293T) were generous gifts from Prof Paul Digard, Roslin Institute, UK.

3.6.2 Cell culture

Cells were cultured in complete media constituting Dulbecco's modified Eagle's medium (DMEM, Gibco®, 21969035) supplemented with fetal bovine serum (FBS, Gibco®, ThermoFisher, 10500064), 10% (v/v), 200 mM L-glutamine (Life Technologies, 25030-024), and 100 U/ml penicillin, 10 µg/ml streptomycin (Biowest, L0022-100, 1% (v/v)). Every 3-4 days, confluent cells were sub-cultured in T75 flasks using trypsin-EDTA (Biowest, X0930-100) and incubated at 37ºC, 5% CO_2.

3.6.3 Transfection

To tag vRNPs during in infection, A549 or GFP-Rab11-WT cells grown to 70% confluency in 8-well glass-bottomed dish (Ibidi), infected with PR8 virus and transfected with plasmids encoding mcherry-NP (200 ng/ µL), GFP-NP (200 ng/ µL) or mcherry-NP (100ng/ µL) and photoactivatable GFP-NP (200 ng/ µL), using Lipofectamine LTX (ThermoFisher, 15338100) or jetPRIME (Polyplus, 101000015) in Reduced Serum Medium Glutamax™ (OptiMEM™; Gibco™, ThermoFisher, 51985026) according to the manufacturer's instructions, and incubated for 12- 16 hours.

3.6.4 Influenza A virus strains

Reverse-genetics (RG) derived A/Puerto Rico/8/34 (PR8, H1N1) (kindly provided by Prof. Ron Fouchier) was used as model virus. Viruses were grown in eggs as following: embryonated chicken eggs were incubated at 37ºC for 10 days. After that, the eggshell was lightly sanded with a rotary tool and a hole was pierced with a sterile 27G needle on top of the egg and on the opposite side of the embryo. Through that hole, 100 PFU of virus diluted in 200µl PBS were injected into the allantoic fluid of the egg. Infected eggs were incubated at 37ºC for 2-3 days, and then at -20ºC for 2h. Viruses were collected by opening the eggs and carefully retrieving the allantoic fluid. After centrifugation at 3500g, 5min, 4ºC to remove debris, the virus solution titrated by plaque assay and aliquoted and kept at -80ºC.

3.6.5 Viral infection

Cells were seeded in culture plates at appropriate density and incubated overnight. Virus inoculum was added in serum-free DMEM at the MOI of 3 (for fixed samples) or MOI of10 (for live imaging) and incubated for 45min. Afterwards, cells were overlaid with complete media and incubated at 37ºC, 5% CO2 for the indicated time.

3.6.6 Drug treatment

Nucleozin was dissolved in dimethyl sulfoxide (DMSO) and used at a final concentration of 2 µM (immunofluorescence staining and virus titres) or 5 µM (live imaging), while 1,6-Hexanediol was dissolved in DMEM and used at 5 % (w/v). Also, Nocodazole (Noc) (Sigma) was dissolved in DMSO and used at a final concentration of 10 µg/ mL.

3.6.7 Condensate shock treatment

PR8 infected cells grown in OptiMEM media were replaced with either 80%(v/v) of H_2O or 5%(w/v) 1,6-Hexanediol in OptiMEM for 10 min or 30 min respectively. Thereafter, cells were either directly fixed or allowed to recover in OptiMEM for 1 h before fixing and processing for immunofluorescence imaging. The number of cells expressing inclusions were quantified manually and normalised to conditions in normal media.

3.6.8 Immunofluorescence

Cells were fixed for 10 min with 4% formaldehyde and permeabilized for 7 min with 0.2% (v/v) Triton-X-100 in PBS. Thereafter, they were incubated with the indicated primary antibodies for 1 h at RT, washed thrice with 1% (v/v) neonatal calf serum (NCS) in phosphase buffered saline (PBS) and incubated for 45 min with Alexa fluor conjugated secondary antibodies and Hoechst. Antibodies used were rabbit polyclonal against Rab11a (1:100; Life Technologies, 715300), and mouse monoclonal against NP (1:1000; Abcam, 20343). Secondary antibodies were all from the Alexa Fluor range (1:1000; Life Technologies). Following washing, cells were mounted with Dako Faramount Aqueous Mounting Medium.

3.6.9 Immunofluorescence imaging

Using a ×100 oil immersion objective (Plan Apo 1.49), a bandpass filter (525/45 Chroma), and a photometrics 512 EMCCD camera, single optical sections immunofluorescence images of fixed cells were taken with a Leica SP5 live confocal microscope (using photon counter mode). Alternatively, the Z-stacks images were acquired using Marianas SoRa (CSU) or Zeiss LSM 900 with AiryScan2.

3.6.10 Image segmentation

Immunofluorescence images were converted to 8-bit color, background was removed, and the threshold was adjusted. Thereafter, the "analyze particle" function in FIJI (Fiji Is Just) ImageJ 2.1.0/1.53p) was selected to quantify and categorise the area of segmented inclusions in the selected cell. Images were postprocessed using FIJI and Adobe Illustrator.

3.6.11 Determining inclusion topology and thermodynamics

To determine the total concentration of vRNPs (NP as proxy) transported to the cytoplasm in relation to vRNPs produced in the nucleus ($\frac{Ccytoplasm}{Cnucleus}$), a sum of slices of z-stacked images were used, otherwise, single plane images were analysed in the experiment assessing change in temperature. We used a custom (Fiji Is Just) ImageJ 2.1.0/1.53p script for image processing using the following pipeline: **(1.)** Segment cell periphery. **(2.)** Segment and remove nucleus from the cell to make the cytoplasm. **(3.)** From the cytoplasm, segment inclusions **(4.)** Analyse the cytoplasm, nucleus, and inclusions for number and topological shape descriptors **(5.)** Using the appropriate segmented region, measure the mean fluorescence intensity (as proxy of concentration) of cell, nucleus, cytoplasm, and cytoplasmic inclusion (*See* **Figure 3.1***B*).

Using the method published by Riback *et al. 2020* as template, we determined C_{dense} as the mean fluorescence intensity of the segmented inclusion while C_{dilute} was extrapolated from remaining cytoplasmic vRNP intensity outside the inclusions. We picked the best approach out of three to measure C_{dilute}. **(1.)** Use ROIs from randomly selected cytoplasmic areas lacking inclusions. The limitation with this method is that inclusions are highly abundant in the cytoplasm of infected cells and are nearly impossible to manually or automatically draw without selecting regions containing inclusions. **(2.)** Use an enlarged ROI band around the inclusions. This was

easy to automate but limited by the overlap with other ROI bands due to the density of IAV inclusions in the infected cell. **(3.)** Use ROI of the entire cytoplasm devoid of viral inclusions. This was easy to automate, lacks overlap with other ROIs and serves as the cleanest strategy when compared to strategy 2 (**Figure 3.20 S**1 and ***Figure 3.21* S**2). We used strategy 3 to determine the $C_{dilute.}$

Partition coefficient (K) and free energy (ΔG) were derived based on (Riback et al., 2020); where K = $\frac{Cdense}{Cdilute}$, and ΔG = -RT*ln*K. Inclusion saturation concentration (C_{sat}) is the threshold C_{dilute} where inclusion begins to appear (~ 6hpi) and is calculated as the minimum C_{dilute} in cells with observable viral inclusions. The change in free energy was normalised to 3hpi (an infection stage with nuclear vRNP staining lacking cytoplasmic inclusions and was represented as $\Delta\Delta G = \Delta G - \Delta G_{(3\ hpi)}$.

3.6.12 Live cell imaging

Cells were grown in chambered 8-well glass-bottomed dish (Ibidi) containing OptiMEM medium (Gibco) and incubated for 14 h at 37 ºC and 5% CO_2. Media was substituted for Leibovitz L-15 media to buffer CO_2 and data acquisition started on a Roper TIRF Spinning Disk (Yokogawa CSU-X1) or Zeiss LSM 980 AiryScan2 with a cage incubator to control temperature at 37 °C. After excitation with a 491 nm laser (Cobolt 491, 100 mW), fluorescence from GFP was detected with a ×100 oil immersion objective (Plan Apo 1.49), a bandpass filter (525/45 Chroma), and a photometrics 512 EMCCD camera. Images were post-processed with ImageJ (NIH) and Adobe Illustrator.

3.6.13 Particle tracking and mean square displacement

TrackMate plugin ((Fiji Is Just) ImageJ 2.1.0/1.53p, FIJI) was used to track inclusions at a timescale of 1 s / frame in live imaging samples and XY

trajectories were subsequently analysed in a custom R (version 4.1.0) script to calculate the mean square displacement (MSD).

3.6.14 Coarsening assay

After nucleozin or DMSO treatment of PR8-infected cells, time lapse image acquisition of inclusions was taken. Coarsening assays were calculated from two biological replicates in which several events were imaged. Coarsening assay was analysed from time-lapsed tracking of two inclusions, starting from the point they first touch to the point they relax into a rounded puncta with an aspect ratio (AR) of 1. Fusion time and shape changes (aspect ratio, AR) of 2 inclusions were quantified using FIJI. Images were post-processed with ImageJ (NIH) and Adobe Illustrator.

3.6.15 Fluorescence recovery after photobleaching (FRAP)

For FRAP analysis, cells were transfected with 250 ng of GFP-NP and immediately superinfected with PR8 at an MOI of 10. At 12 hpi, media was substituted for Leibovitz L-15 media to buffer CO2 and data acquisition started on a Roper TIRF (total internal reflection fluorescence) Spinning Disk (Yokogawa CSU-X1) with a cage incubator to control temperature at 37 °C. After excitation with a 491 nm laser (Cobolt 491, 100 mW), fluorescence from GFP was detected with a ×100 oil immersion objective (Plan Apo 1.49), a bandpass filter (525/45 Chroma), and a photometrics 512 EMCCD camera. All FRAP experiments were performed similarly using iLas FRAP module (Rope Scientific): 2 s prebleach, 12.18 ms μm−2 bleach, 60 s postbleach at a frame rate of three images per second. Bleaching was performed in a variable circular area to target complete viral inclusions. For FRAP analysis, samples were corrected for background fluorescence and acquisition photobleaching as described previously by the Phair method (Phair et al., 2003). After normalization, FRAP curves were fitted following the exponential function: Y = Y0 + (Plateau-Y0) * (1-exp(-D*x)), where: Y0: Y value when X

(time) is zero. It is expressed in the same units as Y. Plateau (must be less than one): Y value at infinite times, expressed in the same units as Y. D: rate constant, expressed in reciprocal of the x axis time units. Tau: time constant, expressed in the same units as the x axis. It is computed as the reciprocal of D. Half time: time units of the x axis. It is computed as *ln*(2) D−1. Span (mobile phase): difference between Y0 and Plateau, expressed in the same units as your Y values.

3.6.16 Fluorescence loss after photoactivation (FLAPh)

FLAPh protocol followed the same sequence as was done for FRAP. In fact, the same microscope and imaging setup was used, except at the point of photobleaching. In place of photobleaching the cells were photoactivated with a 405nm laser excitation. Live images were obtained at 1frame/ s

For photoactivation experiment, cells were cotransfected with cherry-NP (100ng/ µL) and photoGFP-NP (250ng/ µL) using lipofectamine LTX and immediately superinfected with PR8 at an MOI of 10. At 12 hpi, media was substituted for Leibovitz L-15 media to buffer CO2 and data acquisition started on a Roper TIRF Spinning Disk (Yokogawa CSU-X1) with a cage incubator to control temperature at 37 °C. After excitation with a 405 nm laser (blue light), fluorescence from the activated GFP was detected with a ×100 oil immersion objective (Plan Apo 1.49), a bandpass filter (525/45 Chroma), and a photometrics 512 EMCCD camera. All FLAPh experiments were performed similarly using iLas FRAP module (Rope Scientific): 5 s pre-activation, 80% laser power activation, 120 s post-activation at a frame rate of one image per second and imaged using 488 nm and 568 nm lasers for GFP and cherry respectively. Bleaching was performed in a variable circular area to target a pool of viral inclusions. Photoactivation data were post-processed in FIJI (Image J) using a modified FLAPh algorithm and analysed with a lab-custom R script. After normalization, model was obtained using

single exponential curve fitting: $y = (1-a) + ae^{-kt}$, where a = mobile fraction, K = decay rate constant (per second, s^{-1}), t = time (s).

3.6.17 Statistical analysis

Data were analysed using the R statistical package (R version 4.1.0). To quantify thermodynamics and topological variables, we extracted imaging data using an Image J custom plugin and a custom R analytics pipeline. For particle tracking, coarsening assay, photoactivation, photobleaching and shock treatments, we compared two groups: cells treated with DMSO and Ncz. After data transformation in R, we assessed for homogeneity of variance. Homogenously distributed data were assessed by parametric test using either One-way ANOVA to analyse independent variables, followed by a post-hoc analysis by Tukey multiple comparisons of means or t-test for comparison of two groups only. When the data is not homogenous, we used non-parametric analysis with statistical levels determined after Kruskal-Wallis Bonferroni treatment. For simplicity, the details of the test used for each experiment are included in the figure legends. In our case, when two groups were compared, they were not homogenously distributed, hence a non-parametric analysis was done instead of a t-test. Alphabets above each boxplot represents the statistical differences between groups. Same alphabets indicate lack of significant difference between groups while different alphabets infer a statistically significant difference at $\alpha = 0.05$.

3.7 Acknowledgement

We thank all members of CBV lab for helpful discussion and general input in this project, as well as Prof. Ron Fouchier (Erasmus University, Rotterdam) and Prof. Paul Digard (Roslin Institute, UK) for providing reverse genetics virus and cells respectively. We are especially grateful to Victor Hugo Mello for his contribution in designing data analytics pipelines used in this study. We gratefully acknowledge the advanced imaging and quantitative biology units of the Instituto Gulbenkian de Ciência (IGC) for their support & assistance in this work (especially Gabriel Martins (PhD), Maria Hanulova (PhD), Jose Marques (M.Sc.) and Tiago Paixão (PhD)).

Financial support for this work was provided by Fundaçao para a Ciencia e a Technologia (**FCT**) (PD/BD/128436/2017 and COVID/BD/151646/2021), Fundação Calouste Gulbenkian (**FCG**), and the European Research Council (**ERC**) under the European Union's Horizon 2020 research and innovation programme (grant agreement No. 101001521).

3.8 Supplementary Information

Access to data quantification tables and videos from which time-lapsed images were extracted are available on:

https://doi.org/10.5281/zenodo.7473398.

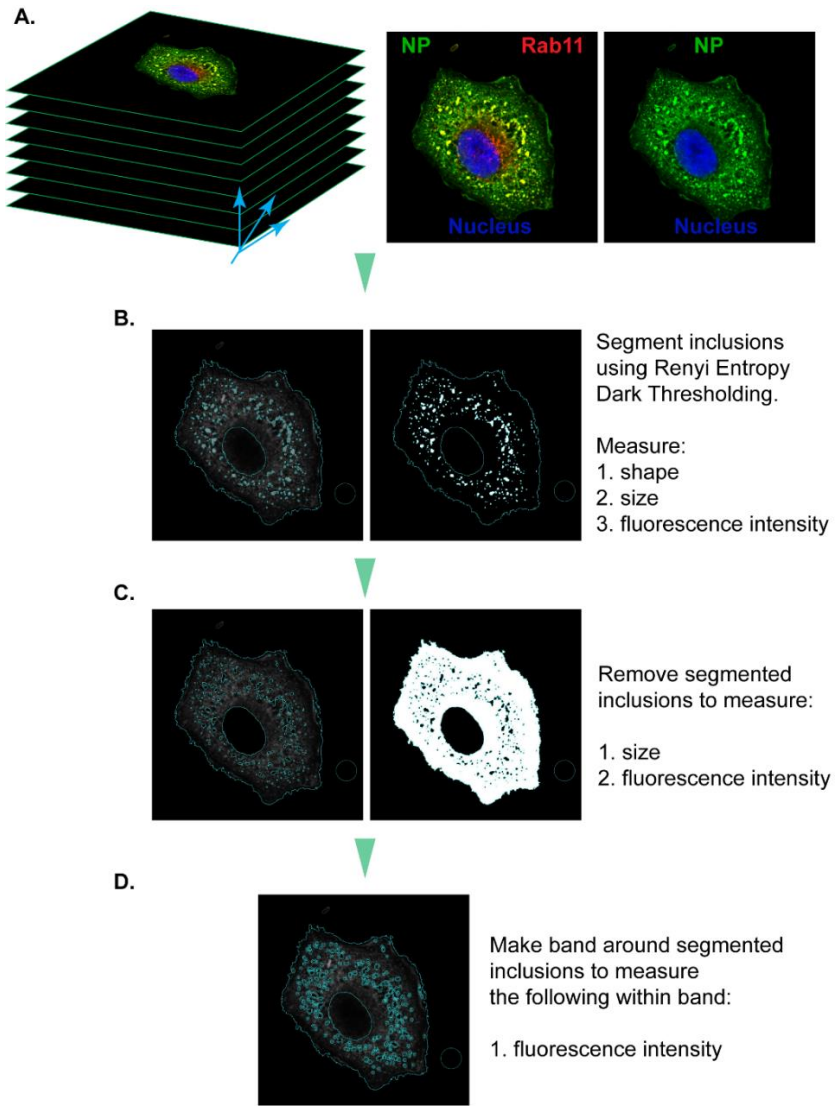

Figure 3.20 S1- Representative images depicting the workflow of Image segmentation and analysis using ImageJ/ FIJI.

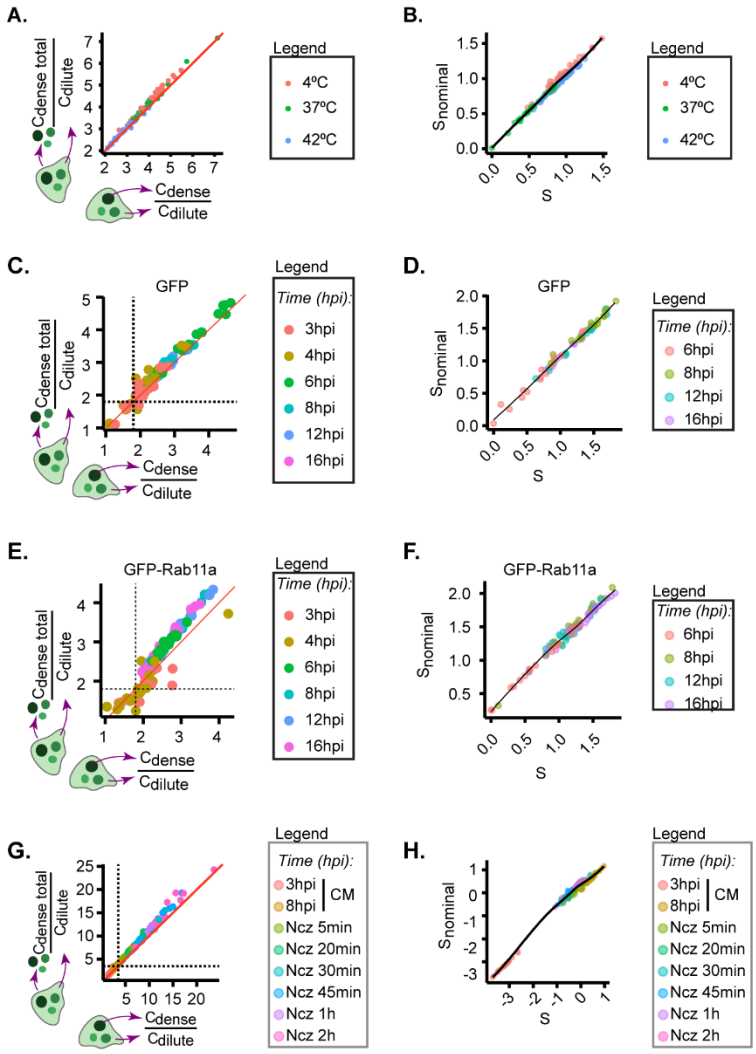

Figure 3.21 S2- Validation of method analysing thermodynamics parameters.

A549 cells expressing (A – D, G – H) endogenous levels of Rab11a or (E - F) over expressing Rab11a were infected at a MOI of 3 with PR8 virus for (A – B, G - H) 8 h before incubating the cells at the indicated (A - B) temperatures, (G - H) Ncz residence time or (C - F) at the indicated timepoints. After this, the cells were fixed, and analysed by immunofluorescence using antibody against NP (as a proxy for vRNPs). Each dot is the average value of measured parameter within or outside IAV inclusions per cell, while the

continuous black lines are non-linear fitted models for all data. (A, C, E, G) are the scatterplots comparing image segmentation strategies to calculate partition coefficient and extrapolate the free energy (see Methods) while (B,D,F,H) is a scatter plot comparing methods for calculating the degree of supersaturation.

Chapter 4 - Solubility proteome profiling of liquid and hardened IAV inclusions

4.1 Author contributions

The experiments presented in this chapter were designed and planned by Temitope Akhigbe Etibor and Maria João Amorim. Coarsening assay and thermodynamic analysis was performed by Temitope Akhigbe Etibor. Supervised by Maria João Amorim, Silvia Vale-Costa performed experiments and analysis of viral titer, topology, and thermodynamics in drug-treated Rab11a-(DN and WT) cell lines. Furthermore, Temitope Akhigbe Etibor, under the supervision of Maria João Amorim, carried out the solubility proteome profiling experiment until the snap-freezing of samples. Afterward, Isabelle Becher and Sindhuja Srinivasan lysed the sample and prepared them for mass spectrometry and data analysis under the supervision of Mikhail Savitski.

Temitope Akhigbe Etibor wrote the chapter with Maria João Amorim supervision. A section of this chapter (co-reviewed by Silvia Vale-Costa, Isabelle Becher, Sindhuja Srinivasan, Mikhail Savitski, and Maria João Amorim) is part of a manuscript currently undergoing peer-review in an open-source journal which can be assessed from bioRxiv:

Temitope Akhigbe Etibor, Sílvia Vale-Costa, Sindhuja Sridharan, Daniela Brás, Isabelle Becher, Victor Hugo Mello, Filipe Ferreira, Marta Alenquer, Mikhail M Savitski and Maria João Amorim. Rules for hardening influenza A virus liquid condensates (2022) bioRxiv 2022.08.03.502602; doi: https://doi.org/10.1101/2022.08.03.502602

4.2 Summary

Previous chapters indicate that IAV inclusions display liquid properties that can be targeted for pharmacological hardening with antiviral function. For this work, we employed conventional condensate strategies to assess phase transitions in IAV inclusions. These approaches were unable to capture unknown molecular factors that may contribute to or deter phase transitions during viral infection. To overcome this limitation, we used proteome-wide solubility profiling to determine the molecular alterations induced by IAV infection as inclusions form. We envisaged that evenly distributed cytoplasmic molecules and those that partition into specific cytoplasmic compartments would display a soluble and insoluble profile respectively.

We analysed phase transitions occurring throughout infection, thereby detecting 6,629 proteins, of which 174 cellular proteins and 10 viral proteins underwent changes in protein abundance and 413 in solubility. Phase transitions in the cell correlated with mitochondria, translation, cell-substrate junction proteins and established LLPS processes (stress granule formation, nucleoli function, splicing). Phase transitions in viral proteins/complexes showed that three viral factors become insoluble with infection – vRNPs, as observed by changes in its components, and surprisingly, NS1 as well as NA.

We validated our screen observing that vRNPs become insoluble in a Rab11a-dependent manner by solubility proteome profiling (SPP) and applied it to Ncz treated infected cells. By doing this, we showed for the first time that through hardening, it is possible to selectively affect viral inclusions without imposing changes in the host proteome abundance and solubility. Our solubility approach may be applied to probe cryptic condensates while simultaneously identifying the molecules present within specific condensates. This work opens new avenues to explore how alterations in cellular and viral material properties regulate cellular function, contribute to viral infection, and may be targeted as novel antiviral approaches.

4.3 Introduction

Generally, viruses and, in our case, the IAV, have been reported to alter the host interactome landscape upon infection ((Bogdanow et al., 2019; Coombs et al., 2010; Domingues et al., 2015; Kummer et al., 2014; Lietzén et al., 2011; Ye et al., 2022) reviewed in (Iselin et al., 2022; Saha et al., 2022; Schneider et al., 2016)). Particularly, infections such as mumps and SARS-CoV-2 were recently reported to influence global intracellular condensates (in)solubility while simultaneously forming virus-specific condensates (Selkrig et al., 2021; Zhang et al., 2022). Such proteome (in)solubility may also be true in the case of IAV since they are able to form liquid inclusions.

Our study so far has concentrated in how vRNPs condensed in the cytosolic IAV inclusions, however, infection could interfere with the cell in a multitude of ways that are important to characterize. This characterization may provide a new layer of understanding to viral-host interactions and especially detailing how viruses utilize phase transitions to regulate cellular function. Some of these assembled, modified, or disassembled condensates are readily identifiable by microscopy, while others may remain cryptic due to the underlying technical limitations associated with the reductionist approach for studying biomolecular condensates.

A gateway to exploring the cryptic virus-induced or disrupted condensates would be a dynamic proteome-wide snapshot along the course of viral infection. In order to explore unknown condensates that might be formed or disrupted by IAV infection, we employed a ultracentrifugation-based solubility proteome profiling (SPP) (Sridharan et al., 2022; Zhang et al., 2022), which enables the capturing of molecular events along the course of IAV infection (encompassing the infection timepoint when inclusions are yet to emerge up till the period when inclusions form and grow).

SPP is a biophysical strategy devised as post-development of TPP (Thermal proteome profiling), an unbiased quantitative mass spectrometry-based profiling for identifying proteome stability across a thermal gradient and used for verification of drug engagement and potency in living cells without the need for compound labeling (Becher et al., 2018; Delport and Hewer, 2022; Franken et al., 2015; J. X. Huang et al., 2019; Kalxdorf et al., 2021; Mateus et al., 2018, 2017; Molina et al., 2013; Potel et al., 2021; Reinhard et al., 2015; Sanchez et al., 2022; Savitski et al., 2014; Selkrig et al., 2021; Sridharan et al., 2019).

SPP was validated in many studies (Sridharan et al., 2019; Sui et al., 2020; Zhang et al., 2022), and serves to discriminate soluble from insoluble proteins in cells, without however being able to associate the phase transitions with specific mechanisms (such as binding to membranes, formation of insoluble complexes, phase separation, phase separation coupled to percolation, and so on). In the context of IAV infection, insoluble proteins would include proteins that partition inside inclusions, but may also involve the partitioning of lipid membranes and well as viral RNAs, which are not readily identified by our SPP methodology. As was shown in healthy (Sridharan et al., 2019), stressed (Sui et al., 2020) and virus infected cells (Zhang et al., 2022), this screen serves a dual purpose: the identification of cryptic molecular component(s) that partition into IAV inclusions and/ or novel viral condensates.

We therefore compared SPP at different timepoints (4, 8, 12, and 16 hpi) of IAV infection, covering the period where inclusions have not yet emerged (at 4 hpi) till when inclusions are formed (8 hpi) and increase in size (12 -16 hpi). Our data demonstrated that IAV infection changed the host proteome landscape. Importantly, we found that vRNPs (which were previously reported to colocalize with Rab11a in IAV inclusions (Amorim et al., 2011; Bruce et al., 2010; Chou et al., 2013; Eisfeld et al., 2011a; Momose

et al., 2011)) become insoluble as inclusions form and mature over time. Critically, through SPP, we were able to identify a novel and yet to be characterized IAV induced insoluble material comprising of viral protein (NS1) and host protein (TRIM25).

Next, we validated this finding by recapitulating the time-resolved SPP strategy on non-functional Rab11a-DN cell lines, which are known to form homogenously distributed vRNPs in the cytosol, but unable to form viral inclusions (Amorim et al., 2011; Bruce et al., 2010; Chou et al., 2013; Eisfeld et al., 2011a; Momose et al., 2011). Here, we expect SPP to resolve the solubility differences between Rab11a-DN and Rab11a-WT expressing cell lines, with vRNP becoming more soluble in the former compared to the higher vRNP insolubility in the later, thereby, validating our initial SPP analysis. Critically, we found as predicted that vRNPs only become insoluble in the presence of Rab11a as cells overexpressing a non-functional Rab11 (known as Rab11a-DN) that do not form inclusions have more soluble vRNPs.

Finally, we employed the SPP assay of Rab11a-DN cell lines to explore solubility changes upon treatment with our c-mod, nucleozin. Since IAV Rab11a-DN cell lines display a soluble vRNP profile and nucleozin are known to harden viral inclusions, we speculate that nucleozin may rescue a hardened inclusion from the soluble vRNP-rich cytoplasm, resulting in higher insolubility of vRNPs. Interestingly, we found that the inclusion hardening effect of nucleozin only affected vRNPs without changing host proteome abundance or solubility, pointing to minimal off-target effects.

In sum, the SPP of IAV infected cells corroborates the thermodynamics profiling of IAV inclusions, indicating that inclusions can be selectively modified through drug targeting, with a resultant reduction of viral replication. This novel screening approach can be applied to many other cellular phase transitions and serves as proof-of-concept that cellular biomolecular condensates may be selectively targeted.

4.4 Results

4.4.1 IAV infection alters proteome abundance in cells.

To understand how both the viral and host cellular proteomes remodel because of IAV infection in the absence and presence of nucleozin, we used a recently developed quantitative mass spectrometry-based approach called solubility proteome profiling (SPP, **Figure 4.1**) (Sridharan et al., 2022, 2019; Zhang et al., 2022). This is a lysate centrifugation assay which can distinguish the soluble (supernatant) from insoluble (dense assemblies) protein pools. Most proteins annotated to be part of membraneless organelles, as well as many cytoskeletal proteins, exhibit prominent insolubility.

In SPP, two aliquots of cellular lysates are extracted with either a strong ionic (SDS) or a mild non-ionic (NP40) detergent. Protein extracted with SDS represent the total proteome, while the supernatant of NP40-extracted lysate represents the soluble sub-pool (**Figure 4.1**). The ratio of NP40- and SDS-derived protein abundance represents the solubility of a protein (**Figure 4.1**). Protein solubility is proxy to track phase transition events in different cellular states. However, this measurement cannot distinguish between different events, such as solidification, phase separation, percolation and gelation (reviewed in (Alberti and Hyman, 2021; Mittag and Pappu, 2022)) that may underlie the phase transition. To establish the physiological changes in protein abundance and solubility occurring along the infection, we performed a time course of PR8 infection in A549 cells followed by SPP as shown in **Figure 4.1**.

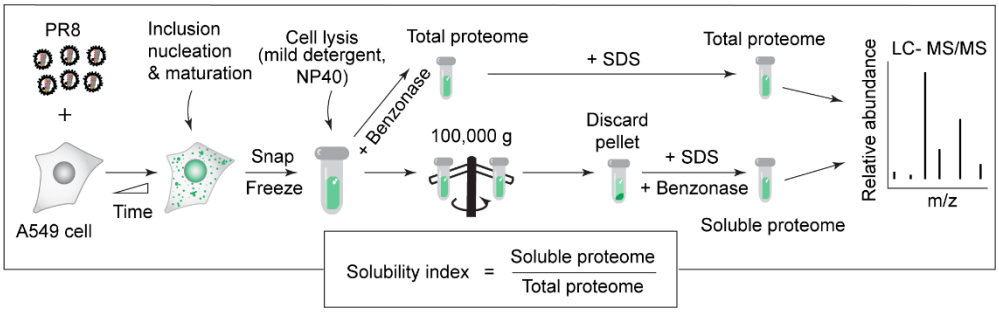

Figure 4.1- Experimental scheme for solubility assay over time of infection.

Cells infected with influenza virus at different time points were lysed in mild (NP40) or strong detergent (SDS) after snap-freezing. Solubility index was determined as the ratio of soluble proteome of the ultracentrifuged NP40 supernatant versus the total proteome from the SDS fraction as measured by mass spectrometry.

Overall, we identified and quantified 6,619 host proteins and 10 viral proteins with at least 2 unique peptides. In comparison to the uninfected cells, 174 host proteins underwent changes in abundance along the infection time course (**Figure 4.2**). Euclidean distances-based clustering of the abundance profiles of these proteins resulted in 6 distinct clusters which enriched for proteins associated with different GO terms “Biological processes” and/or “Cellular Compartments” (**Figure 4.2**).

Most of these proteins (78.2 %, 136 proteins) exhibited a consistent decrease in abundance in line with the previous observations (Nacken et al., 2021), while a small subset (21.8%, 38 proteins) exhibited a sharp increase in abundance in response to the infection. The downregulated host proteins (from cluster 1-3, **Figure 4.2**) are associated with processes such as extracellular matrix organization, cell cycle and cell adhesion. The upregulated proteins (from cluster 6, **Figure 4.2**) were primarily effectors of type-I interferon pathway (**Figure 4.2**), in agreement with the well-known anti-viral response to the infection mounted by host cell. We observed a time

dependent increase in abundance for all identified and quantified viral proteins (**Figure 4.2**E), as expected, from uninfected to infected state.

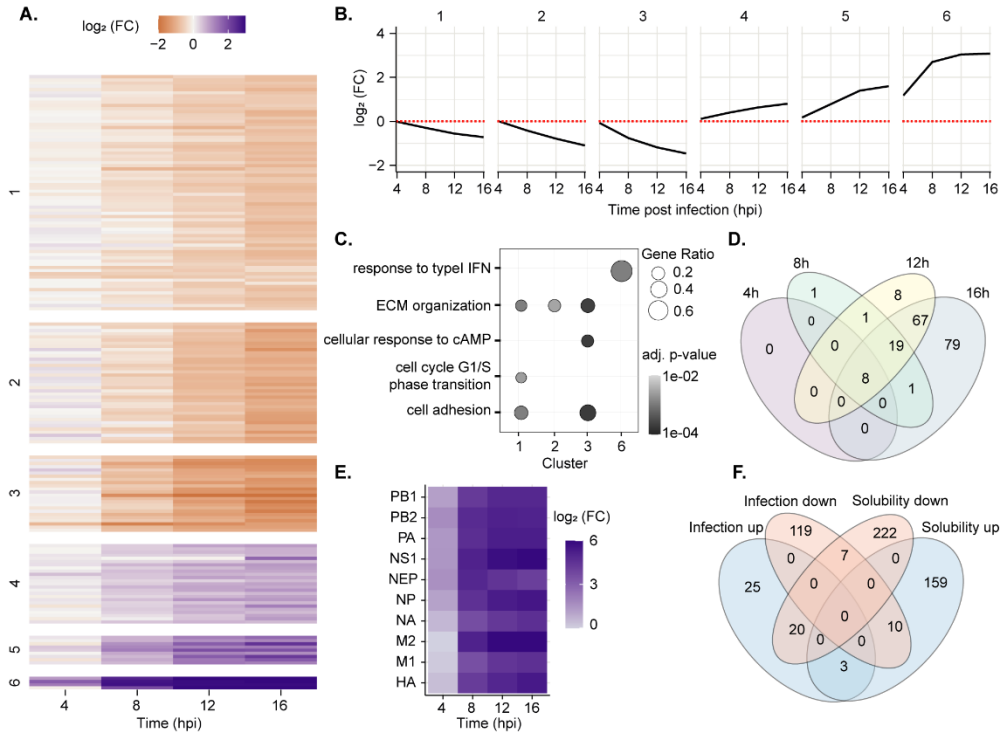

Figure 4.2- Proteome-wide abundance and solubility changes of host and influenza proteins.

A549 cells were mock-infected for 12 hours or PR8 infected for 4, 8, 12 & 16 hours at a multiplicity of infection (MOI) of 5. Thereafter, cells were lysed in mild (NP40) or strong detergent (SDS), while NP40 lysate was ultracentrifuged (100,000 g) to pellet materials in condensates from the soluble fraction in the supernatant. Soluble and total host and viral proteome were identified by LC-MS/MS and solubility was determined as the ratio of soluble NP40- to SDS- derived total proteome abundances at the indicated hour post infection (hpi). ***(A)*** *Hierarchically clustered heat map showing relative abundance of host proteome along the indicated time course of infection in comparison to mock infection. Host proteins that are significantly (see methods) altered in abundance within any of the assayed time points*

were clustered to 6 distinct clusters based on the Euclidean distance. ***(B)*** *Line plot representing the median relative abundance (log_2 fold change, with respect to mock infection) of host proteins from 6 distinct clusters (shown in panel a) over the assayed time course of infection. Red dotted line shows unchanged log_2(FC) at 0 (where low relative abundance < 0 < low relative abundance).* ***(C)*** *Dot plots representing the gene ontology (GO) with terms of biological processes overrepresented among significant hits from proteome-wide abundance (shown in panel a). The dot size corresponds to the ratio of genes per cluster that belong to the indicated biological process, and the grey fill shows the adjusted p-value.* ***(D)*** *Venn diagram showing sets of proteins from the relative host proteome abundance at different infection time.* ***(E)*** *Heat map showing changes in median relative abundance (in log2 scale) of the PR8 influenza proteome along time of infection.* ***(F)*** *Venn diagram of infection-solubility interaction in host proteome at different infection time.*

4.4.2 IAV infection alters solubility profile in cells.

In terms of protein solubility, we observe no significant changes in the host proteome until 4 hpi (**Figure 4.3**A-D). However, from 8 hpi, several host proteins underwent changes in solubility (236 and 171, loosing and gaining solubility, respectively) providing cues on how infection remodels the cellular systems (**Figure 4.3**A-D). Euclidean distance-based clustering of the solubility profiles of host proteins (significantly changing) along the time course resulted in 6 distinct clusters (**Figure 4.3**A-D). We found that proteins involved in interferon pathway, cell division, cellular RNA biology, and ER processes lost solubility, whilst metabolic related processes, mitochondrial organization and ribosomal RNA processing became more soluble (**Figure 4.3**C,D). The phase transitions in the cytosol correlated with inner

mitochondrial membrane, cytoskeleton, translation, and cell-substrate junction proteins (**Figure 4.3**D).

Interestingly, changes progressed steadily until 12 hpi. More so, between 12 and 16 hpi, the profile altered in many ways; for instance, cluster 1, 4 and 6 plateaus, cluster 2 and 5 have steeper slope and cluster 3 reverts trend, which may be related with cytopathic effects (**Figure 4.3**A-D). It is noteworthy that only 35 host proteins (among 407 proteins that alter solubility) – overrepresented in interferon pathway related proteins – change in both abundance and solubility. This indicates that except for interferon related proteins, changes in protein concentration were not the underlying cause of the changes in solubility (**Figure 4.2**).

In terms of solubility, we found 5 viral proteins, namely all vRNP components PB1, PB2, PA and NP (*P* <0.0001 at least), and the non-structural protein-1 (NS1, *P* < 1,31E-08 at least, Fig. 3f), became strongly insoluble with infection from 8 hpi. At a later stage of infection (beyond 12 hpi), neuraminidase (NA) became modestly insoluble (fold changes of 0.64, *P* = 0.008639, and 0.47, *P* = 0.000334, at 12 and 16hpi, respectively, **Figure 4.3**E). NS1 and NA undergoing phase transitions has not been reported. Like NS1 (**Figure 4.3**E), host protein TRIM25 also exhibited significant insolubility at 12 and 16 hpi (fold changes = 0.34, 0.31, *P* = 5,12E-04 and 0,000306289 respectively) in our solubility assay. This protein was recently shown to undergo a type of phase transition, de-mixing from the cytosol by liquid-liquid phase separation (Gack et al., 2009, p. 25; Haubrich et al., 2021; Koliopoulos et al., 2018). Overall, our results indicate that many host proteins undergo dynamic phase transitions during IAV infection. Of note, only 40 proteins (6.7%), including 10 viral proteins, changed abundance and solubility at the same time, out of 597 proteins suffering alterations, which means that alterations in concentration were not the underlying cause of the changes in solubility (**Figure 4.2**D,F). Among the viral components, vRNPs which are

synthesized in the nucleus and transported to the cytosol where they accumulate in viral inclusions exhibit high insolubility.

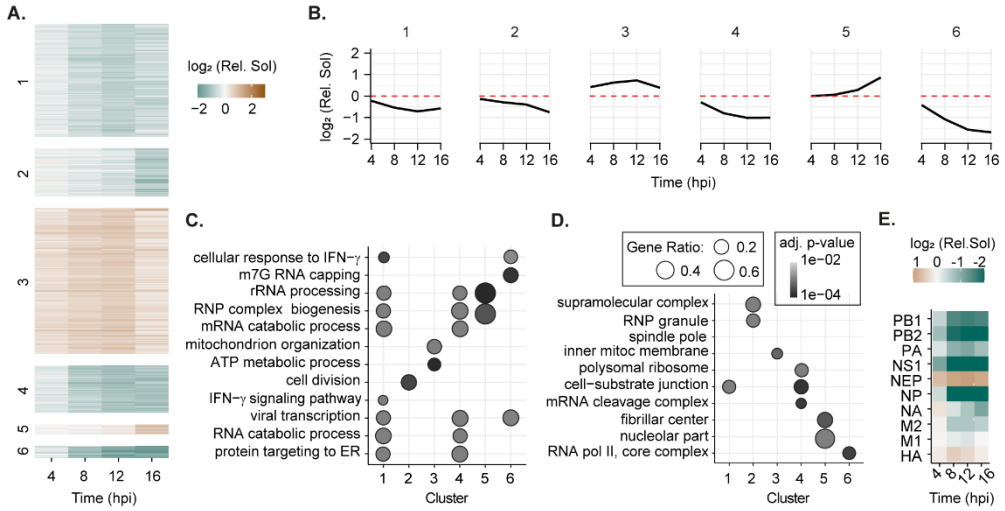

Figure 4.3- Host and viral factors change solubility in a proteome-wide manner.

A549 cells were mock-infected for 12 hours or PR8 infected for 4, 8, 12 & 16 hours at a multiplicity of infection (MOI) of 5. Thereafter, cells were lysed in mild (NP40) or strong detergent (SDS), while NP40 lysate was ultracentrifuged (100,000 g) to pellet materials in condensates from the soluble fraction in the supernatant. Soluble and total host and viral proteome were identified by LC-MS/MS and solubility was determined as the ratio of soluble NP40- to SDS- derived total proteome abundances at the indicated hour post infection (hpi). ***(A)*** *Hierarchically clustered heat map showing relative solubility of host proteome at the indicated times of infection in comparison to 12 hrs of mock-infection. Significant solubility changes were grouped in 6 distinct clusters based on the Euclidean distances.* ***(B)*** *Line plot representing the median relative solubility of host proteins from the 6 distinct clusters (from* ***A.****, in log_2 scale) in relation to the time of infection. Red dashed line indicates no change in relative solubility (log_2 FC = 0). Fold change (FC)*

> 0 means more soluble than control (12 hr Mock) and vice-versa. ***(C)*** *Dot plots representing the gene ontology (GO), biological processes over-represented among significant hits from proteome-wide solubility (shown in panel* ***A.****). Selected enriched biological processes in relation to the individual clusters (1-6) are shown. The size of the dots relates with the ratio of genes per cluster that belong to the indicated biological process, and the grey fill shows the adjusted p-value.* ***(D)*** *Dot plots representing the gene ontology (GO), cellular compartments over-represented among significant hits from proteome-wide solubility (shown in panel* ***B****). Selected enriched cellular compartments for the individual clusters (1-6) are shown. The size of dot relates with the ratio of genes per cluster that belong to the indicated cellular compartment, and the grey fill shows the adjusted p-value.* ***(E)*** *Heat map depicting the relative solubility (log_2) of viral proteins at the indicated times of infection in comparison to 12hrs mock infection.*

4.4.3 Validation of the SPP.

We used two strategies to validate the SPP analysis. First, we used fluorescence microscopy to track two proteins that became insoluble during infection and that are known to interact (Gack et al., 2009; Koliopoulos et al., 2018): the viral protein NS1 and the key host protein – a E3 ubiquitin ligase Tripartite motif 25 (TRIM25) (Gack et al., 2009; Koliopoulos et al., 2018). TRIM25 activates an antiviral state once an infected cell senses pathogen-associated molecular patterns. NS1 counteracts this activation by directly binding to TRIM25 (Gack et al., 2009; Koliopoulos et al., 2018). Until 12 hpi, both TRIM25 and NS1 are homogenously distributed in the cytosol (**Figure 4.4**). From 12 hpi, a time at which TRIM25 insolubility is statistically significant, both NS1 and TRIM25 accumulated in non-spherical, network-like structures (**Figure 4.4**), that are not homogenously distributed in the cytosol. This suggests that they are not solubilised but rather demixed by a yet uncharacterised physical process. At the moment, the hosting laboratory is carrying out experiments using *in vitro* reconstitution assays and analysis in

tissue cultured cells to understand the underlying mechanism of NS1 and of TRIM25 phase transitions.

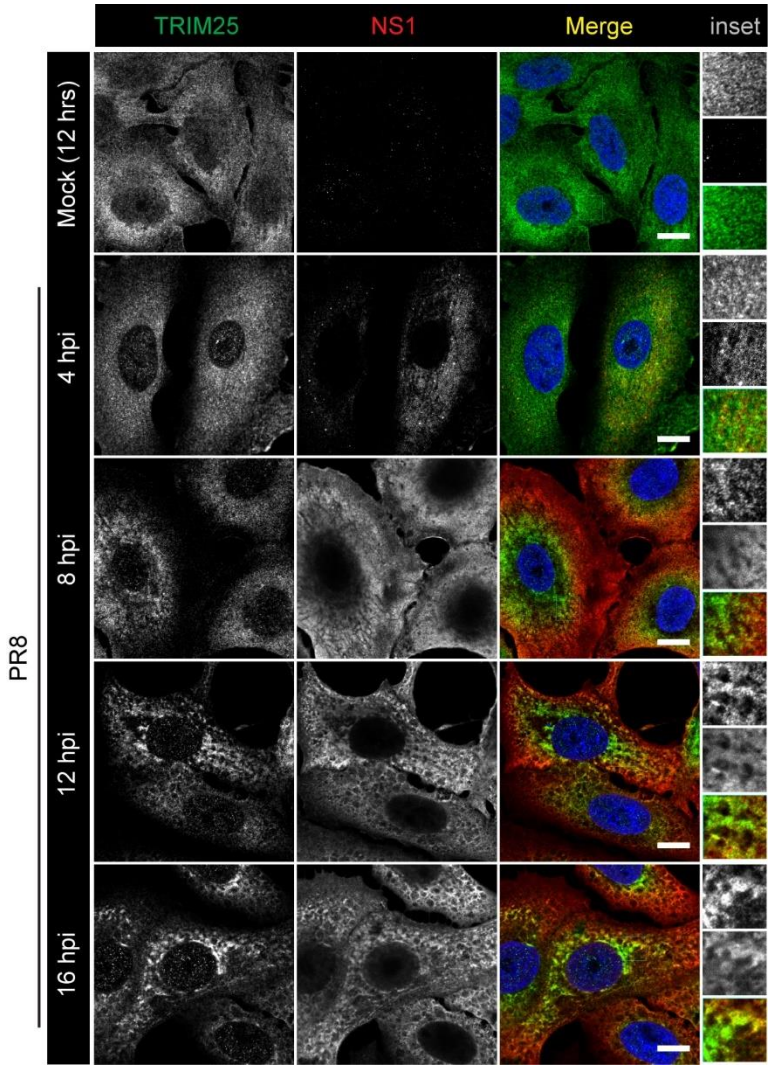

Figure 4.4- IAV induces condensates formation in a time-dependent manner.

A549 cells were mock-infected for 12 hours or PR8 infected for 4, 8, 12 & 16 hours at a multiplicity of infection (MOI) of 5 before fixing for immunofluorescence staining. Immunofluorescence images depicts the

distribution and localisation of host protein TRIM25 (in green) and viral protein NS1 (in red) by immunofluorescence. Inlets show areas of colocalization between TRIM25 and NS1. Nuclei stained using Hoechst. Scale bar = 10 µm.

Second, many laboratories have reported independently that Rab11a is a driver for the formation of IAV liquid inclusions (Amorim et al., 2011; Bruce et al., 2010; Chou et al., 2013; Eisfeld et al., 2011a; Momose et al., 2011). Hence, to validate the SPP screen, we compared proteome abundance and solubility profiles of Rab11a-DN cell lines – where the formation of liquid inclusion is blocked (**Figure 4.5**A,B) – with that of Rab11a-WT cell lines at 12 hpi (**Figure 4.5**B). This strategy aimed at demonstrating by SPP that the insolubility of vRNPs relates to liquid inclusion formation. After a 12 hpi PR8 virus infection, according to **Figure 4.5**B, the ultracentrifugation-based SPP of cell that form vRNP-containing inclusions (Rab11a-WT) were compared to cells (Rab11a-DN) able to make homogeneously distributed vRNPs without forming inclusions.

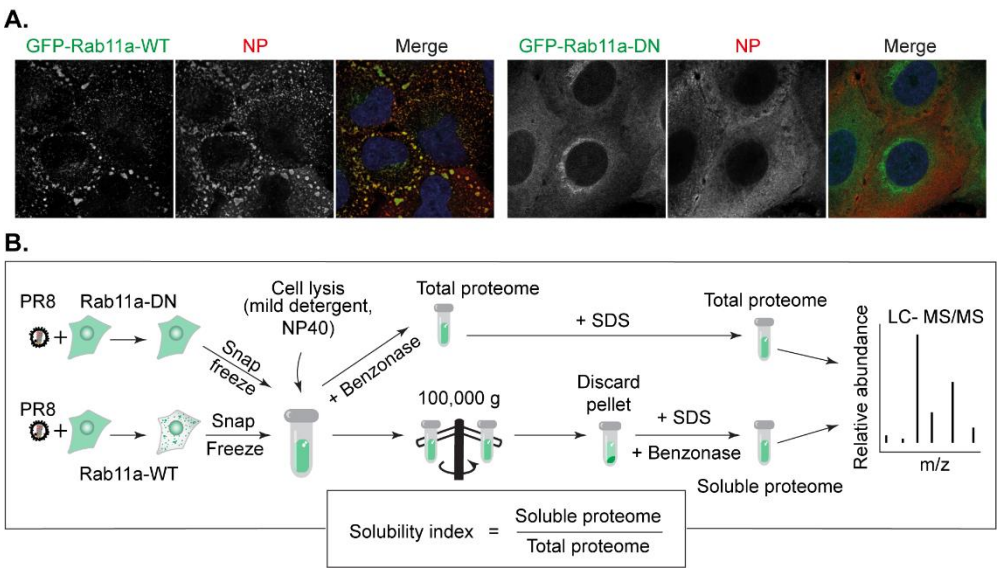

Figure 4.5- Experimental scheme for solubility assay in infected Rab11a-WT and Rab11a-DN cell lines

Inclusion-expressing (Rab11a-WT), and non-expressing (Rab11a-DN) cell lines infected with influenza virus were lysed in mild (NP40) or strong detergent (SDS) after snap-freezing. Solubility index was determined as the ratio of soluble proteome of the ultracentrifuged NP40 supernatant versus the total proteome from the SDS fraction as measured by mass spectrometry. ***(A)*** *Representative images of cells analysed by immunofluorescence staining using antibodies against viral protein (NP, red) and nucleus (blue).* ***(B)*** *Experimental scheme.*

Upon analysis, we found that Rab11a-DN cells exhibited changes in abundance of 582 proteins relative to Rab11a-WT cells (**Figure 4.6**A). Proteins of the metabolic pathways (DHCR24, LSR, CP,), ECM (CDH17) and pro-viral ARRB1 were highly abundant, while the following proteins are of low abundance: cytoskeleton regulator (DPYSL3), interferon (IFI16), metabolic protein (CA2), ECM (GPC6) (**Figure 4.6**A)**.** In terms of the viral proteome, the abundance of all protein components of vRNPs (NP, PB1, PB2, PA and M1) show a modest increase in infected Rab11a-DN cell lines relative to Rab11a/WT (**Figure 4.6**B).

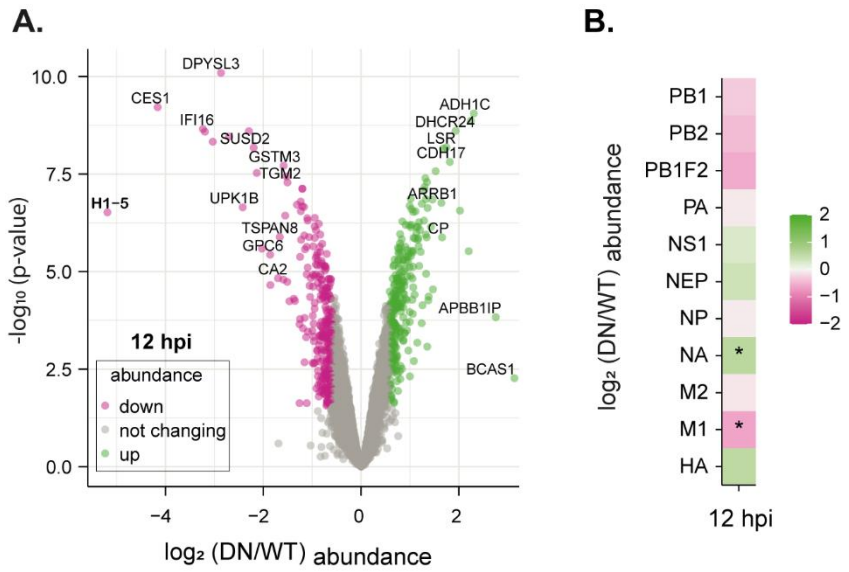

Figure 4.6-Changes in host proteomes abundance in infected Rab11a-DN and Rab11a-WT cell lines.

Cell lines constitutively expressing GFP-(Rab11a-WT and Rab11a-DN; which do not form inclusion upon infection) were infected for 12 hrs with PR8 at a multiplicity of infection (MOI) of 5. Thereafter, cells were lysed in strong detergent (SDS) for total host and viral proteome mapping by LC-MS/MS. ***(A)*** *Volcano plot representing the differentially abundance host proteins in 12hpi infected Rab11a-DN cell line compared to Rab11a-WT line. High abundance and low abundance proteins are represented in green and magenta dots respectively.* ***(B)*** *Heat map showing changes in median relative abundance (in log2 scale) of the influenza proteome at 12hpi in Rab11a-DN cell line compared to Rab11a-WT line. High abundance and low abundance proteins are represented in green and magenta colours respectively.*

We then looked at soluble versus insoluble changes in Rab11a-DN versus Rab11a-WT cells and found that Rab11a-DN cells exhibited altered solubility for 127 host proteins (**Figure 4.7**A) in comparison to the Rab11a-WT cells. We found that proteins associated with mitochondrial translation (e.g. mitochondrial ribosomal protein L15/3/4, MRPL15, MRPL3, MRPL4)

exhibited decreased solubility in Rab11a-DN lines (**Figure 4.6**C and **Figure 4.7**A). So far, the reason for mitochondrial-inclusion association is unknown and currently being investigated in our laboratory.

Interestingly, pro-viral factors ADAR (Chassey et al., 2013), and RRPB1 (Su et al., 2015) as well as anti-viral protein cGAS (Holm et al., 2016) become more soluble in Rab11a-DN cell line (**Figure 4.7**A). In terms of viral proteins, NP exhibited a prominent change by being more soluble in Rab11a-DN lines compared to Rab11a-WT infected cells (**Figure 4.7**B). This corroborates the observation that vRNPs remain uniformly distributed in Rab11a-DN cells (**Figure 4.5**A).

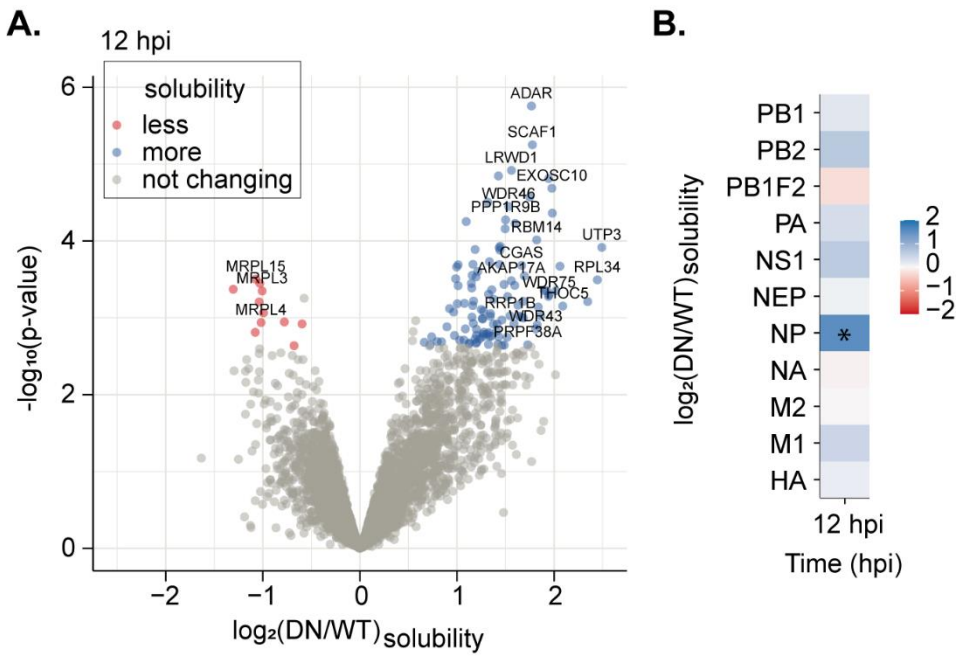

Figure 4.7- Inclusions are insoluble and interact with mitochondria.

Cell lines constitutively expressing GFP-(Rab11a-WT and Rab11a-DN; which do not form inclusion upon infection) were infected for 12 hrs with PR8 at a multiplicity of infection (MOI) of 5. Thereafter, cells were lysed in mild (NP40) or strong detergent (SDS), while NP40 lysate was ultracentrifuged (100,000

g) to pellet materials in condensates from the soluble fraction in the supernatant. Soluble and total host and viral proteome were identified by LC-MS/MS and solubility was determined as the ratio of soluble NP40- to SDS-derived total proteome abundances at the indicated hour post infection (hpi). ***(A)*** *Volcano plot of host proteome solubility in a 12-hr infected Rab11a-DN cell line relative to Rab11a-WT line. Red and blue dots signify insoluble (mitochondria) and soluble proteins respectively.* ***(B)*** *Heat map showing the* log_2 *relative solubility of all influenza proteins (y-axis) in Rab11a-DN mutant cell line in comparison to wild type Rab11a-WT cells at 12 hours post infection (hpi). Asterisk (*) represents proteins changing in a statistically significant manner (see methods).*

Comparing the relative abundances of Rab11a-DN versus Rab11a-WT, many of the top hits in the upregulated and downregulated proteins related to DNA damage, phosphatase activity, cell adhesion, nucleolar RNA processing, cell cycle and cholesterol metabolism (**Figure 4.8**A). Proteins that exhibited increased solubility in Rab11a-DN line were over-represented in cellular processes such as RNA biology, ribosome processing, ribonucleoprotein complex biology (**Figure 4.8**B).

Correlative analysis of host proteome abundance in infected Rab11a-DN relative to Rab11-WT versus PR8 infected A549 relative to mock-infection presented a slight correlation (**Figure 4.8**A). For instance, CD55 (also known as DAF) did not change in abundance in Rab11a-DN despite reduced abundance in infected A549, however immune related proteins (OASL, IFIT1 and IFIT2) becomes less abundant in Rab11a-DN while being more abundant in A549 infected cells (**Figure 4.8**A).

Interestingly, we found that host soluble proteins in infected Rab11a-DN relative to Rab11a-WT correlates with insoluble proteins in A549 PR8 infection relative to mock-infection and vice-versa (**Figure 4.8**D), while proteins such as lysosomal protein ATP6V0A1 retained its insolubility in both

conditions (**Figure 4.8**D). Examples include immune related proteins (TRIM25, OASL), LMNB1, WDR18, CIT and COA3 (**Figure 4.8**D).

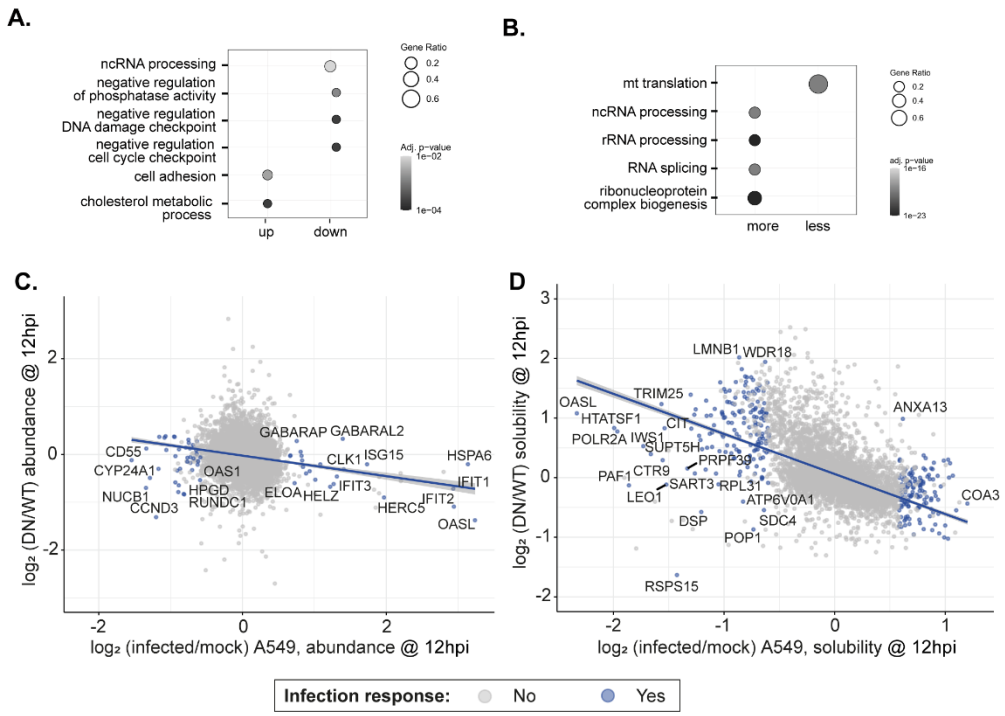

Figure 4.8- Association of host proteome abundance and solubility in different cell states.

(A) *Dot plots representing the gene ontology (GO) with terms of biological processes overrepresented among significant hits from proteome-wide upregulated and downregulated proteins at 12hpi in Rab11a-DN cell line compared to Rab11a-WT line. The size of dot relates with the ratio of genes per cluster (1-6) that belong to the indicated biological process, and the grey fill represents the adjusted p-value.* ***(B)*** *Dot plots representing the gene ontology (GO) with terms of biological processes overrepresented among significant hits from proteome-wide differentially soluble proteins at 12hpi in Rab11a-DN cell line compared to Rab11a-WT line. The size of dot relates with the ratio of genes per cluster (1-6) that belong to the indicated biological process, and the grey fill shows the adjusted p-value.* ***(C)*** *Scatter plot*

comparing relative changes in host protein abundance at 12 hpi with respect to mock infection in GFP-Rab11a-WT (x-axis) with relative changes in protein abundance between GFP-Rab11a-DN and GFP-Rab11a-WT (y-axis) in log_2 scale. Blue dots represent proteins with significant infection response in Rab11a-DN versus Rab11a-WT cell lines at 12 hpi. ***(D)*** *Scatter plot comparing relative host proteome solubility change at 12 hpi in Rab11a-DN with respect to Rab11a-WT scaled to log_2. Blue dots represent proteins with significant solubility response at 12hpi infection in Rab11a-DN versus Rab11a-WT cell lines.*

Altogether, validation of the SPP using cells that are unable to form inclusions further corroborates its ability to identify (un)known proteins that may partition into inclusions as well as uncharacterised condensates. Using this assay, condensate dissolution that leads to more soluble proteome fraction may be easily identified.

4.4.4 Nucleozin induced insolubility on vRNPs relates to formation of IAV liquid inclusions.

Having explored the potential of SPP to identify key differences in protein abundance and solubility, we sought to understand the system-wide response triggered by nucleozin. Exploring the changes imposed by nucleozin on host proteome abundance and solubility in IAV infected cells is critical to determining its selective engagement of host and/ or viral targets.

To achieve this, we measured the protein solubility and abundance changes of both host and viral proteomes in response to 1 h treatment with nucleozin in Rab11a-WT and Rab11a-DN cells infected with PR8 for 12 h (**Figure 4.9**A-D). Nucleozin-treatment did not induce significant alteration in host proteome abundance in both cell lines (**Figure 4.9**A,B). Crucially, no major changes in terms of protein solubility were observed for the host proteome during this treatment period (**Figure 4.9**C). Interestingly, the solubility of vRNPs in Rab11a-WT cell lines treated with either nucleozin or

DMSO remain unaltered (**Figure 4.9**D), while increasing the proportion of NP in insoluble pool in Rab11a-DN cells (**Figure 4.9**D).

Overall, our results suggest that nucleozin does not induce promiscuous changes in cellular protein levels or their solubility.

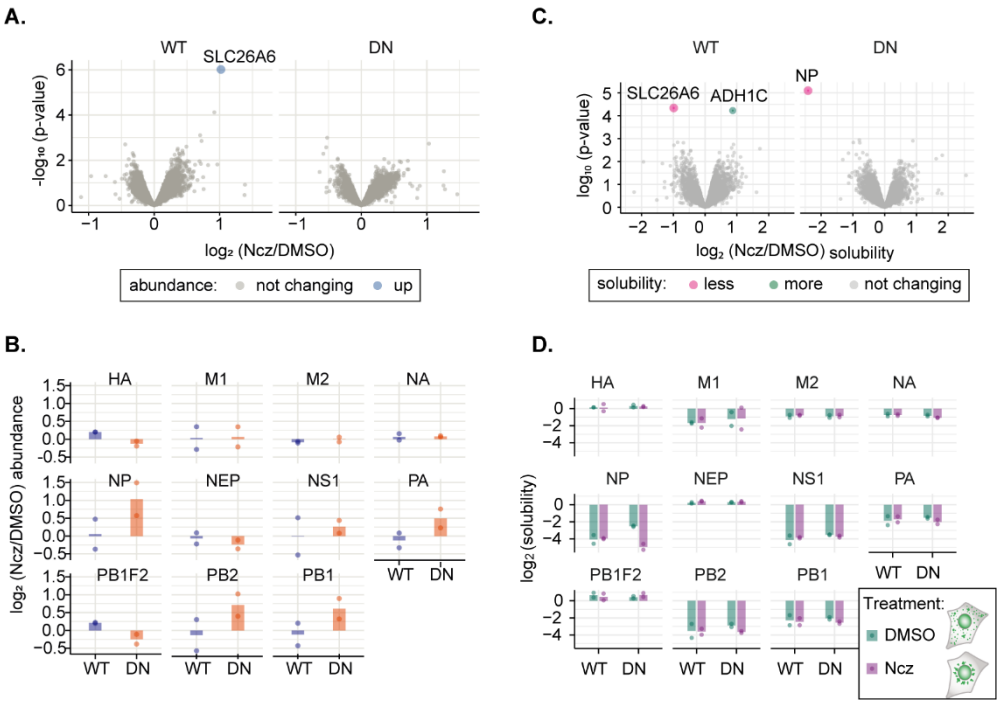

Figure 4.9- The insolubility of IAV inclusions is dependent on Rab11a.

Cell lines constitutively expressing GFP-(Rab11a-WT and Rab11a-DN; which do not form inclusion upon infection) were infected for 12 hrs with PR8 at a multiplicity of infection (MOI) of 5 and treated with nucleozin (Ncz) or control vehicle (DMSO). Thereafter, cells were lysed in mild (NP40) or strong detergent (SDS), while NP40 lysate was ultracentrifuged (100,000 g) to pellet materials in condensates from the soluble fraction in the supernatant. Soluble and total host and viral proteome were identified by LC-MS/MS and solubility was determined as the ratio of soluble NP40- to SDS- derived total proteome abundances at the indicated hour post infection (hpi). ***(A)*** *Volcano plot*

representing relative host protein abundance in Rab11a-WT and Rab11a-DN infected cell lines (at 12 hpi) after treatment with nucleozin or DMSO. Differentially upregulated proteins in these conditions (statistical significance – see methods) are indicated in blue dots. ***(B)*** *BaGr graph comparing viral proteins abundances (in log_2 scale) in Rab11a-WT and Rab11a-DN cell lines PR8-infected (12 hpi) and treated with either nucleozin or DMSO.* ***(C)*** *Volcano plot representing relative solubility of host and viral proteins in Rab11a-WT and Rab11a-DN infected cell lines (at 12 hpi) after treatment with nucleozin. Differentially soluble proteins in these conditions (statistical significance – see methods) are indicated in pink and green dots.* ***(D).*** *Bar graph comparing solubility (in log_2 scale) of viral proteins when PR8 infected (12 hpi) Rab11a-WT and Rab11a-DN cell lines were treated with either nucleozin (Ncz) or sham vehicle (DMSO).*

Although, SPP data was similar, we observed IAV inclusions growing larger and hardening upon nucleozin treatment on the microscopy level in Rab11a-WT cells (**Figure 4.10**). This can be explained as vRNPs are already insoluble in viral inclusions before nucleozin treatment and the net increase in size of the inclusions does not result in higher insolubility of vRNPs. Both SPP and microscopy complement each other in the case of Rab11a-DN cells as viral inclusions change from soluble to insoluble and become bigger upon nucleozin treatment. Overall, the data substantiates our finding that vRNPs form Rab11a-dependent insoluble and liquid inclusions which undergo a distinctive phase transition upon nucleozin treatment.

Given the possibility to harden IAV inclusions, it is important to define the molecular mechanisms conferring the material properties of these condensates, which remain elusive. As Rab11a drive the formation of IAV inclusions (Alenquer et al., 2019; Amorim et al., 2011; Eisfeld et al., 2011a; Lakdawala et al., 2014; Vale-Costa et al., 2016b; Veler et al., 2022), we asked if nucleozin could artificially reform viral inclusion and mimic its behaviour in the absence of Rab11a. Stable cell lines expressing Rab11a dominant

negative (DN) (henceforward Rab11a-DN) did not form IAV inclusions as expected maintaining vRNPs dispersed throughout the cytosol (**Figure 4.10**).

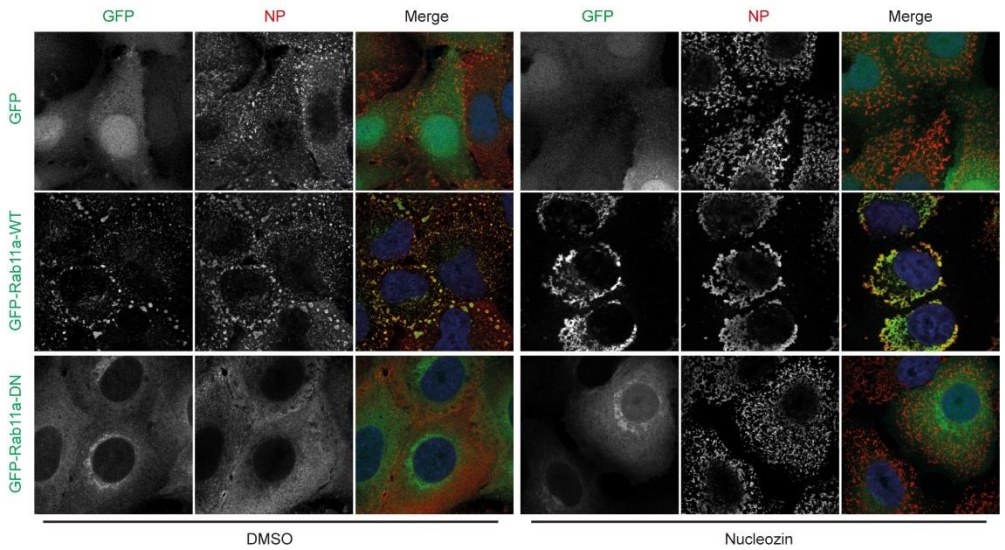

Figure 4.10- Only hardened inclusions emerge in nucleozin treated Rab11a-DN cell line

A549 cells constitutively expressing GFP-(Rab11a-WT or Rab11a-DN, green) were mock- or PR8-infected for 12 hrs and thereafter, treated with nucleozin (Ncz) or sham vehicle-DMSO. Representative images of cells analysed by Immunofluorescence staining using antibody against viral protein NP (magenta). Scale bar = 10 µm.

Interestingly, both Rab11a-WT and Rab11a-DN cell lines, in the presence of nucleozin, exhibited irregularly shaped cytosolic puncta (which are smaller in Rab11a-DN lines, **Figure 4.11**A) and are more deficient in producing progeny virions (**Figure 4.11**B). This indicates that nucleozin bypasses the need for Rab11a to concentrate vRNPs.

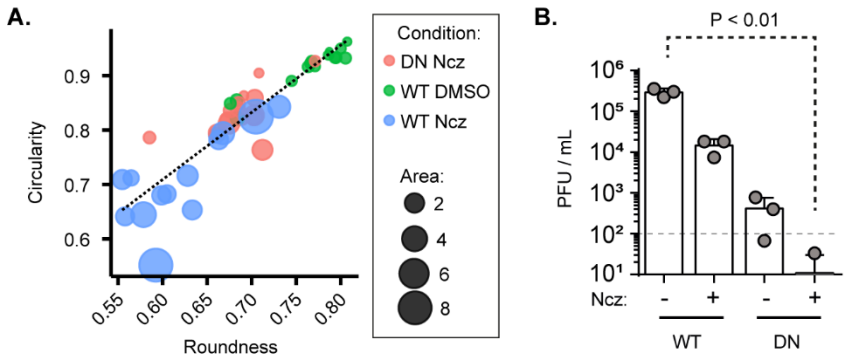

Figure 4.11- Hardened inclusions attenuate viral replication.

Cells in **Figure 4.10** *were analysed for inclusions shape and viral titre* ***(A)*** *Scatter plot of circularity versus roundness of inclusion in mock- or PR8-infected Rab11a-DN and Rab11a-WT cell lines treated with nucleozin or DMSO.* ***(B)*** *Bar chart showing viral titre (PFU/ mL) of mock- or PR8-infected Rab11a-DN and Rab11a-WT cell lines treated with nucleozin or DMSO.*

We next tested the fusion ability of nucleozin-induced IAV inclusions in Rab11a-DN lines. Unlike inclusions in Rab11a-WT cells, nucleozin-induced IAV inclusions in Rab11a-DN infected cells are not able to fuse in coarsening assays (**Figure 4.12**A-C) but exhibited a more stable free energy of partitioning (with lower Gibbs free energy **Figure 4.12**D).

This shows that aberrant inclusions rescued by nucleozin treatment are hardened.

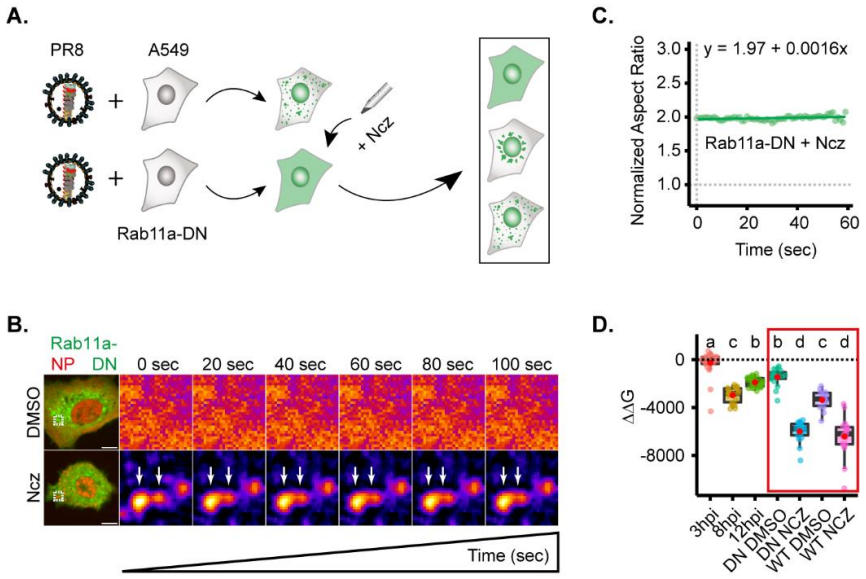

Figure 4.12- Nucleozin-induced inclusions that emerge in Rab11a-DN cell lines are unable to coalesce.

*A549 cells stably expressing a dominant negative version of Rab11a fused to GFP (Rab11a-DN) and unable to form IAV inclusions were transfected with cherry-NP (**B.** or later stained for NP, **D.**, as proxy for inclusions) and co-infected with PR8 at a multiplicity of infection (MOI) of 3, before treating with 5 μM nucleozin or DMSO at 12hpi. **(A)** Schematic depicting the possible outcomes when Rab11a-DN cell lines are treated with nucleozin (Ncz) **(B)** Representative time lapse pseudocolor images show fusion of IAV inclusions in a coarsening assay of PR8 infected Rab11a-DN cell line treated with nucleozin or DMSO. **(C)** Plot depicting the normalised aspect ratio of fusing inclusions over time in infected Rab11a-DN cell line treated with nucleozin (Ncz) **(D)** Boxplot comparing the fold change in free energy of partition (ΔΔG, cal.mol^{-1}) of IAV inclusions, normalized to 3hpi, in PR8 infected cells overexpressing Rab11a (DN and WT, red box) at 12 hpi. $P < 0.01$; Kruskal Wallis Bonferroni treatment. Above each boxplot, same letters indicate no significant difference between them, while different letters indicate a statistical significance at $\alpha = 0.05$.*

4.5 Discussion

Cellular substructures including condensates possess specific signatures and properties that are contingent on their molecular constituents and the interactions they establish (Alexander et al., 2016; Qamar et al., 2018; A. Wang et al., 2018; Yang et al., 2020) and these may be modified by stress including viral infections. Viruses are excellent cellular mimics, able to recruit conserved machinery and molecular pathways to support viral replication. It is now evident that other than the endomembrane systems, viruses also utilise cellular condensates at key stages of their life cycles (reviewed in (Etibor et al., 2021; H. Li et al., 2022; Lopez et al., 2021; Luzak, 2022; Wei et al., 2022; Wu et al., 2022)). At the same time, viruses are capable of counteracting certain cellular condensates (reviewed in (Etibor et al., 2021; H. Li et al., 2022; Lopez et al., 2021; Luzak, 2022; Wei et al., 2022; Wu et al., 2022)).

In fact, condensates have been shown to exhibit distinct solubility profiles when compared to cellular proteins that are evenly distributed in the cytoplasm (Sridharan et al., 2022, 2019; Zhang et al., 2022). However, not much is known about condensate solubility during stress and infection. Therefore, our work addressed the critical challenge to identify how changes in solubility alter cellular function using IAV infection as a model.

As expected, IAV infection resulted in the global alteration of cellular architecture and biochemistry. We found that mitochondrial proteins and proteins of ATP metabolic process were more soluble with time of infection, which may relate to the hydrotrope properties of ATP (Patel et al., 2017; Sridharan et al., 2019). Crucially, key members of the interferon signalling pathway and cellular ribonucleoprotein (RNP) granules displayed insolubility. Despite the increase in viral protein abundance with time of infection, only vRNP components (PA, PB1, PB2, NP) that segregate into IAV inclusion were found to be insoluble together with NS1.

Noticeably, through SPP, we identified novel virus-induced insoluble components that grows through the course of IAV infection, consisting of host (TRIM25) and viral (NS1) proteins. Since RIG-I and TRIM25 are cellular antiviral proteins that target viral RNAs for degradation (Gack et al., 2009; Haubrich et al., 2021; Koliopoulos et al., 2018), we speculate that NS1 sequesters both proteins into specialized condensates, shielding vRNAs in IAV inclusions from catabolic degraders in order to facilitate IAV genome assembly. As this mechanism is important for viral function, future work in the Amorim lab will test this hypothesis and investigate the phase transition mechanism involved.

We validated the solubility hits using Rab11a-DN cell lines (that do not produce inclusions despite exporting vRNPs into the cytosol) to demonstrate that constituents of IAV inclusions are indeed insoluble. Importantly, the host proteome screening of infected Rab11a-DN cell line relative to Rab11a-WT identified mitochondrial proteins as being more insoluble, contrasting with our initial finding in infected A549 cells, where they become more soluble. This raises critical questions as to the role of mitochondria in IAV condensate regulation, which in fact, has been a long-standing interest and line of research in the Amorim lab. We speculate that ATP-related processes of the mitochondria may regulate condensate properties and function, via unknown mechanisms.

Additionally, ADAR and an innate immunity related protein (cGAS) were more soluble in Rab11a-DN cells. It was previously shown that NS1 interacts synergistically with ADAR1 (Chassey et al., 2013) to enhance its editing activity for viral replication, while cGAS is a cytosolic DNA sensor, an adaptor of STING that activates type I interferon (IFN-1) (Gao et al., 2013; Lahaye et al., 2013; Li et al., 2013; L. Sun et al., 2013; Wu et al., 2013; Zhang et al., 2013). Their function in regulating viral RNA sensing and replication may be tied to their ability to partition into condensates or retaining a soluble state. In fact, very recently, it was shown that ADAR1 (Corbet et al., 2022) and cGAS

(Du and Chen, 2018) containing condensates may be induced by dsRNA and DNA respectively. This suggest that IAV infection could trigger a functional ADAR or cGAS insolubility, which may relate to inclusion formation since ADAR and cGAS become more soluble in Rab11a-DN cell line. A similar mechanism may be in play in the case of OASL due to the increased abundance and insolubility of OASL in infected A549, which is reversed in Rab11a-DN cells. This could relate to the formation of NS1 condensate, since NS1 was reported to be involved in the OASL pathway (reviewed in (Goraya et al., 2015)).

Having validated condensate SPP in IAV infection, we then used it to evaluate the changes imposed by condensate hardening drug nucleozin on proteome abundance and solubility changes. Interestingly, we found that nucleozin did not originate *de novo* changes in host proteome abundance and solubility but increases NP insolubility in Rab11a-DN cells, pointing to its selectivity. Of note, aberrant inclusions with hardened phenotype were formed in infected Rab11a-DN cells treated with nucleozin, thereby, validating the insolubility profile. Since hardened and liquid inclusions were already phase transitioned in infected Rab11a-WT cells treated with nucleozin or DMSO respectively, SPP could not resolve their differences as the expected phenotype in both conditions would be of insolubility. In our case, this challenge was circumvented by using cell lines (Rab11a-DN) that do not naturally form inclusion despite being loaded with vRNPs.

Taken together, we demonstrated a strategy for pharmacologically targeting the molecules of viral condensates, which results in the hardening of the material state of IAV inclusions for the abrogation of viral replication. This work serves as a proof-of-concept for selective drug targeting that may be applied to future condensate hardening therapeutics development.

4.6 Materials and methods

4.6.1 Cell lines

GFP-Rab11a-WT and GFP-Rab11a-DN cell lines were produced in-house and characterised in (Alenquer et al., 2019), while human basal alveolar epithelial cell (A549) was a largess from Prof Paul Digard, Roslin Institute, UK.

4.6.2 Cell culture

Cells were cultured in complete media constituting Reduced Serum Medium Glutamax™ (OptiMEM™; Gibco™, ThermoFisher, 51985026) supplemented with fetal bovine serum (FBS, Gibco®, S181i-500), 10% (v/v), 200 mM L-glutamine (Life Technologies, 25030-024), and 100 U/ml penicillin, 10 µg/ml streptomycin (Biowest, L0022-100, 1% (v/v)). Every 3-4 days, confluent 293T cells were sub-cultured in T75 flasks using trypsin-EDTA (Biowest, X0930-100).and incubated at 37ºC, 5% CO_2.

4.6.3 Influenza A virus strains

Reverse-genetics (RG) derived A/Puerto Rico/8/34 (PR8, H1N1) (kindly provided by Prof. Ron Fouchier) was used as model virus. Viruses were grown in eggs as following: embryonated chicken eggs were incubated at 37ºC for 10 days. After that, the eggshell was lightly sanded with a rotary tool and a hole was pierced with a sterile 27G needle on top of the egg and on the opposite side of the embryo. Through that hole, 100 PFU of virus diluted in 200µl PBS were injected into the allantoic fluid of the egg. Infected eggs were incubated at 37ºC for 2-3 days, and then at -20ºC for 2h. Viruses were collected by opening the eggs and carefully retrieving the allantoic fluid. After centrifugation at 3500g, 5min, 4ºC to remove debris, the virus solution titrated by plaque assay and aliquoted and kept at -80ºC.

4.6.4 Viral infection

Cells were seeded in culture plates at appropriate density and incubated overnight. Virus inoculum was added in serum-free DMEM at the MOI of 3 (for fixed samples) or MOI of 10 (for live imaging) and incubated for 45min. Afterwards, cells were overlaid with complete media and incubated at 37ºC, 5% CO2 for the indicated time.

4.6.5 Immunofluorescence and Imaging

Cells were fixed for 10 min with 4% formaldehyde and permeabilized for 7 min with 0.2% (v/v) Triton-X-100 in PBS. Thereafter, they were incubated with the indicated primary antibodies for 1 h at RT, washed thrice with 1% (v/v) NCS in PBS and incubated for 45 min with Alexa fluor conjugated secondary antibodies and Hoechst. Antibodies used were rabbit polyclonal against NP (1:1000; gift from Prof Paul Digard). Secondary antibodies were all from the Alexa Fluor range (1:1000; Life Technologies). Following washing, cells were mounted with Dako Faramount Aqueous Mounting Medium and single optical sections were imaged with a Leica SP5 live confocal microscope. Images were postprocessed using FIJI and Adobe Illustrator.

4.6.6 Live cell imaging

Cells were grown in chambered 8-well glass-bottomed dish (Ibidi) containing OptiMEM medium (Gibco) and incubated for 14 h at 37 ºC and 5% CO_2. Media was substituted for Leibovitz L-15 media to buffer CO_2 and data acquisition started on a Roper TIRF Spinning Disk (Yokogawa CSU-X1) or Zeiss LSM 980 AiryScan2 with a cage incubator to control temperature at 37 °C. After excitation with a 491 nm laser (Cobolt 491, 100 mW), fluorescence from GFP was detected with a ×100 oil immersion objective (Plan Apo 1.49),

a bandpass filter (525/45 Chroma), and a photometrics 512 EMCCD camera. Images were post-processed with ImageJ (NIH) and Adobe Illustrator.

4.6.7 Solubility Proteome Profiling

A549, GFP-Rab11a-WT and GFP-Rab11a-DN cells were mock-infected or infected with PR8 virus between 4 to 16hpi and treated with nucleozin or DMSO. Frozen cell pellets containing $1x10^6$ cells were shipped to Proteomics Core Facility at EMBL, Heidelberg for further sample processing.

Samples for mass spectrometry analysis were prepared as described [53]. Briefly, $1x10^6$ cells were resuspended in 100 µl lysis buffer (0.8 % NP-40, 1x cOmplete protease inhibitor cocktail (Roche), 1x PhosphoStop (Roche), 1 U/ml RNAsin (Promega), 1.5 mM $MgCl_2$ in PBS (2.67 mM KCl, 1.5 mM KH2PO4, 137 mM NaCl, and 8.1 mM NaH2PO4, pH 7.4). The sample aliquot for total proteome was incubated directly with benzonase on ice, while the sample aliquot for the soluble proteome was spun down at 100,000 g at 4 °C for 20 min. The supernatant was incubated with benzonase. Both total and soluble aliquots were incubated for 10 min with final 1 % SDS. Protein concentration was determined for the total proteome sample and aliquots equal to 5 µg protein were taken for sample preparation for MS analysis. Both soluble and total lysate of each sample was combined in a multiplexing MS experiment.

4.6.7.1 Mass spectrometry sample preparation

Sample preparation for mass spectrometric measurements were performed as described in [28,54] .

4.6.7.2 Protein digestion and labelling

Protein digestion was performed using a modified SP3 protocol [55,56]. 5 µg of proteins (per condition) were diluted to a final volume of 20 µl with 0.5% SDS and mixed with a bead slurry (Sera-Mag Speed beads, Thermo Fisher Scientific) in ethanol) and incubated on a shaker at room temperature for 15 min. The beads were washed four times with 70% ethanol. Proteins on beads were overnight reduced (1.7mM TECP), alkylated (5mM chloroacetamide) and digested (0.2 µg trypsin, 0.2µg LysC) 100 mM HEPES, pH8. On the next day, peptides were eluted from the beads, dried under vacuum, reconstituted in 10 µl of water and labelled with TMT-16plex reagents for one hour at room temperature. The labelling reaction was quenched with 4 µl of 5% hydroxylamine and the conditions belonging to a single MS experiment were pooled together.

The pooled sample was desalted with solid-phase extraction after acidification with 0.1 % formic acid. The samples were loaded on a Waters OASIS HLB µelution plate (30µm), washed twice with 0.05% formic acid and finally eluted in 100 µl of 80% acetonitrile containing 0.05% formic acid. The desalted peptides were dried under vacuum and reconstituted in 20 mM ammonium formate. The samples were fractionated using C18-based reversed-phase chromatography running at high pH. Mobile phases constituted of 20 mM Ammonium formate pH 10 (buffer A) and acetonitrile (buffer B). This system was run at 0.1 ml/min on the following gradient: 0% B for 0 – 2 min, linear increase 0 - 35% B in 2 – 60 min, 35 – 85% B in 60 – 62 min, maintain at 85% B until 68 min, linear decrease to 0% in 68 – 70 min and finally equilibrated the system at 0% B until 85 min. Fractions were collected between 2 – 70 min and every 12th fraction was pooled together and vacuum dried.

4.6.7.3 LC-MS-MS measurement

Samples were re-suspended in 0.05% formic acid, 4% ACN in LC-MS grade water and analyzed on Q Exactive Plus mass spectrometer (Thermo Fisher Scientific) connected to UltiMate 3000 RSLC nano system (Thermo Fisher Scientific) equipped with a trapping cartridge (Precolumn; C18 PepMap 100, 5 µm, 300 µm i.d. × 5 mm, 100 Å) and an analytical column (Waters nanoEase HSS C18 T3, 75 µm × 25 cm, 1.8 µm, 100 Å) for chromatographic separation. Mobile phase constituted of 0.1% formic acid in LC-MS grade water (Buffer A) and 0.1% formic acid in LC-MS grade acetonitrile (Buffer B). The peptides were loaded on the trap column (30 µl/min of 0.05% trifluoroacetic acid in LC-MS grade water for 3 min) and eluted using a gradient from 2 % to 30 % Buffer B over 103 min at 0.3 µl/min (followed by an increase to 40 % B, and a final wash to 80 % B for 2 min before re-equilibration to initial conditions).

The outlet of the LC- system was directly fed for MS analysis using a Nanospray-Flex ion source and a Pico-Tip Emitter 360 µm OD × 20 µm ID; 10 µm tip (New Objective). The mass spectrometer was operated in positive ion mode. The spray voltage and capillary temperature was set to 2.2 kV and 275°C respectively. Full-scan MS spectra with a mass range of 375–1,200 m/z were acquired in profile mode using a resolution of 70,000 (maximum fill time of 250 ms or a maximum of 3e6 ions (automatic gain control, AGC)). Fragmentation was triggered for the top 10 peaks with charge 2–4 on the MS scan (data-dependent acquisition) with a 30-s dynamic exclusion window (normalized collision energy was 30), and MS/MS spectra were acquired in profile mode with a resolution of 35,000 (maximum fill time of 120 ms or an AGC target of 2e5 ions).

4.6.7.4 Protein identification and quantification

The MS data was processed as described in [28]. Briefly, the raw MS data was processed with isobarQuant (and identification of peptides and proteins was performed with Mascot 2.4 (Matrix Science) against a database containing *Homo sapiens* Uniprot FASTA ((proteome ID: UP000005640, downloaded on 14 May 2016) and Influenza A virus (strain A/Puerto Rico/8/1934 H1N1, proteome ID: UP000009255) along with known contaminants and the reverse protein sequences (search parameters: trypsin; missed cleavages 3; peptide tolerance 10 ppm; MS/MS tolerance 0.02 Da; fixed modifications included carbamidomethyl on cysteines and TMT16plex on lysine; variable modifications included acetylation of protein N-terminus, methionine oxidation and TMT16plex on peptide N-termini).

4.6.7.5 Mass spectrometry data analysis and normalization.

All MS data analysis was performed using R studio (version 1.2.1335 and R version 3.6.1). Data normalization of NP40- and SDS- derived proteomes was performed with *vsn* [57]. The overall signal sum intensities distributions from all TMT channels of all replicates were corrected for technical variations.

4.6.7.6 Differential analysis of protein abundance

The $\log_2$ transformed *vsn* normalized SDS-derived signal sum intensities of proteins from different samples were analysed for differential abundances using *limma* [58]. Proteins with $|\log_2(\text{fold change})| > 0.5$ and adjusted p-value (Benjamini Hochberg) < 0.1 were considered significantly changed.

4.6.7.7 Differential analysis of protein solubility

Solubility is defined as the ratio of NP40- and SDS- derived abundances of proteins. This ratio was computed for all proteins measured in a dataset. The log2 transformed protein solubility was compared between different conditions (time points of infection or different cell line at 12 hours post infection) using *limma*. Proteins with $|\log_2(\text{fold change})| > 0.5$ and adjusted p-value (Benjamini Hochberg) < 0.1 were considered significantly changed.

4.6.7.8 Gene ontology over representation analysis

Differential abundant or soluble human proteins from infection time course or different cell line datasets were used for GO term “Biological processes” and/or “Cellular Compartments” overrepresentation analysis using clusterProfiler (R Bioconductor) [59]. All identified proteins in each dataset served as the background. Standard settings were used for representing enriched GO terms (p-value cutoff: 0.05, Benjamini-Hochberg procedure for multiple testing adjustment and q-value cutoff of 0.2).

4.7 Acknowledgement

We thank our collaborator Mikhail Savitski (EMBL, Heidelberg) and member of his Lab (Sindhuja Srinivasan and Isabelle Becher) and the members of CBV lab for helpful discussion and general input in this project, as well as Prof. Ron Fouchier (Erasmus University, Rotterdam) and Prof. Paul Digard (Roslin Institute, UK) for providing reverse genetics virus and cells respectively. We are especially grateful to Victor Hugo Mello for his contribution in data analysis. We gratefully acknowledge the advanced imaging units of the Instituto Gulbenkian de Ciência (IGC) for their support & assistance in this work (especially Gabriel Martins (PhD) and Jose Marques (M.Sc.)).

Financial support for this work was provided by Fundaçao para a Ciencia e a Technologia (**FCT**) (PD/BD/128436/2017 and COVID/BD/151646/2021), Fundação Calouste Gulbenkian (**FCG**), the European Research Council (**ERC**) under the European Union's Horizon 2020 research and innovation programme (grant agreement No. 101001521), and **SymbNET** "Genomics and Metabolomics in a Host-Microbe Symbiosis Network", a European Union's Horizon 2020 research and innovation programme(grant agreement 952537).

4.8 Supplementary Information

Access to data quantification tables and videos from which time-lapsed images were extracted are available on:

https://doi.org/10.5281/zenodo.7473398

Chapter 5 - General discussion

5.1 General discussion and caveats

Predating historical records, humans have been plagued with all sorts of epidemic and pandemic events (Morens and Taubenberger, 2011; Pappas et al., 2008). Among others, notable outbreaks include smallpox, bubonic plague, measles, malaria, tuberculosis, yellow fever, leprosy, dengue, cholera, typhus, influenza, and the current coronavirus disease 2019 (COVID-19) pandemic caused by the SARS-CoV-2 virus. Asides the socio-economic burdens, infectious diseases pose a biosafety and/ or biosecurity risks of which the current human population has a first-hand experience through COVID-19, highlighting the need to better understand their disease mechanisms to proffer alternative therapeutic solution.

Like other viruses, the IAV is known to use and/ or perturb diverse host cellular resources for successful infection and propagation. Importantly, IAV was shown to abrogate innate immune response/s while using key cellular pathways to complete its life cycle. Fitting with classical infection biology, IAV manipulates membrane bound structures such as mitochondria, ER, lysosome, recycling endosomes, PM etc (Etibor et al., 2021). For example, IAV entry requires early and late endosomes, viral transcription and replication takes place in the nucleus, while the late stage involves the utilise Rab11 recycling endosome, ER, and the PM to form the viral assembly site, the budozone and promote virion release to the ECM (Amorim, 2019; Chen et al., 2001; Etibor et al., 2021; Hutchinson and Yamauchi, 2018; Moriyama et al., 2019; Pila-Castellanos et al., 2021; Tsai et al., 2017; Sílvia Vale-Costa and Amorim, 2016b).

Beside utilizing membrane bound organelles, it is now apparent that viruses can recruit or modify host condensates while assembling virus-specific condensate *de novo* to promote their life cycles. This was demonstrated for the IAV which was proposed to use liquid viral inclusion for genome assembly (Alenquer et al., 2019; Vale-Costa et al., 2016b; Sílvia

Vale-Costa and Amorim, 2016a). The genome of IAV is constituted by eight vRNPs, suggesting that intersegment interactions may be the driving force for inclusion assembly. Despite the lack of mechanistic insight, the formation and maintenance of viral inclusions is a conserved and robust process as co-infection with two distinct human IAV strains resulted in the co-lodging of their vRNPs in the same inclusions (Alenquer et al., 2019). Formation of reassortant viruses with mixed genomes from human and avian adapted strains have been associated with pandemic viruses. Hence, understanding the mechanism of emergence and the biophysical properties of IAV inclusions may provide insight on their contribution to the production of reassortants.

In **Chapter 2** of this work, we demonstrated that intersegment interaction is not necessary for the formation of IAV inclusions (**Figure 5.1**). In comparison to PR8 infected cells, our CLEM data showed that single vRNP inclusions consist of vRNP enriched clusters of vesicles, which originate from Rab11 recycling endosome, but are not delimited by membrane. Importantly, single vRNP type inclusions phenocopied infection system by displayed adaptive responses to hypotonic shock and 1,6-hexanediol stimuli, suggesting that single vRNP type inclusions are inherently liquid biomolecular condensates that emerge by phase transition. As shown for other systems, phase transition could operate as a signal amplifier (Su et al., 2016), repressor or activator of specific cellular pathways by excluding or including a specific molecules (Delarue et al., 2018). Coupling these traits to our system, we hereby propose that inclusions are non-membrane delimited micro-compartments with liquid properties, able to spatially restrict vRNPs, increasing their concentration at specific sites to facilitate dynamic vRNP exchanges for better genome assembly kinetics. The caveat here lies in our inability to recapitulate single vRNP inclusions in IAV genomic segments other than segments 7 or segment 8. There is a possibility that other segments are unable to form inclusions independently, suggesting that viral genomic segments 7 or 8 may serve as the master regulator vRNP-vRNP

interactions and together with Rab11a control inclusion biogenesis. On the other hand, other segment might require the transfection of vRNA at high concentration and/ or a combination of specific viral or host components to form single vRNP inclusions.

Having met the necessary criteria, molecules can segregate into distinct membraneless microcompartments via phase transition. In thermodynamics, the demixing from the surrounding media implies a preference of alike molecules to interact, self-sort, and exclude the milieu. This is well understood for binary systems but deviate considerably for muticomponent systems, even *in vitro* (Klein et al., 2020; Klosin et al., 2020; Riback et al., 2020; Snead et al., 2022). The operational mechanism of living cells that are complex multicomponent systems at non-equilibrium is yet to be understood. However, small alterations in molecular interactions, caused by changes in the environment or the interactome of the condensate, originate different self-assembled structures (Franzmann et al., 2018; Fuller et al., 2020; Quiroz and Chilkoti, 2015; Riback et al., 2020; Seim et al., 2022; Snead et al., 2022) that respond distinctly to thermodynamic variables such as concentration, temperature and type/strength of interactions. For example, increasing the concentration in a system is mostly associated with more ordered, less flexible structures, however higher ordered structures were reported to arise in response to a concentration reduction (Helmich et al., 2010). Therefore, understanding how physical modulators of phase transitions impact the properties of condensates is key to comprehend how biological systems may be regulated, which is essential, for instance, in designing condensate-targeting drugs with specific activities.

To meet this critical need, in **Chapter 3**, we address the fundamental questions of whether the material properties of IAV inclusions may be modulated and what are the most efficient methods (**Figure 5.1**). We show that they may be hardened by targeting vRNP interactions but not by lowering the temperature down to 4 ºC nor by altering the concentration of the factors

that drive their formation. The data on temperature reveals that a decrease in the entropic contribution leads to a growth of condensates, as observed for other systems (Falahati and Haji-Akbari, 2019; Hyman et al., 2014; Riback and Brangwynne, 2020), that is, however, mild and does not significantly impact the stability of the structures. Similarly, altering the concentration of drivers of IAV inclusions impact their size but not their material properties. This is unexpected because many studies have shown that changing the temperature or concentration of condensate drivers dramatically impacts their phase diagrams (Bracha et al., 2018; Riback et al., 2020; Zhu et al., 2019) and material properties (Shin and Brangwynne, 2017).

For influenza, these minor effects demonstrate that the system is flexible, which may result from the necessity to maintain the liquid character over a wide range of vRNP concentration in the cytosol (low levels in the beginning and high at later stages of infection). The maintenance of the liquid character may be a regulated process involving fission and fusion events associated with the ER, as reported for other systems (Lee et al., 2020). In fact, IAV liquid inclusions develop in proximity to a particular part of a modified ER (de Castro Martin et al., 2017), the ERES (Alenquer et al., 2019). In addition, the fusion and fission events of inclusions may be necessary to promote vRNP interactions, which is essential for genome assembly, as proposed before (Amorim et al., 2011; Eisfeld et al., 2015; Lakdawala et al., 2014; Nturibi et al., 2017).

Our findings are exciting but bear a few constraints that necessitate addressing. Firstly, understanding condensate biology in living cells is complex because the systems are heterotypic and away from equilibria. This is especially challenging for influenza liquid inclusions that are formed by 8 different vRNP complexes, that although sharing the same structure (the vRNP complex), vary in length, valency and RNA sequence. In addition, liquid IAV inclusions result from an incompletely understood network of interactions where vRNPs engage in multiple and distinct intersegment interactions

bridging cognate vRNP-Rab11 units on flexible membranes (Alenquer et al., 2019; Amorim et al., 2011; Bruce et al., 2010; Chou et al., 2013; Gavazzi et al., 2013a, 2013b; Haralampiev et al., 2020; Le Sage et al., 2020; Nturibi et al., 2017; Shafiuddin and Boon, 2019; Sugita et al., 2013). Presently, we lack an *in vitro* reconstitution system to understand the underlying mechanism governing demixing of vRNP-Rab11a-host membranes from the cytosol. This *in vitro* system would be useful to explore how the different segments independently modulate the material properties of inclusions, explore if condensates are sites of IAV genome assembly, determine thermodynamic values, thresholds accurately, and perform rheological measurements for viscosity and elasticity and validate our findings.

One of the constraints of using cells in this work relates to the range and precision of the concentrations and temperature we can vary in our system. Testing gradient temperature and concentration of Rab11 would have been ideal, however, this is challenged by a need to reach balance between thermal degrees and exposure time necessary for an observable physiological effect on inclusions. Moreover, gradient concentration levels of Rab11a in cells is not easy to control as overexpression for too long may be toxic to the cell. We circumvent this challenge, we compared endogenous Rab11a cellular levels to a single pool of transduced cells that contained low, but still heterogeneous, levels of Rab11a to avoid toxicity and/or uncharacterized effects of overly expressing Rab11a in the cell. To minimize this limitation, we combined overexpressing Rab11a with a range of low and high levels of vRNPs (analysing the entire time course of infection) to understand if a combination of high levels of vRNPs and of Rab11a could synergistically change the material properties of IAV inclusions. Also, we used controllable temperatures (4 ºC, 37 ºC and 42 ºC) specified to the available incubators in the Laboratory.

Defining the rules for hardening condensates is important for understanding how biological condensates may be manipulated in cells and

has consequences for development of novel antiviral treatments. In **Chapter 4**, we demonstrated that using nucleozin, as a way to target the type/strength of interactions of viral inclusions, led to hardening of these structures in a way that does not impact host proteome abundance or additional changes in proteome solubility (**Figure 5.1**). How to target the type/strength of interactions within viral inclusions in ways that do not promote immediate viral resistance is a challenge for the future. Earlier, we showed that the development of molecules that affect the interactions between two components (such as post-translational modifications, local pH or ionic strength or pharmaceutical stickers/spacers) could be a solution. Such targeting may prevent off-target effects, especially by developing compounds able to distinguish free vRNP components from those in the supramolecular complex. Importantly, using SPP, we identified many host and viral factors whose abundance and/or solubility changes during infection, opening many interesting questions on how these changes impact cellular function

Overall, our work showed that IAV inclusions are biomolecular condensates with inherent liquid properties that could support genome assembly by a yet uncharacterised molecular mechanism leading to formation of a hetero 8-vRNP complex. We also show that these strutures can be selectively hardened to abrogate viral replication. This may in the future constitute a novel therapeutic strategy that could be recapitulated for other condensate related diseases. As such, we provide a framework for identifying how key physical parameters control condensate formation and material properties.

We are just beginning to understand the involvement of phase transition in virology, but we anticipate that, given the ancient co-evolution between viruses and eukaryotic cells and the diversity of host strategies used by viruses, the next years will provide an interesting overlap between the two fields.

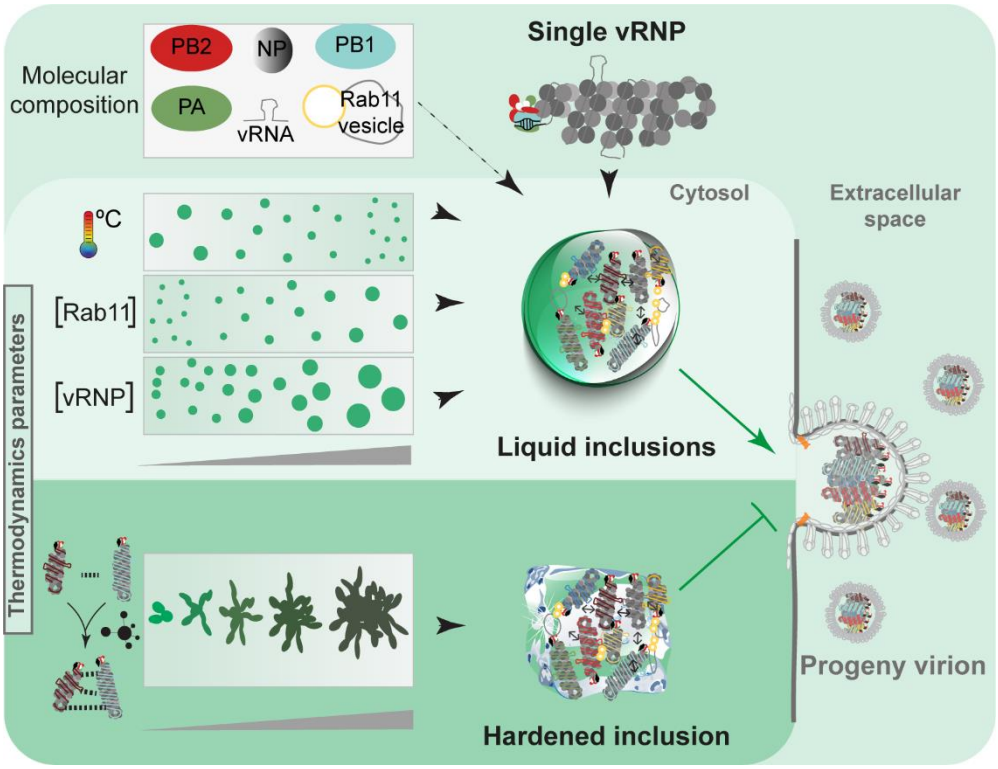

Figure 5.1- Schematics depicting the pharmacological hardening liquid IAV inclusions in situ and in vivo.

IAV inclusions are liquid biomolecular condensates which segregate from the cytoplasm to concentrate vRNPs for posterior genome assembly. In the presence of nucleozin, IAV liquid inclusion become hardened and loses its material properties, thereby subverting viral infection.

5.2 Future perspectives

Altogether, this work bridges a new field of cell biology viz. phase transition to virology, thereby clearing the path to better understand novel cellular mechanism for IAV inclusion biogenesis, genome assembly and targeted therapeutic intervention. However, key questions remain to be addressed.

One of the key curiosities that would be of interest in the future is the determination of inclusion forming mechanism for each of vRNA segments 1-6. We propose one of two possible hypotheses: that a master vRNA segment (7 or 8) is required or other viral and host components are necessary in specific stoichiometry. To address this question, different host proteins e.g., CRM1 and viral proteins such as NS2 and M1 might need to be expressed at different level while employing our minireplicon system. Also, plasmid encoding the vRNAs of either of segment 7 or 8 should be co-transfected with one of other vRNAs (segment 1-6) in the complete minireplicon ratio. Also, the time of transfection of the minireplicon system may require tweaking from the 16 hours we used in our system.

During IAV infection, liquid inclusions are formed by an unknown molecular mechanism. We postulate that the liquid character is maintained by an incompletely understood network of intersegment interactions bridging several cognate vRNP-Rab11 units on flexible membranes. To address this challenge, an *in vitro* reconstitution system of viral inclusions needs to be developed. This in vitro system could, in addition, determine thermodynamic values, thresholds accurately, perform rheological measurements for viscosity and elasticity and validate our findings. However, we find that the most interesting utility of this system would be to explore if and how IAV inclusions promote IAV genome assembly. In fact, inclusions are in a state of dynamic mixing, exchanging vRNP materials as they approach the budozone (Alenquer et al., 2019; Amorim et al., 2011; Avilov et al., 2012b;

Eisfeld et al., 2011a; Lakdawala et al., 2014; Vale-Costa et al., 2016b). How demixing of vRNPs into inclusions could promote formation of complete genomes and how these would be excluded from viral inclusions to reach the plasma membrane remains unknown.

In this work, we explored the rules for hardening IAV liquid condensates by employing some *in vitro* strategies to tease intracellular thermodynamics of IAV inclusions. Technically, we retrieved thermodynamic parameters (such as C_{dense}, C_{dilute}, shape, size) from images in z-stacks as the sum of slices at specific snapshots of infection. However, although requiring a very complex image analysis that we lack, in an ideal scenario, the analysis should have been done using the whole volumetry of each viral inclusion, and using live images quantified over time that is yet to be reported.

Most of our strategies were proxies for cellular mechanisms that regulate transport of material, energy of local reactions and/or parameters that modulate their interactions such as PTM. For IAV inclusion hardening, we showed that increasing molecular valency by drug targeting is the best strategy. However, a cost of targeting conserved molecules is the evolution of escape mutants (Hu et al., 2017; Kao et al., 2010; Li et al., 2012). Therefore, a concern to address in the future is how to design suitable combinatory therapies able to reduce their emergence. Since single nucleotide mutations underpin numerous resistance mechanisms to antivirals (Lampejo, 2020), an alternative is to engineer condensate hardening drugs that require multiple amino acid changes for escaping or targeting conserved motifs that are not subjected to high evolutionary pressure.

In the future, our framework can be improved by probing other specific thermodynamics parameters such as pH, ionic strength, and PTM to identify the potential to target more specific pathways. Other alternatives to modulate the material properties tailored for function can also be developed. For example, accumulating evidence shows that blocking viral inclusion formation

hinders viral infection (Amorim, 2019; Amorim et al., 2011; Bruce et al., 2010; de Castro Martin et al., 2017; Eisfeld et al., 2011a; Momose et al., 2011; Nturibi et al., 2017; Pila-Castellanos et al., 2021; Vale-Costa et al., 2016b; Veler et al., 2022). We demonstrated that increase in temperature biases the system to dissolving viral inclusions, therefore, activating exothermic reactions close to IAV inclusions may lead to their dissolution. This may be achieved by targeting ATP hydrotropes to viral inclusions. Previously, it was demonstrated that blocking Rab11 pathway, directly or indirectly, hampers viral infection (Amorim et al., 2011; Eisfeld et al., 2011a; Han et al., 2021; Momose et al., 2011), hence, future research could also explore this route. Since Rab11a has emerged as a key factor for the replication of members of many unrelated viral families relevant for human health (*Bunyaviridae*, *Filoviridae*, *Orthomyxoviridae*, *Paramyxoviridae* and *Pneumoviridae*), targeting its activity may serve as a pan-antiviral strategy (Amorim et al., 2011; Bruce et al., 2010; Cosentino et al., 2022; Nakatsu et al., 2013; Nanbo and Ohba, 2018).

Finally, our SPP data identified some interesting hits of interest that we were unable to investigate. These includes the biophysical behaviour and function of NS1, TRIM25, OASL microstructures during IAV infection, and how they can be physically modified as a potential antiviral mechanism. For this, *in vitro* reconstitution of molecule, imaging, and rheological analysis, supplemented with *in situ* exploration would be critical.

.

5.3 Bibliography

Adams, M.J., Lefkowitz, E.J., King, A.M.Q., Harrach, B., Harrison, R.L., Knowles, N.J., Kropinski, A.M., Krupovic, M., Kuhn, J.H., Mushegian, A.R., Nibert, M., Sabanadzovic, S., Sanfaçon, H., Siddell, S.G., Simmonds, P., Varsani, A., Zerbini, F.M., Gorbalenya, A.E., Davison, A.J., 2017. Changes to taxonomy and the International Code of Virus Classification and Nomenclature ratified by the International Committee on Taxonomy of Viruses (2017). Arch Virol 162, 2505–2538. https://doi.org/10.1007/s00705-017-3358-5

Akarsu, H., Burmeister, W.P., Petosa, C., Petit, I., Müller, C.W., Ruigrok, R.W.H., Baudin, F., 2003. Crystal structure of the M1 protein-binding domain of the influenza A virus nuclear export protein (NEP/NS2). The EMBO Journal 22, 4646–4655. https://doi.org/10.1093/emboj/cdg449

Alberti, S., 2017. Phase separation in biology. Current Biology 27, R1097–R1102. https://doi.org/10.1016/j.cub.2017.08.069

Alberti, S., Carra, S., 2018. Quality Control of Membraneless Organelles. Journal of Molecular Biology, Phase Separation in Biology and Disease 430, 4711–4729. https://doi.org/10.1016/j.jmb.2018.05.013

Alberti, S., Dormann, D., 2019. Liquid–Liquid Phase Separation in Disease. Annual Review of Genetics 53. https://doi.org/10.1146/annurev-genet-112618-043527

Alberti, S., Gladfelter, A., Mittag, T., 2019. Considerations and Challenges in Studying Liquid-Liquid Phase Separation and Biomolecular Condensates. Cell 176, 419–434. https://doi.org/10.1016/j.cell.2018.12.035

Alberti, S., Hyman, A.A., 2021. Biomolecular condensates at the nexus of cellular stress, protein aggregation disease and ageing. Nat Rev Mol Cell Biol 22, 196–213. https://doi.org/10.1038/s41580-020-00326-6

Alberti, S., Mateju, D., Mediani, L., Carra, S., 2017. Granulostasis: Protein Quality Control of RNP Granules. Frontiers in Molecular Neuroscience 10. https://doi.org/10.3389/fnmol.2017.00084

Alenquer, M., Vale-Costa, S., Etibor, T.A., Ferreira, F., Sousa, A.L., Amorim, M.J., 2019. Influenza A virus ribonucleoproteins form liquid organelles at endoplasmic reticulum exit sites. Nature Communications 10. https://doi.org/10.1038/s41467-019-09549-4

Alexander, Gül, Mittal, J., Nicolas, 2016. ALS Mutations Disrupt Phase Separation Mediated by α-Helical Structure in the TDP-43 Low-Complexity C-Terminal Domain. Structure 24, 1537–1549. https://doi.org/10.1016/j.str.2016.07.007

Alfonso, R., Lutz, T., Rodriguez, A., Chavez, J.P., Rodriguez, P., Gutierrez, S., Nieto, A., 2011. CHD6 chromatin remodeler is a negative modulator of influenza virus replication that relocates to inactive chromatin upon infection. Cell Microbiol 13, 1894–1906. https://doi.org/10.1111/j.1462-5822.2011.01679.x

Ali, A., Avalos, R.T., Ponimaskin, E., Nayak, D.P., 2000. Influenza virus assembly: effect of influenza virus glycoproteins on the membrane association of M1 protein. J Virol 74, 8709–8719. https://doi.org/10.1128/jvi.74.18.8709-8719.2000

Alshareedah, I., Kaur, T., Ngo, J., Seppala, H., Kounatse, L.-A.D., Wang, W., Moosa, M.M., Banerjee, P.R., 2019. Interplay between Short-Range Attraction and Long-Range Repulsion Controls Reentrant Liquid Condensation of Ribonucleoprotein–RNA Complexes. J. Am. Chem. Soc. 141, 14593–14602. https://doi.org/10.1021/jacs.9b03689

Alshareedah, I., Moosa, M.M., Pham, M., Potoyan, D.A., Banerjee, P.R., 2021. Programmable viscoelasticity in protein-RNA condensates with disordered sticker-spacer polypeptides. Nat Commun 12, 6620. https://doi.org/10.1038/s41467-021-26733-7

Amorim, M.J., 2019. A Comprehensive Review on the Interaction Between the Host GTPase Rab11 and Influenza A Virus. Front Cell Dev Biol 6, 176. https://doi.org/10.3389/fcell.2018.00176

Amorim, M.J., Bruce, E.A., Read, E.K.C., Foeglein, A., Mahen, R., Stuart, A.D., Digard, P., 2011. A Rab11- and microtubule-dependent mechanism for cytoplasmic transport of influenza A virus viral RNA. J Virol 85, 4143–4156. https://doi.org/10.1128/JVI.02606-10

Amorim, M.J., Digard, P., 2006. Influenza A virus and the cell nucleus. Vaccine, Proceedings of the Second European Influenza Conference 24, 6651–6655. https://doi.org/10.1016/j.vaccine.2006.05.066

Amorim, M.J., Kao, R.Y., Digard, P., 2013. Nucleozin Targets Cytoplasmic Trafficking of Viral Ribonucleoprotein-Rab11 Complexes in Influenza A Virus Infection. J Virol 87, 4694–4703. https://doi.org/10.1128/JVI.03123-12

An, S., Kumar, R., Sheets, E.D., Benkovic, S.J., 2008. Reversible Compartmentalization of de Novo Purine Biosynthetic Complexes in Living Cells. Science 320, 103–106. https://doi.org/10.1126/science.1152241

Archetti, I., 1955. Appearances associated with filamentous forms of influenza viruses. Archiv f Virusforschung 6, 29–35. https://doi.org/10.1007/BF01242050

Arranz, R., Coloma, R., Chichón, F.J., Conesa, J.J., Carrascosa, J.L., Valpuesta, J.M., Ortín, J., Martín-Benito, J., 2012. The Structure of Native Influenza Virion Ribonucleoproteins. Science 338, 1634–1637. https://doi.org/10.1126/science.1228172

Asadi, S., Gaaloul ben Hnia, N., Barre, R.S., Wexler, A.S., Ristenpart, W.D., Bouvier, N.M., 2020. Influenza A virus is transmissible via aerosolized fomites. Nat Commun 11, 4062. https://doi.org/10.1038/s41467-020-17888-w

Asha, K., Kumar, B., 2019. Emerging Influenza D Virus Threat: What We Know so Far! Journal of Clinical Medicine 8, 192. https://doi.org/10.3390/jcm8020192

Austin, F.J., Hinshaw, V.S., 1984. The isolation of influenza A viruses and paramyxoviruses from feral ducks in New Zealand. Aust J Exp Biol Med Sci 62 (Pt 3), 355–360. https://doi.org/10.1038/icb.1984.35

Avilov, S.V., Moisy, D., Munier, S., Schraidt, O., Naffakh, N., Cusack, S., 2012a. Replication-Competent Influenza A Virus That Encodes a Split-Green Fluorescent Protein-Tagged PB2 Polymerase Subunit Allows Live-Cell Imaging of the Virus Life Cycle. J Virol 86, 1433–1448. https://doi.org/10.1128/JVI.05820-11

Avilov, S.V., Moisy, D., Naffakh, N., Cusack, S., 2012b. Influenza A virus progeny vRNP trafficking in live infected cells studied with the virus-encoded fluorescently tagged PB2 protein. Vaccine, Fourth ESWI Influenza Conference 30, 7411–7417. https://doi.org/10.1016/j.vaccine.2012.09.077

Banani, S.F., Lee, H.O., Hyman, A.A., Rosen, M.K., 2017. Biomolecular condensates: organizers of cellular biochemistry. Nature Reviews Molecular Cell Biology 18, 285–298. https://doi.org/10.1038/nrm.2017.7

Banani, S.F., Rice, A.M., Peeples, W.B., Lin, Y., Jain, S., Parker, R., Rosen, M.K., 2016. Compositional Control of Phase-Separated Cellular Bodies. Cell 166, 651–663. https://doi.org/10.1016/j.cell.2016.06.010

Banerjee, I., Miyake, Y., Nobs, S.P., Schneider, C., Horvath, P., Kopf, M., Matthias, P., Helenius, A., Yamauchi, Y., 2014. Influenza A virus uses the aggresome processing machinery for host cell entry. Science 346, 473–477. https://doi.org/10.1126/science.1257037

Banerjee, P.R., Milin, A.N., Moosa, M.M., Onuchic, P.L., Deniz, A.A., 2017. Reentrant Phase Transition Drives Dynamic Substructure Formation in Ribonucleoprotein Droplets. Angewandte Chemie International Edition 56, 11354–11359. https://doi.org/10.1002/anie.201703191

Banjade, S., Rosen, M.K., 2014. Phase transitions of multivalent proteins can promote clustering of membrane receptors. eLife 3. https://doi.org/10.7554/elife.04123

Barman, S., Adhikary, L., Chakrabarti, A.K., Bernas, C., Kawaoka, Y., Nayak, D.P., 2004. Role of Transmembrane Domain and Cytoplasmic Tail Amino Acid Sequences of Influenza A Virus Neuraminidase in Raft Association and Virus Budding. Journal of Virology 78, 5258–5269. https://doi.org/10.1128/JVI.78.10.5258-5269.2004

Batra, J., Tripathi, S., Kumar, A., Katz, J.M., Cox, N.J., Lal, R.B., Sambhara, S., Lal, S.K., 2016. Human Heat shock protein 40 (Hsp40/DnaJB1) promotes influenza A virus replication by assisting nuclear import of viral ribonucleoproteins. Sci Rep 6, 19063. https://doi.org/10.1038/srep19063

Baudin, F., Petit, I., Weissenhorn, W., Ruigrok, R.W., 2001. In vitro dissection of the membrane and RNP binding activities of influenza virus M1 protein. Virology 281, 102–108. https://doi.org/10.1006/viro.2000.0804

Bavagnoli, L., Cucuzza, S., Campanini, G., Rovida, F., Paolucci, S., Baldanti, F., Maga, G., 2015. The novel influenza A virus protein PA-X and its naturally deleted variant show different enzymatic properties in comparison to the viral endonuclease PA. Nucleic Acids Res 43, 9405–9417. https://doi.org/10.1093/nar/gkv926

Beaton, A.R., Krug, R.M., 1986. Transcription antitermination during influenza viral template RNA synthesis requires the nucleocapsid protein and the absence of a 5' capped end. Proc Natl Acad Sci U S A 83, 6282–6286. https://doi.org/10.1073/pnas.83.17.6282

Beaton, A.R., Krug, R.M., 1981. Selected host cell capped RNA fragments prime influenza viral RNA transcription in vivo. Nucleic Acids Res 9, 4423–4436.

Becher, I., Andrés-Pons, A., Romanov, N., Stein, F., Schramm, M., Baudin, F., Helm, D., Kurzawa, N., Mateus, A., Mackmull, M.-T., Typas, A., Müller, C.W., Bork, P., Beck, M., Savitski, M.M., 2018. Pervasive Protein Thermal Stability Variation during the Cell Cycle. Cell 173, 1495-1507.e18. https://doi.org/10.1016/j.cell.2018.03.053

Belshaw, R., Gardner, A., Rambaut, A., Pybus, O.G., 2008. Pacing a small cage: mutation and RNA viruses. Trends in Ecology & Evolution 23, 188–193. https://doi.org/10.1016/j.tree.2007.11.010

Benhaim, M.A., Mangala Prasad, V., Garcia, N.K., Guttman, M., Lee, K.K., 2020. Structural monitoring of a transient intermediate in the hemagglutinin fusion machinery on influenza virions. Science Advances 6, eaaz8822. https://doi.org/10.1126/sciadv.aaz8822

Bergeron-Sandoval, L.-P., Safaee, N., Michnick, S.W., 2016. Mechanisms and Consequences of Macromolecular Phase Separation. Cell 165, 1067–1079. https://doi.org/10.1016/j.cell.2016.05.026

Berry, J., Brangwynne, C.P., Haataja, M., 2018. Physical principles of intracellular organization via active and passive phase transitions. Rep. Prog. Phys. 81, 046601. https://doi.org/10.1088/1361-6633/aaa61e

Berry, J., Weber, S.C., Vaidya, N., Haataja, M., Brangwynne, C.P., 2015. RNA transcription modulates phase transition-driven nuclear body assembly. Proceedings of the National Academy of Sciences 112, E5237–E5245. https://doi.org/10.1073/pnas.1509317112

Bertram, S., Glowacka, I., Steffen, I., Kühl, A., Pöhlmann, S., 2010. Novel insights into proteolytic cleavage of influenza virus hemagglutinin. Rev Med Virol 20, 298–310. https://doi.org/10.1002/rmv.657

Bertram, S., Heurich, A., Lavender, H., Gierer, S., Danisch, S., Perin, P., Lucas, J.M., Nelson, P.S., Pöhlmann, S., Soilleux, E.J., 2012. Influenza and SARS-coronavirus activating proteases TMPRSS2 and HAT are expressed at multiple sites in human respiratory and gastrointestinal tracts. PLoS One 7, e35876. https://doi.org/10.1371/journal.pone.0035876

Bhagwat, A.R., Le Sage, V., Lakdawala, S.S., 2018. Live Imaging of Influenza Viral Ribonucleoproteins Using Light-Sheet Microscopy, in:

Yamauchi, Y. (Ed.), Influenza Virus: Methods and Protocols, Methods in Molecular Biology. Springer, New York, NY, pp. 303–327. https://doi.org/10.1007/978-1-4939-8678-1_15

Bi, Y., Tan, S., Yang, Y., Wong, G., Zhao, M., Zhang, Q., Wang, Q., Zhao, X., Li, L., Yuan, J., Li, Hao, Li, Hong, Xu, W., Shi, W., Quan, C., Zou, R., Li, J., Zheng, H., Yang, L., Liu, W.J., Liu, D., Wang, H., Qin, Y., Liu, L., Jiang, C., Liu, W., Lu, L., Gao, G.F., Liu, Y., 2019. Clinical and Immunological Characteristics of Human Infections With H5N6 Avian Influenza Virus. Clin Infect Dis 68, 1100–1109. https://doi.org/10.1093/cid/ciy681

Bier, K., York, A., Fodor, E., 2011. Cellular cap-binding proteins associate with influenza virus mRNAs. J Gen Virol 92, 1627–1634. https://doi.org/10.1099/vir.0.029231-0

Binder, K., Stauffer, D., 1976. Statistical theory of nucleation, condensation and coagulation. Advances in Physics 25, 343–396. https://doi.org/10.1080/00018737600101402

Biswas, S.K., Boutz, P.L., Nayak, D.P., 1998. Influenza Virus Nucleoprotein Interacts with Influenza Virus Polymerase Proteins. J Virol 72, 5493–5501.

Biswas, S.K., Nayak, D.P., 1994. Mutational analysis of the conserved motifs of influenza A virus polymerase basic protein 1. Journal of Virology 68, 1819–1826. https://doi.org/10.1128/jvi.68.3.1819-1826.1994

Boeynaems, S., Alberti, S., Fawzi, N.L., Mittag, T., Polymenidou, M., Rousseau, F., Schymkowitz, J., Shorter, J., Wolozin, B., Van Den Bosch, L., Tompa, P., Fuxreiter, M., 2018. Protein Phase Separation: A New Phase in Cell Biology. Trends in Cell Biology 28, 420–435. https://doi.org/10.1016/j.tcb.2018.02.004

Bogdanow, B., Wang, X., Eichelbaum, K., Sadewasser, A., Husic, I., Paki, K., Budt, M., Hergeselle, M., Vetter, B., Hou, J., Chen, W., Wiebusch, L., Meyer, I.M., Wolff, T., Selbach, M., 2019. The dynamic proteome of influenza A virus infection identifies M segment splicing as a host range determinant. Nat Commun 10, 5518. https://doi.org/10.1038/s41467-019-13520-8

Boke, E., Mitchison, T.J., 2017. The balbiani body and the concept of physiological amyloids. Cell Cycle 16, 153–154. https://doi.org/10.1080/15384101.2016.1241605

Bonilla-Aldana, D.K., Aguirre-Florez, M., Villamizar-Peña, R., Gutiérrez-Ocampo, E., Henao-Martínez, J.F., Cvetkovic-Vega, A., Dhama, K., Rabaan, A.A., Sah, R., Rodriguez-Morales, A.J., Schlagenhauf, P., Paniz-Mondolfi, A., 2020. After SARS-CoV-2, will H5N6 and other influenza viruses follow the pandemic path? Infez. Med. 28, 475–485.

Bos, T.J., Davis, A.R., Nayak, D.P., 1984. NH2-terminal hydrophobic region of influenza virus neuraminidase provides the signal function in translocation. Proceedings of the National Academy of Sciences 81, 2327–2331. https://doi.org/10.1073/pnas.81.8.2327

Böttcher, E., Matrosovich, T., Beyerle, M., Klenk, H.-D., Garten, W., Matrosovich, M., 2006. Proteolytic Activation of Influenza Viruses by Serine Proteases TMPRSS2 and HAT from Human Airway Epithelium. J Virol 80, 9896–9898. https://doi.org/10.1128/JVI.01118-06

Böttcher-Friebertshäuser, E., Klenk, H., Garten, W., 2013. Activation of influenza viruses by proteases from host cells and bacteria in the human airway epithelium. Pathog Dis 69, 87–100. https://doi.org/10.1111/2049-632X.12053

Bracha, D., Walls, M.T., Wei, M.-T., Zhu, L., Kurian, M., Avalos, J.L., Toettcher, J.E., Brangwynne, C.P., 2018. Mapping Local and Global Liquid Phase Behavior in Living Cells Using Photo-Oligomerizable Seeds. Cell 175, 1467-1480.e13. https://doi.org/10.1016/j.cell.2018.10.048

Bradel-Tretheway, B.G., Mattiacio, J.L., Krasnoselsky, A., Stevenson, C., Purdy, D., Dewhurst, S., Katze, M.G., 2011. Comprehensive proteomic analysis of influenza virus polymerase complex reveals a novel association with mitochondrial proteins and RNA polymerase accessory factors. J Virol 85, 8569–8581. https://doi.org/10.1128/JVI.00496-11

Brangwynne, C.P., 2011. Soft active aggregates: mechanics, dynamics and self-assembly of liquid-like intracellular protein bodies. Soft Matter 7, 3052–3059. https://doi.org/10.1039/C0SM00981D

Brangwynne, C.P., Eckmann, C.R., Courson, D.S., Rybarska, A., Hoege, C., Gharakhani, J., Julicher, F., Hyman, A.A., 2009. Germline P Granules Are Liquid Droplets That Localize by Controlled Dissolution/Condensation. Science (New York, N.Y.) 324, 1729–1732. https://doi.org/10.1126/science.1172046

Brangwynne, C.P., Johnson, T.L., 2013. The micro and macro of RNA function. MBoC 24, 679–679. https://doi.org/10.1091/mbc.e13-01-0012

Brangwynne, C.P., Tompa, P., Pappu, R.V., 2015. Polymer physics of intracellular phase transitions. Nature Phys 11, 899–904. https://doi.org/10.1038/nphys3532

Brocca, S., Grandori, R., Longhi, S., Uversky, V., 2020. Liquid–Liquid Phase Separation by Intrinsically Disordered Protein Regions of Viruses: Roles in Viral Life Cycle and Control of Virus–Host Interactions. International Journal of Molecular Sciences 21, 9045. https://doi.org/10.3390/ijms21239045

Brooke, C.B., Ince, W.L., Wrammert, J., Ahmed, R., Wilson, P.C., Bennink, J.R., Yewdell, J.W., 2013. Most Influenza A Virions Fail To Express at Least One Essential Viral Protein. Journal of Virology 87, 3155–3162. https://doi.org/10.1128/JVI.02284-12

Bruce, E.A., Digard, P., Stuart, A.D., 2010. The Rab11 Pathway Is Required for Influenza A Virus Budding and Filament Formation. Journal of Virology 84, 5848–5859. https://doi.org/10.1128/JVI.00307-10

Bui, M., Whittaker, G., Helenius, A., 1996. Effect of M1 protein and low pH on nuclear transport of influenza virus ribonucleoproteins. J Virol 70, 8391–8401. https://doi.org/10.1128/JVI.70.12.8391-8401.1996

Bui, M., Wills, E.G., Helenius, A., Whittaker, G.R., 2000. Role of the Influenza Virus M1 Protein in Nuclear Export of Viral Ribonucleoproteins. J Virol 74, 1781–1786.

Bullido, R., Gómez-Puertas, P., Saiz, M.J., Portela, A., 2001. Influenza A virus NEP (NS2 protein) downregulates RNA synthesis of model template RNAs. J Virol 75, 4912–4917. https://doi.org/10.1128/JVI.75.10.4912-4917.2001

Bullough, P.A., Hughson, F.M., Skehel, J.J., Wiley, D.C., 1994. Structure of influenza haemagglutinin at the pH of membrane fusion. Nature 371, 37–43. https://doi.org/10.1038/371037a0

Burnet, F.M., Bull, D.R., 1943. CHANGES IN INFLUENZA VIRUS ASSOCIATED WITH ADAPTATION TO PASSAGE IN CHICK EMBRYOS. [WWW Document]. URL https://web.s.ebscohost.com/abstract?direct=true&profile=ehost&scope=site&authtype=crawler&jrnl=0004945X&AN=17413485&h=d73xa2p7rCgDZiCGk3W0lbFpuA3BG0d4Mnb0jcG5MOd0fxHhRd5Zg8ESlm2MFfZLVue%2beQX6aaEAaF73OsA6Cg%3d%3d&crl=c&resultNs=AdminWebAuth&resultLocal=ErrCrlNotAuth&crlhashurl=login.aspx%3fdirect%3dtrue%26profile%3dehost%26scope%3dsite%26authtype%3dcrawler%26jrnl%3d0004945X%26AN%3d17413485 (accessed 11.21.22).

Butt, H.-J., Graf, K., Kappl, M., 2006. Physics and Chemistry of Interfaces. John Wiley & Sons.

Butt, H.-J., Graf, K., Kappl, M., 2003. Physics and Chemistry of Interfaces. Wiley-VCH GmbH & Co. KGaA 376.

Caini, S., Kusznierz, G., Garate, V.V., Wangchuk, S., Thapa, B., Júnior, F.J. de P., Almeida, W.A.F. de, Njouom, R., Fasce, R.A., Bustos, P., Feng, L., Peng, Z., Araya, J.L., Bruno, A., Mora, D. de, Gámez, M.J.B. de, Pebody, R., Zambon, M., Higueros, R., Rivera, R., Kosasih, H., Castrucci, M.R., Bella, A., Kadjo, H.A., Daouda, C., Makusheva, A., Bessonova, O., Chaves, S.S., Emukule, G.O., Heraud, J.-M., Razanajatovo, N.H., Barakat, A., Falaki, F.E., Meijer, A., Donker, G.A., Huang, Q.S., Wood, T., Balmaseda, A., Palekar, R., Arévalo, B.M., Rodrigues, A.P., Guiomar, R., Lee, V.J.M., Ang, L.W., Cohen, C., Treurnicht, F., Mironenko, A., Holubka, O., Bresee, J., Brammer, L., Le, M.T.Q., Hoang, P.V.M., Guerche-Séblain, C.E., Paget, J., Team, the G.I.B.S., 2019. The epidemiological signature of influenza B virus and its B/Victoria and B/Yamagata lineages in the 21st century. PLOS ONE 14, e0222381. https://doi.org/10.1371/journal.pone.0222381

Calder, L.J., Wasilewski, S., Berriman, J.A., Rosenthal, P.B., 2010. Structural organization of a filamentous influenza A virus. Proceedings of the

National Academy of Sciences 107, 10685–10690. https://doi.org/10.1073/pnas.1002123107
Calvo, C., García-García, M.L., Borrell, B., Pozo, F., Casas, I., 2013. Prospective Study of Influenza C in Hospitalized Children. The Pediatric Infectious Disease Journal 32, 916–919. https://doi.org/10.1097/INF.0b013e31828fca10
Caragliano, E., Bonazza, S., Frascaroli, G., Tang, J., Soh, T.K., Grünewald, K., Bosse, J.B., Brune, W., 2022a. Human cytomegalovirus forms phase-separated compartments at viral genomes to facilitate viral replication. Cell Reports 38, 110469. https://doi.org/10.1016/j.celrep.2022.110469
Caragliano, E., Brune, W., Bosse, J.B., 2022b. Herpesvirus Replication Compartments: Dynamic Biomolecular Condensates. Viruses 14, 960. https://doi.org/10.3390/v14050960
Carlson, C.R., Asfaha, J.B., Ghent, C.M., Howard, C.J., Hartooni, N., Safari, M., Frankel, A.D., Morgan, D.O., 2020. Phosphoregulation of Phase Separation by the SARS-CoV-2 N Protein Suggests a Biophysical Basis for its Dual Functions. Molecular Cell 80, 1092-1103.e4. https://doi.org/10.1016/j.molcel.2020.11.025
Cascarina, S.M., Ross, E.D., 2022. Phase separation by the SARS-CoV-2 nucleocapsid protein: Consensus and open questions. J Biol Chem 298, 101677. https://doi.org/10.1016/j.jbc.2022.101677
Cascarina, S.M., Ross, E.D., 2020. A proposed role for the SARS-CoV-2 nucleocapsid protein in the formation and regulation of biomolecular condensates. The FASEB Journal 34, 9832–9842. https://doi.org/10.1096/fj.202001351
Case, L.B., Ditlev, J.A., Rosen, M.K., 2019a. Regulation of Transmembrane Signaling by Phase Separation. Annual Review of Biophysics 48, 465–494. https://doi.org/10.1146/annurev-biophys-052118-115534
Case, L.B., Zhang, X., Ditlev, J.A., Rosen, M.K., 2019b. Stoichiometry controls activity of phase-separated clusters of actin signaling proteins. Science 363, 1093–1097. https://doi.org/10.1126/science.aau6313
CDC, 2022. Avian Influenza in Birds [WWW Document]. Centers for Disease Control and Prevention. URL https://www.cdc.gov/flu/avianflu/avian-in-birds.htm (accessed 11.22.22).
CDC, 2021. How Flu Viruses Can Change [WWW Document]. Centers for Disease Control and Prevention. URL https://www.cdc.gov/flu/about/viruses/change.htm (accessed 11.21.22).
Chaipan, C., Kobasa, D., Bertram, S., Glowacka, I., Steffen, I., Tsegaye, T.S., Takeda, M., Bugge, T.H., Kim, S., Park, Y., Marzi, A., Pöhlmann, S., 2009. Proteolytic activation of the 1918 influenza virus hemagglutinin. J Virol 83, 3200–3211. https://doi.org/10.1128/JVI.02205-08
Chan, W.-H., Ng, A.K.-L., Robb, N.C., Lam, M.K.-H., Chan, P.K.-S., Au, S.W.-N., Wang, J.-H., Fodor, E., Shaw, P.-C., 2010. Functional Analysis of

the Influenza Virus H5N1 Nucleoprotein Tail Loop Reveals Amino Acids That Are Crucial for Oligomerization and Ribonucleoprotein Activities. J Virol 84, 7337–7345. https://doi.org/10.1128/JVI.02474-09

Chang, P., Sealy, J.E., Sadeyen, J.-R., Bhat, S., Lukosaityte, D., Sun, Y., Iqbal, M., 2020. Immune Escape Adaptive Mutations in the H7N9 Avian Influenza Hemagglutinin Protein Increase Virus Replication Fitness and Decrease Pandemic Potential. J Virol 94, e00216-20. https://doi.org/10.1128/JVI.00216-20

Chase, G.P., Rameix-Welti, M.-A., Zvirbliene, A., Zvirblis, G., Götz, V., Wolff, T., Naffakh, N., Schwemmle, M., 2011. Influenza Virus Ribonucleoprotein Complexes Gain Preferential Access to Cellular Export Machinery through Chromatin Targeting. PLOS Pathogens 7, e1002187. https://doi.org/10.1371/journal.ppat.1002187

Chassey, B. de, Aublin-Gex, A., Ruggieri, A., Meyniel-Schicklin, L., Pradezynski, F., Davoust, N., Chantier, T., Tafforeau, L., Mangeot, P.-E., Ciancia, C., Perrin-Cocon, L., Bartenschlager, R., André, P., Lotteau, V., 2013. The Interactomes of Influenza Virus NS1 and NS2 Proteins Identify New Host Factors and Provide Insights for ADAR1 Playing a Supportive Role in Virus Replication. PLOS Pathogens 9, e1003440. https://doi.org/10.1371/journal.ppat.1003440

Chen, B.J., Leser, G.P., Morita, E., Lamb, R.A., 2007. Influenza Virus Hemagglutinin and Neuraminidase, but Not the Matrix Protein, Are Required for Assembly and Budding of Plasmid-Derived Virus-Like Particles. Journal of Virology 81, 7111–7123. https://doi.org/10.1128/JVI.00361-07

Chen, C., Zhuang, X., 2008. Epsin 1 is a cargo-specific adaptor for the clathrin-mediated endocytosis of the influenza virus. Proc Natl Acad Sci U S A 105, 11790–11795. https://doi.org/10.1073/pnas.0803711105

Chen, G.-W., Chang, S.-C., Mok, C.-K., Lo, Y.-L., Kung, Y.-N., Huang, J.-H., Shih, Y.-H., Wang, J.-Y., Chiang, C., Chen, C.-J., Shih, S.-R., 2006. Genomic Signatures of Human versus Avian Influenza A Viruses. Emerg Infect Dis 12, 1353–1360. https://doi.org/10.3201/eid1209.060276

Chen, H., Cui, Y., Han, X., Hu, W., Sun, M., Zhang, Y., Wang, P.-H., Song, G., Chen, W., Lou, J., 2020. Liquid–liquid phase separation by SARS-CoV-2 nucleocapsid protein and RNA. Cell Res 30, 1143–1145. https://doi.org/10.1038/s41422-020-00408-2

Chen, H., Huang, L., Li, Hui, Zhou, X., Li, Huanan, Sun, N., Qi, W., Xiao, C., Ni, X., Liu, M., Liao, M., 2015. High Pathogenicity of Influenza A (H10N8) Virus in Mice. Am J Trop Med Hyg 93, 1360–1363. https://doi.org/10.4269/ajtmh.15-0064

Chen, J., Lee, K.H., Steinhauer, D.A., Stevens, D.J., Skehel, J.J., Wiley, D.C., 1998. Structure of the hemagglutinin precursor cleavage site, a determinant of influenza pathogenicity and the origin of the labile

conformation. Cell 95, 409–417. https://doi.org/10.1016/s0092-8674(00)81771-7
Chen, W., Calvo, P.A., Malide, D., Gibbs, J., Schubert, U., Bacik, I., Basta, S., O'Neill, R., Schickli, J., Palese, P., Henklein, P., Bennink, J.R., Yewdell, J.W., 2001. A novel influenza A virus mitochondrial protein that induces cell death. Nat Med 7, 1306–1312. https://doi.org/10.1038/nm1201-1306
Chizhmakov, I.V., Geraghty, F.M., Ogden, D.C., Hayhurst, A., Antoniou, M., Hay, A.J., 1996. Selective proton permeability and pH regulation of the influenza virus M2 channel expressed in mouse erythroleukaemia cells. The Journal of Physiology 494, 329–336. https://doi.org/10.1113/jphysiol.1996.sp021495
Chizhmakov, I.V., Ogden, D.C., Geraghty, F.M., Hayhurst, A., Skinner, A., Betakova, T., Hay, A.J., 2003. Differences in conductance of M2 proton channels of two influenza viruses at low and high pH. The Journal of Physiology 546, 427–438. https://doi.org/10.1113/jphysiol.2002.028910
Chlanda, P., Schraidt, O., Kummer, S., Riches, J., Oberwinkler, H., Prinz, S., Kräusslich, H.-G., Briggs, J.A.G., 2015. Structural Analysis of the Roles of Influenza A Virus Membrane-Associated Proteins in Assembly and Morphology. Journal of Virology 89, 8957–8966. https://doi.org/10.1128/JVI.00592-15
Choi, J.-M., Holehouse, A.S., Pappu, R.V., 2020. Physical Principles Underlying the Complex Biology of Intracellular Phase Transitions. Annual Review of Biophysics 49, 107–133. https://doi.org/10.1146/annurev-biophys-121219-081629
Choi, J.-M., Pappu, R.V., 2020. The Stickers and Spacers Framework for Describing Phase Behavior of Multivalent Intrinsically Disordered Proteins. Biophysical Journal 118, 492a. https://doi.org/10.1016/j.bpj.2019.11.2723
Chou, Y., Heaton, N.S., Gao, Q., Palese, P., Singer, R., Lionnet, T., 2013. Colocalization of Different Influenza Viral RNA Segments in the Cytoplasm before Viral Budding as Shown by Single-molecule Sensitivity FISH Analysis. PLOS Pathogens 9, e1003358. https://doi.org/10.1371/journal.ppat.1003358
Chutiwitoonchai, N., Aida, Y., 2016. NXT1, a Novel Influenza A NP Binding Protein, Promotes the Nuclear Export of NP via a CRM1-Dependent Pathway. Viruses 8, 209. https://doi.org/10.3390/v8080209
Cianci, C., Gerritz, S.W., Deminie, C., Krystal, M., 2013. Influenza Nucleoprotein: Promising Target for Antiviral Chemotherapy. Antivir Chem Chemother 23, 77–91. https://doi.org/10.3851/IMP2235
Cianci, C., Tiley, L., Krystal, M., 1995. Differential activation of the influenza virus polymerase via template RNA binding. J Virol 69, 3995–3999. https://doi.org/10.1128/JVI.69.7.3995-3999.1995

Ciminski, K., Schwemmle, M., 2021. Bat-Borne Influenza A Viruses: An Awakening. Cold Spring Harb Perspect Med 11, a038612. https://doi.org/10.1101/cshperspect.a038612

Clohisey, S., Parkinson, N., Wang, B., Bertin, N., Wise, H., Tomoiu, A., Summers, K.M., Hendry, R.W., Carninci, P., Forrest, A.R.R., Hayashizaki, Y., Digard, P., Hume, D.A., Baillie, J.K., 2020. Comprehensive Characterization of Transcriptional Activity during Influenza A Virus Infection Reveals Biases in Cap-Snatching of Host RNA Sequences. J Virol 94, e01720-19. https://doi.org/10.1128/JVI.01720-19

Cohen, M., Zhang, X.-Q., Senaati, H.P., Chen, H.-W., Varki, N.M., Schooley, R.T., Gagneux, P., 2013. Influenza A penetrates host mucus by cleaving sialic acids with neuraminidase. Virology Journal 10, 321. https://doi.org/10.1186/1743-422X-10-321

Collin, E.A., Sheng, Z., Lang, Y., Ma, W., Hause, B.M., Li, F., 2015. Cocirculation of Two Distinct Genetic and Antigenic Lineages of Proposed Influenza D Virus in Cattle. J Virol 89, 1036–1042. https://doi.org/10.1128/JVI.02718-14

Colman, P.M., Varghese, J.N., Laver, W.G., 1983. Structure of the catalytic and antigenic sites in influenza virus neuraminidase. Nature 303, 41–44. https://doi.org/10.1038/303041a0

Compans, R.W., Content, J., Duesberg, P.H., 1972. Structure of the ribonucleoprotein of influenza virus. J Virol 10, 795–800. https://doi.org/10.1128/JVI.10.4.795-800.1972

Coombs, K.M., Berard, A., Xu, W., Krokhin, O., Meng, X., Cortens, J.P., Kobasa, D., Wilkins, J., Brown, E.G., 2010. Quantitative Proteomic Analyses of Influenza Virus-Infected Cultured Human Lung Cells. Journal of Virology 84, 10888–10906. https://doi.org/10.1128/JVI.00431-10

Copeland, C.S., Doms, R.W., Bolzau, E.M., Webster, R.G., Helenius, A., 1986. Assembly of influenza hemagglutinin trimers and its role in intracellular transport. Journal of Cell Biology 103, 1179–1191. https://doi.org/10.1083/jcb.103.4.1179

Corbet, G.A., Burke, J.M., Bublitz, G.R., Tay, J.W., Parker, R., 2022. dsRNA-induced condensation of antiviral proteins modulates PKR activity. Proc. Natl. Acad. Sci. U.S.A. 119, e2204235119. https://doi.org/10.1073/pnas.2204235119

Cosentino, G., Marougka, K., Desquesnes, A., Welti, N., Sitterlin, D., Gault, E., Rameix-Welti, M.-A., 2022. Respiratory syncytial virus ribonucleoproteins hijack microtubule Rab11 dependent transport for intracellular trafficking. PLOS Pathogens 18, e1010619. https://doi.org/10.1371/journal.ppat.1010619

Cros, J.F., García-Sastre, A., Palese, P., 2005. An unconventional NLS is critical for the nuclear import of the influenza A virus nucleoprotein and ribonucleoprotein. Traffic 6, 205–213. https://doi.org/10.1111/j.1600-0854.2005.00263.x

Cuylen, S., Blaukopf, C., Politi, A.Z., Müller-Reichert, T., Neumann, B., Poser, I., Ellenberg, J., Hyman, A.A., Gerlich, D.W., 2016. Ki-67 acts as a biological surfactant to disperse mitotic chromosomes. Nature 535, 308–312. https://doi.org/10.1038/nature18610

Czabotar, P.E., Martin, S.R., Hay, A.J., 2004. Studies of structural changes in the M2 proton channel of influenza A virus by tryptophan fluorescence. Virus Research 99, 57–61. https://doi.org/10.1016/j.virusres.2003.10.004

Dadonaite, B., Vijayakrishnan, S., Fodor, E., Bhella, D., Hutchinson, E.C., 2016. Filamentous Influenza Viruses. J Gen Virol 97, 1755–1764. https://doi.org/10.1099/jgv.0.000535

Danieli, A., Martens, S., 2018. p62-mediated phase separation at the intersection of the ubiquitin-proteasome system and autophagy. Journal of Cell Science 131, jcs214304. https://doi.org/10.1242/jcs.214304

Daniels, R., Kurowski, B., Johnson, A.E., Hebert, D.N., 2003. N-Linked Glycans Direct the Cotranslational Folding Pathway of Influenza Hemagglutinin. Molecular Cell 11, 79–90. https://doi.org/10.1016/S1097-2765(02)00821-3

Dao, T.P., Kolaitis, R.-M., Kim, H.J., O'Donovan, K., Martyniak, B., Colicino, E., Hehnly, H., Taylor, J.P., Castañeda, C.A., 2018. Ubiquitin Modulates Liquid-Liquid Phase Separation of UBQLN2 via Disruption of Multivalent Interactions. Molecular Cell 69, 965-978.e6. https://doi.org/10.1016/j.molcel.2018.02.004

Das, D.K., Govindan, R., Nikić-Spiegel, I., Krammer, F., Lemke, E.A., Munro, J.B., 2018. Direct Visualization of the Conformational Dynamics of Single Influenza Hemagglutinin Trimers. Cell 174, 926-937.e12. https://doi.org/10.1016/j.cell.2018.05.050

Davis, A.R., Hiti, A.L., Nayak, D.P., 1980. Influenza defective interfering viral RNA is formed by internal deletion of genomic RNA. Proc Natl Acad Sci U S A 77, 215–219.

Davis, D., Yuan, H., Liang, F.-X., Yang, Y.-M., Westley, J., Petzold, C., Dancel-Manning, K., Deng, Y., Sall, J., Sehgal, P.B., 2019. Human Antiviral Protein MxA Forms Novel Metastable Membraneless Cytoplasmic Condensates Exhibiting Rapid Reversible Tonicity-Driven Phase Transitions. Journal of Virology 93, e01014-19. https://doi.org/10.1128/JVI.01014-19

de Castro Martin, I.F., Fournier, G., Sachse, M., Pizarro-Cerda, J., Risco, C., Naffakh, N., 2017. Influenza virus genome reaches the plasma membrane via a modified endoplasmic reticulum and Rab11-dependent vesicles. Nat Commun 8, 1396. https://doi.org/10.1038/s41467-017-01557-6

de Vries, E., Tscherne, D.M., Wienholts, M.J., Cobos-Jiménez, V., Scholte, F., García-Sastre, A., Rottier, P.J.M., de Haan, C.A.M., 2011. Dissection of the Influenza A Virus Endocytic Routes Reveals

Macropinocytosis as an Alternative Entry Pathway. PLoS Pathog 7, e1001329. https://doi.org/10.1371/journal.ppat.1001329
Deibel, R., Emord, D.E., Dukelow, W., Hinshaw, V.S., Wood, J.M., 1985. Influenza viruses and paramyxoviruses in ducks in the Atlantic flyway, 1977-1983, including an H5N2 isolate related to the virulent chicken virus. Avian Dis 29, 970–985.
Delarue, M., Brittingham, G.P., Pfeffer, S., Surovtsev, I.V., Pinglay, S., Kennedy, K.J., Schaffer, M., Gutierrez, J.I., Sang, D., Poterewicz, G., Chung, J.K., Plitzko, J.M., Groves, J.T., Jacobs-Wagner, C., Engel, B.D., Holt, L.J., 2018. mTORC1 Controls Phase Separation and the Biophysical Properties of the Cytoplasm by Tuning Crowding. Cell 174, 338-349.e20. https://doi.org/10.1016/j.cell.2018.05.042
Delport, A., Hewer, R., 2022. A superior loading control for the cellular thermal shift assay. Sci Rep 12, 6672. https://doi.org/10.1038/s41598-022-10653-7
Deng, T., Vreede, F.T., Brownlee, G.G., 2006. Different de novo initiation strategies are used by influenza virus RNA polymerase on its cRNA and viral RNA promoters during viral RNA replication. J Virol 80, 2337–2348. https://doi.org/10.1128/JVI.80.5.2337-2348.2006
Detjen, B.M., St Angelo, C., Katze, M.G., Krug, R.M., 1987. The three influenza virus polymerase (P) proteins not associated with viral nucleocapsids in the infected cell are in the form of a complex. Journal of Virology 61, 16–22. https://doi.org/10.1128/jvi.61.1.16-22.1987
Dhillon, P., Rao, C.D., 2018. Rotavirus Induces Formation of Remodeled Stress Granules and P Bodies and Their Sequestration in Viroplasms To Promote Progeny Virus Production. Journal of Virology 92. https://doi.org/10.1128/jvi.01363-18
Dias, A., Bouvier, D., Crépin, T., McCarthy, A.A., Hart, D.J., Baudin, F., Cusack, S., Ruigrok, R.W.H., 2009. The cap-snatching endonuclease of influenza virus polymerase resides in the PA subunit. Nature 458, 914–918. https://doi.org/10.1038/nature07745
Digard, P., Elton, D., Bishop, K., Medcalf, E., Weeds, A., Pope, B., 1999. Modulation of Nuclear Localization of the Influenza Virus Nucleoprotein through Interaction with Actin Filaments. J Virol 73, 2222–2231.
Dignon, G.L., Best, R.B., Mittal, J., 2020. Biomolecular Phase Separation: From Molecular Driving Forces to Macroscopic Properties. Annual Review of Physical Chemistry 71, 53–75. https://doi.org/10.1146/annurev-physchem-071819-113553
Dolnik, O., Gerresheim, G.K., Biedenkopf, N., 2021. New Perspectives on the Biogenesis of Viral Inclusion Bodies in Negative-Sense RNA Virus Infections. Cells 10, 1460. https://doi.org/10.3390/cells10061460
Domingues, P., Golebiowski, F., Tatham, M.H., Lopes, A.M., Taggart, A., Hay, R.T., Hale, B.G., 2015. Global Reprogramming of Host SUMOylation during Influenza Virus Infection. Cell Reports 13, 1467–1480. https://doi.org/10.1016/j.celrep.2015.10.001

Dong, X., Biswas, A., Süel, K.E., Jackson, L.K., Martinez, R., Gu, H., Chook, Y.M., 2009. Structural basis for leucine-rich nuclear export signal recognition by CRM1. Nature 458, 1136–1141. https://doi.org/10.1038/nature07975

Dou, D., da Silva, D.V., Nordholm, J., Wang, H., Daniels, R., 2014. Type II transmembrane domain hydrophobicity dictates the cotranslational dependence for inversion. MBoC 25, 3363–3374. https://doi.org/10.1091/mbc.e14-04-0874

Dou, D., Hernández-Neuta, I., Wang, H., Östbye, H., Qian, X., Thiele, S., Resa-Infante, P., Kouassi, N.M., Sender, V., Hentrich, K., Mellroth, P., Henriques-Normark, B., Gabriel, G., Nilsson, M., Daniels, R., 2017. Analysis of IAV Replication and Co-infection Dynamics by a Versatile RNA Viral Genome Labeling Method. Cell Rep 20, 251–263. https://doi.org/10.1016/j.celrep.2017.06.021

Dou, D., Revol, R., Östbye, H., Wang, H., Daniels, R., 2018. Influenza A Virus Cell Entry, Replication, Virion Assembly and Movement. Frontiers in Immunology 9.

Drino, A., Schaefer, M.R., 2018. RNAs, Phase Separation, and Membrane-Less Organelles: Are Post-Transcriptional Modifications Modulating Organelle Dynamics? BioEssays 40, 1800085. https://doi.org/10.1002/bies.201800085

Du, M., Chen, Z.J., 2018. DNA-induced liquid phase condensation of cGAS activates innate immune signaling. Science 361, 704–709. https://doi.org/10.1126/science.aat1022

Duhaut, S.D., Dimmock, N.J., 1998. Heterologous Protection of Mice from a Lethal Human H1N1 Influenza A Virus Infection by H3N8 Equine Defective Interfering Virus: Comparison of Defective RNA Sequences Isolated from the DI Inoculum and Mouse Lung. Virology 248, 241–253. https://doi.org/10.1006/viro.1998.9267

Duhaut, S.D., Mccauley, J.W., 1996. Defective RNAs Inhibit the Assembly of Influenza Virus Genome Segments in a Segment-Specific Manner. Virology 216, 326–337. https://doi.org/10.1006/viro.1996.0068

Eisfeld, A.J., Kawakami, E., Watanabe, T., Neumann, G., Kawaoka, Y., 2011a. RAB11A Is Essential for Transport of the Influenza Virus Genome to the Plasma Membrane. Journal of Virology 85, 6117–6126. https://doi.org/10.1128/JVI.00378-11

Eisfeld, A.J., Neumann, G., Kawaoka, Y., 2015. At the centre: influenza A virus ribonucleoproteins. Nat Rev Microbiol 13, 28–41. https://doi.org/10.1038/nrmicro3367

Eisfeld, A.J., Neumann, G., Kawaoka, Y., 2011b. Human Immunodeficiency Virus Rev-Binding Protein Is Essential for Influenza A Virus Replication and Promotes Genome Trafficking in Late-Stage Infection ▿. J Virol 85, 9588–9598. https://doi.org/10.1128/JVI.05064-11

Elbaum-Garfinkle, S., Brangwynne, C.P., 2015. Liquids, Fibers, and Gels: The Many Phases of Neurodegeneration. Developmental Cell 35, 531–532. https://doi.org/10.1016/j.devcel.2015.11.014

Elleman, C.J., Barclay, W.S., 2004. The M1 matrix protein controls the filamentous phenotype of influenza A virus. Virology 321, 144–153. https://doi.org/10.1016/j.virol.2003.12.009

Elton, D., Medcalf, E., Bishop, K., Digard, P., 1999. Oligomerization of the Influenza Virus Nucleoprotein: Identification of Positive and Negative Sequence Elements. Virology 260, 190–200. https://doi.org/10.1006/viro.1999.9818

Elton, D., Simpson-Holley, M., Archer, K., Medcalf, L., Hallam, R., McCauley, J., Digard, P., 2001. Interaction of the Influenza Virus Nucleoprotein with the Cellular CRM1-Mediated Nuclear Export Pathway. Journal of Virology 75, 408–419. https://doi.org/10.1128/JVI.75.1.408-419.2001

Engelhardt, O.G., Smith, M., Fodor, E., 2005. Association of the Influenza A Virus RNA-Dependent RNA Polymerase with Cellular RNA Polymerase II. Journal of Virology 79, 5812–5818. https://doi.org/10.1128/JVI.79.9.5812-5818.2005

Etibor, T.A., Sridharan, S., Vale-Costa, S., Bras, D., Becher, I., Vello, V., Ferreira, F., Alenquer, M., Savitski, M.M., Amorim, M.J., 2022. Influenza A virus liquid condensates can undergo pharmacological hardening. https://doi.org/10.1101/2022.08.03.502602

Etibor, T.A., Yamauchi, Y., Amorim, M.J., 2021. Liquid Biomolecular Condensates and Viral Lifecycles: Review and Perspectives. Viruses 13, 366. https://doi.org/10.3390/v13030366

Etkind, P.R., Krug, R.M., 1975. Purification of influenza viral complementary RNA: its genetic content and activity in wheat germ cell-free extracts. Journal of Virology 16, 1464–1475. https://doi.org/10.1128/jvi.16.6.1464-1475.1975

Exner, H.E., Lukas, H.L., 1971. The experimental verification of the stationary Wagner-Lifshitz distribution of coarse particles. Metallography 4, 325–338. https://doi.org/10.1016/0026-0800(71)90061-9

Falahati, H., Haji-Akbari, A., 2019. Thermodynamically driven assemblies and liquid–liquid phase separations in biology. Soft Matter 15, 1135–1154. https://doi.org/10.1039/C8SM02285B

Fechter, P., Mingay, L., Sharps, J., Chambers, A., Fodor, E., Brownlee, G.G., 2003. Two Aromatic Residues in the PB2 Subunit of Influenza A RNA Polymerase Are Crucial for Cap Binding*. Journal of Biological Chemistry 278, 20381–20388. https://doi.org/10.1074/jbc.M300130200

Feldmann, A., Schäfer, M.K.-H., Garten, W., Klenk, H.-D., 2000. Targeted Infection of Endothelial Cells by Avian Influenza Virus A/FPV/Rostock/34 (H7N1) in Chicken Embryos. J Virol 74, 8018–8027.

Ferhadian, D., Contrant, M., Printz-Schweigert, A., Smyth, R.P., Paillart, J.-C., Marquet, R., 2018. Structural and Functional Motifs in Influenza Virus RNAs. Front Microbiol 9, 559. https://doi.org/10.3389/fmicb.2018.00559

Feric, M., Vaidya, N., Harmon, T.S., Mitrea, D.M., Zhu, L., Richardson, T.M., Kriwacki, R.W., Pappu, R.V., Brangwynne, C.P., 2016. Coexisting Liquid Phases Underlie Nucleolar Subcompartments. Cell 165, 1686–1697. https://doi.org/10.1016/j.cell.2016.04.047

Firth, A.E., Jagger, B.W., Wise, H.M., Nelson, C.C., Parsawar, K., Wills, N.M., Napthine, S., Taubenberger, J.K., Digard, P., Atkins, J.F., 2012. Ribosomal frameshifting used in influenza A virus expression occurs within the sequence UCC_UUU_CGU and is in the +1 direction. Open Biol. 2, 120109. https://doi.org/10.1098/rsob.120109

Fodor, E., 2013. The RNA polymerase of influenza A virus: mechanisms of viral transcription and replication. av 57, 113–122. https://doi.org/10.4149/av_2013_02_113

Fodor, E., Seong, B.L., Brownlee, G.G., 1993. Photochemical cross-linking of influenza A polymerase to its virion RNA promoter defines a polymerase binding site at residues 9 to 12 of the promoter. J Gen Virol 74 (Pt 7), 1327–1333. https://doi.org/10.1099/0022-1317-74-7-1327

Fodor, E., Velthuis, A.J.W. te, 2020. Structure and Function of the Influenza Virus Transcription and Replication Machinery. Cold Spring Harb Perspect Med 10, a038398. https://doi.org/10.1101/cshperspect.a038398

Fournier, G., Chiang, C., Munier, S., Tomoiu, A., Demeret, C., Vidalain, P.-O., Jacob, Y., Naffakh, N., 2014. Recruitment of RED-SMU1 Complex by Influenza A Virus RNA Polymerase to Control Viral mRNA Splicing. PLOS Pathogens 10, e1004164. https://doi.org/10.1371/journal.ppat.1004164

Franken, H., Mathieson, T., Childs, D., Sweetman, G.M.A., Werner, T., Tögel, I., Doce, C., Gade, S., Bantscheff, M., Drewes, G., Reinhard, F.B.M., Huber, W., Savitski, M.M., 2015. Thermal proteome profiling for unbiased identification of direct and indirect drug targets using multiplexed quantitative mass spectrometry. Nat Protoc 10, 1567–1593. https://doi.org/10.1038/nprot.2015.101

Franzmann, T.M., Alberti, S., 2019. Protein Phase Separation as a Stress Survival Strategy. Cold Spring Harbor Perspectives in Biology 11, a034058. https://doi.org/10.1101/cshperspect.a034058

Franzmann, T.M., Jahnel, M., Pozniakovsky, A., Mahamid, J., Holehouse, A.S., Nüske, E., Richter, D., Baumeister, W., Grill, S.W., Pappu, R.V., Hyman, A.A., Alberti, S., 2018. Phase separation of a yeast prion protein promotes cellular fitness. Science (New York, N.Y.) 359, eaao5654. https://doi.org/10.1126/science.aao5654

Freeman Rosenzweig, E.S., Xu, B., Kuhn Cuellar, L., Martinez-Sanchez, A., Schaffer, M., Strauss, M., Cartwright, H.N., Ronceray, P., Plitzko, J.M., Förster, F., Wingreen, N.S., Engel, B.D., Mackinder, L.C.M., Jonikas, M.C., 2017. The Eukaryotic CO2-Concentrating Organelle Is Liquid-like and Exhibits Dynamic Reorganization. Cell 171, 148-162.e19. https://doi.org/10.1016/j.cell.2017.08.008

Fritsch, A., Schweiger, B., Biere, B., 2019. Influenza C virus in pre-school children with respiratory infections: retrospective analysis of data from the national influenza surveillance system in Germany, 2012 to 2014. Euro Surveill 24, 1800174. https://doi.org/10.2807/1560-7917.ES.2019.24.10.1800174

Frottin, F., Schueder, F., Tiwary, S., Gupta, R., Körner, R., Schlichthaerle, T., Cox, J., Jungmann, R., Hartl, F.U., Hipp, M.S., 2019. The nucleolus functions as a phase-separated protein quality control compartment. Science 365, 342–347. https://doi.org/10.1126/science.aaw9157

Frymus, T., Belák, S., Egberink, H., Hofmann-Lehmann, R., Marsilio, F., Addie, D.D., Boucraut-Baralon, C., Hartmann, K., Lloret, A., Lutz, H., Pennisi, M.G., Thiry, E., Truyen, U., Tasker, S., Möstl, K., Hosie, M.J., 2021. Influenza Virus Infections in Cats. Viruses 13, 1435. https://doi.org/10.3390/v13081435

Fujii, Y., Goto, H., Watanabe, T., Yoshida, T., Kawaoka, Y., 2003. Selective incorporation of influenza virus RNA segments into virions. Proceedings of the National Academy of Sciences 100, 2002–2007. https://doi.org/10.1073/pnas.0437772100

Fuller, G.G., Han, T., Freeberg, M.A., Moresco, J.J., Ghanbari Niaki, A., Roach, N.P., Yates, J.R., III, Myong, S., Kim, J.K., 2020. RNA promotes phase separation of glycolysis enzymes into yeast G bodies in hypoxia. eLife 9, e48480. https://doi.org/10.7554/eLife.48480

Gabriel, G., Herwig, A., Klenk, H.-D., 2008. Interaction of polymerase subunit PB2 and NP with importin alpha1 is a determinant of host range of influenza A virus. PLoS Pathog 4, e11. https://doi.org/10.1371/journal.ppat.0040011

Gack, M.U., Albrecht, R.A., Urano, T., Inn, K.-S., Huang, I.-C., Carnero, E., Farzan, M., Inoue, S., Jung, J.U., García-Sastre, A., 2009. Influenza A Virus NS1 Targets the Ubiquitin Ligase TRIM25 to Evade Recognition by the Host Viral RNA Sensor RIG-I. Cell Host & Microbe 5, 439–449. https://doi.org/10.1016/j.chom.2009.04.006

Ganti, K., Han, J., Manicassamy, B., Lowen, A.C., 2021. Rab11a mediates cell-cell spread and reassortment of influenza A virus genomes via tunneling nanotubes. PLOS Pathogens 17, e1009321. https://doi.org/10.1371/journal.ppat.1009321

Gao, D., Wu, J., Wu, Y.-T., Du, F., Aroh, C., Yan, N., Sun, L., Chen, Z.J., 2013. Cyclic GMP-AMP synthase is an innate immune sensor of HIV and other retroviruses. Science 341, 903–906. https://doi.org/10.1126/science.1240933

Gao, S., Song, L., Li, J., Zhang, Z., Peng, H., Jiang, W., Wang, Q., Kang, T., Chen, S., Huang, W., 2012. Influenza A virus-encoded NS1 virulence factor protein inhibits innate immune response by targeting IKK. Cellular Microbiology 14, 1849–1866. https://doi.org/10.1111/cmi.12005

Garcia-Jove Navarro, M., Kashida, S., Chouaib, R., Souquere, S., Pierron, G., Weil, D., Gueroui, Z., 2019. RNA is a critical element for the sizing

and the composition of phase-separated RNA–protein condensates. Nat Commun 10, 3230. https://doi.org/10.1038/s41467-019-11241-6
García-Sastre, A., 2017. Ten Strategies of Interferon Evasion by Viruses. Cell Host & Microbe 22, 176–184. https://doi.org/10.1016/j.chom.2017.07.012
Gavazzi, C., Isel, C., Fournier, E., Moules, V., Cavalier, A., Thomas, D., Lina, B., Marquet, R., 2013a. An in vitro network of intermolecular interactions between viral RNA segments of an avian H5N2 influenza A virus: comparison with a human H3N2 virus. Nucleic Acids Research 41, 1241–1254. https://doi.org/10.1093/nar/gks1181
Gavazzi, C., Yver, M., Isel, C., Smyth, R.P., Rosa-Calatrava, M., Lina, B., Moulès, V., Marquet, R., 2013b. A functional sequence-specific interaction between influenza A virus genomic RNA segments. Proceedings of the National Academy of Sciences 110, 16604–16609. https://doi.org/10.1073/pnas.1314419110
Gaymard, A., Le Briand, N., Frobert, E., Lina, B., Escuret, V., 2016. Functional balance between neuraminidase and haemagglutinin in influenza viruses. Clinical Microbiology and Infection 22, 975–983. https://doi.org/10.1016/j.cmi.2016.07.007
Geiger, F., Acker, J., Papa, G., Wang, X., Arter, W.E., Saar, K.L., Erkamp, N.A., Qi, R., Bravo, J.P., Strauss, S., Krainer, G., Burrone, O.R., Jungmann, R., Knowles, T.P., Engelke, H., Borodavka, A., 2021. Liquid-liquid phase separation underpins the formation of replication factories in rotaviruses. EMBO J 40, e107711. https://doi.org/10.15252/embj.2021107711
Gerber, M., Isel, C., Moules, V., Marquet, R., 2014. Selective packaging of the influenza A genome and consequences for genetic reassortment. Trends in Microbiology 22, 446–455. https://doi.org/10.1016/j.tim.2014.04.001
Giotis, E.S., Carnell, G., Young, E.F., Ghanny, S., Soteropoulos, P., Wang, L.-F., Barclay, W.S., Skinner, M.A., Temperton, N., 2019. Entry of the bat influenza H17N10 virus into mammalian cells is enabled by the MHC class II HLA-DR receptor. Nat Microbiol 4, 2035–2038. https://doi.org/10.1038/s41564-019-0517-3
Gog, J.R., Afonso, E.D.S., Dalton, R.M., Leclercq, I., Tiley, L., Elton, D., von Kirchbach, J.C., Naffakh, N., Escriou, N., Digard, P., 2007. Codon conservation in the influenza A virus genome defines RNA packaging signals. Nucleic Acids Research 35, 1897–1907. https://doi.org/10.1093/nar/gkm087
Goldstein, T., Mena, I., Anthony, S.J., Medina, R., Robinson, P.W., Greig, D.J., Costa, D.P., Lipkin, W.I., Garcia-Sastre, A., Boyce, W.M., 2013. Pandemic H1N1 Influenza Isolated from Free-Ranging Northern Elephant Seals in 2010 off the Central California Coast. PLOS ONE 8, e62259. https://doi.org/10.1371/journal.pone.0062259
Gómez-Puertas, P., Albo, C., Pérez-Pastrana, E., Vivo, A., Portela, A., 2000. Influenza Virus Matrix Protein Is the Major Driving Force in Virus

Budding. Journal of Virology 74, 11538–11547. https://doi.org/10.1128/JVI.74.24.11538-11547.2000
González, Susana, Ortín, J., 1999. Characterization of Influenza Virus PB1 Protein Binding to Viral RNA: Two Separate Regions of the Protein Contribute to the Interaction Domain. J Virol 73, 631–637.
González, S, Ortín, J., 1999. Distinct regions of influenza virus PB1 polymerase subunit recognize vRNA and cRNA templates. EMBO J 18, 3767–3775. https://doi.org/10.1093/emboj/18.13.3767
Gorai, T., Goto, H., Noda, T., Watanabe, T., Kozuka-Hata, H., Oyama, M., Takano, R., Neumann, G., Watanabe, S., Kawaoka, Y., 2012. F1Fo-ATPase, F-type proton-translocating ATPase, at the plasma membrane is critical for efficient influenza virus budding. Proceedings of the National Academy of Sciences 109, 4615–4620. https://doi.org/10.1073/pnas.1114728109
Goraya, M.U., Wang, S., Munir, M., Chen, J.-L., 2015. Induction of innate immunity and its perturbation by influenza viruses. Protein Cell 6, 712–721. https://doi.org/10.1007/s13238-015-0191-z
Gosling, P., 2003. DORLAND'S ILLUSTRATED MEDICAL DICTIONARY. Australas Chiropr Osteopathy 11, 65.
Goto, H., Muramoto, Y., Noda, T., Kawaoka, Y., 2013. The Genome-Packaging Signal of the Influenza A Virus Genome Comprises a Genome Incorporation Signal and a Genome-Bundling Signal. Journal of Virology 87, 11316–11322. https://doi.org/10.1128/JVI.01301-13
Gotoh, B., Ogasawara, T., Toyoda, T., Inocencio, N.M., Hamaguchi, M., Nagai, Y., 1990. An endoprotease homologous to the blood clotting factor X as a determinant of viral tropism in chick embryo. EMBO J 9, 4189–4195. https://doi.org/10.1002/j.1460-2075.1990.tb07643.x
Gschweitl, M., Ulbricht, A., Barnes, C.A., Enchev, R.I., Stoffel-Studer, I., Meyer-Schaller, N., Huotari, J., Yamauchi, Y., Greber, U.F., Helenius, A., Peter, M., 2016. A SPOPL/Cullin-3 ubiquitin ligase complex regulates endocytic trafficking by targeting EPS15 at endosomes. eLife 5, e13841. https://doi.org/10.7554/eLife.13841
Gu, W., Gallagher, G.R., Dai, W., Liu, P., Li, R., Trombly, M.I., Gammon, D.B., Mello, C.C., Wang, J.P., Finberg, R.W., 2015. Influenza A virus preferentially snatches noncoding RNA caps. RNA 21, 2067–2075. https://doi.org/10.1261/rna.054221.115
Guillén-Boixet, J., Kopach, A., Holehouse, A.S., Wittmann, S., Jahnel, M., Schlüßler, R., Kim, K., Trussina, I.R.E.A., Wang, J., Mateju, D., Poser, I., Maharana, S., Ruer-Gruß, M., Richter, D., Zhang, X., Chang, Y.-T., Guck, J., Honigmann, A., Mahamid, J., Hyman, A.A., Pappu, R.V., Alberti, S., Franzmann, T.M., 2020. RNA-Induced Conformational Switching and Clustering of G3BP Drive Stress Granule Assembly by Condensation. Cell 181, 346-361.e17. https://doi.org/10.1016/j.cell.2020.03.049
Guilligay, D., Tarendeau, F., Resa-Infante, P., Coloma, R., Crepin, T., Sehr, P., Lewis, J., Ruigrok, R.W.H., Ortin, J., Hart, D.J., Cusack, S., 2008.

The structural basis for cap binding by influenza virus polymerase subunit PB2. MOLECULAR BIOLOGY 15, 7.
Guo, S., Kang, G., Phan, D.T., Hsu, M.N., Por, Y.C., Chen, C.H., 2018. Polymerization-Induced Phase Separation Formation of Structured Hydrogel Particles via Microfluidics for Scar Therapeutics. Sci Rep 8, 2245. https://doi.org/10.1038/s41598-018-20516-9
Guo, Y.J., Jin, F.G., Wang, P., Wang, M., Zhu, J.M., 1983. Isolation of influenza C virus from pigs and experimental infection of pigs with influenza C virus. J Gen Virol 64 (Pt 1), 177–182. https://doi.org/10.1099/0022-1317-64-1-177
Guseva, S., Milles, S., Jensen, M.R., Salvi, N., Kleman, J.-P., Maurin, D., Ruigrok, R.W.H., Blackledge, M., 2020. Measles virus nucleo- and phosphoproteins form liquid-like phase-separated compartments that promote nucleocapsid assembly. Sci Adv 6, eaaz7095. https://doi.org/10.1126/sciadv.aaz7095
Güttler, T., Madl, T., Neumann, P., Deichsel, D., Corsini, L., Monecke, T., Ficner, R., Sattler, M., Görlich, D., 2010. NES consensus redefined by structures of PKI-type and Rev-type nuclear export signals bound to CRM1. Nat Struct Mol Biol 17, 1367–1376. https://doi.org/10.1038/nsmb.1931
Hagen, M., Chung, T.D., Butcher, J.A., Krystal, M., 1994. Recombinant influenza virus polymerase: requirement of both 5' and 3' viral ends for endonuclease activity. Journal of Virology 68, 1509–1515. https://doi.org/10.1128/jvi.68.3.1509-1515.1994
Hampson, A.W., Mackenzie, J.S., 2006. The influenza viruses. Med J Aust 185, S39-43. https://doi.org/ham10884_fm [pii]
Han, J., Ganti, K., Sali, V.K., Twigg, C., Zhang, Y., Manivasagam, S., Liang, C.-Y., Vogel, O.A., Huang, I., Emmanuel, S.N., Plung, J., Radoshevich, L., Perez, J.T., Lowen, A.C., Manicassamy, B., 2021. Host factor Rab11a is critical for efficient assembly of influenza A virus genomic segments. PLOS Pathogens 17, e1009517. https://doi.org/10.1371/journal.ppat.1009517
Haralampiev, I., Prisner, S., Nitzan, M., Schade, M., Jolmes, F., Schreiber, M., Loidolt-Krüger, M., Jongen, K., Chamiolo, J., Nilson, N., Winter, F., Friedman, N., Seitz, O., Wolff, T., Herrmann, A., 2020. Selective flexible packaging pathways of the segmented genome of influenza A virus. Nat Commun 11, 4355. https://doi.org/10.1038/s41467-020-18108-1
Harmon, T.S., Holehouse, A.S., Rosen, M.K., Pappu, R.V., 2017. Intrinsically disordered linkers determine the interplay between phase separation and gelation in multivalent proteins. eLife 6, e30294. https://doi.org/10.7554/eLife.30294
Harrington, W.N., Kackos, C.M., Webby, R.J., 2021. The evolution and future of influenza pandemic preparedness. Exp Mol Med 53, 737–749. https://doi.org/10.1038/s12276-021-00603-0

Harris, A., Cardone, G., Winkler, D.C., Heymann, J.B., Brecher, M., White, J.M., Steven, A.C., 2006. Influenza virus pleiomorphy characterized by cryoelectron tomography. Proceedings of the National Academy of Sciences 103, 19123–19127. https://doi.org/10.1073/pnas.0607614103

Harrison, S.C., 2008. Viral membrane fusion. Nat Struct Mol Biol 15, 690–698. https://doi.org/10.1038/nsmb.1456

Hatada, E., Hasegawa, M., Mukaigawa, J., Shimizu, K., Fukuda, R., 1989. Control of influenza virus gene expression: quantitative analysis of each viral RNA species in infected cells. J Biochem 105, 537–546. https://doi.org/10.1093/oxfordjournals.jbchem.a122702

Hatta, M., Zhong, G., Gao, Y., Nakajima, N., Fan, S., Chiba, S., Deering, K.M., Ito, M., Imai, M., Kiso, M., Nakatsu, S., Lopes, T.J., Thompson, A.J., McBride, R., Suarez, D.L., Macken, C.A., Sugita, S., Neumann, G., Hasegawa, H., Paulson, J.C., Toohey-Kurth, K.L., Kawaoka, Y., 2018. Characterization of a Feline Influenza A(H7N2) Virus. Emerg Infect Dis 24, 75–86. https://doi.org/10.3201/eid2401.171240

Haubrich, K., Augsten, S., Álvarez, L., Huppertz, I., Simon, B., Perez, K., Masiewicz, P., Lethier, M., Rittinger, K., Gabel, F., Hentze, M.W., Cusack, S., Hennig, J., 2021. Mechanistic insights into RNA binding and RNA-regulated RIG-I ubiquitination by TRIM25. https://doi.org/10.1101/2020.05.04.070177

Hause, B.M., Ducatez, M., Collin, E.A., Ran, Z., Liu, R., Sheng, Z., Armien, A., Kaplan, B., Chakravarty, S., Hoppe, A.D., Webby, R.J., Simonson, R.R., Li, F., 2013. Isolation of a Novel Swine Influenza Virus from Oklahoma in 2011 Which Is Distantly Related to Human Influenza C Viruses. PLOS Pathogens 9, e1003176. https://doi.org/10.1371/journal.ppat.1003176

He, X., Zhou, J., Bartlam, M., Zhang, R., Ma, J., Lou, Z., Li, X., Li, J., Joachimiak, A., Zeng, Z., Ge, R., Rao, Z., Liu, Y., 2008. Crystal structure of the polymerase PAC–PB1N complex from an avian influenza H5N1 virus. Nature 454, 1123–1126. https://doi.org/10.1038/nature07120

Heinrich, B.S., Maliga, Z., Stein, D.A., Hyman, A.A., Whelan, S.P.J., 2018. Phase Transitions Drive the Formation of Vesicular Stomatitis Virus Replication Compartments. mBio 9, e02290-17. https://doi.org/10.1128/mBio.02290-17

Helmich, F., Lee, C.C., Nieuwenhuizen, M.M.L., Gielen, J.C., Christianen, P.C.M., Larsen, A., Fytas, G., Leclère, P.E.L.G., Schenning, A.P.H.J., Meijer, E.W., 2010. Dilution-Induced Self-Assembly of Porphyrin Aggregates: A Consequence of Coupled Equilibria. Angewandte Chemie International Edition 49, 3939–3942. https://doi.org/10.1002/anie.201000162

Hernández-Vega, A., Braun, M., Scharrel, L., Jahnel, M., Wegmann, S., Hyman, B.T., Alberti, S., Diez, S., Hyman, A.A., 2017. Local Nucleation of Microtubule Bundles through Tubulin Concentration into

a Condensed Tau Phase. Cell reports 20, 2304–2312. https://doi.org/10.1016/j.celrep.2017.08.042
Herrera, A.L., Suso, K., Allison, S., Simon, A., Schlenker, E., Huber, V.C., Chaussee, M.S., 2017. Binding host proteins to the M protein contributes to the mortality associated with influenza–Streptococcus pyogenes superinfections. Microbiology (Reading) 163, 1445–1456. https://doi.org/10.1099/mic.0.000532
Herz, C., Stavnezer, E., Krug, R.M., Gurney, T., 1981. Influenza virus, an RNA virus, synthesizes its messenger RNA in the nucleus of infected cells. Cell 26, 391–400. https://doi.org/10.1016/0092-8674(81)90208-7
Hidalgo, P., Gonzalez, R.A., 2019. Formation of adenovirus DNA replication compartments. FEBS Letters 593, 3518–3530. https://doi.org/10.1002/1873-3468.13672
Hilsch, M., Goldenbogen, B., Sieben, C., Höfer, C.T., Rabe, J.P., Klipp, E., Herrmann, A., Chiantia, S., 2014. Influenza A Matrix Protein M1 Multimerizes upon Binding to Lipid Membranes. Biophys J 107, 912–923. https://doi.org/10.1016/j.bpj.2014.06.042
Hinshaw, V., Webster, R., Turner, B., 1980. The perpetuation of orthomyxoviruses and paramyxoviruses in Canadian waterfowl. Can. J. Microbiol. 26, 622–629. https://doi.org/10.1139/m80-108
Hnisz, D., Shrinivas, K., Young, R.A., Chakraborty, A.K., Sharp, P.A., 2017. A Phase Separation Model for Transcriptional Control. Cell 169, 13–23. https://doi.org/10.1016/j.cell.2017.02.007
Ho, J.S.Y., Angel, M., Ma, Y., Sloan, E., Wang, G., Martinez-Romero, C., Alenquer, M., Roudko, V., Chung, L., Zheng, S., Chang, M., Fstkchyan, Y., Clohisey, S., Dinan, A.M., Gibbs, J., Gifford, R., Shen, R., Gu, Q., Irigoyen, N., Campisi, L., Huang, C., Zhao, N., Jones, J.D., van Knippenberg, I., Zhu, Z., Moshkina, N., Meyer, L., Noel, J., Peralta, Z., Rezelj, V., Kaake, R., Rosenberg, B., Wang, B., Wei, J., Paessler, S., Wise, H.M., Johnson, J., Vannini, A., Amorim, M.J., Baillie, J.K., Miraldi, E.R., Benner, C., Brierley, I., Digard, P., Łuksza, M., Firth, A.E., Krogan, N., Greenbaum, B.D., MacLeod, M.K., van Bakel, H., Garcìa-Sastre, A., Yewdell, J.W., Hutchinson, E., Marazzi, I., 2020. Hybrid Gene Origination Creates Human-Virus Chimeric Proteins during Infection. Cell 181, 1502-1517.e23. https://doi.org/10.1016/j.cell.2020.05.035
Hofweber, M., Dormann, D., 2019. Friend or foe—Post-translational modifications as regulators of phase separation and RNP granule dynamics. Journal of Biological Chemistry 294, 7137–7150. https://doi.org/10.1074/jbc.TM118.001189
Holehouse, A.S., Pappu, R.V., 2018. Functional Implications of Intracellular Phase Transitions. Biochemistry 57, 2415–2423. https://doi.org/10.1021/acs.biochem.7b01136
Holm, C.K., Rahbek, S.H., Gad, H.H., Bak, R.O., Jakobsen, M.R., Jiang, Z., Hansen, A.L., Jensen, S.K., Sun, C., Thomsen, M.K., Laustsen, A.,

Nielsen, C.G., Severinsen, K., Xiong, Y., Burdette, D.L., Hornung, V., Lebbink, R.J., Duch, M., Fitzgerald, K.A., Bahrami, S., Mikkelsen, J.G., Hartmann, R., Paludan, S.R., 2016. Influenza A virus targets a cGAS-independent STING pathway that controls enveloped RNA viruses. Nat Commun 7, 10680. https://doi.org/10.1038/ncomms10680

Holsinger, L.J., Alams, R., 1991. Influenza virus M2 integral membrane protein is a homotetramer stabilized by formation of disulfide bonds. Virology 183, 32–43. https://doi.org/10.1016/0042-6822(91)90115-R

Honda, A., Mukaigawa, J., Yokoiyama, A., Kato, A., Ueda, S., Nagata, K., Krystal, M., Nayak, D.P., Ishihama, A., 1990. Purification and Molecular Structure of RNA Polymerase from Influenza Virus A/PR8. The Journal of Biochemistry 107, 624–628.

Honda, A., Uéda, K., Nagata, K., Ishihama, A., 1988. RNA polymerase of influenza virus: role of NP in RNA chain elongation. J Biochem 104, 1021–1026. https://doi.org/10.1093/oxfordjournals.jbchem.a122569

Hondele, M., Heinrich, S., De Los Rios, P., Weis, K., 2020. Membraneless organelles: phasing out of equilibrium. Emerging Topics in Life Sciences 4, 343–354. https://doi.org/10.1042/ETLS20190190

Hondele, M., Sachdev, R., Heinrich, S., Wang, J., Vallotton, P., Fontoura, B.M.A., Weis, K., 2019. DEAD-box ATPases are global regulators of phase-separated organelles. Nature 573, 144–148. https://doi.org/10.1038/s41586-019-1502-y

Horimoto, T., Nakayama, K., Smeekens, S.P., Kawaoka, Y., 1994. Proprotein-processing endoproteases PC6 and furin both activate hemagglutinin of virulent avian influenza viruses. J Virol 68, 6074–6078. https://doi.org/10.1128/JVI.68.9.6074-6078.1994

Horisberger, M.A., 1980. The large P proteins of influenza A viruses are composed of one acidic and two basic polypeptides. Virology 107, 302–305. https://doi.org/10.1016/0042-6822(80)90296-2

Hsu, M.T., Parvin, J.D., Gupta, S., Krystal, M., Palese, P., 1987. Genomic RNAs of influenza viruses are held in a circular conformation in virions and in infected cells by a terminal panhandle. Proceedings of the National Academy of Sciences 84, 8140–8144. https://doi.org/10.1073/pnas.84.22.8140

Hu, J., Fu, R., Nishimura, K., Zhang, L., Zhou, H.-X., Busath, D.D., Vijayvergiya, V., Cross, T.A., 2006. Histidines, heart of the hydrogen ion channel from influenza A virus: Toward an understanding of conductance and proton selectivity. Proceedings of the National Academy of Sciences 103, 6865–6870. https://doi.org/10.1073/pnas.0601944103

Hu, Y., Sneyd, H., Dekant, R., Wang, J., 2017. Influenza A virus nucleoprotein: a highly conserved multi-functional viral protein as a hot antiviral drug target. Curr Top Med Chem 17, 2271–2285. https://doi.org/10.2174/1568026617666170224122508

Huang, J.S., Vernon, S., Wong, N.C., 1974. Homogeneous Nucleation in a Critical Binary Fluid Mixture. Phys. Rev. Lett. 33, 140–143. https://doi.org/10.1103/PhysRevLett.33.140

Huang, J.X., Lee, G., Cavanaugh, K.E., Chang, J.W., Gardel, M.L., Moellering, R.E., 2019. High throughput discovery of functional protein modifications by Hotspot Thermal Profiling. Nat Methods 16, 894–901. https://doi.org/10.1038/s41592-019-0499-3

Huang, S., Chen, Jingjing, Chen, Q., Wang, H., Yao, Y., Chen, Jianjun, Chen, Z., 2013. A Second CRM1-Dependent Nuclear Export Signal in the Influenza A Virus NS2 Protein Contributes to the Nuclear Export of Viral Ribonucleoproteins. J Virol 87, 767–778. https://doi.org/10.1128/JVI.06519-11

Huang, W.Y.C., Alvarez, S., Kondo, Y., Lee, Y.K., Chung, J.K., Lam, H.Y.M., Biswas, K.H., Kuriyan, J., Groves, J.T., 2019. A molecular assembly phase transition and kinetic proofreading modulate Ras activation by SOS. Science 363, 1098–1103. https://doi.org/10.1126/science.aau5721

Huang, W.Y.C., Yan, Q., Lin, W.-C., Chung, J.K., Hansen, S.D., Christensen, S.M., Tu, H.-L., Kuriyan, J., Groves, J.T., 2016. Phosphotyrosine-mediated LAT assembly on membranes drives kinetic bifurcation in recruitment dynamics of the Ras activator SOS. Proc Natl Acad Sci U S A 113, 8218–8223. https://doi.org/10.1073/pnas.1602602113

Hughey, P.G., Compans, R.W., Zebedee, S.L., Lamb, R.A., 1992. Expression of the influenza A virus M2 protein is restricted to apical surfaces of polarized epithelial cells. Journal of Virology 66, 5542–5552. https://doi.org/10.1128/jvi.66.9.5542-5552.1992

Hull, J.D., Gilmore, R., Lamb, R.A., 1988. Integration of a small integral membrane protein, M2, of influenza virus into the endoplasmic reticulum: analysis of the internal signal-anchor domain of a protein with an ectoplasmic NH2 terminus. Journal of Cell Biology 106, 1489–1498. https://doi.org/10.1083/jcb.106.5.1489

Huotari, J., Helenius, A., 2011. Endosome maturation. The EMBO Journal 30, 3481–3500. https://doi.org/10.1038/emboj.2011.286

Huotari, J., Meyer-Schaller, N., Hubner, M., Stauffer, S., Katheder, N., Horvath, P., Mancini, R., Helenius, A., Peter, M., 2012. Cullin-3 regulates late endosome maturation. Proc. Natl. Acad. Sci. U.S.A. 109, 823–828. https://doi.org/10.1073/pnas.1118744109

Hurt, A.C., Chotpitayasunondh, T., Cox, N.J., Daniels, R., Fry, A.M., Gubareva, L.V., Hayden, F.G., Hui, D.S., Hungnes, O., Lackenby, A., Lim, W., Meijer, A., Penn, C., Tashiro, M., Uyeki, T.M., Zambon, M., WHO Consultation on Pandemic Influenza A (H1N1) 2009 Virus Resistance to Antivirals, 2012. Antiviral resistance during the 2009 influenza A H1N1 pandemic: public health, laboratory, and clinical perspectives. Lancet Infect Dis 12, 240–248. https://doi.org/10.1016/S1473-3099(11)70318-8

Hussain, M., Galvin, H.D., Haw, T.Y., Nutsford, A.N., Husain, M., 2017. Drug resistance in influenza A virus: the epidemiology and management. IDR 10, 121–134. https://doi.org/10.2147/IDR.S105473

Hutchinson, E.C., Charles, P.D., Hester, S.S., Thomas, B., Trudgian, D., Martínez-Alonso, M., Fodor, E., 2014. Conserved and host-specific features of influenza virion architecture. Nat Commun 5, 4816. https://doi.org/10.1038/ncomms5816

Hutchinson, E.C., Curran, M.D., Read, E.K., Gog, J.R., Digard, P., 2008. Mutational Analysis of cis-Acting RNA Signals in Segment 7 of Influenza A Virus. Journal of Virology 82, 11869–11879. https://doi.org/10.1128/JVI.01634-08

Hutchinson, E.C., Fodor, E., 2013. Transport of the Influenza Virus Genome from Nucleus to Nucleus. Viruses 5, 2424–2446. https://doi.org/10.3390/v5102424

Hutchinson, E.C., von Kirchbach, J.C., Gog, J.R., Digard, P. 2010, 2010. Genome packaging in influenza A virus. Journal of General Virology 91, 313–328. https://doi.org/10.1099/vir.0.017608-0

Hutchinson, E.C., Yamauchi, Y., 2018. Understanding Influenza, in: Yamauchi, Y. (Ed.), Influenza Virus: Methods and Protocols, Methods in Molecular Biology. Springer, New York, NY, pp. 1–21. https://doi.org/10.1007/978-1-4939-8678-1_1

Hyman, A.A., Simons, K., 2012. Beyond Oil and Water—Phase Transitions in Cells. Science 337, 1047–1049. https://doi.org/10.1126/science.1223728

Hyman, A.A., Weber, C.A., Jülicher, F., 2014. Liquid-Liquid Phase Separation in Biology. Annual Review of Cell and Developmental Biology 30, 39–58. https://doi.org/10.1146/annurev-cellbio-100913-013325

ICTV, 2017. Family: Orthomyxoviridae Chapter Version: ICTV Ninth Report; 2009 Taxonomy Release [WWW Document]. URL https://ictv.global/report_9th/RNAneg/Orthomyxoviridae (accessed 9.22.22).

Inagaki, A., Goto, H., Kakugawa, S., Ozawa, M., Kawaoka, Y., 2012. Competitive Incorporation of Homologous Gene Segments of Influenza A Virus into Virions. J Virol 86, 10200–10202. https://doi.org/10.1128/JVI.01204-12

Inglis, S.C., Carroll, A.R., Lamb, R.A., Mahy, B.W.J., 1976. Polypeptides specified by the influenza virus genome: I. Evidence for eight distinct gene products specified by fowl plague virus. Virology 74, 489–503. https://doi.org/10.1016/0042-6822(76)90355-X

Isel, C., Munier, S., Naffakh, N., 2016. Experimental Approaches to Study Genome Packaging of Influenza A Viruses. Viruses 8, 218. https://doi.org/10.3390/v8080218

Iselin, L., Palmalux, N., Kamel, W., Simmonds, P., Mohammed, S., Castello, A., 2022. Uncovering viral RNA–host cell interactions on a proteome-wide scale. Trends in Biochemical Sciences 47, 23–38. https://doi.org/10.1016/j.tibs.2021.08.002

Iserman, C., Roden, C., Boerneke, M., Sealfon, R., McLaughlin, G., Jungreis, I., Park, C., Boppana, A., Fritch, E., Hou, Y.J., Theesfeld, C., Troyanskaya, O.G., Baric, R.S., Sheahan, T.P., Weeks, K., Gladfelter, A.S., 2020a. Specific viral RNA drives the SARS CoV-2 nucleocapsid to phase separate. https://doi.org/10.1101/2020.06.11.147199

Iserman, C., Roden, C.A., Boerneke, M.A., Sealfon, R.S.G., McLaughlin, G.A., Jungreis, I., Fritch, E.J., Hou, Y.J., Ekena, J., Weidmann, C.A., Theesfeld, C.L., Kellis, M., Troyanskaya, O.G., Baric, R.S., Sheahan, T.P., Weeks, K.M., Gladfelter, A.S., 2020b. Genomic RNA Elements Drive Phase Separation of the SARS-CoV-2 Nucleocapsid. Molecular Cell 80, 1078-1091.e6. https://doi.org/10.1016/j.molcel.2020.11.041

Ito, T., Couceiro, J.N.S.S., Kelm, S., Baum, L.G., Krauss, S., Castrucci, M.R., Donatelli, I., Kida, H., Paulson, J.C., Webster, R.G., Kawaoka, Y., 1998. Molecular Basis for the Generation in Pigs of Influenza A Viruses with Pandemic Potential. Journal of Virology 72, 7367–7373. https://doi.org/10.1128/JVI.72.9.7367-7373.1998

Ito, T., Suzuki, Y., Suzuki, T., Takada, A., Horimoto, T., Wells, K., Kida, H., Otsuki, K., Kiso, M., Ishida, H., Kawaoka, Y., 2000. Recognition of N-Glycolylneuraminic Acid Linked to Galactose by the α2,3 Linkage Is Associated with Intestinal Replication of Influenza A Virus in Ducks. Journal of Virology 74, 9300–9305. https://doi.org/10.1128/JVI.74.19.9300-9305.2000

Iuliano, A.D., Roguski, K.M., Chang, H.H., Muscatello, D.J., Palekar, R., Tempia, S., Cohen, C., Gran, J.M., Schanzer, D., Cowling, B.J., Wu, P., Kyncl, J., Ang, L.W., Park, M., Redlberger-Fritz, M., Yu, H., Espenhain, L., Krishnan, A., Emukule, G., van Asten, L., Pereira da Silva, S., Aungkulanon, S., Buchholz, U., Widdowson, M.-A., Bresee, J.S., Azziz-Baumgartner, E., Cheng, P.-Y., Dawood, F., Foppa, I., Olsen, S., Haber, M., Jeffers, C., MacIntyre, C.R., Newall, A.T., Wood, J.G., Kundi, M., Popow-Kraupp, T., Ahmed, M., Rahman, M., Marinho, F., Sotomayor Proschle, C.V., Vergara Mallegas, N., Luzhao, F., Sa, L., Barbosa-Ramírez, J., Sanchez, D.M., Gomez, L.A., Vargas, X.B., Acosta Herrera, aBetsy, Llanés, M.J., Fischer, T.K., Krause, T.G., Mølbak, K., Nielsen, J., Trebbien, R., Bruno, A., Ojeda, J., Ramos, H., an der Heiden, M., del Carmen Castillo Signor, L., Serrano, C.E., Bhardwaj, R., Chadha, M., Narayan, V., Kosen, S., Bromberg, M., Glatman-Freedman, A., Kaufman, Z., Arima, Y., Oishi, K., Chaves, S., Nyawanda, B., Al-Jarallah, R.A., Kuri-Morales, P.A., Matus, C.R., Corona, M.E.J., Burmaa, A., Darmaa, O., Obtel, M., Cherkaoui, I., van den Wijngaard, C.C., van der Hoek, W., Baker, M., Bandaranayake, D., Bissielo, A., Huang, S., Lopez, L., Newbern, C., Flem, E., Grøneng, G.M., Hauge, S., de Cosío, F.G., de Moltó, Y., Castillo, L.M., Cabello, M.A., von Horoch, M., Medina Osis, J., Machado, A., Nunes, B., Rodrigues, A.P., Rodrigues, E., Calomfirescu, C., Lupulescu, E., Popescu, R., Popovici, O., Bogdanovic, D., Kostic, M., Lazarevic, K., Milosevic, Z., Tiodorovic, B., Chen, M., Cutter, J., Lee, V., Lin, R., Ma,

S., Cohen, A.L., Treurnicht, F., Kim, W.J., Delgado-Sanz, C., de mateo Ontañón, S., Larrauri, A., León, I.L., Vallejo, F., Born, R., Junker, C., Koch, D., Chuang, J.-H., Huang, W.-T., Kuo, H.-W., Tsai, Y.-C., Bundhamcharoen, K., Chittaganpitch, M., Green, H.K., Pebody, R., Goñi, N., Chiparelli, H., Brammer, L., Mustaquim, D., 2018. Estimates of global seasonal influenza-associated respiratory mortality: a modelling study. The Lancet 391, 1285–1300. https://doi.org/10.1016/S0140-6736(17)33293-2

Jackson, D.A., Caton, A.J., McCready, S.J., Cook, P.R., 1982. Influenza virus RNA is synthesized at fixed sites in the nucleus. Nature 296, 366–368. https://doi.org/10.1038/296366a0

Jagger, B.W., Wise, H.M., Kash, J.C., Walters, K.-A., Wills, N.M., Xiao, Y.-L., Dunfee, R.L., Schwartzman, L.M., Ozinsky, A., Bell, G.L., Dalton, R.M., Lo, A., Efstathiou, S., Atkins, J.F., Firth, A.E., Taubenberger, J.K., Digard, P., 2012. An Overlapping Protein-Coding Region in Influenza A Virus Segment 3 Modulates the Host Response. Science 337, 199–204. https://doi.org/10.1126/science.1222213

Jin, H., Leser, G.P., Zhang, J., Lamb, R.A., 1997. Influenza virus hemagglutinin and neuraminidase cytoplasmic tails control particle shape. EMBO J 16, 1236–1247. https://doi.org/10.1093/emboj/16.6.1236

Jones, I.M., Reay, P.A., Philpott, K.L., 1986. Nuclear location of all three influenza polymerase proteins and a nuclear signal in polymerase PB2. The EMBO Journal 5, 2371–2376. https://doi.org/10.1002/j.1460-2075.1986.tb04506.x

Jones, J.E., Le Sage, V., Lakdawala, S.S., 2021. Viral and host heterogeneity and their effects on the viral life cycle. Nat Rev Microbiol 19, 272–282. https://doi.org/10.1038/s41579-020-00449-9

Jonges, M., Welkers, M.R.A., Jeeninga, R.E., Meijer, A., Schneeberger, P., Fouchier, R.A.M., de Jong, M.D., Koopmans, M., 2014. Emergence of the Virulence-Associated PB2 E627K Substitution in a Fatal Human Case of Highly Pathogenic Avian Influenza Virus A(H7N7) Infection as Determined by Illumina Ultra-Deep Sequencing. J Virol 88, 1694–1702. https://doi.org/10.1128/JVI.02044-13

Jorba, N., Coloma, R., Ortín, J., 2009. Genetic trans-Complementation Establishes a New Model for Influenza Virus RNA Transcription and Replication. PLOS Pathogens 5, e1000462. https://doi.org/10.1371/journal.ppat.1000462

Joseph, U., Su, Y.C.F., Vijaykrishna, D., Smith, G.J.D., 2017a. The ecology and adaptive evolution of influenza A interspecies transmission. Influenza and Other Respiratory Viruses 11, 74–84. https://doi.org/10.1111/irv.12412

Joseph, U., Su, Y.C.F., Vijaykrishna, D., Smith, G.J.D., 2017b. The ecology and adaptive evolution of influenza A interspecies transmission. Influenza and Other Respiratory Viruses 11, 74–84. https://doi.org/10.1111/irv.12412

Jung, T.E., Brownlee, G.G., 2006. A new promoter-binding site in the PB1 subunit of the influenza A virus polymerase. J Gen Virol 87, 679–688. https://doi.org/10.1099/vir.0.81453-0

Kaján, G.L., Doszpoly, A., Tarján, Z.L., Vidovszky, M.Z., Papp, T., 2020. Virus–Host Coevolution with a Focus on Animal and Human DNA Viruses. J Mol Evol 88, 41–56. https://doi.org/10.1007/s00239-019-09913-4

Kajiwara, N., Nomura, N., Ukaji, M., Yamamoto, N., Kohara, M., Yasui, F., Sakoda, Y., Kida, H., Shibasaki, F., 2020. Cell-penetrating peptide-mediated cell entry of H5N1 highly pathogenic avian influenza virus. Sci Rep 10, 18008. https://doi.org/10.1038/s41598-020-74604-w

Kalxdorf, M., Günthner, I., Becher, I., Kurzawa, N., Knecht, S., Savitski, M.M., Eberl, H.C., Bantscheff, M., 2021. Cell surface thermal proteome profiling tracks perturbations and drug targets on the plasma membrane. Nat Methods 18, 84–91. https://doi.org/10.1038/s41592-020-01022-1

Kandeil, A., Gomaa, M.R., Shehata, M.M., El Taweel, A.N., Mahmoud, S.H., Bagato, O., Moatasim, Y., Kutkat, O., Kayed, A.S., Dawson, P., Qiu, X., Bahl, J., Webby, R.J., Karesh, W.B., Kayali, G., Ali, M.A., 2019. Isolation and Characterization of a Distinct Influenza A Virus from Egyptian Bats. Journal of Virology 93, e01059-18. https://doi.org/10.1128/JVI.01059-18

Kao, R.Y., Yang, D., Lau, L.-S., Tsui, W.H.W., Hu, L., Dai, J., Chan, M.-P., Chan, C.-M., Wang, P., Zheng, B.-J., Sun, J., Huang, J.-D., Madar, J., Chen, G., Chen, H., Guan, Y., Yuen, K.-Y., 2010. Identification of influenza A nucleoprotein as an antiviral target. Nat Biotechnol 28, 600–605. https://doi.org/10.1038/nbt.1638

Kar, M., Dar, F., Welsh, T.J., Vogel, L.T., Kühnemuth, R., Majumdar, A., Krainer, G., Franzmann, T.M., Alberti, S., Seidel, C.A.M., Knowles, T.P.J., Hyman, A.A., Pappu, R.V., 2022. Phase-separating RNA-binding proteins form heterogeneous distributions of clusters in subsaturated solutions. Proceedings of the National Academy of Sciences 119, e2202222119. https://doi.org/10.1073/pnas.2202222119

Karakus, U., Thamamongood, T., Ciminski, K., Ran, W., Günther, S.C., Pohl, M.O., Eletto, D., Jeney, C., Hoffmann, D., Reiche, S., Schinköthe, J., Ulrich, R., Wiener, J., Hayes, M.G.B., Chang, M.W., Hunziker, A., Yángüez, E., Aydillo, T., Krammer, F., Oderbolz, J., Meier, M., Oxenius, A., Halenius, A., Zimmer, G., Benner, C., Hale, B.G., García-Sastre, A., Beer, M., Schwemmle, M., Stertz, S., 2019. MHC class II proteins mediate cross-species entry of bat influenza viruses. Nature 567, 109–112. https://doi.org/10.1038/s41586-019-0955-3

Kauppila, J., Rönkkö, E., Juvonen, R., Saukkoriipi, A., Saikku, P., Bloigu, A., Vainio, O., Ziegler, T., 2014. Influenza C virus infection in military recruits—symptoms and clinical manifestation. Journal of Medical Virology 86, 879–885. https://doi.org/10.1002/jmv.23756

Kaur, T., Alshareedah, I., Wang, W., Ngo, J., Moosa, M.M., Banerjee, P.R., 2019. Molecular Crowding Tunes Material States of Ribonucleoprotein Condensates. Biomolecules 9, 71. https://doi.org/10.3390/biom9020071

Kawaguchi, A., Hirohama, M., Harada, Y., Osari, S., Nagata, K., 2015. Influenza Virus Induces Cholesterol-Enriched Endocytic Recycling Compartments for Budozone Formation via Cell Cycle-Independent Centrosome Maturation. PLOS Pathogens 11, e1005284. https://doi.org/10.1371/journal.ppat.1005284

Kawaguchi, A., Matsumoto, K., Nagata, K., 2012. YB-1 Functions as a Porter To Lead Influenza Virus Ribonucleoprotein Complexes to Microtubules. Journal of Virology 86, 11086–11095. https://doi.org/10.1128/JVI.00453-12

Kawaguchi, A., Momose, F., Nagata, K., 2011. Replication-coupled and host factor-mediated encapsidation of the influenza virus genome by viral nucleoprotein. J Virol 85, 6197–6204. https://doi.org/10.1128/JVI.00277-11

Kawaguchi, A., Nagata, K., 2007. De novo replication of the influenza virus RNA genome is regulated by DNA replicative helicase, MCM. EMBO J 26, 4566–4575. https://doi.org/10.1038/sj.emboj.7601881

Kawakami, E., Watanabe, T., Fujii, K., Goto, H., Watanabe, S., Noda, T., Kawaoka, Y., 2011. Strand-specific real-time RT-PCR for distinguishing influenza vRNA, cRNA, and mRNA. Journal of Virological Methods 173, 1–6. https://doi.org/10.1016/j.jviromet.2010.12.014

Kawaoka, Y., Krauss, S., Webster, R.G., 1989. Avian-to-human transmission of the PB1 gene of influenza A viruses in the 1957 and 1968 pandemics. Journal of Virology 63, 4603–4608. https://doi.org/10.1128/jvi.63.11.4603-4608.1989

Kawaoka, Y., Webster, R.G., 1988. Sequence requirements for cleavage activation of influenza virus hemagglutinin expressed in mammalian cells. Proceedings of the National Academy of Sciences 85, 324–328. https://doi.org/10.1073/pnas.85.2.324

Kemler, I., Whittaker, G., Helenius, A., 1994. Nuclear Import of Microinjected Influenza Virus Ribonucleoproteins. Virology 202, 1028–1033. https://doi.org/10.1006/viro.1994.1432

Kido, H., Yokogoshi, Y., Sakai, K., Tashiro, M., Kishino, Y., Fukutomi, A., Katunuma, N., 1992. Isolation and characterization of a novel trypsin-like protease found in rat bronchiolar epithelial Clara cells. A possible activator of the viral fusion glycoprotein. The Journal of Biological Chemistry 267, 7.

Kim, T.H., Tsang, B., Vernon, R.M., Sonenberg, N., Kay, L.E., Forman-Kay, J.D., 2019. Phospho-dependent phase separation of FMRP and CAPRIN1 recapitulates regulation of translation and deadenylation. Science 365, 825–829. https://doi.org/10.1126/science.aax4240

Kimura, H., Abiko, C., Peng, G., Muraki, Y., Sugawara, K., Hongo, S., Kitame, F., Mizuta, K., Numazaki, Y., Suzuki, H., Nakamura, K., 1997. Interspecies transmission of influenza C virus between humans and pigs. Virus Res 48, 71–79. https://doi.org/10.1016/s0168-1702(96)01427-x

Kingsbury, D.W., 1970. Replication and functions of myxovirus ribonucleic acids. Prog Med Virol 12, 49–77.

Klein, I.A., Boija, A., Afeyan, L.K., Hawken, S.W., Fan, M., Dall'Agnese, A., Oksuz, O., Henninger, J.E., Shrinivas, K., Sabari, B.R., Sagi, I., Clark, V.E., Platt, J.M., Kar, M., McCall, P.M., Zamudio, A.V., Manteiga, J.C., Coffey, E.L., Li, C.H., Hannett, N.M., Guo, Y.E., Decker, T.-M., Lee, T.I., Zhang, T., Weng, J.-K., Taatjes, D.J., Chakraborty, A., Sharp, P.A., Chang, Y.T., Hyman, A.A., Gray, N.S., Young, R.A., 2020. Partitioning of cancer therapeutics in nuclear condensates. Science 368, 1386–1392. https://doi.org/10.1126/science.aaz4427

Klenk, H.D., Rott, R., Orlich, M., Blödorn, J., 1975. Activation of influenza A viruses by trypsin treatment. Virology 68, 426–439. https://doi.org/10.1016/0042-6822(75)90284-6

Klosin, A., Oltsch, F., Harmon, T., Honigmann, A., Jülicher, F., Hyman, A.A., Zechner, C., 2020. Phase separation provides a mechanism to reduce noise in cells. Science 367, 464–468. https://doi.org/10.1126/science.aav6691

Koga, S., Williams, D.S., Perriman, A.W., Mann, S., 2011. Peptide–nucleotide microdroplets as a step towards a membrane-free protocell model. Nature Chem 3, 720–724. https://doi.org/10.1038/nchem.1110

Koliopoulos, M.G., Lethier, M., van der Veen, A.G., Haubrich, K., Hennig, J., Kowalinski, E., Stevens, R.V., Martin, S.R., Reis e Sousa, C., Cusack, S., Rittinger, K., 2018. Molecular mechanism of influenza A NS1-mediated TRIM25 recognition and inhibition. Nat Commun 9, 1820. https://doi.org/10.1038/s41467-018-04214-8

Koppstein, D., Ashour, J., Bartel, D.P., 2015. Sequencing the cap-snatching repertoire of H1N1 influenza provides insight into the mechanism of viral transcription initiation. Nucleic Acids Res 43, 5052–5064. https://doi.org/10.1093/nar/gkv333

Krainer, G., Welsh, T.J., Joseph, J.A., Espinosa, J.R., Wittmann, S., de Csilléry, E., Sridhar, A., Toprakcioglu, Z., Gudiškytė, G., Czekalska, M.A., Arter, W.E., Guillén-Boixet, J., Franzmann, T.M., Qamar, S., George-Hyslop, P.S., Hyman, A.A., Collepardo-Guevara, R., Alberti, S., Knowles, T.P.J., 2021. Reentrant liquid condensate phase of proteins is stabilized by hydrophobic and non-ionic interactions. Nat Commun 12, 1085. https://doi.org/10.1038/s41467-021-21181-9

Krammer, F., 2019. The human antibody response to influenza A virus infection and vaccination. Nat Rev Immunol 19, 383–397. https://doi.org/10.1038/s41577-019-0143-6

Krammer, F., Smith, G.J.D., Fouchier, R.A.M., Peiris, M., Kedzierska, K., Doherty, P.C., Palese, P., Shaw, M.L., Treanor, J., Webster, R.G.,

García-Sastre, A., 2018. Influenza. Nat Rev Dis Primers 4, 1–21. https://doi.org/10.1038/s41572-018-0002-y
Krasnopolsky, S., Marom, L., Victor, R.A., Kuzmina, A., Schwartz, J.C., Fujinaga, K., Taube, R., 2019. Fused in sarcoma silences HIV gene transcription and maintains viral latency through suppressing AFF4 gene activation. Retrovirology 16. https://doi.org/10.1186/s12977-019-0478-x
Krishnamoorthy, G., Roques, B., Darlix, J., Mély, Y., 2003. DNA condensation by the nucleocapsid protein of HIV-1: a mechanism ensuring DNA protection. Nucleic Acids Research 31, 5425–5432. https://doi.org/10.1093/nar/gkg738
Kroschwald, S., Maharana, S., Simon, A., 2017. Hexanediol: a chemical probe to investigate the material properties of membrane-less compartments 7.
Kroschwald, S., Munder, M.C., Maharana, S., Franzmann, T.M., Richter, D., Ruer, M., Hyman, A.A., Alberti, S., 2018. Different Material States of Pub1 Condensates Define Distinct Modes of Stress Adaptation and Recovery. Cell reports 23, 3327–3339. https://doi.org/10.1016/j.celrep.2018.05.041
Kuchipudi, S.V., Nelli, R.K., Gontu, A., Satyakumar, R., Surendran Nair, M., Subbiah, M., 2021. Sialic Acid Receptors: The Key to Solving the Enigma of Zoonotic Virus Spillover. Viruses 13, 262. https://doi.org/10.3390/v13020262
Kuiken, T., Holmes, E.C., McCauley, J., Rimmelzwaan, G.F., Williams, C.S., Grenfell, B.T., 2006. Host Species Barriers to Influenza Virus Infections. Science 312, 394–397. https://doi.org/10.1126/science.1122818
Kumar, B., Asha, K., Khanna, M., Ronsard, L., Meseko, C.A., Sanicas, M., 2018. The emerging influenza virus threat: status and new prospects for its therapy and control. Arch Virol 163, 831–844. https://doi.org/10.1007/s00705-018-3708-y
Kummer, S., Flöttmann, M., Schwanhäusser, B., Sieben, C., Veit, M., Selbach, M., Klipp, E., Herrmann, A., 2014. Alteration of Protein Levels during Influenza Virus H1N1 Infection in Host Cells: A Proteomic Survey of Host and Virus Reveals Differential Dynamics. PLoS One 9, e94257. https://doi.org/10.1371/journal.pone.0094257
Kuo, R.-L., Li, L.-H., Lin, S.-J., Li, Z.-H., Chen, G.-W., Chang, C.-K., Wang, Y.-R., Tam, E.-H., Gong, Y.-N., Krug, R.M., Shih, S.-R., 2016. Role of N Terminus-Truncated NS1 Proteins of Influenza A Virus in Inhibiting IRF3 Activation. J Virol 90, 4696–4705. https://doi.org/10.1128/JVI.02843-15
Labaronne, A., Swale, C., Monod, A., Schoehn, G., Crépin, T., Ruigrok, R.W.H., 2016. Binding of RNA by the Nucleoproteins of Influenza Viruses A and B. Viruses 8, 247. https://doi.org/10.3390/v8090247
Lahaye, X., Satoh, T., Gentili, M., Cerboni, S., Conrad, C., Hurbain, I., El Marjou, A., Lacabaratz, C., Lelièvre, J.-D., Manel, N., 2013. The

capsids of HIV-1 and HIV-2 determine immune detection of the viral cDNA by the innate sensor cGAS in dendritic cells. Immunity 39, 1132–1142. https://doi.org/10.1016/j.immuni.2013.11.002

Lahaye, X., Vidy, A., Pomier, C., Obiang, L., Harper, F., Gaudin, Y., Blondel, D., 2009. Functional Characterization of Negri Bodies (NBs) in Rabies Virus-Infected Cells: Evidence that NBs Are Sites of Viral Transcription and Replication. Journal of Virology 83, 7948–7958. https://doi.org/10.1128/JVI.00554-09

Lai, J.C.C., Chan, W.W.L., Kien, F., Nicholls, J.M., Peiris, J.S.M., Garcia, J.-M. 2010, 2010. Formation of virus-like particles from human cell lines exclusively expressing influenza neuraminidase. Journal of General Virology 91, 2322–2330. https://doi.org/10.1099/vir.0.019935-0

Lakdawala, S.S., Wu, Y., Wawrzusin, P., Kabat, J., Broadbent, A.J., Lamirande, E.W., Fodor, E., Altan-Bonnet, N., Shroff, H., Subbarao, K., 2014. Influenza A Virus Assembly Intermediates Fuse in the Cytoplasm. PLOS Pathogens 10, e1003971. https://doi.org/10.1371/journal.ppat.1003971

Lampejo, T., 2020. Influenza and antiviral resistance: an overview. Eur J Clin Microbiol Infect Dis 39, 1201–1208. https://doi.org/10.1007/s10096-020-03840-9

Landeras-Bueno, S., Jorba, N., Pérez-Cidoncha, M., Ortín, J., 2011. The Splicing Factor Proline-Glutamine Rich (SFPQ/PSF) Is Involved in Influenza Virus Transcription. PLOS Pathogens 7, e1002397. https://doi.org/10.1371/journal.ppat.1002397

Langdon, E.M., Gladfelter, A.S., 2018. A New Lens for RNA Localization: Liquid-Liquid Phase Separation. Annual Review of Microbiology 72, 255–271. https://doi.org/10.1146/annurev-micro-090817-062814

Lazarowitz, S.G., Choppin, P.W., 1975. Enhancement of the infectivity of influenza A and B viruses by proteolytic cleavage of the hemagglutinin polypeptide. Virology 68, 440–454. https://doi.org/10.1016/0042-6822(75)90285-8

Le Sage, V., Kanarek, J.P., Snyder, D.J., Cooper, V.S., Lakdawala, S.S., Lee, N., 2020. Mapping of Influenza Virus RNA-RNA Interactions Reveals a Flexible Network. Cell Rep 31, 107823. https://doi.org/10.1016/j.celrep.2020.107823

Lebarbenchon, C., Poulson, R., Shannon, K., Slagter, J., Slusher, M.J., Wilcox, B.R., Berdeen, J., Knutsen, G.A., Cardona, C.J., Stallknecht, D.E., 2013. Isolation of Influenza A Viruses from Wild Ducks and Feathers in Minnesota (2010—2011). Avian Diseases 57, 677–680.

Lee, J.E., Cathey, P.I., Wu, H., Parker, R., Voeltz, G.K., 2020. Endoplasmic reticulum contact sites regulate the dynamics of membraneless organelles. Science 367, eaay7108. https://doi.org/10.1126/science.aay7108

Lee, N., Le Sage, V., Nanni, A.V., Snyder, D.J., Cooper, V.S., Lakdawala, S.S., 2017. Genome-wide analysis of influenza viral RNA and

nucleoprotein association. Nucleic Acids Research 45, 8968–8977. https://doi.org/10.1093/nar/gkx584

Leiding, T., Wang, J., Martinsson, J., DeGrado, W.F., Årsköld, S.P., 2010. Proton and cation transport activity of the M2 proton channel from influenza A virus. Proceedings of the National Academy of Sciences 107, 15409–15414. https://doi.org/10.1073/pnas.1009997107

Li, H., Ernst, C., Kolonko-Adamska, M., Greb-Markiewicz, B., Man, J., Parissi, V., Ng, B.W.-L., 2022. Phase separation in viral infections. Trends in Microbiology 0. https://doi.org/10.1016/j.tim.2022.06.005

Li, J., Zhang, M., Ma, W., Yang, B., Lu, H., Zhou, F., Zhang, L., 2022. Post-translational modifications in liquid-liquid phase separation: a comprehensive review. Mol Biomed 3, 13. https://doi.org/10.1186/s43556-022-00075-2

Li, M.L., Ramirez, B.C., Krug, R.M., 1998. RNA-dependent activation of primer RNA production by influenza virus polymerase: different regions of the same protein subunit constitute the two required RNA-binding sites. EMBO J 17, 5844–5852. https://doi.org/10.1093/emboj/17.19.5844

Li, M.L., Rao, P., Krug R.M., 2001. The active sites of the influenza cap-dependent endonuclease are on different polymerase subunits. The EMBO Journal 20, 2078–2086. https://doi.org/10.1093/emboj/20.8.2078

Li, P., Banjade, S., Cheng, H.-C., Kim, S., Chen, B., Guo, L., Llaguno, M., Hollingsworth, J.V., King, D.S., Banani, S.F., Russo, P.S., Jiang, Q.-X., Nixon, B.T., Rosen, M.K., 2012. Phase transitions in the assembly of multivalent signalling proteins. Nature 483, 336–340. https://doi.org/10.1038/nature10879

Li, S., Sieben, C., Ludwig, K., Höfer, C.T., Chiantia, S., Herrmann, A., Eghiaian, F., Schaap, I.A.T., 2014. pH-Controlled Two-Step Uncoating of Influenza Virus. Biophysical Journal 106, 1447–1456. https://doi.org/10.1016/j.bpj.2014.02.018

Li, X.-D., Wu, J., Gao, D., Wang, H., Sun, L., Chen, Z.J., 2013. Pivotal roles of cGAS-cGAMP signaling in antiviral defense and immune adjuvant effects. Science 341, 1390–1394. https://doi.org/10.1126/science.1244040

Liang, Y., Hong, Y., Parslow, T.G., 2005. cis-Acting Packaging Signals in the Influenza Virus PB1, PB2, and PA Genomic RNA Segments. Journal of Virology 79, 10348–10355. https://doi.org/10.1128/JVI.79.16.10348-10355.2005

Liang, Yuhong, Huang, T., Ly, H., Parslow, T.G., Liang, Yuying, 2008. Mutational Analyses of Packaging Signals in Influenza Virus PA, PB1, and PB2 Genomic RNA Segments. Journal of Virology 82, 229–236. https://doi.org/10.1128/JVI.01541-07

Lietzén, N., Öhman, T., Rintahaka, J., Julkunen, I., Aittokallio, T., Matikainen, S., Nyman, T.A., 2011. Quantitative Subcellular Proteome and Secretome Profiling of Influenza A Virus-Infected Human Primary

Macrophages. PLOS Pathogens 7, e1001340. https://doi.org/10.1371/journal.ppat.1001340
Lifshitz, I.M., Slyozov, V.V., 1961. The kinetics of precipitation from supersaturated solid solutions. Journal of Physics and Chemistry of Solids 19, 35–50. https://doi.org/10.1016/0022-3697(61)90054-3
Lin, B.C., Lai, C.J., 1983. The influenza virus nucleoprotein synthesized from cloned DNA in a simian virus 40 vector is detected in the nucleus. Journal of Virology 45, 434–438. https://doi.org/10.1128/jvi.45.1.434-438.1983
Lin, R.-W., Chen, G.-W., Sung, H.-H., Lin, R.-J., Yen, L.-C., Tseng, Y.-L., Chang, Y.-K., Lien, S.-P., Shih, S.-R., Liao, C.-L., 2019. Naturally occurring mutations in PB1 affect influenza A virus replication fidelity, virulence, and adaptability. Journal of Biomedical Science 26, 55. https://doi.org/10.1186/s12929-019-0547-4
Lin, Y.-C., Jeng, K.-S., Lai, M.M.C., 2017. CNOT4-Mediated Ubiquitination of Influenza A Virus Nucleoprotein Promotes Viral RNA Replication. mBio 8, e00597-17. https://doi.org/10.1128/mBio.00597-17
Ling, Y.-H., Wang, H., Han, M.-Q., Wang, D., Hu, Y.-X., Zhou, K., Li, Y., 2022. Nucleoporin 85 interacts with influenza A virus PB1 and PB2 to promote its replication by facilitating nuclear import of ribonucleoprotein. Frontiers in Microbiology 13.
Liu, R., Sheng, Z., Huang, C., Wang, D., Li, F., 2020. Influenza D virus. Current Opinion in Virology, Preventive and therapeutic vaccines * Viral Immunology 44, 154–161. https://doi.org/10.1016/j.coviro.2020.08.004
Long, J.S., Giotis, E.S., Moncorgé, O., Frise, R., Mistry, B., James, J., Morisson, M., Iqbal, M., Vignal, A., Skinner, M.A., Barclay, W.S., 2016. Species difference in ANP32A underlies influenza A virus polymerase host restriction. Nature 529, 101–104. https://doi.org/10.1038/nature16474
Long, J.S., Mistry, B., Haslam, S.M., Barclay, W.S., 2019. Host and viral determinants of influenza A virus species specificity. Nat Rev Microbiol 17, 67–81. https://doi.org/10.1038/s41579-018-0115-z
Lopez, N., Camporeale, G., Salgueiro, M., Borkosky, S.S., Visentín, A., Peralta-Martinez, R., Loureiro, M.E., Prat-Gay, G. de, 2021. Deconstructing virus condensation. PLOS Pathogens 17, e1009926. https://doi.org/10.1371/journal.ppat.1009926
López-Turiso, J.A., Martínez, C., Tanaka, T., Ortín, J., 1990. The synthesis of influenza virus negative-strand RNA takes place in insoluble complexes present in the nuclear matrix fraction. Virus Res 16, 325–337. https://doi.org/10.1016/0168-1702(90)90056-h
Lowen, A.C., 2017. Constraints, Drivers, and Implications of Influenza A Virus Reassortment. Annual Review of Virology 4, 105–121. https://doi.org/10.1146/annurev-virology-101416-041726
Lukarska, M., Fournier, G., Pflug, A., Resa-Infante, P., Reich, S., Naffakh, N., Cusack, S., 2017. Structural basis of an essential interaction between

influenza polymerase and Pol II CTD. Nature 541, 117–121. https://doi.org/10.1038/nature20594
Luzak, V., 2022. Nuclear Condensates: New Targets to Combat Parasite Immune Evasion? Frontiers in Cellular and Infection Microbiology 12.
Lyonnais, S., Sadiq, S.K., Lorca-Oró, C., Dufau, L., Nieto-Marquez, S., Escribà, T., Gabrielli, N., Tan, X., Ouizougun-Oubari, M., Okoronkwo, J., Reboud-Ravaux, M., Gatell, J.M., Marquet, R., Paillart, J.-C., Meyerhans, A., Tisné, C., Gorelick, R.J., Mirambeau, G., 2021. The HIV-1 Nucleocapsid Regulates Its Own Condensation by Phase-Separated Activity-Enhancing Sequestration of the Viral Protease during Maturation. Viruses 13, 2312. https://doi.org/10.3390/v13112312
Ma, K., Roy, A.M., Whittaker, G.R., 2001. Nuclear export of influenza virus ribonucleoproteins: identification of an export intermediate at the nuclear periphery. Virology 282, 215–220. https://doi.org/10.1006/viro.2001.0833
Ma, W., Mayr, C., 2018. A Membraneless Organelle Associated with the Endoplasmic Reticulum Enables 3′UTR-Mediated Protein-Protein Interactions. Cell 175, 1492-1506.e19. https://doi.org/10.1016/j.cell.2018.10.007
Machkovech, H.M., Bloom, J.D., Subramaniam, A.R., 2019. Comprehensive profiling of translation initiation in influenza virus infected cells. PLOS Pathogens 15, e1007518. https://doi.org/10.1371/journal.ppat.1007518
Maeda, T., Kawasaki, K., Ohnishi, S., 1981. Interaction of influenza virus hemagglutinin with target membrane lipids is a key step in virus-induced hemolysis and fusion at pH 5.2. Proceedings of the National Academy of Sciences 78, 4133–4137. https://doi.org/10.1073/pnas.78.7.4133
Maeda, T., Ohnishi, S., 1980. Activation of influenza virus by acidic media causes hemolysis and fusion of erythrocytes. FEBS Letters 122, 283–287. https://doi.org/10.1016/0014-5793(80)80457-1
Maharana, S., Wang, J., Papadopoulos, D.K., Richter, D., Pozniakovsky, A., Poser, I., Bickle, M., Rizk, S., Guillén-Boixet, J., Franzmann, T.M., Jahnel, M., Marrone, L., Chang, Y.-T., Sterneckert, J., Tomancak, P., Hyman, A.A., Alberti, S., 2018. RNA buffers the phase separation behavior of prion-like RNA binding proteins. Science 360, 918–921. https://doi.org/10.1126/science.aar7366
Malinovska, L., Kroschwald, S., Alberti, S., 2013. Protein disorder, prion propensities, and self-organizing macromolecular collectives. Biochim Biophys Acta 1834, 918–931. https://doi.org/10.1016/j.bbapap.2013.01.003
Manuguerra, J.C., Hannoun, C., 1992. Natural infection of dogs by influenza C virus. Res Virol 143, 199–204. https://doi.org/10.1016/s0923-2516(06)80104-4

Mänz, B., Brunotte, L., Reuther, P., Schwemmle, M., 2012. Adaptive mutations in NEP compensate for defective H5N1 RNA replication in cultured human cells. Nat Commun 3, 802. https://doi.org/10.1038/ncomms1804

Mänz, B., Schwemmle, M., Brunotte, L., 2013. Adaptation of avian influenza A virus polymerase in mammals to overcome the host species barrier. J Virol 87, 7200–7209. https://doi.org/10.1128/JVI.00980-13

Marazzi, I., Ho, J.S.Y., Kim, J., Manicassamy, B., Dewell, S., Albrecht, R.A., Seibert, C.W., Schaefer, U., Jeffrey, K.L., Prinjha, R.K., Lee, K., García-Sastre, A., Roeder, R.G., Tarakhovsky, A., 2012. Suppression of the antiviral response by an influenza histone mimic. Nature 483, 428–433. https://doi.org/10.1038/nature10892

Marcos-Villar, L., Pazo, A., Nieto, A., 2016. Influenza Virus and Chromatin: Role of the CHD1 Chromatin Remodeler in the Virus Life Cycle. J Virol 90, 3694–3707. https://doi.org/10.1128/JVI.00053-16

Marjuki, H., Alam, M.I., Ehrhardt, C., Wagner, R., Planz, O., Klenk, H.-D., Ludwig, S., Pleschka, S., 2006. Membrane Accumulation of Influenza A Virus Hemagglutinin Triggers Nuclear Export of the Viral Genome via Protein Kinase Cα-mediated Activation of ERK Signaling *. Journal of Biological Chemistry 281, 16707–16715. https://doi.org/10.1074/jbc.M510233200

Marjuki, H., Yen, H.-L., Franks, J., Webster, R.G., Pleschka, S., Hoffmann, E., 2007. Higher polymerase activity of a human influenza virus enhances activation of the hemagglutinin-induced Raf/MEK/ERK signal cascade. Virology Journal 4, 134. https://doi.org/10.1186/1743-422X-4-134

Markwell, D.D., Shortridge, K.F., 1982. Possible waterborne transmission and maintenance of influenza viruses in domestic ducks. Appl Environ Microbiol 43, 110–115. https://doi.org/10.1128/aem.43.1.110-115.1982

Marrone, L., Poser, I., Casci, I., Japtok, J., Reinhardt, P., Janosch, A., Andree, C., Lee, H.O., Moebius, C., Koerner, E., Reinhardt, L., Cicardi, M.E., Hackmann, K., Klink, B., Poletti, A., Alberti, S., Bickle, M., Hermann, A., Pandey, U.B., Hyman, A.A., Sterneckert, J.L., 2018. Isogenic FUS-eGFP iPSC Reporter Lines Enable Quantification of FUS Stress Granule Pathology that Is Rescued by Drugs Inducing Autophagy. Stem Cell Reports 10, 375–389. https://doi.org/10.1016/j.stemcr.2017.12.018

Marsh, G.A., Hatami, R., Palese, P., 2007. Specific Residues of the Influenza A Virus Hemagglutinin Viral RNA Are Important for Efficient Packaging into Budding Virions. Journal of Virology 81, 9727–9736. https://doi.org/10.1128/JVI.01144-07

Martin, E.W., Harmon, T.S., Hopkins, J.B., Chakravarthy, S., Incicco, J.J., Schuck, P., Soranno, A., Mittag, T., 2021. A multi-step nucleation process determines the kinetics of prion-like domain phase

separation. Nat Commun 12, 4513. https://doi.org/10.1038/s41467-021-24727-z
Martin, K., Helenius, A., 1991. Nuclear transport of influenza virus ribonucleoproteins: the viral matrix protein (M1) promotes export and inhibits import. Cell 67, 117–130. https://doi.org/10.1016/0092-8674(91)90576-k
Martin, K, Helenius, A., 1991. Transport of incoming influenza virus nucleocapsids into the nucleus. Journal of Virology 65, 232–244. https://doi.org/10.1128/jvi.65.1.232-244.1991
Martin-Benito, J., Ortin, J., 2013. Influenza virus transcription and replication. Adv Virus Res 87, 113–137. https://doi.org/10.1016/B978-0-12-407698-3.00004-1
Martínez-Alonso, M., Hengrung, N., Fodor, E., 2016. RNA-Free and Ribonucleoprotein-Associated Influenza Virus Polymerases Directly Bind the Serine-5-Phosphorylated Carboxyl-Terminal Domain of Host RNA Polymerase II. Journal of Virology 90, 6014–6021. https://doi.org/10.1128/JVI.00494-16
Mateus, A., Bobonis, J., Kurzawa, N., Stein, F., Helm, D., Hevler, J., Typas, A., Savitski, M.M., 2018. Thermal proteome profiling in bacteria: probing protein state in vivo. Molecular Systems Biology 14, e8242. https://doi.org/10.15252/msb.20188242
Mateus, A., Määttä, T.A., Savitski, M.M., 2017. Thermal proteome profiling: unbiased assessment of protein state through heat-induced stability changes. Proteome Science 15, 13. https://doi.org/10.1186/s12953-017-0122-4
Matsuzaki, Y., Katsushima, N., Nagai, Y., Shoji, M., Itagaki, T., Sakamoto, M., Kitaoka, S., Mizuta, K., Nishimura, H., 2006. Clinical Features of Influenza C Virus Infection in Children. The Journal of Infectious Diseases 193, 1229–1235. https://doi.org/10.1086/502973
McAuley, J.L., Hornung, F., Boyd, K.L., Smith, A.M., McKeon, R., Bennink, J., Yewdell, J.W., McCullers, J.A., 2007. Expression of the 1918 influenza A virus PB1-F2 enhances the pathogenesis of viral and secondary bacterial pneumonia. Cell Host Microbe 2, 240–249. https://doi.org/10.1016/j.chom.2007.09.001
Mehle, A., Doudna, J.A., 2008. An inhibitory activity in human cells restricts the function of an avian-like influenza virus polymerase. Cell Host Microbe 4, 111–122. https://doi.org/10.1016/j.chom.2008.06.007
Melen, K., Fagerlund, R., Franke, J., Kohler, M., Kinnunen, L., Julkunen, I., 2003. Importin alpha nuclear localization signal binding sites for STAT1, STAT2, and influenza A virus nucleoprotein. J Biol Chem 278, 28193–28200. https://doi.org/10.1074/jbc.M303571200
Mettelman, R.C., Thomas, P.G., 2021. Human Susceptibility to Influenza Infection and Severe Disease. Cold Spring Harb Perspect Med 11, a038711. https://doi.org/10.1101/cshperspect.a038711
Mettier, J., Marc, D., Sedano, L., Da Costa, B., Chevalier, C., Le Goffic, R., 2021. Study of the host specificity of PB1-F2-associated virulence.

Virulence 12, 1647–1660. https://doi.org/10.1080/21505594.2021.1933848
Milin, A.N., Deniz, A.A., 2018. Reentrant Phase Transitions and Non-Equilibrium Dynamics in Membraneless Organelles. Biochemistry 57, 2470–2477. https://doi.org/10.1021/acs.biochem.8b00001
Milovanovic, D., De Camilli, P., 2017. Synaptic vesicle clusters at synapses: a distinct liquid phase? Neuron 93, 995–1002. https://doi.org/10.1016/j.neuron.2017.02.013
Milovanovic, D., Wu, Y., Bian, X., De Camilli, P., 2018. A liquid phase of synapsin and lipid vesicles. Science (New York, N.Y.) 361, 604–607. https://doi.org/10.1126/science.aat5671
Min, J.-Y., Krug, R.M., 2006. The primary function of RNA binding by the influenza A virus NS1 protein in infected cells: Inhibiting the 2′-5′ oligo (A) synthetase/RNase L pathway. Proceedings of the National Academy of Sciences 103, 7100–7105. https://doi.org/10.1073/pnas.0602184103
Mitrea, D.M., Cika, J.A., Stanley, C.B., Nourse, A., Onuchic, P.L., Banerjee, P.R., Phillips, A.H., Park, C.-G., Deniz, A.A., Kriwacki, R.W., 2018. Self-interaction of NPM1 modulates multiple mechanisms of liquid–liquid phase separation. Nat Commun 9, 842. https://doi.org/10.1038/s41467-018-03255-3
Mitrea, D.M., Mittasch, M., Gomes, B.F., Klein, I.A., Murcko, M.A., 2022. Modulating biomolecular condensates: a novel approach to drug discovery. Nat Rev Drug Discov 1–22. https://doi.org/10.1038/s41573-022-00505-4
Mittag, T., Pappu, R.V., 2022. A conceptual framework for understanding phase separation and addressing open questions and challenges. Molecular Cell 82, 2201–2214. https://doi.org/10.1016/j.molcel.2022.05.018
Mittag, T., Parker, R., 2018. Multiple Modes of Protein–Protein Interactions Promote RNP Granule Assembly. Journal of Molecular Biology, Phase Separation in Biology and Disease 430, 4636–4649. https://doi.org/10.1016/j.jmb.2018.08.005
Miyake, Y., Keusch, J.J., Decamps, L., Ho-Xuan, H., Iketani, S., Gut, H., Kutay, U., Helenius, A., Yamauchi, Y., 2019. Influenza virus uses transportin 1 for vRNP debundling during cell entry. Nat Microbiol 4, 578–586. https://doi.org/10.1038/s41564-018-0332-2
Moeller, A., Kirchdoerfer, R.N., Potter, C.S., Carragher, B., Wilson, I.A., 2012. Organization of the Influenza Virus Replication Machinery. Science 338, 1631–1634. https://doi.org/10.1126/science.1227270
Moisy, D., Avilov, S.V., Jacob, Y., Laoide, B.M., Ge, X., Baudin, F., Naffakh, N., Jestin, J.-L., 2012. HMGB1 protein binds to influenza virus nucleoprotein and promotes viral replication. J Virol 86, 9122–9133. https://doi.org/10.1128/JVI.00789-12
Molina, D.M., Jafari, R., Ignatushchenko, M., Seki, T., Larsson, E.A., Dan, C., Sreekumar, L., Cao, Y., Nordlund, P., 2013. Monitoring Drug Target

Engagement in Cells and Tissues Using the Cellular Thermal Shift Assay. Science 341, 84–87. https://doi.org/10.1126/science.1233606
Molliex, A., Temirov, J., Lee, J., Coughlin, M., Kanagaraj, A.P., Kim, H.J., Mittag, T., Taylor, J.P., 2015. Phase Separation by Low Complexity Domains Promotes Stress Granule Assembly and Drives Pathological Fibrillization. Cell 163, 123–133. https://doi.org/10.1016/j.cell.2015.09.015
Momose, F., Basler, C.F., O'Neill, R.E., Iwamatsu, A., Palese, P., Nagata, K., 2001. Cellular splicing factor RAF-2p48/NPI-5/BAT1/UAP56 interacts with the influenza virus nucleoprotein and enhances viral RNA synthesis. J Virol 75, 1899–1908. https://doi.org/10.1128/JVI.75.4.1899-1908.2001
Momose, F., Kikuchi, Y., Komase, K., Morikawa, Y., 2007. Visualization of microtubule-mediated transport of influenza viral progeny ribonucleoprotein. Microbes and Infection 9, 1422–1433. https://doi.org/10.1016/j.micinf.2007.07.007
Momose, F., Sekimoto, T., Ohkura, T., Jo, S., Kawaguchi, A., Nagata, K., Morikawa, Y., 2011. Apical Transport of Influenza A Virus Ribonucleoprotein Requires Rab11-positive Recycling Endosome. PLOS ONE 6, e21123. https://doi.org/10.1371/journal.pone.0021123
Monette, A., Niu, M., Chen, L., Rao, S., Gorelick, R.J., Mouland, A.J., 2020. Pan-retroviral Nucleocapsid-Mediated Phase Separation Regulates Genomic RNA Positioning and Trafficking. Cell Reports 31, 107520. https://doi.org/10.1016/j.celrep.2020.03.084
Morens, D.M., Taubenberger, J.K., 2011. Pandemic influenza: certain uncertainties. Reviews in Medical Virology 21, 262–284. https://doi.org/10.1002/rmv.689
Morgan, C., Ellison, S.A., Rose, H.M., Moore, D.H., 1954. STRUCTURE AND DEVELOPMENT OF VIRUSES OBSERVED IN THE ELECTRON MICROSCOPE : II. VACCINIA AND FOWL POX VIRUSES. Journal of Experimental Medicine 100, 301–310. https://doi.org/10.1084/jem.100.3.301
Moriyama, M., Koshiba, T., Ichinohe, T., 2019. Influenza A virus M2 protein triggers mitochondrial DNA-mediated antiviral immune responses. Nat Commun 10, 4624. https://doi.org/10.1038/s41467-019-12632-5
Mosley, V.M., Wyckoff, R.W.G., 1946. Electron Micrography of the Virus of Influenza. Nature 157, 263–263. https://doi.org/10.1038/157263a0
Mould, J.A., Drury, J.E., Frings, S.M., Kaupp, U.B., Pekosz, A., Lamb, R.A., Pinto, L.H., 2000. Permeation and Activation of the M2 Ion Channel of Influenza A Virus *. Journal of Biological Chemistry 275, 31038–31050. https://doi.org/10.1074/jbc.M003663200
Mubareka, S., Lowen, A.C., Steel, J., Coates, A.L., García-Sastre, A., Palese, P., 2009. Transmission of Influenza Virus via Aerosols and Fomites in the Guinea Pig Model. J Infect Dis 199, 858–865. https://doi.org/10.1086/597073

Munder, M.C., Midtvedt, D., Franzmann, T., NüSke, E., Otto, O., Herbig, M., Ulbricht, E., Müller, P., Taubenberger, A., Maharana, S., Malinovska, L., Richter, D., Guck, J., Zaburdaev, V., Alberti, S., 2016. A pH-driven transition of the cytoplasm from a fluid- to a solid-like state promotes entry into dormancy. eLife 5. https://doi.org/10.7554/elife.09347

Murakami, M., Towatari, T., Ohuchi, M., Shiota, M., Akao, M., Okumura, Y., Parry, M.A., Kido, H., 2001. Mini-plasmin found in the epithelial cells of bronchioles triggers infection by broad-spectrum influenza A viruses and Sendai virus. Eur J Biochem 268, 2847–2855. https://doi.org/10.1046/j.1432-1327.2001.02166.x

Muramoto, Y., Noda, T., Kawakami, E., Akkina, R., Kawaoka, Y., 2013. Identification of novel influenza A virus proteins translated from PA mRNA. J Virol 87, 2455–2462. https://doi.org/10.1128/JVI.02656-12

Muramoto, Y., Takada, A., Fujii, K., Noda, T., Iwatsuki-Horimoto, K., Watanabe, S., Horimoto, T., Kida, H., Kawaoka, Y., 2006. Hierarchy among Viral RNA (vRNA) Segments in Their Role in vRNA Incorporation into Influenza A Virions. Journal of Virology 80, 2318–2325. https://doi.org/10.1128/JVI.80.5.2318-2325.2006

Murti, K.G., Webster, R.G., Jones, I.M., 1988. Localization of RNA polymerases on influenza viral ribonucleoproteins by immunogold labeling. Virology 164, 562–566. https://doi.org/10.1016/0042-6822(88)90574-0

Nacken, W., Schreiber, A., Masemann, D., Ludwig, S., 2021. The Effector Domain of the Influenza A Virus Nonstructural Protein NS1 Triggers Host Shutoff by Mediating Inhibition and Global Deregulation of Host Transcription When Associated with Specific Structures in the Nucleus. mBio 12, e02196-21. https://doi.org/10.1128/mBio.02196-21

Naito, T., Kiyasu, Y., Sugiyama, K., Kimura, A., Nakano, R., Matsukage, A., Nagata, K., 2007. An influenza virus replicon system in yeast identified Tat-SF1 as a stimulatory host factor for viral RNA synthesis. Proceedings of the National Academy of Sciences 104, 18235–18240. https://doi.org/10.1073/pnas.0705856104

Naito, T., Shirai, K., Mori, K., Muratsu, H., Ushirogawa, H., Ohniwa, R.L., Hanada, K., Saito, M., 2019. Tyr82 Amino Acid Mutation in PB1 Polymerase Induces an Influenza Virus Mutator Phenotype. J Virol 93, e00834-19. https://doi.org/10.1128/JVI.00834-19

Nakach, M., Authelin, J.-R., Voignier, C., Tadros, T., Galet, L., Chamayou, A., 2016. Assessment of formulation robustness for nano-crystalline suspensions using failure mode analysis or derisking approach. International Journal of Pharmaceutics 506, 320–331. https://doi.org/10.1016/j.ijpharm.2016.04.043

Nakamura, H., Lee, A.A., Afshar, A.S., Watanabe, S., Rho, E., Razavi, S., Suarez, A., Lin, Y.-C., Tanigawa, M., Huang, B., DeRose, R., Bobb, D., Hong, W., Gabelli, S.B., Goutsias, J., Inoue, T., 2018. Intracellular production of hydrogels and synthetic RNA granules by multivalent

molecular interactions. Nature Mater 17, 79–89. https://doi.org/10.1038/nmat5006
Nakano, M., Sugita, Y., Kodera, N., Miyamoto, S., Muramoto, Y., Wolf, M., Noda, T., 2021. Ultrastructure of influenza virus ribonucleoprotein complexes during viral RNA synthesis. Commun Biol 4, 1–10. https://doi.org/10.1038/s42003-021-02388-4
Nakashima, K.K., Baaij, J.F., Spruijt, E., 2018. Reversible generation of coacervate droplets in an enzymatic network. Soft Matter 14, 361–367. https://doi.org/10.1039/C7SM01897E
Nakashima, K.K., Vibhute, M.A., Spruijt, E., 2019. Biomolecular Chemistry in Liquid Phase Separated Compartments. Frontiers in Molecular Biosciences 6.
Nakatsu, S., Sagara, H., Sakai-Tagawa, Y., Sugaya, N., Noda, T., Kawaoka, Y., 2016. Complete and Incomplete Genome Packaging of Influenza A and B Viruses. mBio 7, e01248-16. https://doi.org/10.1128/mBio.01248-16
Nakatsu, Y., Ma, X., Seki, F., Suzuki, T., Iwasaki, M., Yanagi, Y., Komase, K., Takeda, M., 2013. Intracellular Transport of the Measles Virus Ribonucleoprotein Complex Is Mediated by Rab11A-Positive Recycling Endosomes and Drives Virus Release from the Apical Membrane of Polarized Epithelial Cells. J Virol 87, 4683–4693. https://doi.org/10.1128/JVI.02189-12
Nanbo, A., Ohba, Y., 2018. Budding of Ebola Virus Particles Requires the Rab11-Dependent Endocytic Recycling Pathway. The Journal of Infectious Diseases 218, S388–S396. https://doi.org/10.1093/infdis/jiy460
Nayak, D.P., Balogun, R.A., Yamada, H., Zhou, Z.H., Barman, S., 2009. Influenza virus morphogenesis and budding. Virus Res 143, 147–161. https://doi.org/10.1016/j.virusres.2009.05.010
Nedelsky, N.B., Taylor, J.P., 2019. Bridging biophysics and neurology: aberrant phase transitions in neurodegenerative disease. Nature reviews. Neurology 15, 272–286. https://doi.org/10.1038/s41582-019-0157-5
Netherton, C., Moffat, K., Brooks, E., Wileman, T., 2007. A Guide to Viral Inclusions, Membrane Rearrangements, Factories, and Viroplasm Produced During Virus Replication, in: Advances in Virus Research. Academic Press, pp. 101–182. https://doi.org/10.1016/S0065-3527(07)70004-0
Netherton, C.L., Wileman, T., 2011. Virus factories, double membrane vesicles and viroplasm generated in animal cells. Current Opinion in Virology 1, 381–387. https://doi.org/10.1016/j.coviro.2011.09.008
Neumann, G., Castrucci, M.R., Kawaoka, Y., 1997. Nuclear import and export of influenza virus nucleoprotein. J Virol 71, 9690–9700.
Neumann, G., Hughes, M.T., Kawaoka, Y., 2000. Influenza A virus NS2 protein mediates vRNP nuclear export through NES-independent

interaction with hCRM1. EMBO J 19, 6751–6758. https://doi.org/10.1093/emboj/19.24.6751
Neumann, G., Noda, T., Kawaoka, Y., 2009. Emergence and pandemic potential of swine-origin H1N1 influenza virus. Nature 459, 931–939. https://doi.org/10.1038/nature08157
Ng, A.K.-L., Chan, W.-H., Choi, S.-T., Lam, M.K.-H., Lau, K.-F., Chan, P.K.-S., Au, S.W.-N., Fodor, E., Shaw, P.-C., 2012. Influenza Polymerase Activity Correlates with the Strength of Interaction between Nucleoprotein and PB2 through the Host-Specific Residue K/E627. PLOS ONE 7, e36415. https://doi.org/10.1371/journal.pone.0036415
Ng, A.K.-L., Zhang, H., Tan, K., Li, Z., Liu, J., Chan, P.K.-S., Li, S.-M., Chan, W.-Y., Au, S.W.-N., Joachimiak, A., Walz, T., Wang, J.-H., Shaw, P.-C., 2008. Structure of the influenza virus A H5N1 nucleoprotein: implications for RNA binding, oligomerization, and vaccine design. FASEB J 22, 3638–3647. https://doi.org/10.1096/fj.08-112110
Nikolic, J., Civas, A., Lama, Z., Lagaudrière-Gesbert, C., Blondel, D., 2016. Rabies Virus Infection Induces the Formation of Stress Granules Closely Connected to the Viral Factories. PLOS Pathogens 12, e1005942. https://doi.org/10.1371/journal.ppat.1005942
Nikolic, J., Le Bars, R., Lama, Z., Scrima, N., Lagaudrière-Gesbert, C., Gaudin, Y., Blondel, D., 2017. Negri bodies are viral factories with properties of liquid organelles. Nat Commun 8, 58. https://doi.org/10.1038/s41467-017-00102-9
Nilsson-Payant, B.E., 2022. The Host Factor ANP32A Is Required for Influenza A Virus vRNA and cRNA Synthesis. Journal of Virology 96, 15.
Nobusawa, E., Sato, K., 2006. Comparison of the Mutation Rates of Human Influenza A and B Viruses. Journal of Virology 80, 3675–3678. https://doi.org/10.1128/JVI.80.7.3675-3678.2006
Noda, T., 2012. Native Morphology of Influenza Virions. Frontiers in Microbiology 2.
Noda, T., Kawaoka, Y., 2010. Structure of Influenza Virus Ribonucleoprotein Complexes and Their Packaging into Virions. Rev Med Virol 20, 380–391. https://doi.org/10.1002/rmv.666
Noda, T., Murakami, S., Nakatsu, S., Imai, H., Muramoto, Y., Shindo, K., Sagara, H., Kawaoka, Y., 2018. Importance of the 1+7 configuration of ribonucleoprotein complexes for influenza A virus genome packaging. Nat Commun 9, 54. https://doi.org/10.1038/s41467-017-02517-w
Noda, T., Sagara, H., Yen, A., Takada, A., Kida, H., Cheng, R.H., Kawaoka, Y., 2006. Architecture of ribonucleoprotein complexes in influenza A virus particles. Nature 439, 490–492. https://doi.org/10.1038/nature04378
Noton, S.L., Medcalf, E., Fisher, D., Mullin, A.E., Elton, D., Digard, P., 2007. Identification of the domains of the influenza A virus M1 matrix protein

required for NP binding, oligomerization and incorporation into virions. J Gen Virol 88, 2280–2290. https://doi.org/10.1099/vir.0.82809-0
Nott, T.J., Craggs, T.D., Baldwin, A.J., 2016. Membraneless organelles can melt nucleic acid duplexes and act as biomolecular filters. Nature Chem 8, 569–575. https://doi.org/10.1038/nchem.2519
Nott, T.J., Petsalaki, E., Farber, P., Jervis, D., Fussner, E., Plochowietz, A., Craggs, T.D., Bazett-Jones, D.P., Pawson, T., Forman-Kay, J.D., Baldwin, A.J., 2015. Phase Transition of a Disordered Nuage Protein Generates Environmentally Responsive Membraneless Organelles. Molecular Cell 57, 936–947. https://doi.org/10.1016/j.molcel.2015.01.013
Nturibi, E., Bhagwat, A.R., Coburn, S., Myerburg, M.M., Lakdawala, S.S., 2017. Intracellular Colocalization of Influenza Viral RNA and Rab11A Is Dependent upon Microtubule Filaments. Journal of Virology 91, e01179-17. https://doi.org/10.1128/JVI.01179-17
Odagiri, T., Tobita, K., 1990. Mutation in NS2, a nonstructural protein of influenza A virus, extragenically causes aberrant replication and expression of the PA gene and leads to generation of defective interfering particles. Proc Natl Acad Sci U S A 87, 5988–5992.
Odagiri, T., Tominaga, K., Tobita, K., Ohta, S., 1994. An amino acid change in the non-structural NS2 protein of an influenza A virus mutant is responsible for the generation of defective interfering (DI) particles by amplifying DI RNAs and suppressing complementary RNA synthesis. J Gen Virol 75 (Pt 1), 43–53. https://doi.org/10.1099/0022-1317-75-1-43
Ohkura, T., Momose, F., Ichikawa, R., Takeuchi, K., Morikawa, Y., 2014. Influenza A Virus Hemagglutinin and Neuraminidase Mutually Accelerate Their Apical Targeting through Clustering of Lipid Rafts. J Virol 88, 10039–10055. https://doi.org/10.1128/JVI.00586-14
Oltrogge, L.M., Chaijarasphong, T., Chen, A.W., Bolin, E.R., Marqusee, S., Savage, D.F., 2020. Multivalent interactions between CsoS2 and Rubisco mediate α-carboxysome formation. Nat Struct Mol Biol 27, 281–287. https://doi.org/10.1038/s41594-020-0387-7
O'Neill, R.E., Jaskunas, R., Blobel, G., Palese, P., Moroianu, J., 1995. Nuclear import of influenza virus RNA can be mediated by viral nucleoprotein and transport factors required for protein import. J Biol Chem 270, 22701–22704. https://doi.org/10.1074/jbc.270.39.22701
O'Neill, R.E., Palese, P., 1995. NPI-1, the human homolog of SRP-1, interacts with influenza virus nucleoprotein. Virology 206, 116–125. https://doi.org/10.1016/s0042-6822(95)80026-3
O'Neill, R.E., Talon, J., Palese, P., 1998. The influenza virus NEP (NS2 protein) mediates the nuclear export of viral ribonucleoproteins. EMBO J 17, 288–296. https://doi.org/10.1093/emboj/17.1.288
Ong, J.Y., Torres, J.Z., 2020. Phase Separation in Cell Division. Molecular Cell 80, 9–20. https://doi.org/10.1016/j.molcel.2020.08.007

Ortega, J., Martín-Benito, J., Zürcher, T., Valpuesta, J.M., Carrascosa, J.L., Ortín, J., 2000. Ultrastructural and Functional Analyses of Recombinant Influenza Virus Ribonucleoproteins Suggest Dimerization of Nucleoprotein during Virus Amplification. J Virol 74, 156–163.

Ou, J., Zheng, F., Cheng, J., Ye, S.S., Ye, C., Jia, K., Lu, G., Li, S., 2022. Isolation and Genetic Characterization of Emerging H3N2 Canine Influenza Virus in Guangdong Province, Southern China, 2018–2021. Frontiers in Veterinary Science 9.

Ozawa, M., Fujii, K., Muramoto, Y., Yamada, S., Yamayoshi, S., Takada, A., Goto, H., Horimoto, T., Kawaoka, Y., 2007. Contributions of Two Nuclear Localization Signals of Influenza A Virus Nucleoprotein to Viral Replication. Journal of Virology 81, 30–41. https://doi.org/10.1128/JVI.01434-06

Pappas, G., Kiriaze, I.J., Falagas, M.E., 2008. Insights into infectious disease in the era of Hippocrates. International Journal of Infectious Diseases 12, 347–350. https://doi.org/10.1016/j.ijid.2007.11.003

Parchure, A., Tian, M., Stalder, D., Boyer, C.K., Bearrows, S.C., Rohli, K.E., Zhang, J., Rivera-Molina, F., Ramazanov, B.R., Mahata, S.K., Wang, Y., Stephens, S.B., Gershlick, D.C., von Blume, J., 2022. Liquid-liquid phase separation facilitates the biogenesis of secretory storage granules. J Cell Biol 221, e202206132. https://doi.org/10.1083/jcb.202206132

Park, H.-S., Liu, G., Thulasi Raman, S.N., Landreth, S.L., Liu, Q., Zhou, Y., 2018. NS1 Protein of 2009 Pandemic Influenza A Virus Inhibits Porcine NLRP3 Inflammasome-Mediated Interleukin-1 Beta Production by Suppressing ASC Ubiquitination. Journal of Virology 92, e00022-18. https://doi.org/10.1128/JVI.00022-18

Parrish, C.R., Murcia, P.R., Holmes, E.C., 2015. Influenza Virus Reservoirs and Intermediate Hosts: Dogs, Horses, and New Possibilities for Influenza Virus Exposure of Humans. J Virol 89, 2990–2994. https://doi.org/10.1128/JVI.03146-14

Patel, A., Lee, H.O., Jawerth, L., Maharana, S., Jahnel, M., Hein, M.Y., Stoynov, S., Mahamid, J., Saha, S., Franzmann, T.M., Pozniakovski, A., Poser, I., Maghelli, N., Royer, L.A., Weigert, M., Myers, E.W., Grill, S., Drechsel, D., Hyman, A.A., Alberti, S., 2015. A Liquid-to-Solid Phase Transition of the ALS Protein FUS Accelerated by Disease Mutation. Cell 162, 1066–1077. https://doi.org/10.1016/j.cell.2015.07.047

Patel, A., Malinovska, L., Saha, S., Wang, J., Alberti, S., Krishnan, Y., Hyman, A.A., 2017. ATP as a biological hydrotrope. Science 356, 753–756. https://doi.org/10.1126/science.aaf6846

Patel, A., Mitrea, D., Namasivayam, V., Murcko, M.A., Wagner, M., Klein, I.A., 2022. Principles and functions of condensate modifying drugs. Frontiers in Molecular Biosciences 9.

Paterson, D., Fodor, E., 2012. Emerging Roles for the Influenza A Virus Nuclear Export Protein (NEP). PLOS Pathogens 8, e1003019. https://doi.org/10.1371/journal.ppat.1003019

Pauly, M.D., Procario, M.C., Lauring, A.S., 2017. A novel twelve class fluctuation test reveals higher than expected mutation rates for influenza A viruses. eLife 6, e26437. https://doi.org/10.7554/eLife.26437

Peacock, T.P., Sheppard, C.M., Staller, E., Frise, R., Swann, O.C., Goldhill, D.H., Long, J.S., Barclay, W.S., 2020a. Mammalian ANP32A and ANP32B proteins drive alternative avian influenza virus polymerase adaptations. https://doi.org/10.1101/2020.09.03.282384

Peacock, T.P., Swann, O.C., Salvesen, H.A., Staller, E., Leung, P.B., Goldhill, D.H., Zhou, H., Lillico, S.G., Whitelaw, C.B.A., Long, J.S., Barclay, W.S., 2020b. Swine ANP32A Supports Avian Influenza Virus Polymerase. J Virol 94, e00132-20. https://doi.org/10.1128/JVI.00132-20

Peeples, W., Rosen, M.K., 2021. Mechanistic dissection of increased enzymatic rate in a phase-separated compartment. Nat Chem Biol 17, 693–702. https://doi.org/10.1038/s41589-021-00801-x

Perales, B., de la Luna, S., Palacios, I., Ortín, J., 1996. Mutational analysis identifies functional domains in the influenza A virus PB2 polymerase subunit. J Virol 70, 1678–1686. https://doi.org/10.1128/JVI.70.3.1678-1686.1996

Perez, J.T., Varble, A., Sachidanandam, R., Zlatev, I., Manoharan, M., García-Sastre, A., tenOever, B.R., 2010. Influenza A virus-generated small RNAs regulate the switch from transcription to replication. Proc Natl Acad Sci U S A 107, 11525–11530. https://doi.org/10.1073/pnas.1001984107

Perry, S.L., 2019. Phase separation: Bridging polymer physics and biology. Current Opinion in Colloid & Interface Science, Special Topic Section: Outstanding Young Researchers in Colloid and Interface Science 39, 86–97. https://doi.org/10.1016/j.cocis.2019.01.007

Petrova, V.N., Russell, C.A., 2018. The evolution of seasonal influenza viruses. Nat Rev Microbiol 16, 47–60. https://doi.org/10.1038/nrmicro.2017.118

Pflug, A., Lukarska, M., Resa-Infante, P., Reich, S., Cusack, S., 2017. Structural insights into RNA synthesis by the influenza virus transcription-replication machine. Virus Research, Viral polymerases 234, 103–117. https://doi.org/10.1016/j.virusres.2017.01.013

Phair, R.D., Gorski, S.A., Misteli, T., 2003. Measurement of Dynamic Protein Binding to Chromatin In Vivo, Using Photobleaching Microscopy, in: Methods in Enzymology, Chromatin and Chromatin Remodeling Enzymes, Part A. Academic Press, pp. 393–414. https://doi.org/10.1016/S0076-6879(03)75025-3

Pichlmair, A., Schulz, O., Tan, C.P., Näslund, T.I., Liljeström, P., Weber, F., Reis e Sousa, C., 2006. RIG-I-Mediated Antiviral Responses to

Single-Stranded RNA Bearing 5'-Phosphates. Science 314, 997–1001. https://doi.org/10.1126/science.1132998
Pila-Castellanos, I., Molino, D., McKellar, J., Lines, L., Graca, J.D., Tauziet, M., Chanteloup, L., Mikaelian, I., Meyniel-Schicklin, L., Codogno, P., Vonderscher, J., Delevoye, C., Moncorgé, O., Meldrum, E., Goujon, C., Morel, E., Chassey, B. de, 2021. Mitochondrial morphodynamics alteration induced by influenza virus infection as a new antiviral strategy. PLOS Pathogens 17, e1009340. https://doi.org/10.1371/journal.ppat.1009340
Pinto, L.H., Dieckmann, G.R., Gandhi, C.S., Papworth, C.G., Braman, J., Shaughnessy, M.A., Lear, J.D., Lamb, R.A., DeGrado, W.F., 1997. A functionally defined model for the M2 proton channel of influenza A virus suggests a mechanism for its ion selectivity. Proceedings of the National Academy of Sciences 94, 11301–11306. https://doi.org/10.1073/pnas.94.21.11301
Pinto, L.H., Holsinger, L.J., Lamb, R.A., 1992. Influenza virus M2 protein has ion channel activity. Cell 69, 517–528. https://doi.org/10.1016/0092-8674(92)90452-I
Pinto, R.M., Lycett, S., Gaunt, E., Digard, P., 2021. Accessory Gene Products of Influenza A Virus. Cold Spring Harb Perspect Med 11, a038380. https://doi.org/10.1101/cshperspect.a038380
Pleschka, S., Wolff, T., Ehrhardt, C., Hobom, G., Planz, O., Rapp, U.R., Ludwig, S., 2001. Influenza virus propagation is impaired by inhibition of the Raf/MEK/ERK signalling cascade. Nat Cell Biol 3, 301–305. https://doi.org/10.1038/35060098
Plotch, S.J., Bouloy, M., Ulmanen, I., Krug, R.M., 1981. A unique cap(m7GpppXm)-dependent influenza virion endonuclease cleaves capped RNAs to generate the primers that initiate viral RNA transcription. Cell 23, 847–858. https://doi.org/10.1016/0092-8674(81)90449-9
Pohl, M.O., Lanz, C., Stertz, S., 2016. Late stages of the influenza A virus replication cycle-a tight interplay between virus and host. J Gen Virol 97, 2058–2072. https://doi.org/10.1099/jgv.0.000562
Pons, M.W., Schulze, I.T., Hirst, G.K., 1969. Isolation and characterization of the ribonucleoprotein of influenza virus. Virology 39, 250–259. https://doi.org/10.1016/0042-6822(69)90045-2
Poon, L.L., Fodor, E., Brownlee, G.G., 2000. Polyuridylated mRNA synthesized by a recombinant influenza virus is defective in nuclear export. J Virol 74, 418–427. https://doi.org/10.1128/jvi.74.1.418-427.2000
Poon, L.L., Pritlove, D.C., Fodor, E., Brownlee, G.G., 1999. Direct evidence that the poly(A) tail of influenza A virus mRNA is synthesized by reiterative copying of a U track in the virion RNA template. J Virol 73, 3473–3476. https://doi.org/10.1128/JVI.73.4.3473-3476.1999
Portela, A., Digard, P., 2002. The influenza virus nucleoprotein: a multifunctional RNA-binding protein pivotal to virus replication. Journal

of General Virology 83, 723–734. https://doi.org/10.1099/0022-1317-83-4-723
Portz, B., Shorter, J., 2021. Biochemical Timekeeping Via Reentrant Phase Transitions. Journal of Molecular Biology, Phase Separation in Biology and Disease: The Next Chapter 433, 166794. https://doi.org/10.1016/j.jmb.2020.166794
Posey, A.E., Holehouse, A.S., Pappu, R.V., 2018. Chapter One - Phase Separation of Intrinsically Disordered Proteins, in: Rhoades, E. (Ed.), Methods in Enzymology, Intrinsically Disordered Proteins. Academic Press, pp. 1–30. https://doi.org/10.1016/bs.mie.2018.09.035
Potel, C.M., Kurzawa, N., Becher, I., Typas, A., Mateus, A., Savitski, M.M., 2021. Impact of phosphorylation on thermal stability of proteins. Nat Methods 18, 757–759. https://doi.org/10.1038/s41592-021-01177-5
Pumroy, R.A., Ke, S., Hart, D.J., Zachariae, U., Cingolani, G., 2015. Molecular determinants for nuclear import of Influenza A PB2 by importin α isoforms 3 and 7. Structure 23, 374–384. https://doi.org/10.1016/j.str.2014.11.015
Qamar, S., Wang, G., Randle, S.J., Ruggeri, F.S., Varela, J.A., Lin, J.Q., Phillips, E.C., Miyashita, A., Williams, D., Ströhl, F., Meadows, W., Ferry, R., Dardov, V.J., Tartaglia, G.G., Farrer, L.A., Kaminski Schierle, G.S., Kaminski, C.F., Holt, C.E., Fraser, P.E., Schmitt-Ulms, G., Klenerman, D., Knowles, T., Vendruscolo, M., St George-Hyslop, P., 2018. FUS Phase Separation Is Modulated by a Molecular Chaperone and Methylation of Arginine Cation-π Interactions. Cell 173, 720-734.e15. https://doi.org/10.1016/j.cell.2018.03.056
Quiroz, F.G., Chilkoti, A., 2015. Sequence heuristics to encode phase behaviour in intrinsically disordered protein polymers. Nat Mater 14, 1164–1171. https://doi.org/10.1038/nmat4418
Rabouille, C., Alberti, S., 2017. Cell adaptation upon stress: the emerging role of membrane-less compartments. Current Opinion in Cell Biology, Cell Organelles 47, 34–42. https://doi.org/10.1016/j.ceb.2017.02.006
Rai, A.K., Chen, J.-X., Selbach, M., Pelkmans, L., 2018. Kinase-controlled phase transition of membraneless organelles in mitosis. Nature 559, 211–216. https://doi.org/10.1038/s41586-018-0279-8
Rajsbaum, R., Albrecht, R.A., Wang, M.K., Maharaj, N.P., Versteeg, G.A., Nistal-Villán, E., García-Sastre, A., Gack, M.U., 2012. Species-Specific Inhibition of RIG-I Ubiquitination and IFN Induction by the Influenza A Virus NS1 Protein. PLOS Pathogens 8, e1003059. https://doi.org/10.1371/journal.ppat.1003059
Ramos-Nascimento, A., Kellen, B., Ferreira, F., Alenquer, M., Vale-Costa, S., Raposo, G., Delevoye, C., Amorim, M.J., 2017. KIF13A mediates trafficking of influenza A virus ribonucleoproteins. Journal of Cell Science 130, 4038–4050. https://doi.org/10.1242/jcs.210807
Ranganathan, S., Shakhnovich, E.I., 2020. Dynamic metastable long-living droplets formed by sticker-spacer proteins. eLife 9, e56159. https://doi.org/10.7554/eLife.56159

Rao, P., Yuan, W., Krug, R.M., 2003. Crucial role of CA cleavage sites in the cap-snatching mechanism for initiating viral mRNA synthesis. EMBO J 22, 1188–1198. https://doi.org/10.1093/emboj/cdg109

Reich, S., Guilligay, D., Pflug, A., Malet, H., Berger, I., Crépin, T., Hart, D., Lunardi, T., Nanao, M., Ruigrok, R.W.H., Cusack, S., 2014. Structural insight into cap-snatching and RNA synthesis by influenza polymerase. Nature 516, 361–366. https://doi.org/10.1038/nature14009

Reineke, L.C., Tsai, W.-C., Jain, A., Kaelber, J.T., Jung, S.Y., Lloyd, R.E., 2017. Casein Kinase 2 Is Linked to Stress Granule Dynamics through Phosphorylation of the Stress Granule Nucleating Protein G3BP1. Molecular and Cellular Biology 37, e00596-16. https://doi.org/10.1128/MCB.00596-16

Reinhard, F.B.M., Eberhard, D., Werner, T., Franken, H., Childs, D., Doce, C., Savitski, M.F., Huber, W., Bantscheff, M., Savitski, M.M., Drewes, G., 2015. Thermal proteome profiling monitors ligand interactions with cellular membrane proteins. Nat Methods 12, 1129–1131. https://doi.org/10.1038/nmeth.3652

Ren, H., Jin, Y., Hu, M., Zhou, J., Song, T., Huang, Z., Li, B., Li, K., Zhou, W., Dai, H., Shi, W., Yue, J., Liang, L., 2016. Ecological dynamics of influenza A viruses: cross-species transmission and global migration. Sci Rep 6, 36839. https://doi.org/10.1038/srep36839

Riback, J.A., Brangwynne, C.P., 2020. Can phase separation buffer cellular noise? Science 367, 364–365. https://doi.org/10.1126/science.aba0446

Riback, J.A., Zhu, L., Ferrolino, M.C., Tolbert, M., Mitrea, D.M., Sanders, D.W., Wei, M.-T., Kriwacki, R.W., Brangwynne, C.P., 2020. Composition-dependent thermodynamics of intracellular phase separation. Nature 581, 209–214. https://doi.org/10.1038/s41586-020-2256-2

Richardson, J.C., Akkina, R.K., 1991. NS2 protein of influenza virus is found in purified virus and phosphorylated in infected cells. Archives of Virology 116, 69–80. https://doi.org/10.1007/BF01319232

Rigby, R.E., Wise, H.M., Smith, N., Digard, P., Rehwinkel, J., 2019. PA-X antagonises MAVS-dependent accumulation of early type I interferon messenger RNAs during influenza A virus infection. Sci Rep 9, 7216. https://doi.org/10.1038/s41598-019-43632-6

Risso-Ballester, J., Galloux, M., Cao, J., Le Goffic, R., Hontonnou, F., Jobart-Malfait, A., Desquesnes, A., Sake, S.M., Haid, S., Du, M., Zhang, X., Zhang, H., Wang, Z., Rincheval, V., Zhang, Y., Pietschmann, T., Eléouët, J.-F., Rameix-Welti, M.-A., Altmeyer, R., 2021. A condensate-hardening drug blocks RSV replication in vivo. Nature 595, 596–599. https://doi.org/10.1038/s41586-021-03703-z

Robb, N.C., Chase, G., Bier, K., Vreede, F.T., Shaw, P.-C., Naffakh, N., Schwemmle, M., Fodor, E., 2011. The influenza A virus NS1 protein

interacts with the nucleoprotein of viral ribonucleoprotein complexes. J Virol 85, 5228–5231. https://doi.org/10.1128/JVI.02562-10
Robb, N.C., Smith, M., Vreede, F.T., Fodor, E., 2009. NS2/NEP protein regulates transcription and replication of the influenza virus RNA genome. Journal of General Virology 90, 1398–1407. https://doi.org/10.1099/vir.0.009639-0
Roberts, P.C., Lamb, R.A., Compans, R.W., 1998. The M1 and M2 Proteins of Influenza A Virus Are Important Determinants in Filamentous Particle Formation. Virology 240, 127–137. https://doi.org/10.1006/viro.1997.8916
Robertson, J.S., Schubert, M., Lazzarini, R.A., 1981. Polyadenylation sites for influenza virus mRNA. J Virol 38, 157–163. https://doi.org/10.1128/JVI.38.1.157-163.1981
Rodriguez, A., Pérez-González, A., Nieto, A., 2011. Cellular human CLE/C14orf166 protein interacts with influenza virus polymerase and is required for viral replication. J Virol 85, 12062–12066. https://doi.org/10.1128/JVI.00684-11
Rosenthal, P.B., Zhang, X., Formanowski, F., Fitz, W., Wong, C.-H., Meier-Ewert, H., Skehel, J.J., Wiley, D.C., 1998. Structure of the haemagglutinin-esterase-fusion glycoprotein of influenza C virus. Nature 396, 92–96. https://doi.org/10.1038/23974
Rosowski, K.A., Vidal-Henriquez, E., Zwicker, D., Style, R.W., Dufresne, E.R., 2020. Elastic stresses reverse Ostwald ripening. Soft Matter 16, 5892–5897. https://doi.org/10.1039/D0SM00628A
Rossman, J.S., Lamb, R.A., 2011. Influenza virus assembly and budding. Virology, Special Reviews Issue 2011 411, 229–236. https://doi.org/10.1016/j.virol.2010.12.003
Roy, A.-M.M., Parker, J.S., Parrish, C.R., Whittaker, G.R., 2000. Early Stages of Influenza Virus Entry into Mv-1 Lung Cells: Involvement of Dynamin. Virology 267, 17–28. https://doi.org/10.1006/viro.1999.0109
Ruigrok, R.W., Baudin, F., 1995. Structure of influenza virus ribonucleoprotein particles. II. Purified RNA-free influenza virus ribonucleoprotein forms structures that are indistinguishable from the intact influenza virus ribonucleoprotein particles. J Gen Virol 76 (Pt 4), 1009–1014. https://doi.org/10.1099/0022-1317-76-4-1009
Runnström, J., 1963. Sperm-induced protrusions in sea urchin oocytes: A study of phase separation and mixing in living cytoplasm. Developmental Biology 7, 38–50. https://doi.org/10.1016/0012-1606(63)90105-2
Rust, M.J., Lakadamyali, M., Zhang, F., Zhuang, X., 2004. Assembly of endocytic machinery around individual influenza viruses during viral entry. Nat Struct Mol Biol 11, 567–573. https://doi.org/10.1038/nsmb769
Saha, D., Iannuccelli, M., Brun, C., Zanzoni, A., Licata, L., 2022. The Intricacy of the Viral-Human Protein Interaction Networks: Resources, Data, and Analyses. Frontiers in Microbiology 13.

Saini, B., Mukherjee, T.K., 2022. Biomolecular Condensate Regulates Enzymatic Activity under Crowded Milieu: Synchronization of Liquid-Liquid Phase separation and Enzymatic Transformation. https://doi.org/10.1101/2022.06.16.496378

Saito, M., Hess, D., Eglinger, J., Fritsch, A.W., Kreysing, M., Weinert, B.T., Choudhary, C., Matthias, P., 2019. Acetylation of intrinsically disordered regions regulates phase separation. Nat Chem Biol 15, 51–61. https://doi.org/10.1038/s41589-018-0180-7

Sakai, T., Nishimura, S.I., Naito, T., Saito, M., 2017. Influenza A virus hemagglutinin and neuraminidase act as novel motile machinery. Sci Rep 7, 45043. https://doi.org/10.1038/srep45043

Sanchez, T.W., Ronzetti, M.H., Owens, A.E., Antony, M., Voss, T., Wallgren, E., Talley, D., Balakrishnan, K., Leyes Porello, S.E., Rai, G., Marugan, J.J., Michael, S.G., Baljinnyam, B., Southall, N., Simeonov, A., Henderson, M.J., 2022. Real-Time Cellular Thermal Shift Assay to Monitor Target Engagement. ACS Chem. Biol. 17, 2471–2482. https://doi.org/10.1021/acschembio.2c00334

Sanders, D.W., Kedersha, N., Lee, D.S.W., Strom, A.R., Drake, V., Riback, J.A., Bracha, D., Eeftens, J.M., Iwanicki, A., Wang, A., Wei, M.-T., Whitney, G., Lyons, S.M., Anderson, P., Jacobs, W.M., Ivanov, P., Brangwynne, C.P., 2020. Competing Protein-RNA Interaction Networks Control Multiphase Intracellular Organization. Cell 181, 306-324.e28. https://doi.org/10.1016/j.cell.2020.03.050

Sarkies, K.W., Frankel, N.E., 1971. Nucleation Theory with a Nonclassical Free Energy. J. Chem. Phys. 54, 433–434. https://doi.org/10.1063/1.1674627

Sato, M., Yoshida, S., Iida, K., Tomozawa, T., Kido, H., Yamashita, M., 2003. A Novel Influenza A Virus Activating Enzyme from Porcine Lung: Purification and Characterization 384, 219–227. https://doi.org/10.1515/BC.2003.024

Sato, R., Okura, T., Kawahara, M., Takizawa, N., Momose, F., Morikawa, Y., 2019. Apical Trafficking Pathways of Influenza A Virus HA and NA via Rab17- and Rab23-Positive Compartments. Frontiers in Microbiology 10.

Saunders-Hastings, P.R., Krewski, D., 2016. Reviewing the History of Pandemic Influenza: Understanding Patterns of Emergence and Transmission. Pathogens 5, 66. https://doi.org/10.3390/pathogens5040066

Savastano, A., Ibáñez de Opakua, A., Rankovic, M., Zweckstetter, M., 2020. Nucleocapsid protein of SARS-CoV-2 phase separates into RNA-rich polymerase-containing condensates. Nat Commun 11, 6041. https://doi.org/10.1038/s41467-020-19843-1

Savitski, M.M., Reinhard, F.B.M., Franken, H., Werner, T., Savitski, M.F., Eberhard, D., Molina, D.M., Jafari, R., Dovega, R.B., Klaeger, S., Kuster, B., Nordlund, P., Bantscheff, M., Drewes, G., 2014. Tracking

cancer drugs in living cells by thermal profiling of the proteome. Science 346, 1255784. https://doi.org/10.1126/science.1255784
Schneider, M., Johnson, J.R., Krogan, N.J., Chanda, S.K., 2016. The Virus–Host Interactome. Viral Pathogenesis 157–167. https://doi.org/10.1016/B978-0-12-800964-2.00012-4
Schrauwen, E.J.A., de Graaf, M., Herfst, S., Rimmelzwaan, G.F., Osterhaus, A.D.M.E., Fouchier, R.A.M., 2014. Determinants of virulence of influenza A virus. Eur J Clin Microbiol Infect Dis 33, 479–490. https://doi.org/10.1007/s10096-013-1984-8
Sederdahl, B.K., Williams, J.V., 2020. Epidemiology and Clinical Characteristics of Influenza C Virus. Viruses 12, 89. https://doi.org/10.3390/v12010089
Seim, I., Posey, A.E., Snead, W.T., Stormo, B.M., Klotsa, D., Pappu, R.V., Gladfelter, A.S., 2022. Dilute phase oligomerization can oppose phase separation and modulate material properties of a ribonucleoprotein condensate. Proceedings of the National Academy of Sciences 119, e2120799119. https://doi.org/10.1073/pnas.2120799119
Seladi-Schulman, J., Steel, J., Lowen, A.C., 2013. Spherical Influenza Viruses Have a Fitness Advantage in Embryonated Eggs, while Filament-Producing Strains Are Selected In Vivo. Journal of Virology 87, 13343–13353. https://doi.org/10.1128/JVI.02004-13
Selkrig, J., Stanifer, M., Mateus, A., Mitosch, K., Barrio-Hernandez, I., Rettel, M., Kim, H., Voogdt, C.G.P., Walch, P., Kee, C., Kurzawa, N., Stein, F., Potel, C., Jarzab, A., Kuster, B., Bartenschlager, R., Boulant, S., Beltrao, P., Typas, A., Savitski, M.M., 2021. SARS-CoV-2 infection remodels the host protein thermal stability landscape. Molecular Systems Biology 17, e10188. https://doi.org/10.15252/msb.202010188
Selman, M., Dankar, S.K., Forbes, N.E., Jia, J.-J., Brown, E.G., 2012. Adaptive mutation in influenza A virus non-structural gene is linked to host switching and induces a novel protein by alternative splicing. Emerg Microbes Infect 1, e42. https://doi.org/10.1038/emi.2012.38
Sengupta, P., Seo, A.Y., Pasolli, H.A., Song, Y.E., Johnson, M.C., Lippincott-Schwartz, J., 2019. A lipid-based partitioning mechanism for selective incorporation of proteins into membranes of HIV particles. Nat Cell Biol 21, 452–461. https://doi.org/10.1038/s41556-019-0300-y
Shafiuddin, M., Boon, A.C.M., 2019. RNA sequence features are at the core of Influenza A virus genome packaging. J Mol Biol 431, 4217–4228. https://doi.org/10.1016/j.jmb.2019.03.018
Shapiro, G.I., Gurney, T., Krug, R.M., 1987. Influenza virus gene expression: control mechanisms at early and late times of infection and nuclear-cytoplasmic transport of virus-specific RNAs. J Virol 61, 764–773.
Shapiro, G.I., Krug, R.M., 1988. Influenza virus RNA replication in vitro: synthesis of viral template RNAs and virion RNAs in the absence of

an added primer. J Virol 62, 2285–2290. https://doi.org/10.1128/JVI.62.7.2285-2290.1988
Sharma, K., Tripathi, S., Ranjan, P., Kumar, P., Garten, R., Deyde, V., Katz, J.M., Cox, N.J., Lal, R.B., Sambhara, S., Lal, S.K., 2011. Influenza A Virus Nucleoprotein Exploits Hsp40 to Inhibit PKR Activation. PLOS ONE 6, e20215. https://doi.org/10.1371/journal.pone.0020215
Shaw, M.L., Stone, K.L., Colangelo, C.M., Gulcicek, E.E., Palese, P., 2008. Cellular Proteins in Influenza Virus Particles. PLOS Pathogens 4, e1000085. https://doi.org/10.1371/journal.ppat.1000085
Shaw, M.W., Lamb, R.A., 1984. A specific sub-set of host-cell mRNAs prime influenza virus mRNA synthesis. Virus Research 1, 455–467. https://doi.org/10.1016/0168-1702(84)90003-0
Sheu-Gruttadauria, J., MacRae, I.J., 2018. Phase Transitions in the Assembly and Function of Human miRISC. Cell 173, 946-957.e16. https://doi.org/10.1016/j.cell.2018.02.051
Shevtsov, S.P., Dundr, M., 2011. Nucleation of nuclear bodies by RNA. Nat Cell Biol 13, 167–173. https://doi.org/10.1038/ncb2157
Shih, S.R., Krug, R.M., 1996. Novel exploitation of a nuclear function by influenza virus: the cellular SF2/ASF splicing factor controls the amount of the essential viral M2 ion channel protein in infected cells. EMBO J 15, 5415–5427.
Shimizu, T., Takizawa, N., Watanabe, K., Nagata, K., Kobayashi, N., 2011. Crucial role of the influenza virus NS2 (NEP) C-terminal domain in M1 binding and nuclear export of vRNP. FEBS Letters 585, 41–46. https://doi.org/10.1016/j.febslet.2010.11.017
Shimizu, Y., Abiko, C., Ikeda, T., Mizuta, K., Matsuzaki, Y., 2015. Influenza C Virus and Human Metapneumovirus Infections in Hospitalized Children With Lower Respiratory Tract Illness. The Pediatric Infectious Disease Journal 34, 1273–1275. https://doi.org/10.1097/INF.0000000000000863
Shimobayashi, S.F., Ronceray, P., Sanders, D.W., Haataja, M.P., Brangwynne, C.P., 2021. Nucleation landscape of biomolecular condensates. Nature 599, 503–506. https://doi.org/10.1038/s41586-021-03905-5
Shin, Y., Brangwynne, C.P., 2017. Liquid phase condensation in cell physiology and disease. Science 357, eaaf4382. https://doi.org/10.1126/science.aaf4382
Shope, R.E., 1931. The Etiology of Swine Influenza. Science 73, 214–215. https://doi.org/10.1126/science.73.1886.214
Sieczkarski, S.B., Whittaker, G.R., 2002. Influenza Virus Can Enter and Infect Cells in the Absence of Clathrin-Mediated Endocytosis. Journal of Virology 76, 10455–10464. https://doi.org/10.1128/JVI.76.20.10455-10464.2002
Sikora, D., Rocheleau, L., Brown, E.G., Pelchat, M., 2014. Deep sequencing reveals the eight facets of the influenza A/HongKong/1/1968 (H3N2)

virus cap-snatching process. Sci Rep 4, 6181. https://doi.org/10.1038/srep06181
Silverman, R.H., Weiss, S.R., 2014. Viral Phosphodiesterases That Antagonize Double-Stranded RNA Signaling to RNase L by Degrading 2-5A. Journal of Interferon & Cytokine Research 34, 455–463. https://doi.org/10.1089/jir.2014.0007
Simons, K., Ikonen, E., 1997. Functional rafts in cell membranes. Nature 387, 569–572. https://doi.org/10.1038/42408
Skorko, R., Summers, D.F., Galarza, J.M., 1991. Influenza A virus in vitro transcription: Roles of NS1 and NP proteins in regulating RNA synthesis. Virology 180, 668–677. https://doi.org/10.1016/0042-6822(91)90080-U
Smieszek, T., Lazzari, G., Salathé, M., 2019. Assessing the Dynamics and Control of Droplet- and Aerosol-Transmitted Influenza Using an Indoor Positioning System. Sci Rep 9, 2185. https://doi.org/10.1038/s41598-019-38825-y
Smith, W., Andrewes, C.H., Laidlaw, P.P., 1933. A VIRUS OBTAINED FROM INFLUENZA PATIENTS. The Lancet, Originally published as Volume 2, Issue 5732 222, 66–68. https://doi.org/10.1016/S0140-6736(00)78541-2
Snead, W.T., Gladfelter, A.S., 2019. The Control Centers of Biomolecular Phase Separation: How Membrane Surfaces, PTMs, and Active Processes Regulate Condensation. Molecular Cell 76, 295–305. https://doi.org/10.1016/j.molcel.2019.09.016
Snead, W.T., Jalihal, A.P., Gerbich, T.M., Seim, I., Hu, Z., Gladfelter, A.S., 2022. Membrane surfaces regulate assembly of ribonucleoprotein condensates. Nat Cell Biol 24, 461–470. https://doi.org/10.1038/s41556-022-00882-3
Sousa, A.L., Vale-Costa, S., Amorim, M.J., Tranfield, E.M., 2017. Using correlative light and electron microscopy to understand influenza A viral assembly. Ultrastructural Pathology 41, 80–81. https://doi.org/10.1080/01913123.2016.1269508
Sovinova, O., Tumova, B., Pouska, F., Nemec, J., 1958. Isolation of a virus causing respiratory disease in horses. Acta Virol 2, 52–61.
Spannl, S., Tereshchenko, M., Mastromarco, G.J., Ihn, S.J., Lee, H.O., 2019. Biomolecular condensates in neurodegeneration and cancer. Traffic 20, 890–911. https://doi.org/10.1111/tra.12704
Sreenivasan, C., Thomas, M., Sheng, Z., Hause, B.M., Collin, E.A., Knudsen, D.E.B., Pillatzki, A., Nelson, E., Wang, D., Kaushik, R.S., Li, F., 2015. Replication and Transmission of the Novel Bovine Influenza D Virus in a Guinea Pig Model. Journal of Virology 89, 11990–12001. https://doi.org/10.1128/JVI.01630-15
Sridharan, S., Hernandez-Armendariz, A., Kurzawa, N., Potel, C.M., Memon, D., Beltrao, P., Bantscheff, M., Huber, W., Cuylen-Haering, S., Savitski, M.M., 2022. Systematic discovery of biomolecular

condensate-specific protein phosphorylation. Nat Chem Biol 1–11. https://doi.org/10.1038/s41589-022-01062-y

Sridharan, S., Kurzawa, N., Werner, T., Günthner, I., Helm, D., Huber, W., Bantscheff, M., Savitski, M.M., 2019. Proteome-wide solubility and thermal stability profiling reveals distinct regulatory roles for ATP. Nat Commun 10, 1155. https://doi.org/10.1038/s41467-019-09107-y

Staller, E., Sheppard, C.M., Neasham, P.J., Mistry, B., Peacock, T.P., Goldhill, D.H., Long, J.S., Barclay, W.S., 2019. ANP32 Proteins Are Essential for Influenza Virus Replication in Human Cells. J Virol 93, e00217-19. https://doi.org/10.1128/JVI.00217-19

Stauffer, S., Feng, Y., Nebioglu, F., Heilig, R., Picotti, P., Helenius, A., 2014. Stepwise Priming by Acidic pH and a High K+ Concentration Is Required for Efficient Uncoating of Influenza A Virus Cores after Penetration. Journal of Virology 88, 13029–13046. https://doi.org/10.1128/JVI.01430-14

Stieneke-Gröber, A., Vey, M., Angliker, H., Shaw, E., Thomas, G., Roberts, C., Klenk, H.D., Garten, W., 1992. Influenza virus hemagglutinin with multibasic cleavage site is activated by furin, a subtilisin-like endoprotease. EMBO J 11, 2407–2414. https://doi.org/10.1002/j.1460-2075.1992.tb05305.x

Strom, A.R., Brangwynne, C.P., 2019. The liquid nucleome – phase transitions in the nucleus at a glance. Journal of Cell Science 132, jcs235093. https://doi.org/10.1242/jcs.235093

Su, L., Mosquera, J., Mabesoone, M.F.J., Schoenmakers, S.M.C., Muller, C., Vleugels, M.E.J., Dhiman, S., Wijker, S., Palmans, A.R.A., Meijer, E.W., 2022. Dilution-induced gel-sol-gel-sol transitions by competitive supramolecular pathways in water. Science. https://doi.org/10.1126/science.abn3438

Su, S., Fu, X., Li, G., Kerlin, F., Veit, M., 2017. Novel Influenza D virus: Epidemiology, pathology, evolution and biological characteristics. Virulence 8, 1580–1591. https://doi.org/10.1080/21505594.2017.1365216

Su, W.-C., Chen, Y.-C., Tseng, C.-H., Hsu, P.W.-C., Tung, K.-F., Jeng, K.-S., Lai, M.M.C., 2013. Pooled RNAi screen identifies ubiquitin ligase Itch as crucial for influenza A virus release from the endosome during virus entry. Proceedings of the National Academy of Sciences 110, 17516–17521. https://doi.org/10.1073/pnas.1312374110

Su, W.-C., Hsu, S.-F., Lee, Y.-Y., Jeng, K.-S., Lai, M.M.C., 2015. A Nucleolar Protein, Ribosomal RNA Processing 1 Homolog B (RRP1B), Enhances the Recruitment of Cellular mRNA in Influenza Virus Transcription. J Virol 89, 11245–11255. https://doi.org/10.1128/JVI.01487-15

Su, X., Ditlev, J.A., Hui, E., Xing, W., Banjade, S., Okrut, J., King, D.S., Taunton, J., Rosen, M.K., Vale, R.D., 2016. Phase separation of signaling molecules promotes T cell receptor signal transduction. Science 352, 595–599. https://doi.org/10.1126/science.aad9964

Sugita, Y., Noda, T., Sagara, H., Kawaoka, Y., 2011. Ultracentrifugation deforms unfixed influenza A virions. J Gen Virol 92, 2485–2493. https://doi.org/10.1099/vir.0.036715-0

Sugita, Y., Sagara, H., Noda, T., Kawaoka, Y., 2013. Configuration of Viral Ribonucleoprotein Complexes within the Influenza A Virion. Journal of Virology 87, 12879–12884. https://doi.org/10.1128/JVI.02096-13

Sugiyama, K., Kawaguchi, A., Okuwaki, M., Nagata, K., 2015. pp32 and APRIL are host cell-derived regulators of influenza virus RNA synthesis from cRNA. eLife 4, e08939. https://doi.org/10.7554/eLife.08939

Sugiyama, K., Obayashi, E., Kawaguchi, A., Suzuki, Y., Tame, J.R.H., Nagata, K., Park, S.-Y., 2009. Structural insight into the essential PB1–PB2 subunit contact of the influenza virus RNA polymerase. EMBO J 28, 1803–1811. https://doi.org/10.1038/emboj.2009.138

Sui, X., Pires, D.E.V., Ormsby, A.R., Cox, D., Nie, S., Vecchi, G., Vendruscolo, M., Ascher, D.B., Reid, G.E., Hatters, D.M., 2020. Widespread remodeling of proteome solubility in response to different protein homeostasis stresses. Proceedings of the National Academy of Sciences 117, 2422–2431. https://doi.org/10.1073/pnas.1912897117

Sun, L., Wu, J., Du, F., Chen, X., Chen, Z.J., 2013. Cyclic GMP-AMP synthase is a cytosolic DNA sensor that activates the type I interferon pathway. Science 339, 786–791. https://doi.org/10.1126/science.1232458

Sun, X., Shi, Y., Lu, X., He, J., Gao, F., Yan, J., Qi, J., Gao, G.F., 2013. Bat-Derived Influenza Hemagglutinin H17 Does Not Bind Canonical Avian or Human Receptors and Most Likely Uses a Unique Entry Mechanism. Cell Reports 3, 769–778. https://doi.org/10.1016/j.celrep.2013.01.025

Suzuki, Y., Ito, T., Suzuki, T., Holland, R.E., Chambers, T.M., Kiso, M., Ishida, H., Kawaoka, Y., 2000. Sialic Acid Species as a Determinant of the Host Range of Influenza A Viruses. Journal of Virology 74, 11825–11831. https://doi.org/10.1128/JVI.74.24.11825-11831.2000

Swale, C., Monod, A., Tengo, L., Labaronne, A., Garzoni, F., Bourhis, J.-M., Cusack, S., Schoehn, G., Berger, I., Ruigrok, R.W., Crépin, T., 2016. Structural characterization of recombinant IAV polymerase reveals a stable complex between viral PA-PB1 heterodimer and host RanBP5. Sci Rep 6, 24727. https://doi.org/10.1038/srep24727

Swann, O.C., Rasmussen, A.B., Peacock, T.P., Sheppard, C.M., Barclay, W.S., 2022. Avian Influenza A Virus polymerase can utilise human ANP32 proteins to support cRNA but not vRNA synthesis. https://doi.org/10.1101/2022.06.27.497881

Tai, C.E., Tayeb-Fligelman, E., Griner, S., Salwinski, L., Bowler, J.T., Abskharon, R., Cheng, X., Seidler, P.M., Jiang, Y.X., Eisenberg, D.S., Guo, F., 2021. The SARS-CoV-2 nucleocapsid protein preferentially

binds long and structured RNAs (preprint). Biochemistry. https://doi.org/10.1101/2021.12.25.474155
Takeda, M., Leser, G.P., Russell, C.J., Lamb, R.A., 2003. Influenza virus hemagglutinin concentrates in lipid raft microdomains for efficient viral fusion. Proceedings of the National Academy of Sciences 100, 14610–14617. https://doi.org/10.1073/pnas.2235620100
Takizawa, N., Watanabe, K., Nouno, K., Kobayashi, N., Nagata, K., 2006. Association of functional influenza viral proteins and RNAs with nuclear chromatin and sub-chromatin structure. Microbes Infect 8, 823–833. https://doi.org/10.1016/j.micinf.2005.10.005
Talon, J., Horvath, C.M., Polley, R., Basler, C.F., Muster, T., Palese, P., García-Sastre, A., 2000. Activation of Interferon Regulatory Factor 3 Is Inhibited by the Influenza A Virus NS1 Protein. Journal of Virology 74, 7989–7996. https://doi.org/10.1128/JVI.74.17.7989-7996.2000
Tanaka, A., Nakano, T., Watanabe, K., Masuda, K., Honda, G., Kamata, S., Yasui, R., Kozuka-Hata, H., Watanabe, C., Chinen, T., Kitagawa, D., Sawai, S., Oyama, M., Yanagisawa, M., Kunieda, T., 2022. Stress-dependent cell stiffening by tardigrade tolerance proteins that reversibly form a filamentous network and gel. PLOS Biology 20, e3001780. https://doi.org/10.1371/journal.pbio.3001780
Tang, Y., Zaitseva, F., Lamb, R.A., Pinto, L.H., 2002. The Gate of the Influenza Virus M2 Proton Channel Is Formed by a Single Tryptophan Residue *. Journal of Biological Chemistry 277, 39880–39886. https://doi.org/10.1074/jbc.M206582200
Tarakhovsky, A., Prinjha, R.K., 2018. Drawing on disorder: How viruses use histone mimicry to their advantage. Journal of Experimental Medicine 215, 1777–1787. https://doi.org/10.1084/jem.20180099
Tarendeau, F., Boudet, J., Guilligay, D., Mas, P.J., Bougault, C.M., Boulo, S., Baudin, F., Ruigrok, R.W.H., Daigle, N., Ellenberg, J., Cusack, S., Simorre, J.-P., Hart, D.J., 2007. Structure and nuclear import function of the C-terminal domain of influenza virus polymerase PB2 subunit. Nat Struct Mol Biol 14, 229–233. https://doi.org/10.1038/nsmb1212
Taubenberger, J.K., Kash, J.C., 2010. Influenza Virus Evolution, Host Adaptation, and Pandemic Formation. Cell Host & Microbe 7, 440–451. https://doi.org/10.1016/j.chom.2010.05.009
Taubenberger, J.K., Morens, D.M., 2008. The Pathology of Influenza Virus Infections. Annual Review of Pathology: Mechanisms of Disease 3, 499–522. https://doi.org/10.1146/annurev.pathmechdis.3.121806.154316
Taubenberger, J.K., Morens, D.M., 2006. 1918 Influenza: the Mother of All Pandemics. Emerg Infect Dis 12, 15–22. https://doi.org/10.3201/eid1201.050979
Tauber, S., Ligertwood, Y., Quigg-Nicol, M., Dutia, B.M., Elliott, R.M., 2012. Behaviour of influenza A viruses differentially expressing segment 2 gene products in vitro and in vivo. J Gen Virol 93, 840–849. https://doi.org/10.1099/vir.0.039966-0

Taylor, N., Elbaum-Garfinkle, S., Vaidya, N., Zhang, H., Stone, H.A., Brangwynne, C.P., 2016. Biophysical characterization of organelle-based RNA/protein liquid phases using microfluidics. Soft Matter 12, 9142–9150. https://doi.org/10.1039/C6SM01087C

te Velthuis, A.J.W., Fodor, E., 2016. Influenza virus RNA polymerase: insights into the mechanisms of viral RNA synthesis. Nat Rev Microbiol 14, 479–493. https://doi.org/10.1038/nrmicro.2016.87

Te Velthuis, A.J.W., Robb, N.C., Kapanidis, A.N., Fodor, E., 2016. The role of the priming loop in Influenza A virus RNA synthesis. Nat Microbiol 1, 16029. https://doi.org/10.1038/nmicrobiol.2016.29

Terrier, O., Carron, C., De Chassey, B., Dubois, J., Traversier, A., Julien, T., Cartet, G., Proust, A., Hacot, S., Ressnikoff, D., Lotteau, V., Lina, B., Diaz, J.-J., Moules, V., Rosa-Calatrava, M., 2016. Nucleolin interacts with influenza A nucleoprotein and contributes to viral ribonucleoprotein complexes nuclear trafficking and efficient influenza viral replication. Sci Rep 6, 29006. https://doi.org/10.1038/srep29006

Thierry, E., Guilligay, D., Kosinski, J., Bock, T., Gaudon, S., Round, A., Pflug, A., Hengrung, N., El Omari, K., Baudin, F., Hart, D.J., Beck, M., Cusack, S., 2016. Influenza Polymerase Can Adopt an Alternative Configuration Involving a Radical Repacking of PB2 Domains. Mol Cell 61, 125–137. https://doi.org/10.1016/j.molcel.2015.11.016

Toh, X., Soh, M.L., Ng, M.K., Yap, S.C., Harith, N., Fernandez, C.J., Huangfu, T., 2019. Isolation and characterization of equine influenza virus (H3N8) from an equine influenza outbreak in Malaysia in 2015. Transbound Emerg Dis 66, 1884–1893. https://doi.org/10.1111/tbed.13218

Tom, J.K.A., Deniz, A.A., 2021. Complex dynamics of multicomponent biological coacervates. Current Opinion in Colloid & Interface Science 56, 101488. https://doi.org/10.1016/j.cocis.2021.101488

Tomescu, A.I., Robb, N.C., Hengrung, N., Fodor, E., Kapanidis, A.N., 2014. Single-molecule FRET reveals a corkscrew RNA structure for the polymerase-bound influenza virus promoter. Proceedings of the National Academy of Sciences 111, E3335–E3342. https://doi.org/10.1073/pnas.1406056111

Tong, S., Li, Y., Rivailler, P., Conrardy, C., Castillo, D.A.A., Chen, L.-M., Recuenco, S., Ellison, J.A., Davis, C.T., York, I.A., Turmelle, A.S., Moran, D., Rogers, S., Shi, M., Tao, Y., Weil, M.R., Tang, K., Rowe, L.A., Sammons, S., Xu, X., Frace, M., Lindblade, K.A., Cox, N.J., Anderson, L.J., Rupprecht, C.E., Donis, R.O., 2012. A distinct lineage of influenza A virus from bats. Proceedings of the National Academy of Sciences 109, 4269–4274. https://doi.org/10.1073/pnas.1116200109

Tong, S., Zhu, X., Li, Y., Shi, M., Zhang, J., Bourgeois, M., Yang, H., Chen, X., Recuenco, S., Gomez, J., Chen, L.-M., Johnson, A., Tao, Y., Dreyfus, C., Yu, W., McBride, R., Carney, P.J., Gilbert, A.T., Chang, J., Guo, Z., Davis, C.T., Paulson, J.C., Stevens, J., Rupprecht, C.E.,

Holmes, E.C., Wilson, I.A., Donis, R.O., 2013. New World Bats Harbor Diverse Influenza A Viruses. PLOS Pathogens 9, e1003657. https://doi.org/10.1371/journal.ppat.1003657

Tsai, C.-F., Lin, H.-Y., Hsu, W.-L., Tsai, C.-H., 2017. The novel mitochondria localization of influenza A virus NS1 visualized by FlAsH labeling. FEBS Open Bio 7, 1960–1971. https://doi.org/10.1002/2211-5463.12336

Tsai, P.-L., Chiou, N.-T., Kuss, S., García-Sastre, A., Lynch, K.W., Fontoura, B.M.A., 2013. Cellular RNA Binding Proteins NS1-BP and hnRNP K Regulate Influenza A Virus RNA Splicing. PLOS Pathogens 9, e1003460. https://doi.org/10.1371/journal.ppat.1003460

Turrell, L., Lyall, J.W., Tiley, L.S., Fodor, E., Vreede, F.T., 2013. The role and assembly mechanism of nucleoprotein in influenza A virus ribonucleoprotein complexes. Nat Commun 4, 1591. https://doi.org/10.1038/ncomms2589

Umbach, J.L., Yen, H.-L., Poon, L.L.M., Cullen, B.R., 2010. Influenza A Virus Expresses High Levels of an Unusual Class of Small Viral Leader RNAs in Infected Cells. mBio 1, e00204-10. https://doi.org/10.1128/mBio.00204-10

Valcárcel, J., Portela, A., Ortín, J., 1991. Regulated M1 mRNA splicing in influenza virus-infected cells. J Gen Virol 72 (Pt 6), 1301–1308. https://doi.org/10.1099/0022-1317-72-6-1301

Vale-Costa, S., Alenquer, M., Sousa, A.L., Kellen, B., Ramalho, J., Tranfield, E.M., Amorim, M.J., 2016a. Influenza A virus ribonucleoproteins modulate host recycling by competing with Rab11 effectors. Journal of Cell Science 129, 1697–1710. https://doi.org/10.1242/jcs.188409

Vale-Costa, S., Alenquer, M., Sousa, A.L., Kellen, B., Ramalho, J., Tranfield, E.M., Amorim, M.J., 2016b. Influenza A virus ribonucleoproteins modulate host recycling by competing with Rab11 effectors. J Cell Sci 129, 1697–1710. https://doi.org/10.1242/jcs.188409

Vale-Costa, Silvia, Amorim, M.J., 2016. Clustering of Rab11 vesicles in influenza A virus infected cells creates hotspots containing the 8 viral ribonucleoproteins. Small GTPases 8, 1–7. https://doi.org/10.1080/21541248.2016.1199190

Vale-Costa, Sílvia, Amorim, M.J., 2016a. Clustering of Rab11 vesicles in influenza A virus infected cells creates hotspots containing the 8 viral ribonucleoproteins. Small GTPases 8, 71–77. https://doi.org/10.1080/21541248.2016.1199190

Vale-Costa, Sílvia, Amorim, M.J., 2016b. Recycling Endosomes and Viral Infection. Viruses 8, 64. https://doi.org/10.3390/v8030064

Van Roey, K., Uyar, B., Weatheritt, R.J., Dinkel, H., Seiler, M., Budd, A., Gibson, T.J., Davey, N.E., 2014. Short Linear Motifs: Ubiquitous and Functionally Diverse Protein Interaction Modules Directing Cell Regulation. Chem. Rev. 114, 6733–6778. https://doi.org/10.1021/cr400585q

Van Treeck, B., Protter, D.S.W., Matheny, T., Khong, A., Link, C.D., Parker, R., 2018. RNA self-assembly contributes to stress granule formation and defining the stress granule transcriptome. Proceedings of the National Academy of Sciences 115, 2734–2739. https://doi.org/10.1073/pnas.1800038115

Vantomme, G., Meijer, E.W., 2019. The construction of supramolecular systems. Science 363, 1396–1397. https://doi.org/10.1126/science.aav4677

Vekilov, P.G., 2010. Nucleation. Cryst Growth Des 10, 5007–5019. https://doi.org/10.1021/cg1011633

Veler, H., Fan, H., Keown, J.R., Sharps, J., Fournier, M., Grimes, J.M., Fodor, E., 2022. The C-Terminal Domains of the PB2 Subunit of the Influenza A Virus RNA Polymerase Directly Interact with Cellular GTPase Rab11a. J Virol 96, e0197921. https://doi.org/10.1128/jvi.01979-21

Venev, S.V., Zeldovich, K.B., 2013. Segment Self-Repulsion is the Major Driving Force of Influenza Genome Packaging. Phys. Rev. Lett. 110, 098104. https://doi.org/10.1103/PhysRevLett.110.098104

Ver, L.S., Marcos-Villar, L., Landeras-Bueno, S., Nieto, A., Ortín, J., 2015. The Cellular Factor NXP2/MORC3 Is a Positive Regulator of Influenza Virus Multiplication. J Virol 89, 10023–10030. https://doi.org/10.1128/JVI.01530-15

Vijayakrishnan, S., Loney, C., Jackson, D., Suphamungmee, W., Rixon, F.J., Bhella, D., 2013. Cryotomography of Budding Influenza A Virus Reveals Filaments with Diverse Morphologies that Mostly Do Not Bear a Genome at Their Distal End. PLOS Pathogens 9, e1003413. https://doi.org/10.1371/journal.ppat.1003413

Voorhees, P.W., 1992. Ostwald Ripening of Two-Phase Mixtures. Annual Review of Materials Science 22, 197–215. https://doi.org/10.1146/annurev.ms.22.080192.001213

Vreede, F.T., Brownlee, G.G., 2007. Influenza virion-derived viral ribonucleoproteins synthesize both mRNA and cRNA in vitro. J Virol 81, 2196–2204. https://doi.org/10.1128/JVI.02187-06

Wan, G., Fields, B.D., Spracklin, G., Shukla, A., Phillips, C.M., Kennedy, S., 2018. Spatiotemporal regulation of liquid-like condensates in epigenetic inheritance. Nature 557, 679–683. https://doi.org/10.1038/s41586-018-0132-0

Wan, Z., Kan, Q., Zhao, Z., Shao, H., Deliberto, T.J., Wan, X.-F., Qin, A., Ye, J., 2021. Characterization of Subtype H6 Avian Influenza A Viruses Isolated From Wild Birds in Poyang Lake, China. Frontiers in Veterinary Science 8.

Wandzik, J.M., Kouba, T., Cusack, S., 2021. Structure and Function of Influenza Polymerase. Cold Spring Harb Perspect Med 11, a038372. https://doi.org/10.1101/cshperspect.a038372

Wang, A., Conicella, A.E., Schmidt, H.B., Martin, E.W., Rhoads, S.N., Reeb, A.N., Nourse, A., Ramirez Montero, D., Ryan, V.H., Rohatgi, R., Shewmaker, F., Naik, M.T., Mittag, T., Ayala, Y.M., Fawzi, N.L., 2018.

A single N-terminal phosphomimic disrupts TDP-43 polymerization, phase separation, and RNA splicing. The EMBO journal 37, e97452. https://doi.org/10.15252/embj.201797452

Wang, C., Lamb, R.A., Pinto, L.H., 1995. Activation of the M2 ion channel of influenza virus: a role for the transmembrane domain histidine residue. Biophysical Journal 69, 1363–1371. https://doi.org/10.1016/S0006-3495(95)80003-2

Wang, D., Harmon, A., Jin, J., Francis, D.H., Christopher-Hennings, J., Nelson, E., Montelaro, R.C., Li, F., 2010. The lack of an inherent membrane targeting signal is responsible for the failure of the matrix (M1) protein of influenza A virus to bud into virus-like particles. J Virol 84, 4673–4681. https://doi.org/10.1128/JVI.02306-09

Wang, D., Zhu, W., Yang, L., Shu, Y., 2021. The Epidemiology, Virology, and Pathogenicity of Human Infections with Avian Influenza Viruses. Cold Spring Harb Perspect Med 11, a038620. https://doi.org/10.1101/cshperspect.a038620

Wang, H., Yan, X., Aigner, H., Bracher, A., Nguyen, N.D., Hee, W.Y., Long, B.M., Price, G.D., Hartl, F.U., Hayer-Hartl, M., 2019. Rubisco condensate formation by CcmM in β-carboxysome biogenesis. Nature 566, 131–135. https://doi.org/10.1038/s41586-019-0880-5

Wang, J., Choi, J.-M., Holehouse, A.S., Lee, H.O., Zhang, X., Jahnel, M., Maharana, S., Lemaitre, R., Pozniakovsky, A., Drechsel, D., Poser, I., Pappu, R.V., Alberti, S., Hyman, A.A., 2018. A Molecular Grammar Governing the Driving Forces for Phase Separation of Prion-like RNA Binding Proteins. Cell 174, 688-699.e16. https://doi.org/10.1016/j.cell.2018.06.006

Wang, N., Glidden, E.J., Murphy, S.R., Pearse, B.R., Hebert, D.N., 2008. The cotranslational maturation program for the type II membrane glycoprotein influenza neuraminidase. J Biol Chem 283, 33826–33837. https://doi.org/10.1074/jbc.M806897200

Wang, P., Palese, P., O'Neill, R.E., 1997. The NPI-1/NPI-3 (karyopherin alpha) binding site on the influenza a virus nucleoprotein NP is a nonconventional nuclear localization signal. J Virol 71, 1850–1856.

Wang, Q., Li, Q., Liu, T., Chang, G., Sun, Z., Gao, Z., Wang, F., Zhou, H., Liu, R., Zheng, M., Cui, H., Chen, G., Li, H., Yuan, X., Wen, J., Peng, D., Zhao, G., 2018. Host Interaction Analysis of PA-N155 and PA-N182 in Chicken Cells Reveals an Essential Role of UBA52 for Replication of H5N1 Avian Influenza Virus. Frontiers in Microbiology 9.

Wang, Q., Liu, R., Li, Q., Wang, F., Zhu, B., Zheng, M., Cui, H., Wen, J., Zhao, G., 2019. Host cell interactome of PB1 N40 protein of H5N1 influenza A virus in chicken cells. Journal of Proteomics 197, 34–41. https://doi.org/10.1016/j.jprot.2019.02.011

Wanitchang, A., Patarasirin, P., Jengarn, J., Jongkaewwattana, A., 2011. Atypical characteristics of nucleoprotein of pandemic influenza virus H1N1 and their roles in reassortment restriction. Arch Virol 156, 1031–1040. https://doi.org/10.1007/s00705-011-0947-6

Ward, A.C., Castelli, L.A., Lucantoni, A.C., White, J.F., Azad, A.A., Macreadie, I.G., 1995. Expression and analysis of the NS2 protein of influenza A virus. Archives of Virology 140, 2067–2073. https://doi.org/10.1007/BF01322693

Wasilewski, S., Calder, L.J., Grant, T., Rosenthal, P.B., 2012. Distribution of surface glycoproteins on influenza A virus determined by electron cryotomography. Vaccine, Fourth ESWI Influenza Conference 30, 7368–7373. https://doi.org/10.1016/j.vaccine.2012.09.082

Watanabe, K., Takizawa, N., Katoh, M., Hoshida, K., Kobayashi, N., Nagata, K., 2001. Inhibition of nuclear export of ribonucleoprotein complexes of influenza virus by leptomycin B. Virus Research 77, 31–42. https://doi.org/10.1016/S0168-1702(01)00263-5

Watanabe, T., Watanabe, S., Kawaoka, Y., 2010. Cellular Networks Involved in the Influenza Virus Life Cycle. Cell Host & Microbe 7, 427–439. https://doi.org/10.1016/j.chom.2010.05.008

Watanabe, T., Watanabe, S., Noda, T., Fujii, Y., Kawaoka, Y., 2003. Exploitation of nucleic acid packaging signals to generate a novel influenza virus-based vector stably expressing two foreign genes. J Virol 77, 10575–10583. https://doi.org/10.1128/jvi.77.19.10575-10583.2003

Weber, S.C., Brangwynne, C.P., 2015. Inverse Size Scaling of the Nucleolus by a Concentration-Dependent Phase Transition. Current Biology 25, 641–646. https://doi.org/10.1016/j.cub.2015.01.012

Weber, S.C., Brangwynne, C.P., 2012. Getting RNA and Protein in Phase. Cell 149, 1188–1191. https://doi.org/10.1016/j.cell.2012.05.022

Webster, R.G., Bean, W.J., Gorman, O.T., Chambers, T.M., Kawaoka, Y., 1992. Evolution and ecology of influenza A viruses. Microbiol Rev 56, 152–179. https://doi.org/10.1128/mr.56.1.152-179.1992

Webster, R.G., Yakhno, M., Hinshaw, V.S., Bean, W.J., Copal Murti, K., 1978. Intestinal influenza: Replication and characterization of influenza viruses in ducks. Virology 84, 268–278. https://doi.org/10.1016/0042-6822(78)90247-7

Wei, W., Bai, L., Yan, B., Meng, W., Wang, H., Zhai, J., Si, F., Zheng, C., 2022. When liquid-liquid phase separation meets viral infections. Frontiers in Immunology 13.

Weis, S., Te Velthuis, A.J.W., 2021. Influenza Virus RNA Synthesis and the Innate Immune Response. Viruses 13, 780. https://doi.org/10.3390/v13050780

Weis, W., Brown, J.H., Cusack, S., Paulson, J.C., Skehel, J.J., Wiley, D.C., 1988. Structure of the influenza virus haemagglutinin complexed with its receptor, sialic acid. Nature 333, 426–431. https://doi.org/10.1038/333426a0

Wheeler, R.J., Hyman, A.A., 2018. Controlling compartmentalization by non-membrane-bound organelles. Philosophical Transactions of the Royal Society B: Biological Sciences 373, 20170193. https://doi.org/10.1098/rstb.2017.0193

White, J., Helenius, A., Gething, M.-J., 1982. Haemagglutinin of influenza virus expressed from a cloned gene promotes membrane fusion. Nature 300, 658–659. https://doi.org/10.1038/300658a0
White, S.K., Ma, W., McDaniel, C.J., Gray, G.C., Lednicky, J.A., 2016. Serologic evidence of exposure to influenza D virus among persons with occupational contact with cattle. Journal of Clinical Virology 81, 31–33. https://doi.org/10.1016/j.jcv.2016.05.017
Whittaker, G., Bui, M., Helenius, A., 1996. The role of nuclear import and export in influenza virus infection. Trends Cell Biol 6, 67–71. https://doi.org/10.1016/0962-8924(96)81017-8
WHO, 2018. Influenza (Seasonal) [WWW Document]. URL https://www.who.int/news-room/fact-sheets/detail/influenza-(seasonal) (accessed 8.6.22).
Wikipedia, 2022. Phase separation. Wikipedia.
Wileman, T., 2007. Aggresomes and Pericentriolar Sites of Virus Assembly: Cellular Defense or Viral Design? Annual Review of Microbiology 61, 149–167. https://doi.org/10.1146/annurev.micro.57.030502.090836
Wiley, D.C., Skehel, J.J., 1987. The structure and function of the hemagglutinin membrane glycoprotein of influenza virus. Annual review of biochemistry 56. https://doi.org/10.1146/annurev.bi.56.070187.002053
Wille, M., Holmes, E.C., 2020. The Ecology and Evolution of Influenza Viruses. Cold Spring Harb Perspect Med 10, a038489. https://doi.org/10.1101/cshperspect.a038489
Williams, G.D., Townsend, D., Wylie, K.M., Kim, P.J., Amarasinghe, G.K., Kutluay, S.B., Boon, A.C.M., 2018. Nucleotide resolution mapping of influenza A virus nucleoprotein-RNA interactions reveals RNA features required for replication. Nat Commun 9, 465. https://doi.org/10.1038/s41467-018-02886-w
Wilson, E.B., 1899. The Structure of Protoplasm. Science 10, 33–45. https://doi.org/10.1126/science.10.237.33
Wilson, I.A., Skehel, J.J., Wiley, D.C., 1981. Structure of the haemagglutinin membrane glycoprotein of influenza virus at 3 Å resolution. Nature 289, 366–373. https://doi.org/10.1038/289366a0
Wippich, F., Bodenmiller, B., Trajkovska, M.G., Wanka, S., Aebersold, R., Pelkmans, L., 2013. Dual Specificity Kinase DYRK3 Couples Stress Granule Condensation/Dissolution to mTORC1 Signaling. Cell 152, 791–805. https://doi.org/10.1016/j.cell.2013.01.033
Wise, H.M., Barbezange, C., Jagger, B.W., Dalton, R.M., Gog, J.R., Curran, M.D., Taubenberger, J.K., Anderson, E.C., Digard, P., 2011. Overlapping signals for translational regulation and packaging of influenza A virus segment 2. Nucleic Acids Res 39, 7775–7790. https://doi.org/10.1093/nar/gkr487
Wise, H.M., Foeglein, A., Sun, J., Dalton, R.M., Patel, S., Howard, W., Anderson, E.C., Barclay, W.S., Digard, P., 2009. A Complicated Message: Identification of a Novel PB1-Related Protein Translated

from Influenza A Virus Segment 2 mRNA. Journal of Virology 83, 8021–8031. https://doi.org/10.1128/JVI.00826-09
Wise, H.M., Hutchinson, E.C., Jagger, B.W., Stuart, A.D., Kang, Z.H., Robb, N., Schwartzman, L.M., Kash, J.C., Fodor, E., Firth, A.E., Gog, J.R., Taubenberger, J.K., Digard, P., 2012. Identification of a Novel Splice Variant Form of the Influenza A Virus M2 Ion Channel with an Antigenically Distinct Ectodomain. PLOS Pathogens 8, e1002998. https://doi.org/10.1371/journal.ppat.1002998
Wolff, G., Melia, C.E., Snijder, E.J., Bárcena, M., 2020. Double-Membrane Vesicles as Platforms for Viral Replication. Trends in Microbiology 28, 1022–1033. https://doi.org/10.1016/j.tim.2020.05.009
Woodruff, J.B., Hyman, A.A., Boke, E., 2018. Organization and Function of Non-dynamic Biomolecular Condensates. Trends in biochemical sciences 43, 81–94. https://doi.org/10.1016/j.tibs.2017.11.005
World Health Organization, 2022. FluNet Summary [WWW Document]. FluNet summary. URL https://www.who.int/tools/flunet/flunet-summary (accessed 11.21.22).
Wu, C., Holehouse, A.S., Leung, D.W., Amarasinghe, G.K., Dutch, R.E., 2022. Liquid Phase Partitioning in Virus Replication: Observations and Opportunities. Annual Review of Virology 9, null. https://doi.org/10.1146/annurev-virology-093020-013659
Wu, J., Sun, L., Chen, X., Du, F., Shi, H., Chen, C., Chen, Z.J., 2013. Cyclic GMP-AMP is an endogenous second messenger in innate immune signaling by cytosolic DNA. Science 339, 826–830. https://doi.org/10.1126/science.1229963
Wu, X., Qi, X., Qu, B., Zhang, Z., Liang, M., Li, C., Cardona, C.J., Li, D., Xing, Z., 2014. Evasion of Antiviral Immunity through Sequestering of TBK1/IKKε/IRF3 into Viral Inclusion Bodies. Journal of Virology 88, 3067–3076. https://doi.org/10.1128/JVI.03510-13
Wunder, T., Cheng, S.L.H., Lai, S.-K., Li, H.-Y., Mueller-Cajar, O., 2018. The phase separation underlying the pyrenoid-based microalgal Rubisco supercharger. Nat Commun 9, 5076. https://doi.org/10.1038/s41467-018-07624-w
Wurzer, W.J., Planz, O., Ehrhardt, C., Giner, M., Silberzahn, T., Pleschka, S., Ludwig, S., 2003. Caspase 3 activation is essential for efficient influenza virus propagation. EMBO J 22, 2717–2728. https://doi.org/10.1093/emboj/cdg279
Xue, B., Mizianty, M.J., Kurgan, L., Uversky, V.N., 2012. Protein intrinsic disorder as a flexible armor and a weapon of HIV-1. Cell. Mol. Life Sci. 69, 1211–1259. https://doi.org/10.1007/s00018-011-0859-3
Yamanaka, K., Ishihama, A., Nagata, K., 1990. Reconstitution of influenza virus RNA-nucleoprotein complexes structurally resembling native viral ribonucleoprotein cores. Journal of Biological Chemistry 265, 11151–11155. https://doi.org/10.1016/S0021-9258(19)38570-9

Yamaoka, M., Hotta, H., Itoh, M., Homma, M., 1991. Prevalence of antibody to influenza C virus among pigs in Hyogo Prefecture, Japan. J Gen Virol 72 (Pt 3), 711–714. https://doi.org/10.1099/0022-1317-72-3-711

Yamayoshi, S., Watanabe, M., Goto, H., Kawaoka, Y., 2015. Identification of a Novel Viral Protein Expressed from the PB2 Segment of Influenza A Virus. Journal of Virology 90, 444–456. https://doi.org/10.1128/JVI.02175-15

Yang, P., Mathieu, C., Kolaitis, R.-M., Zhang, P., Messing, J., Yurtsever, U., Yang, Z., Wu, J., Li, Y., Pan, Q., Yu, J., Martin, E.W., Mittag, T., Kim, H.J., Taylor, J.P., 2020. G3BP1 Is a Tunable Switch that Triggers Phase Separation to Assemble Stress Granules. Cell 181, 325-345.e28. https://doi.org/10.1016/j.cell.2020.03.046

Yang, W., Schountz, T., Ma, W., 2021. Bat Influenza Viruses: Current Status and Perspective. Viruses 13, 547. https://doi.org/10.3390/v13040547

Yang, Y., Jones, H.B., Dao, T.P., Castañeda, C.A., 2019. Single Amino Acid Substitutions in Stickers, but Not Spacers, Substantially Alter UBQLN2 Phase Transitions and Dense Phase Material Properties. J. Phys. Chem. B 123, 3618–3629. https://doi.org/10.1021/acs.jpcb.9b01024

Yao, R.-W., Xu, G., Wang, Ying, Shan, L., Luan, P.-F., Wang, Yang, Wu, M., Yang, L.-Z., Xing, Y.-H., Yang, L., Chen, L.-L., 2019. Nascent Pre-rRNA Sorting via Phase Separation Drives the Assembly of Dense Fibrillar Components in the Human Nucleolus. Molecular Cell 76, 767-783.e11. https://doi.org/10.1016/j.molcel.2019.08.014

Yasuda, J., Nakada, S., Kato, A., Toyoda, T., Ishihama, A., 1993. Molecular Assembly of Influenza Virus: Association of the NS2 Protein with Virion Matrix. Virology 196, 249–255. https://doi.org/10.1006/viro.1993.1473

Ye, Q., Krug, R.M., Tao, Y.J., 2006. The mechanism by which influenza A virus nucleoprotein forms oligomers and binds RNA. Nature 444, 1078–1082. https://doi.org/10.1038/nature05379

Ye, Y., Fan, H., Li, Q., Zhang, Z., Miao, P., Zhu, J., Liu, J., Zhang, J., Liao, M., 2022. Differential proteome response to H5N1 highly pathogenic avian influenza (HPAI) viruses infection in duck. Frontiers in Immunology 13.

Ye, Z., Liu, T., Offringa, D.P., McInnis, J., Levandowski, R.A., 1999. Association of influenza virus matrix protein with ribonucleoproteins. J Virol 73, 7467–7473. https://doi.org/10.1128/JVI.73.9.7467-7473.1999

Yewdell, J.W., Antón, L.C., Bennink, J.R., 1996. Defective ribosomal products (DRiPs): a major source of antigenic peptides for MHC class I molecules? The Journal of Immunology 157, 1823–1826.

Yondola, M.A., Fernandes, F., Belicha-Villanueva, A., Uccelini, M., Gao, Q., Carter, C., Palese, P., 2011. Budding Capability of the Influenza Virus Neuraminidase Can Be Modulated by Tetherin. Journal of Virology 85, 2480–2491. https://doi.org/10.1128/JVI.02188-10

Yoon, S.-W., Webby, R.J., Webster, R.G., 2014. Evolution and Ecology of Influenza A Viruses, in: Compans, R.W., Oldstone, M.B.A. (Eds.), Influenza Pathogenesis and Control - Volume I, Current Topics in Microbiology and Immunology. Springer International Publishing, Cham, pp. 359–375. https://doi.org/10.1007/82_2014_396

York, A., 2021. Targeting viral liquid–liquid phase separation. Nat Rev Microbiol 19, 550–550. https://doi.org/10.1038/s41579-021-00608-6

York, A., Fodor, E., 2013. Biogenesis, assembly, and export of viral messenger ribonucleoproteins in the influenza A virus infected cell. RNA Biol 10, 1274–1282. https://doi.org/10.4161/rna.25356

York, A., Hengrung, N., Vreede, F.T., Huiskonen, J.T., Fodor, E., 2013. Isolation and characterization of the positive-sense replicative intermediate of a negative-strand RNA virus. Proc Natl Acad Sci U S A 110, E4238-4245. https://doi.org/10.1073/pnas.1315068110

York, A., Hutchinson, E.C., Fodor, E., 2014. Interactome Analysis of the Influenza A Virus Transcription/Replication Machinery Identifies Protein Phosphatase 6 as a Cellular Factor Required for Efficient Virus Replication. Journal of Virology 88, 13284–13299. https://doi.org/10.1128/JVI.01813-14

Yoshimura, A., Ohnishi, S., 1984. Uncoating of influenza virus in endosomes. Journal of Virology 51, 497–504. https://doi.org/10.1128/jvi.51.2.497-504.1984

Yoshizawa, T., Nozawa, R.-S., Jia, T.Z., Saio, T., Mori, E., 2020. Biological phase separation: cell biology meets biophysics. Biophys Rev 12, 519–539. https://doi.org/10.1007/s12551-020-00680-x

Yuan, P., Bartlam, M., Lou, Z., Chen, S., Zhou, J., He, X., Lv, Z., Ge, R., Li, X., Deng, T., Fodor, E., Rao, Z., Liu, Y., 2009. Crystal structure of an avian influenza polymerase PAN reveals an endonuclease active site. Nature 458, 909–913. https://doi.org/10.1038/nature07720

Zamarin, D., García-Sastre, A., Xiao, X., Wang, R., Palese, P., 2005. Influenza Virus PB1-F2 Protein Induces Cell Death through Mitochondrial ANT3 and VDAC1. PLOS Pathogens 1, e4. https://doi.org/10.1371/journal.ppat.0010004

Zambon, M.C., 1999. Epidemiology and pathogenesis of influenza. Journal of Antimicrobial Chemotherapy 44, 3–9. https://doi.org/10.1093/jac/44.suppl_2.3

Zebedee, S.L., Richardson, C.D., Lamb, R.A., 1985. Characterization of the influenza virus M2 integral membrane protein and expression at the infected-cell surface from cloned cDNA. Journal of Virology 56, 502–511. https://doi.org/10.1128/jvi.56.2.502-511.1985

Zeng, Y., Xu, S., Wei, Y., Zhang, X., Wang, Q., Jia, Y., Wang, W., Han, L., Chen, Z., Wang, Z., Zhang, B., Chen, H., Lei, C.-Q., Zhu, Q., 2021. The PB1 protein of influenza A virus inhibits the innate immune response by targeting MAVS for NBR1-mediated selective autophagic degradation. PLoS Pathog 17, e1009300. https://doi.org/10.1371/journal.ppat.1009300

Zhai, S.-L., Zhang, H., Chen, S.-N., Zhou, X., Lin, T., Liu, R., Lv, D.-H., Wen, X.-H., Wei, W.-K., Wang, D., Li, F., 2017. Influenza D Virus in Animal Species in Guangdong Province, Southern China - Volume 23, Number 8—August 2017 - Emerging Infectious Diseases journal - CDC 23. https://doi.org/10.3201/eid2308.170059

Zhang, H., Elbaum-Garfinkle, S., Langdon, E.M., Taylor, N., Occhipinti, P., Andrew, Clifford, Amy, 2015. RNA Controls PolyQ Protein Phase Transitions 60, 220–230. https://doi.org/10.1016/j.molcel.2015.09.017

Zhang, H., Porter, E., Lohman, M., Lu, N., Peddireddi, L., Hanzlicek, G., Marthaler, D., Liu, X., Bai, J., 2018. Influenza C Virus in Cattle with Respiratory Disease, United States, 2016–2018. Emerg Infect Dis 24, 1926–1929. https://doi.org/10.3201/eid2410.180589

Zhang, J., Lamb, R.A., 1996. Characterization of the membrane association of the influenza virus matrix protein in living cells. Virology 225, 255–266. https://doi.org/10.1006/viro.1996.0599

Zhang, J., Leser, G.P., Pekosz, A., Lamb, R.A., 2000. The cytoplasmic tails of the influenza virus spike glycoproteins are required for normal genome packaging. Virology 269, 325–334. https://doi.org/10.1006/viro.2000.0228

Zhang, X., Sridharan, S., Zagoriy, I., Oegema, C.E., Ching, C., Pflaesterer, T., Fung, H.K.H., Poser, I., Müller, C.W., Hyman, A.A., Savitski, M.M., Mahamid, J., 2022. Molecular mechanisms of stress-induced reactivation in mumps virus condensates. https://doi.org/10.1101/2021.07.10.451879

Zhang, Xu, Shi, H., Wu, J., Zhang, Xuewu, Sun, L., Chen, C., Chen, Z.J., 2013. Cyclic GMP-AMP containing mixed phosphodiester linkages is an endogenous high-affinity ligand for STING. Mol Cell 51, 226–235. https://doi.org/10.1016/j.molcel.2013.05.022

Zhao, H., French, J.B., Fang, Y., Benkovic, S.J., 2013. The purinosome, a multi-protein complex involved in the de novo biosynthesis of purines in humans. Chem. Commun. 49, 4444–4452. https://doi.org/10.1039/C3CC41437J

Zhao, Y.G., Zhang, H., 2020. Phase Separation in Membrane Biology: The Interplay between Membrane-Bound Organelles and Membraneless Condensates. Developmental Cell 55, 30–44. https://doi.org/10.1016/j.devcel.2020.06.033

Zhou, J., Wang, D., Gao, R., Zhao, B., Song, J., Qi, X., Zhang, Yanjun, Shi, Y., Yang, L., Zhu, W., Bai, T., Qin, K., Lan, Y., Zou, S., Guo, J., Dong, J., Dong, L., Zhang, Ye, Wei, H., Li, Xiaodan, Lu, J., Liu, L., Zhao, X., Li, Xiyan, Huang, W., Wen, L., Bo, H., Xin, L., Chen, Y., Xu, C., Pei, Y., Yang, Y., Zhang, X., Wang, S., Feng, Z., Han, J., Yang, W., Gao, G.F., Wu, G., Li, D., Wang, Y., Shu, Y., 2013. Biological features of novel avian influenza A (H7N9) virus. Nature 499, 500–503. https://doi.org/10.1038/nature12379

Zhou, Y., Su, J.M., Samuel, C.E., Ma, D., 2019. Measles Virus Forms Inclusion Bodies with Properties of Liquid Organelles. Journal of Virology 93, e00948-19. https://doi.org/10.1128/JVI.00948-19

Zhou, Z., Cao, M., Guo, Y., Zhao, L., Wang, Jingfeng, Jia, X., Li, J., Wang, C., Gabriel, G., Xue, Q., Yi, Y., Cui, S., Jin, Q., Wang, Jianwei, Deng, T., 2014. Fragile X mental retardation protein stimulates ribonucleoprotein assembly of influenza A virus. Nat Commun 5, 3259. https://doi.org/10.1038/ncomms4259

Zhu, L., Richardson, T.M., Wacheul, L., Wei, M.-T., Feric, M., Whitney, G., Lafontaine, D.L.J., Brangwynne, C.P., 2019. Controlling the material properties and rRNA processing function of the nucleolus using light. Proceedings of the National Academy of Sciences 116, 17330–17335. https://doi.org/10.1073/pnas.1903870116

Zvonarjev, A.Y., Ghendon, Y.Z., 1980. Influence of membrane (M) protein on influenza A virus virion transcriptase activity in vitro and its susceptibility to rimantadine. J Virol 33, 583–586. https://doi.org/10.1128/JVI.33.2.583-586.1980

ITQB NOVA, Avenida da República, 2780-157 Oeiras, Portugal | Tel +351 214 469 100 | itqb.unl.pt